

Novel Sequential Batch Electro-Fenton System for Total Kjeldahl Nitrogen
Removal: Solution for Highly Polluted Industrial Wastewater

Arash Fella Jahromi

A Thesis
in
the Department
of
Building, Civil and Environmental Engineering

Presented in Partial Fulfilment of the Requirements
for the Degree of Master of Applied Science (Civil Engineering)
at Concordia University
Montreal, Quebec, Canada

December 2017

© Arash Fella Jahromi

CONCORDIA UNIVERSITY
School of Graduate studies

This is to certify that the thesis prepared

By: Arash Fella Jahromi

Entitled Novel Sequential Batch Electro-Fenton System for Total Kjeldahl Nitrogen Removal:
Solution for Highly Polluted Industrial Wastewater

And submitted in partial fulfillment of the requirements for the degree of

Master of Applied Science (Civil Engineering)

Complies with the regulations of the University and meets the accepted standards with respect to originality and quality.

Signed by the final Examining Committee:

_____ Chair

Dr. S. Li

_____ Examiner

Dr. X. Wang

_____ Examiner

Dr. C. Mulligan

_____ Examiner

Dr. S. Li

_____ Supervisor

Dr. M. Elektorowicz

Approved by

Chair of Department or Graduate Program Director

December 2017

Dean of Faculty

Abstract

Novel Sequential Batch Electro-Fenton System for Total Kjeldahl Nitrogen Removal: Solution for Highly Polluted Industrial Wastewater

Arash Fella Jahromi

A novel electro-Fenton sequential batch reactor (EF-SBR) was developed in this study which permits to overcome main drawbacks of Fenton process, sludge production. The primary objective of this research is providing a solution for treatment of industrial wastewater containing specifically high amount of Total Kjeldahl Nitrogen (TKN). For sustainable reason, a more detailed objective of this study is simultaneous removal of ammonia, total nitrogen, and organic nitrogen. Thereby, investigations in four phases were conducted to achieve the objectives. The predominant mechanism of this study is electro Fenton oxidation. In Phase 1, fundamental operating parameters were investigated to achieve optimal design for small scale batch system. Throughout phase 2, the medium scale electrokinetic reactor was developed in which the optimal technological parameters were adjusted to scale up process. A multi compartment large scale EK reactor was designed and tested in Phase 3 to optimize the energy consumption. The results of Phase 3 showed above 99% and 99.6% of ammonia and TKN removal by using potent oxidizing agent in an appropriate time interval which leads to an economical retention time. Throughout Phase 4, the EF-SBR (Electro-Fenton Sequential Batch Reactor) was designed to address a industrial situation. The highlights of Phase 4 were reducing retention time of the EF-SBR while obtaining above 99% removal efficiencies for ammonia, TKN, total nitrogen, and organic nitrogen. Conducted research demonstrated the feasibility of proposed method, as well as fractal analysis to find the pathway to construe the transient variations in the target concentrations while analyzing the samples in an adequate number of points over an extended exposure period. The proposed design is sustainable since limits supplying additional chemicals and optimizes energy use. The technology is ready for a full-scale application.

Acknowledgments

I would like to express my deepest gratitude and respect to my supervisor Professor Maria Elektorowicz who supports me throughout my research and study at Concordia University. She has devoted her time and help to support me in entire work and she was always welcome me to meet her even out of office hours. I am also deeply and sincerely grateful to Professor Marek Balazinski from École Polytechnique de Montréal who considers time to discuss with me about fractal analysis and kindly advises me. Also, I express my gratitude to Dr. Xavier Rimpault who collaborated in fractal modeling of the research. Also, I would like to thank Professor Sasha Omanovic, a faculty member of McGill University, for allowing me to attend his course on Electrochemical Engineering and learn from him.

I would like to appreciate the financial support from NSERC Discovery Grant (discerned to Prof. Elektorowicz) and Graduate Scholarship provided by the Faculty of Engineering and Computer Science at Concordia University.

I wish to express my appreciation to all my laboratory colleagues, particularly Alexandre Belanger and Lazar Louis Stevanovic for their friendship and great team work spirit that we shared during these years. Without devoted aid of my colleague, Mr. Vahid Mohseni, it would not be feasible to proceed the precise kinetics investigation of the pollutant degradation over five day exposure time without interruption. Also, it would be my pleasure to appreciate my colleague Hamed Shahnejat Bushehri, for his dedicated help.

It is my pleasure and honor to admire and appreciate my high school chemistry teacher, Mr. Jahantab, who motivated me to chemistry and built my future research interests. I am also thankful to my uncle, Dr. Mohammad Fella Jahromi who is an academic paradigm for me.

Last, but not least, my sincere heartfelt thanks go out to my mother Dr. Shohreh Khaefi, my father Dr. Mahmoud Fella Jahromi, my grandmother Mrs. Tooran Larizadeh, my brother Dr. Ali Fella Jahromi and my sister-in-law Ms. Zahra Rostamkhani.

Dedicated to
My family

Table of contents

List of Figures	viii
List of Tables	xiii
Notation	xvi
Symbols and abbreviations	xviii
CHAPTER 1 Introduction and research objectives	1
1-1. Problem statement.....	1
1-2. Research objectives.....	4
CHAPTER 2 Literature review	5
2-1. Overview of photo processing and wastewater composition	5
2-1-1. Process description.....	5
2-1-2. Composition of photographic wastewater.....	6
2-2. Chemical properties of amides and amines	9
2-2-1. Amide molecular structure, synthesis, and hydrolysis.....	9
2-2-2. Amine molecular structure and synthesis.....	12
2-3. Applicable mechanisms in highly polluted industrial wastewater	15
2-3-1. Ozonation in an alkaline medium.....	18
2-3-2. Ozone and ultraviolet radiation (O_3 / UV).....	19
2-3-3. Ozone, hydrogen peroxide, and ultraviolet radiation ($O_3/ H_2O_2/UV$).....	20
2-3-4. Ozonolysis and ultrasound.....	21
2-3-5. Fenton process.....	22
2-3-6. Sono-Fenton process	27
2-3-7. Photo-Fenton process	29
2-3-8. Electro-Fenton process.....	30
2-3-9. Cost consumption of Fenton, ozonation, and conductive-diamond electrochemical oxidation (CDEO).....	38
CHAPTER 3 Methodology	40
3-1. Methodological approach	40
3-2. Experimental configuration and reactor design.....	43
3-2-1. Reactor and experimental design of Phase 1	48
3-2-2. Reactor and experimental design of Phase 2.....	59
3-2-3. Reactor and experimental design of Phase 3.....	64
3-2-4. Reactor and experimental design of Phase 4.....	67
3-3. Experimental analysis methods	71
3-4. Electrochemical reactions.....	72
3-4-1. Electro-Fenton reactions	73
3-4-2. Mass transfer	74
3-4-3. Kinetics.....	92

CHAPTER 4 Results and discussions	95
4-1. Phase 1 results and discussions	95
4-1-1. Stage 1-1 analysis.....	95
4-1-2. Stage 1-2 analysis.....	112
4-1-3. Stage 1-3 analysis.....	118
4-1-4. Stage 1-4 analysis.....	123
4-1-5. Stage 1-5 analysis.....	128
4-1-6. Stage 1-6 analysis.....	134
4-2. Phase 2 results and discussions	145
4-2-1. Stage 2-1 and Stage 2-2 analysis.....	145
4-2-2. Stage 2-3 analysis.....	150
4-2-3. Stage 2-4 analysis.....	155
4-3. Phase 3 results and discussions	163
4-3-1. Stage 3-1 analysis.....	163
4-3-2. Stage 3-2 analysis.....	174
4-3-3. Stage 3-3 analysis.....	182
4-4. Phase 4 results and discussions	193
4-4-1. Stage 4-1 analysis.....	193
4-4-1-1. Impact of hydrogen peroxide purity on medium scale EF-SBR removal Efficiency	193
4-4-1-2. Impact of hydrogen peroxide purity on large scale EF-SBR removal Efficiency	203
4-4-2. Stage 4-2 analysis.....	222
4-4-2-1. Impact of number of cycles on medium scale EF-SBR efficiency	222
4-4-2-2. Impact of number of cycles on large scale EF-SBR efficiency	230
CHAPTER 5 Investigation of EF-SBR process kinetics	243
5-1. Experimental analysis.....	243
5-2. Kinetics of degradation.....	261
5-3. Fractal analysis	262
CHAPTER 6 Conclusions and future work	268
6-1. Conclusion	268
6-2. Contribution.....	271
6-3. Future works	272
References	274

List of Figures

Figure 2- 1 Groups of amides based on the number of C-N mono bond.....	10
Figure 2- 2 C = O versus C – N distances in (1) formamide (crystal), (2) suberamide, (3) aureomycin, (4) trans-oxamide, (5) benzamide, (6) diketopiprazinc, (7) succinamide (8) N,N,N',N'-tetramethyl- α , α' -dibromosuccinamide (mesoform), (9) chlorocetamide (α -form), (10) acetamide (gas), and (11) formamide (gas) ^[2-7]	11
Figure 2- 3 Amide synthesis methods; a) acylation of amine by alcohols in the presence of silver; b) amidation of aldehyde with amines catalyzed by iron ^{[2-11],[1-13]}	11
Figure 2- 4 Mechanism of acid-catalyzed hydrolysis of amides ^{[2-12],[2-13]}	13
Figure 2- 5 Classification of different types of amine based on number of alkyl or aryl group replaced by hydrogen atoms; a) primary amine; b) secondary amine; c) tertiary amine; d) quaternary amine.....	13
Figure 2- 6 Hofmann degradation reaction; a) Associated three stages reactions to form amine ^[2-15] ; b) Details of three reactions contributed in formation of amine ^[2-14]	14
Figure 2- 7 Advanced oxidation process classification; applied abbreviations: O ₃ ozonation; H ₂ O ₂ hydrogen peroxide; UV ultraviolet radiation; US ultrasound energy; Fe ²⁺ ferrous ion ^[2-32]	18
Figure 2- 8 Proposed reaction pathways for mineralization of aniline at pH 3 following photoelectro-Fenton processes (adopted from Brillas et al. ; 1998).....	38
Figure 3- 1 Overview of the research flowchart of parametric study.....	44
Figure 3- 2 Research flowchart for Phase 1: small scale which consider reactor design, matrix, and interrelated parameters.....	45
Figure 3- 3 Research flowchart for Phase 2: medium scale which consider reactor design and interrelated parameters.....	46
Figure 3- 4 b) Research flowchart for Phase 4: EF-SBR which consider matrix and interrelated parameters in both medium and large scale.....	48
Figure 3- 5 b) Schematic of small scale cylindrical reactor considering associated electro-Fenton reactions	53
Figure 3- 6 Schematic of medium scale electrokinetic cell with 2.2 L volume.....	60
Figure 3- 7 Schematic of large scale electrokinetic cell with 5.8 L volume; the exposure areas of the electrodes are from the side of width* height of the exposure	66
Figure 3- 8 Schematic concept of electro Fenton sequential batch reactor (EF-SBR); the reactor is refilled after the first 72 hours (end of the first cycle) and the second cycle of SBR is ended after 48 hours	69
Figure 3- 9 Schematic of time dependent Fickian diffusion volume element	76
Figure 3- 10 Schematic of proton mobility in structural diffusion phenomenon (Adapted from n Kornyshev et al;2003).....	81
Figure 3- 11 The graphical determination of rate constant of the substrate A and the order of the reaction (adopted from http://www.umich.edu/~elements/fogler&gurmen/html/course/lectures/five/index.htm).....	93

Figure 4- 1 Variations of relevant parameters for experiments of the Stage 1-1; a) voltage versus time; b) pH versus time; c) ORP versus time; d) conductivity versus time; e) temperature versus time	97
Figure 4- 2 Removal efficiency for Stage 1-1 a) ammonia removal; b) TKN removal; c) organic nitrogen removal; d) total nitrogen removal	99
Figure 4- 3 Variations of monitored parameters for the relevant experiments of the 2nd objective of Stage 1-1; a) voltage versus time; b) pH versus time c) ORP versus time; d) conductivity versus time; e) temperature versus time.....	102
Figure 4- 4 Removal efficiency versus time for the 2nd objective of Stage 1-1 considering: a) ammonia; b) TKN; c) organic nitrogen; d) total nitrogen.....	104
Figure 4- 5 Variations of monitored parameters for the relevant experiments of the 3rd objective of Stage 1-1: a) voltage versus time; b) pH versus time; c) ORP versus time; d) conductivity versus time; e) temperature versus time.....	109
Figure 4- 6 Removal efficiency versus time for the 3rd objective of stage 1-1 considering: a) ammonia; b) TKN; c) organic nitrogen; d) total nitrogen.....	111
Figure 4- 7 Variations of monitored parameters for the relevant experiments of Stage 1-2; a) voltage versus time; b) pH versus time c) ORP versus time; d) conductivity versus time; e) temperature versus time	114
Figure 4- 8 Removal efficiencies of the pollutants for stage 1-2 a) ammonia removal efficiency; b) TKN removal efficiency; c) organic nitrogen removal efficiency; d) total nitrogen removal efficiency.....	117
Figure 4- 9 Variations of monitored parameters for the relevant experiments of Stage 1-3; a) voltage versus time; b) pH versus time c) ORP versus time; conductivity versus time e) temperature versus time	119
Figure 4- 10 Removal efficiencies of the pollutants for Stage 1-3; a) ammonia removal efficiency; b) TKN removal efficiency; c) organic nitrogen removal efficiency; d) total nitrogen removal efficiency	121
Figure 4- 11 Variations of monitored parameters for the relevant experiments of Stage 1-4; a) voltage versus time; b) pH versus time c) ORP versus time; d) conductivity versus time e) temperature versus time	127
Figure 4- 12 Removal efficiencies of the pollutants for Stage 1-4; a) ammonia removal efficiency; b) TKN removal efficiency; c) organic nitrogen removal efficiency; d) total nitrogen removal efficiency	128
Figure 4- 13 Variations of monitored parameters for the relevant experiments of Stage 1-5; a) voltage versus time; b) pH versus time c) ORP versus time; d) conductivity versus time e) temperature versus time	129
Figure 4- 14 Removal efficiencies of the pollutant for Stage 1-5; a) ammonia removal efficiency; b) TKN removal efficiency; c) organic nitrogen removal efficiency; d) total nitrogen removal efficiency.....	131
Figure 4- 15 Variation of monitored parameters for the relevant experiments of the Stage 1-6; a) voltage versus time; b) pH versus time c) ORP versus time; d) conductivity versus time e) temperature versus time; f) air flow versus time	136

Figure 4- 16 Removal efficiencies of the pollutants for stage 1-6; a) ammonia removal efficiency; b) TKN removal efficiency; c) organic nitrogen removal efficiency; d) total nitrogen removal efficiency	137
Figure 4- 17 Variations of monitored parameters for the relevant experiments of Stage 2-1 and Stage 2-2; a) voltage versus time; b) pH variation versus time c) ORP versus time; d) conductivity versus time e) temperature versus time.....	147
Figure 4- 18 Removal efficiencies of the pollutants for stage 2-1 and 2-2; a) ammonia removal efficiency; b) TKN removal efficiency; c) organic nitrogen removal efficiency; d) total nitrogen removal efficiency	150
Figure 4- 19 Variations of monitored parameters for the relevant experiments of Stage 2-3; a) voltage versus time; b) pH versus time c) ORP versus time; d) conductivity versus time e) temperature versus time	153
Figure 4- 20 Removal efficiencies of the pollutants for Stage 2-3; a) ammonia removal efficiency; b) TKN removal efficiency; c) organic nitrogen removal efficiency; d) total nitrogen removal efficiency	154
Figure 4- 21 Variations of monitored parameters for the relevant experiments of Stage 2-4; a) voltage versus time; b) pH versus time c) ORP versus time; conductivity versus time e) temperature versus time	159
Figure 4- 22 Removal efficiencies of the pollutants for Stage 2-4; a) ammonia removal efficiency; b) TKN removal efficiency c) organic nitrogen removal efficiency; d) total nitrogen removal efficiency	160
Figure 4- 23 Variations of monitored parameters for the relevant experiments of Stage 3-1; a) voltage versus time; b) pH versus time c) ORP versus time; d) conductivity versus time e) temperature versus time	171
Figure 4- 24 Removal efficiencies of the pollutant for Stage 3-1; a) ammonia removal efficiency; b) TKN removal efficiency; c) organic nitrogen removal efficiency; d) total nitrogen removal efficiency.....	172
Figure 4- 25 Variations of monitored parameters for the relevant experiments of Stage 3-2; a) voltage versus time; b) pH versus time c) ORP versus time; d) conductivity time e) temperature versus time	180
Figure 4- 26 Removal efficiencies of the pollutants for Stage 3-2; a) ammonia removal efficiency; b) TKN removal efficiency; c) organic nitrogen removal efficiency; d) total nitrogen removal efficiency	182
Figure 4- 27 Variations of monitored parameters for the relevant experiments of Stage 3-3; a) voltage versus time; b) pH versus time c) ORP versus time; d) conductivity versus time e) temperature versus time	189
Figure 4- 28 Removal efficiencies of the pollutants for Stage 3-3; a) ammonia removal efficiency; b) TKN removal efficiency; c) organic nitrogen removal efficiency; d) total nitrogen removal efficiency	191
Figure 4- 29 Variations of monitored parameters for the relevant experiments of Stage 4-1 for medium scale EF-SBR; a) voltage versus time; b) pH versus time c) ORP versus time; d) conductivity versus time e) temperature versus time.....	197

Figure 4- 30 Removal efficiencies of the pollutants for Stage 4-1, medium scale EF-SBR; a) ammonia removal efficiency; b) TKN removal efficiency; c) total nitrogen removal efficiency; d) organic nitrogen removal efficiency	203
Figure 4- 31 Variations of monitored parameters for the relevant experiments of the Stage 4-1, large scale EF-SBR; a) voltage versus time; b) pH versus time c) ORP versus time; conductivity versus time e) temperature versus time.....	218
Figure 4- 32 Removal efficiencies of the pollutants for Stage 4-1, large scale EF-SBR; a) ammonia removal efficiency; b) TKN removal efficiency; c) organic nitrogen removal efficiency; d) total nitrogen removal efficiency.....	221
Figure 4- 33 Variations of monitored parameters for the relevant experiments of the Stage 4-2, medium scale EF-SBR; a) voltage versus time; b) pH versus time c) ORP versus time; conductivity versus time e) temperature versus time.....	226
Figure 4- 34 Removal efficiencies of the pollutants versus time for Stage 4-2, medium scale EF-SBR; a) ammonia removal efficiency, b) TKN removal efficiency; c) organic nitrogen removal efficiency; d) total nitrogen removal efficiency.....	229
Figure 4- 35 Variations of monitored parameters for the relevant experiments of the Stage 4-2, large scale EF-SBR; a) voltage versus time; b) pH versus time c) ORP versus time; conductivity versus time e) temperature versus time.....	234
Figure 4- 36 Removal efficiencies of the pollutants with time for Stage 4-2, large scale EF-SBR; a) ammonia removal efficiency; b) TKN removal efficiency; c) total nitrogen removal efficiency; d) organic nitrogen removal efficiency.....	237
Figure 5- 1 Voltage variations versus time for large scale EF-SBR.....	250
Figure 5- 2 pH variations versus time for large scale EF-SBR.....	251
Figure 5- 3 ORP variations versus time for large scale EF-SBR.....	251
Figure 5- 4 Conductivity variations versus time for large scale EF-SBR.....	252
Figure 5- 5 Temperature variations versus time for large scale EF-SBR.....	252
Figure 5- 6 Ammonia concentrations variations versus time for large scale EF-SBR.....	258
Figure 5- 7 TKN concentrations variations versus time for large scale EF-SBR.....	258
Figure 5- 8 Total nitrogen concentrations variations versus time for large scale EF-SBR.....	259
Figure 5- 9 Organic nitrogen concentrations variations versus time for large scale EF-SBR.....	259
Figure 5- 10 Nitrate concentrations variations versus time for large scale EF-SBR.....	260
Figure 5- 11 Sulfate concentration variations versus time for large scale EF-SBR.....	260
Figure 5- 12 regularization dimension curves for ammonia concentrations in compartment1, compartment 2 and, compartment 3 of Exp.48.....	264
Figure 5- 13 regularization dimension curves for TKN concentrations in compartment 1, compartment 2 and, compartment 3.....	264
Figure 5- 14 Regularization dimension curves for total nitrogen concentrations in compartment 1, compartment 2 and, compartment 3.....	265
Figure 5- 15 Regularization dimension curves for organic nitrogen concentrations in compartment 1, compartment 2 and, compartment 3.....	265
Figure 5- 16 Regularization dimension curves for nitrate concentrations in compartment 1, compartment 2 and, compartment 3.....	266

Figure 5- 17 Regularization dimension curves for sulfate concentrations in compartment 1,
compartment 2 and, compartment 3..... 266

List of Tables

Table 2- 1 Effluent limitations of photographic wastewater designated by United States Environmental Protection Agency under the regulation of 40 CFR Part 459	8
Table 2- 2 Characteristics of effluents resulted from three photographic processes of plumbless color, conventional color, and black and white ^[2-2]	9
Table 2- 3 Comparison of applicable treatment processes for emerging contaminants considering advantages and challenges	17
Table 2- 4 Operating cost of advanced oxidation processes ^{a [2-41]}	20
Table 2- 5 Overview of research works conducted on Fenton treatment in recent years	26
Table 2- 6 The impacts of operating parameters on pollutants degradation efficiencies ^[2-125]	33
Table 2- 7 Overview of the conducted researches on pollutant degradation efficiency using electro-Fenton process	34
Table 2- 8 Operation cost of CDEO, ozonation, and Fenton process for 85% COD removal ^[2-129]	39
Table 2- 9 Capital investment of CDEO, ozonation, and Fenton process for 85% COD removal ^[2-129]	39
Table 3- 1 Characteristics of the industrial wastewater	40
Table 3- 2 Experimental design and operating conditions of the Phase 1, Stage 1-1, 1st objective using mesh stainless steel as cathode; impact of anode to cathode surface area ratio and dimensions	53
Table 3- 3 Experimental design and operating conditions of the Phase 1, Stage 1-1, 2nd objective; impact of using different geometries of cathode	54
Table 3- 4 Experimental design and operating conditions of the Phase 1, Stage 1-1, 3rd objective; impact of the geometry of the reactor and position of the anode	54
Table 3- 5 Experimental design and operating conditions of the Phase 1, Stage 1-2; impact of time intervals for hydrogen peroxide supply	55
Table 3- 6 Experimental design and operating conditions of the Phase 1, Stage 1-3; impact of pretreatment of the present sulfate in the influent	56
Table 3- 7 Experimental design and operating conditions of the Phase 1, Stage 1-4; impact of adding Fenton agent	57
Table 3- 8 Experimental design and operating conditions of the Phase 1, Stage 1-5; impact of current density variation	58
Table 3- 9 Experimental design and operating conditions of the Phase 1, Stage 1-6; impact of continuous airflow diffusion	59
Table 3- 10 Experimental design and operating Conditions of the Phase 2, Stage 2-1 and 2-2; impact of anode to cathode surface ratio, the geometry of electrodes and distance between electrodes	61
Table 3- 11 Experimental design and operating conditions of the Phase 2, Stage 2-3; impact of current density variation	63
Table 3- 12 Experimental design and operating conditions of the Phase 2, Stage 2-4; impact of continuous air flow diffusion	63

Table 3- 13 Experimental design and operating conditions of the Phase 3, Stage 3-1; Impact of distance among electrodes	65
Table 3- 14 Experimental design and operating conditions of Phase 3, Stage 3-2; impact of hydrogen peroxide purity	66
Table 3- 15 Experimental design and operating conditions of Phase 3, Stage 3-3; Impact of hydrogen peroxide molar ratio	67
Table 3- 16 Experimental design and operating conditions of the Phase 4, Stage 4-1; impact of hydrogen peroxide purity on medium-scale EF-SBR removal efficiency	70
Table 3- 17 Experimental design and operating conditions of the Phase 4, Stage 4-2; impact of hydrogen peroxide on large-scale EF-SBR removal efficiency	70
Table 3- 18 Experimental design and operating conditions of the Phase 4, Stage 4-2; impact of SBR cycles on medium-scale EF-SBR removal efficiency	71
Table 3- 19 Experimental design and operating conditions of the Phase 4, Stage 4-2; impact of SBR cycles on large-scale EF-SBR removal efficiency	71
Table 3- 20 Analysis methods of measuring pollutant concentration.....	72
Table 3- 21 Limiting molar conductivity of the different ions in dilute solutions (ion-ion interactions can be neglected).....	82
Table 3- 22 Initial boundary value problem describing chronopotentiometry for an electrolyte membrane electrolyte system (Bieniasz;2003)	91
Table 3- 23 The finite difference equations applied for determining the concentration derivatives values versus time in initial, interior, and last point locations.....	94
Table 4- 1 Removal efficiencies of ammonia, TKN, total nitrogen, and organic nitrogen for all experiments of Phase 1	142
Table 4- 2 Removal efficiencies of ammonia, TKN, total nitrogen, and organic nitrogen for all experiments of Phase 2	162
Table 4- 3 Removal efficiencies of ammonia, TKN, total nitrogen, and organic nitrogen for all experiments of Phase 3	192
Table 4- 4 Characteristics of the initial concentrations of the ammonia, TKN, total nitrogen and, organic nitrogen in the raw wastewater and beginning of the second cycle; medium scale results	202
Table 4- 5 Characteristics of the initial concentrations of the ammonia, TKN, total nitrogen, and organic nitrogen in the raw wastewater and the beginning of the second cycle; large scale results	221
Table 4- 6 Characteristics of the initial concentrations of the ammonia, TKN, total nitrogen and, organic nitrogen in the raw wastewater and the beginning of each cycle medium scale results; cycle 1, cycle 2, cycle 3 and cycle 4 initial concentration	228
Table 4- 7 Characteristics of the initial concentrations of the ammonia, TKN, total nitrogen and, organic nitrogen in the raw wastewater and the beginning of each cycle of the large scale; cycle 1, cycle 2, and cycle 3 initial concentration.....	236
Table 4- 8 Removal efficiencies of ammonia, TKN, total nitrogen, and organic nitrogen for all experiments of Phase 4	238

Table 4- 9 Amount of sludge production and sludge mass per liter for small scale, large scale, and medium and large EF-SBR	242
Table 5- 1 Characteristics of the studied wastewater for investigation of the kinetics.....	244
Table 5- 2 The initial concentrations of ammonia, TKN, total nitrogen, organic nitrogen, nitrate, nitrite, and sulfate at the beginning of cycle 1 and cycle 2.....	253

Notations

$\frac{\partial c_k(x)}{\partial x}$	variations of concentration in length scale [mol cm ⁻⁴]
$\langle \Delta r^2 \rangle$	mean-square displacement of the particles in n-dimensional space [cm]
C^s	concentration of a substance at the surface of the electrode [mg/L]
C^b	concentration of a substance in the bulk electrolyte [mg/L]
D_k	diffusion coefficient [cm ² s ⁻¹] or [m ² s ⁻¹]
$f_k(x)$	fickian diffusion [mol cm ⁻² s ⁻¹]
k_A	rate constant with respect to reactant A
t_+	transport number [dimensionless]
z_0	axial beam waist [dimensionless]
\bar{v}	average velocity [cm/s]
ω_0	radial beam waist [dimensionless]
Λ_m°	limiting molar conductivity [S cm ⁻¹ mol ⁻¹] or [cm ² Ω ⁻¹ mol ⁻¹]
ϑ_{Re}	voltage noise generated by the electrolyte resistance [V]
Δ	membrane thickness [cm]
a	width
c_k	molar concentration [mol cm ⁻³]
D_R	regularization dimension
$E(t)$	variation of electrochemical potential across electrochemical interface [V]
F	Faraday constant 96485 C/mol
g_a	kernels
$I(t)$	variation of amperage respect to time [A]
i_{step}	current pulse amplitude [A]

j	current density, A/m ²
K_h	hydrolysis constant [dimensionless]
l_a	finite length
m	number of photon extinction [dimensionless]
p	pressure [atm]
R	8.314 J / mol. K
R_e	resistance of the electrolyte between a working and a reference electrode [Ω]
T	temperature [K]
t	time [s]
t_{step}	current pulse duration [s]
u_j	mobility of species j [m ² V ⁻¹ s ⁻¹]
$V(t)$	variation of voltage with respect to time [V]
z_j	valence (charge) of the ion j [dimensionless]
α	anomalous exponent [dimensionless]
α	reaction order
Γ	transport factor or constant prefactor [cm ² /s]
ε	dielectric permittivity [dimensionless]
σ	parameter of the smoothed unit step function $H^*(x, \sigma)$
τ	time [s]
$\varphi(x)$	potential at distance x [V]
χ^0	fixed charge parameter [C]
λ	molar ionic conductivity [S cm ⁻¹ mol ⁻¹] or [cm ² Ω ⁻¹ mol ⁻¹]
ν	number of associated electrons (valent) [dimensionless]
σ	conductivity [S cm ⁻¹]

Symbols and abbreviations

2-CP	2-chlorophenol
2-NP	2-nitrophenol
AOPs	advanced oxidation processes
CD	current density
CDEO	conductive-diamond electrochemical oxidation
CF	carbon felt
COD	chemical oxygen demand
DQ	dimensional quotient
EAOPs	electrochemical advanced oxidation processes
EDTA	ethylenediaminetetraacetic acid
EF	electro-Fenton
EF-SBR	electro Fenton sequential batch reactor
EPA	environmental protection agency
FCS	fluorescence correlation spectroscopy
MSD	mean-square displacement
NHE	normal hydrogen electrode
NMP	N-Methyl-2-pyrrolidone
O ₃ /H ₂ O ₂ /UV	ozone, hydrogen peroxide and, ultraviolet radiation
O ₃ /UV	ozone and ultraviolet radiation
ON	organic nitrogen
ORP	oxidation reduction potential
PAP	p-Aminophenol
PEF	photo electro-Fenton
PTFE	polytetrafluoroethylene
RDS	rate determining step
RFA	regularization fractal analysis

RVC	reticulated vitreous carbon
SPEF	solar photo electro-Fenton
TD	time dependant
TKN	Total Kjeldahl Nitrogen
TOC	total organic carbon
UV	ultraviolet
WWTP	wastewater treatment plant

Chapter 1 Introduction and research objectives

1-1. Problem statement

Many municipalities (including the City of Montreal) have been paid more attention to presence of organic nitrogen (ON) in their sewage systems. Its presence may affect the quality of effluent at their wastewater treatment plants [1-1],[1-2]. Therefore, there is tendency to implement a better treatment of industrial influents at the source. Unfortunately, traditional approaches and technical solutions in the field of water treatment are often futile for the treatment and discharge of wastewater containing hardly degradable ON, which is measured by Total Kjeldahl Nitrogen (TKN) [1-3],[1-4]. The raw wastewater in such cases can contain thousands mg of TKN per liter.

On the other hand, if nitrogen is not treated adequately at WWTP, its presence in effluent causes eutrophication of waters leading to toxic algae growth, decreasing the dissolved oxygen concentrations, provoking aquatic biota depletion and/or changing in population of affected organisms. When ammonia undergoes oxidation in water, it produces by-products which might generate a serious restriction of oxygen transport in infant bloodstream, Blue Baby Syndrome. In case of organic nitrogen discharge (e.g. amines, amides), a pollution of water resources is evident and dangerous. Unfortunately, the removal of organic nitrogen is minimal in wastewater treatment facilities, while a conventional treatment of ammonia creates other problems related to generation of H₂S emissions and subsequently the acid rain.

One of the most effective and widespread methods of wastewater treatment is biological processes. For this specific industrial wastewater, however, this process cannot be used due to the wastewater's characteristics, specifically a very high conductivity of hundreds of milliSiemens per cm.

There are a number of Advanced Oxidation Processes (AOPs) such as: Ozonation, Photolysis, Fenton Oxidation, Photo-Fenton Oxidation and Electrochemical Advanced Oxidation Processes (EAOPs); however, they have never demonstrated successful treatment of such harsh wastewater. The first disadvantage that limits the use of ozonation in this study is the fact that the compounds like amides are resistant to ozone ^[1-5]. An additional disadvantage is the side effects of the by-products from ozone treatment, which may be more harmful than the parent compounds ^[1-6]. Moreover, the mass transfer of the ozone molecule from the gas to liquid phase is a limiting step, which reduces removal efficiency and increases the cost of treatment ^[1-7].

There are two types of photolysis processes: direct and indirect. In a direct process, organic compounds absorb UV light and undergo self-decomposition ^[1-8]. Since photolysis can be applied to low COD loads and photosensitive compounds ^[1-9], it cannot be used to the wastewater of concern since its chemical oxygen demand (COD) is close to 50 grams per liter. Fenton Oxidation requires the presence of Fe^{2+} and H_2O_2 , where ferrous ions act as a catalyst while hydrogen peroxide produces hydroxyl radicals to degrade organic compounds. Moreover, H_2O_2 can act as an OH scavenger as well as an initiator ^[1-10]. The disadvantages include an expensive treatment of sludge and a limited pH range (pH 2-3), as well as the fact that not all organics are susceptible to this type of oxidation ^[1-11]. However, the costs might be reduced if the addition of chemicals (e.g. iron) can be avoided.

Photo-Fenton Oxidation, a combination of $\text{Fe}^{2+}/\text{H}_2\text{O}_2/\text{UV}$, might decrease the costs, when solar radiation instead of UV is used ^[1-12]. However, such process needs a reactor with a chamber that limits the design parameter selection (e.g. detention time and dimensions of the reactor); furthermore, it requires a continuous source of light, which would not be always available.

Likewise, the installation of UV source causes a significant increase of costs. Thus, Photo-Fenton Oxidation has not been applied in this study.

Electro-Fenton Oxidation is one of the electrochemical advanced oxidation processes that has a possibility of a high mineralization of persistent organics. EAOPs consist of two processes: anodic oxidation and electro-Fenton oxidation. In anodic oxidation, mineralization occurs due to a reaction with the hydroxyl radical formed on the electrode surface, through the reduction reaction of water. While in the electro-Fenton process, the organic compounds are degraded by interaction of both Fenton reagent and anodic oxidation simultaneously ^[1-13]. However, there are a few applications of EAOPs in real wastewater treatment and most of the applications are implemented on synthetic wastewater.

Zhukovskaya ^[1-13] conducted a research on introducing electro-Fenton treatment on the same type of the wastewater, when a significant removal efficiency of target pollutants (ammonia, TKN, total nitrogen, and organic nitrogen) are achieved in small scale (300 mL). The best removal efficiency of TKN, ammonia, and organic nitrogen are reached with the magnitude of 92.4 %, 95.2 % and 81.4 %, respectively. Also, it was proved that enhanced electro-Fenton process with pretreatment from the ammonia can remove TKN and organic nitrogen by 95.8% and 97.2%, respectively in a shorter residence time of 24 hours ^[1-13]. Applying a pretreatment such as ammonia stripping is not feasible in many municipalities including Montreal, due to building height restrictions and air quality limitations. Also, the achieved removal efficiencies of pollutants without pretreatment might not meet the municipal requirements and necessitates to propose a new design to enhance the process efficiency and define a proper experimental upscaling.

1-2. Research objectives

The main objective of this research is finding a solution to treat industrial wastewater highly polluted with Total Kjeldahl Nitrogen. The study focuses on a industrial wastewater containing TKN, ammonia, COD, and iron, in the range of 14000 mg/L, 11000 mg/L, 50000 mg/L, and 2760 mg/L, respectively. Therefore, the objective targets the removal of TKN by 96%.

Further objective of the research is to achieve a scale up process, where determination of operating conditions in designed reactor attain the required effluent quality.

Chapter 2 Literature review

Chapter 2-1 makes an overview of photo-processing and wastewater decompositions. The hydrolysis of Chemical properties of amides and amines are described in Section 2-2. Section 2-3 includes applicable processes to highly polluted industrial wastewater. In the last section of Section 2-4, a cost comparison between the Fenton process, ozonation and one of the EAOPs is provided.

2-1. Overview of photo-processing and wastewater compositions

2-1-1. Process description

Photo-processing can be defined as the development or printing of paper prints, negatives, enlargements, movie film and so forth. The defined process includes 5 main steps which are considered as exposure, development, fixing, bleaching, and stabilizing.

A photographic film can be very simple in structure—a coating of a gelatin—silver halide emulsion on a transparent base (e.g. positive film, used for printing the black-and-white motion pictures). The exposure step is determined as covering positive film which is used for the black and white printing with a coating of a gelatin-silver halide emulsion. Those negative films which are used for pictorial photography are generally more complex in their structure. In many films, two or more coatings of the emulsion are used to derive the sensitometric characteristics that yield a good pictorial tone rendition. On top of this, there is generally an over-coating or surface layer which controls many of the film physical characteristics ^[2-1]. After that, the coated film structure is exposed to the light where formation of “latent image” forms. The obtained image is invisible due to the minimal quality of the silver and draw the necessity of development step to attention. During the development step, silver halide grains are chemically transformed to the metallic silver.

Due to the fact that small portion of emulsion still contains silver halide which introduces the essence of the third stage, fixing. Fixers commonly consist of thiosulfates $S_2O_3^{2-}$ compounds (regularly ammonium thiosulfate) which dissolve remained silver halide from the emulsion and forming stable soluble complex $Ag(S_2O_3)_2^{3-}$ [2-2]. Fixers are also capable to dissolve sensitized salts on the films and provide the appropriate condition for the development of photographic images [2-3]. The next stage, bleaching, is the recovery of silver halide from metallic silver to make the photographic process sustainable. The bleaching is selected to oxidize the silver metal, converting it back to silver halide without destroying gelatin or dye. Two of the most applicable bleaching agents in photographic industry are considered a iron EDTA(amide) and iron PDTA (amine).

Residual chemicals and undesired by-products are essential to be removed to prevent the unwanted reaction between them which finally lead to decline the final product life time. Afterwards, the final step which is stabilizing, comes into consideration. The purpose of stabilizing is protecting the image from aging and light fading by treating the emulsion by stabilizer [2-2].

2-1-2. Compositions of photographic wastewater

The photographic wastewater mainly comprised fixer and bleach solutions which contain high concentration of dissolved silver and other chemicals such as sulphates, nitrates, and silver in all forms. Due to being classified as toxic heavy metal contained wastewater, the environmental protection regulations of hazardous wastes would be applied to forbid discharging to public sewers [2-3].

Bensalah et al. [2-4] consider three sources of wastewater from the film industry which are film and paper wash water, solution make-up water, area, and equipment wash water. The described

wastewater contains heavy metals (silver), toxic organics such as hydroquinone, metol, phenidone, and high concentration of nitrogen-containing organics.

Lunar et al.^[2-5] also describes the possible introduced compounds to wastewater during the development step. Based on the conducted research by Lunar et al. (2000), the main compounds available in photographic wastewater are the developing agent (p-aminophenols and/or hydroquinone, and p-phenylenediamines for the black and white and colour development, respectively), an alkaline buffer (applicable for reduction reactions of the exposed film by silver halide), anti-fog agents (commonly halide ions), and an antioxidant (i.e. sulfite). Multitudinous substances are also expected to be present which are originated from chemical reactions of the developing agent with silver halide, oxygen, and other present compounds in the solution.

EPA regulations for photographic wastewater^[2-6] are effective for dischargers processes more than 150 m² of materials per day. EPA limits the target discharging of the effluents specifically for silver, cyanide, and pH. The allowable discharge characteristics are also provided in Table 2-1.

Table 2- 1 Effluent limitations of photographic wastewater designated by United States Environmental Protection Agency under the regulation of 40 CFR Part 459

Effluent characteristic	Effluent limitations	
	Maximum for any 1 day	Average of daily values for 30 consecutive days shall not exceed
	Metric units (kilograms per 1,000 m ² of product)	
Ag	0.14	0.07
CN	0.18	0.09
pH	6.0 to 9.0	6.0 to 9.0

Wang and Tselung^[2-2] give the characteristics of effluents for three distinctive photographic processes which are considered as plumbless color, conventional color and black and white respectively. The allocated properties are described in Table 2-2 for the all three-mentioned photographic processes.

Table 2- 2 Characteristics of effluents resulted from three photographic processes of plumbless color, conventional color, and black and white [2-2]

Process	BOD5 [mg/L]	COD, [mg/L]	TDS, [mg/L]	TSS, [mg/L]	NH ₃ - N, [mg/L]	TKN, [mg/L]	SO ₄ ²⁻ , [mg/L]	Iron, [mg/L]
Plumbless color	5000- 14000	30000- 36000	60000- 90000	10-50	6000- 10000	8000- 13000	3000- 4000	1400- 2000
Conventional color	200- 3000	400-5000	300-3000	5-50	20-300	30-350	50-250	10-100
Black and white	300- 5000	200- 20000	1500- 30000	5-50	350-4300	400- 4500	100- 300	< 0.5

It is crucial to clarify that high nitrogen contained wastewater is carried out by high concentration of amines and amides originated from developers. Therefore, studying the chemical and electrochemical properties of amides and amines is taken into consideration.

2-2. Chemical properties of amides and amines

2-2-1. Amides molecular structure, synthesis, and hydrolysis

Amides are derivative of carboxylic acids and it is also possible to be prepared from amines, anhydrides, esters, and nitriles. Classifying amides based on the degree of carbon formed mono bond with nitrogen, provides 3 groups: primary, secondary, and tertiary which are illustrated in Figure 2-1. “X” are commonly representative of hydrogen atoms. The other classification is presented based on the nature of substituent and overall structure, and categorized amides to three groups of aromatics (i.e. anilides or benzamides) or cyclic (lactams).

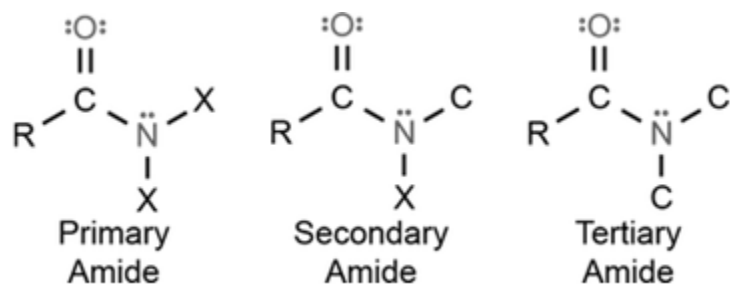


Figure 2- 1 Groups of amides based on the number of C-N mono bond

Zabicky ^[2-7] research determines that the analyses of a variety of amides in crystalline form and gas phase gives the C = O distance in the range between 1.19 Å to 1.21 Å and concomitant opening of the C – N distance to 1.36 -1.37 Å. The angle between <RCN is also 113 – 117°, and the other two are about 120-125° each. A plot of the C = O vs. C – N distances which is resulted based on analysis of several amides in both the gas and crystalline phases suggests a reciprocal dependence which is illustrated in Figure 2-2. The shortest C = O distances having the longest C – N.

Due to the existence of rotational barrier around the C – N bond ^[2-8], amides are considered as stable compounds. Therefore, degradation of amides is expected to require high activation energy barrier to overcome C – N and C = O bonds.

The possibility of amide synthesis meanwhile photographic processes, and presence of resulted amides in wastewater are emerged by two major methods which are considered a: 1) the direct acylation of amines by equimolar amount of alcohols in the presence of silver ^[2-9] and 2) the oxidative amidation of aldehyde with amines which is generally catalyzed by metals such as Cu, Rh, Ru, Ni, Ag, and Fe ^[2-10]. Figure 2-3 presents both methods of amide synthesis ^[2-11].

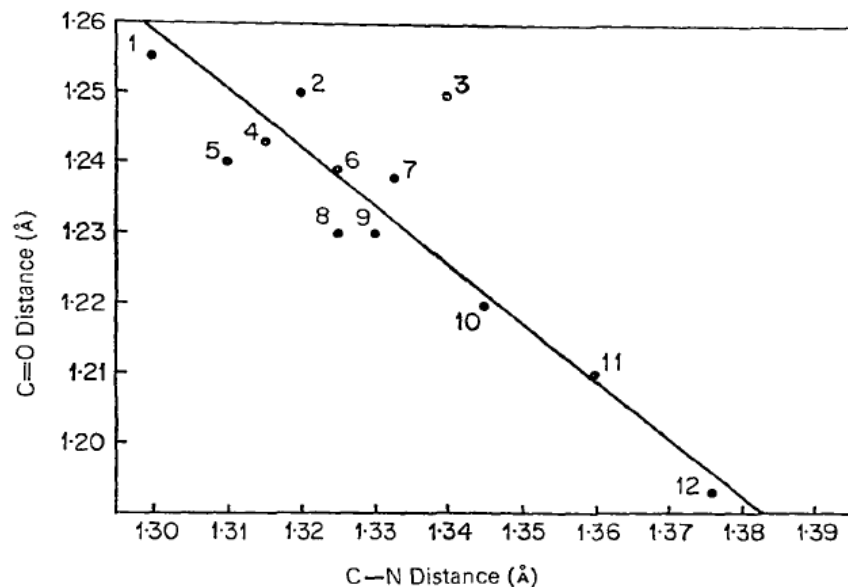
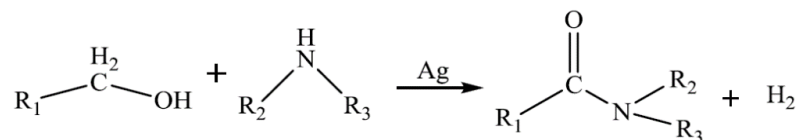


Figure 2- 2 C = O versus C – N distances in (1) formamide (crystal), (2) suberamide, (3) aureomycin, (4) trans-oxamide, (5) benzamide, (6) diketopiprazinc, (7) succinamide (8) N,N,N',N'-tetramethyl- α , α' -dibromosuccinamide (mesoform), (9) chlorocetamide (α -form), (10) acetamide (gas), and (11) formamide (gas) ^[2-7]

a)



b)

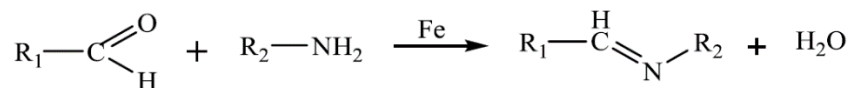


Figure 2- 3 Amide synthesis methods; a) acylation of amine by alcohols in the presence of silver; b) amidation of aldehyde with amines catalyzed by iron ^{[2-11],[1-13]}

Basic hydrolysis is difficult in comparison with the acid-catalyzed reaction due to the nature of amide ion which is poor leaving group. Stabilization of the carbonyl group by the e-donation properties of N atom is also the other reason for experiencing difficulties in amide hydrolysis.

Hunt and Spinney ^[2-12], and Carey and Giuliano ^[2-13] researches provide the mechanism of acid-catalyzed hydrolysis of amides in 6 steps which is presented in Figure 2-4.

The first step is the acid/base reaction. The purpose is to activate amide by protonation of the amidecarbonyl to make amide more electrophilic. The weakness in electrophilicity and nucleophilicity of the neutral amide necessitate the first step reactions. The second step is devoted to reaction of water oxygen function with electrophilic carbon in C = O band which creates tetrahedral intermediate. The third step is an acid/base reaction to deprotonate the oxygen which comes from the water molecule to neutralize the charge.

The fourth step is again an acid/base reaction which is required for -NH₂ removal. However, the preliminary step is providing a condition for facilitation of leaving group by protonation. Step 5 is using the electrons of an adjacent oxygen to help untying the leaving group, a neutral ammonia molecule. The final step is acid/base reaction in which the deprotonation of the oxonium ion reveals the carbonyl in the carboxylic acid product and regenerate the acid catalyst.

2-2-2. Amine molecular structure and synthesis

Based on Lawrence ^[2-14] definition, “the amines can be defined as group of chemical compounds that have the common feature of possessing nitrogen atoms that are sp³ hybridized with three single bonds to other elements.” Based on IUPAC system, Amines are named from the related parent alcohol (i.e. C₂H₅ is called ethylamine). Carbon chain substitutes are identified by number and N- is used for substituents on the nitrogen atom. The simplest amine is also ammonia, NH₃. As well as amides, a classification is proposed based on the replacement of hydrogen with alkyl or aryl (AR). The primary, secondary, and tertiary amine follow the same protocol for naming. However,

the quaternary amine is formed by adding a molecule of amine (e.g. amine hydrobromide to tertiary amine with a bromide counter ion. The different types of amines are shown in Figure 2-5.

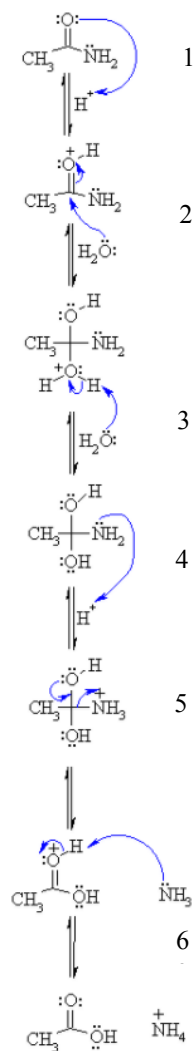


Figure 2- 4 Mechanism of acid-catalyzed hydrolysis of amides ^{[2-12],[2-13]}

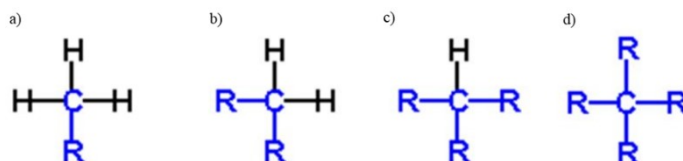


Figure 2- 5 Classification of different types of amine based on number of alkyl or aryl group replaced by hydrogen atoms; a) primary amine; b) secondary amine; c) tertiary amine; d) quaternary amine

Two mechanisms which are reviewed in this study are 1) the Hofmann reaction degradation and 2) Electrochemical reduction. The Hofmann mechanism is simply described in Figure 2-6a and illustrated in detail in Figure 2-6b. In other words, the Hofmann reaction is the organic reaction of primary amide to primary amine with one less carbon.

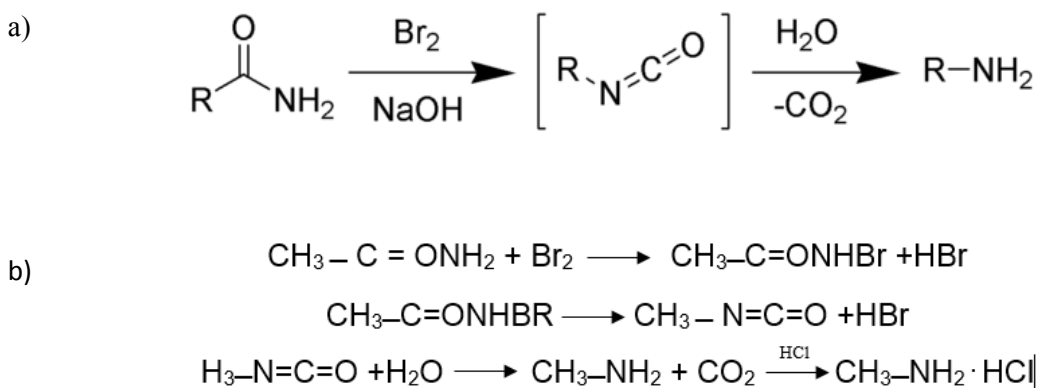
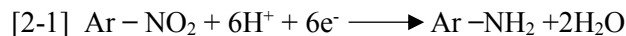


Figure 2- 6 Hofmann degradation reaction; a) Associated three stages reactions to form amine ^[2-15]; b) Details of three reactions contributed in formation of amine ^[2-14]

The electrochemical reduction of nitro-aryls is conducted on electrochemical cell. A typical cell is divided by a semipermeable membrane with 30% sulphuric acid on the anode side and 15% to 20% hydrochloric acid on the cathode side. The applicable types of cathodes are considered as lead, tin, nickel or copper. Due to demand of reducing agent to result in amine production and inorganic compound is introduced to the system, and after reaction with the nitro-aryl, it can be regenerated at the cathode. The reaction is as follows:



A common reaction that is capable of performing electrochemically is the reduction of para-nitrobenzoic acid to para-aminophenol. The expected challenges are stability of cell membrane,

the high power consumption and difficulties in isolating the desired reaction products from the starting material and electrolyte [2-15].

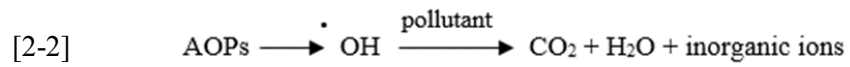
2-3. Applicable mechanisms in highly polluted industrial wastewater

Various treatment processes are implemented for removing synthetic organics which are considered as: 1) conventional; biological activated carbon, 2) microalgae reactor, 3) activated sludge, 4) non-conventional; constructed wetland, 5) MBR, 6) chemical process coagulation, 7) ozonation, 8) AOPs, 9) Fenton and photo-Fenton, 10) photocatalysis (TiO_2), 11) physical process; micro- or ultra filtration, 12) Nanofiltration, and finally 13) reverse osmosis. According to Ahmed et al. [2-16] review on progress in the biological and chemical treatment of emerging contaminants (ECs) including synthetic organics, the advantageous and challenges of each individual treatment process is discussed. Table 2-3 provides all challenges and advantageous of applicable treatment processes on removing ECs.

Due to stability of amides and high concentrations of ammonia, TKN, total nitrogen, and organic nitrogen in plumbless color photographic process (see Tab.2-2) and high conductivity of medium (62 mS/cm), most mechanisms which are effective in treatment of diluted wastewater (i.e. biological treatment) would be impractical in the described scenario. Poyatos et al. [2-32] prove that AOPs are applicable and recommended when there is a high chemical stability and/or low biodegradability in wastewater components.

To generally describe AOPs, photochemical degradation processes (UV/O_3 , $\text{UV}/\text{H}_2\text{O}_2$), photocatalysis (TiO_2/UV , Photo-Fenton reactives), and chemical oxidation processes (O_3 , $\text{O}_3/\text{H}_2\text{O}_2$, $\text{H}_2\text{O}_2/\text{Fe}^{2+}$) are all considered as subcategories. The predominant mechanism produces

hydroxyl radicals (OH^\cdot) which are very reactive and attack the most organic molecules although they are not highly selective [2-33, [2-34].



The methods which are specifically investigated and reviewed in this study are: ozonation in an alkaline medium, ozone and ultraviolet, ozone and ultrasound, ozone, hydrogen peroxide, ultraviolet, Fenton and assisted Fenton processes, electrochemical oxidation, and finally anodic oxidation.

Table 2- 3 Comparison of applicable treatment processes for emerging contaminants considering advantages and challenges

Treatment Process	Advantages	Challenges	Reference
Conventional Biological activated carbon	Provide a wide range of ECs removal from wastewater	Relatively high cost in operation and maintenance Regeneration and disposal issues of high sludge	[2-17], [2-18], [2-19], [2-20]
Activated sludge	More environmentally friendly than chlorination	Large amount of sludge containing ECs Unsuitable where COD levels are greater than 4000 mg/L	[2-17], [2-21], [2-22], [2-23]
Non-conventional Constructed wetlands	Low energy consumption and low operational and maintenance costs High performance on removal of estrogens, PCPs, pesticides and pathogens	Clogging, solids entrapment and sediments formation Biofilm growth, chemical precipitation and seasonal dependent Needs large area of lands and long retention time	[2-24]
Microalgae reactor	Resource recovery of algal biomass, used as fertilizer High quality effluent and no acute toxicity risk associated with ECs	Removal efficiencies affected by cold season and low temperature EDCs cannot be degraded properly	[2-25]
MBR	Effective for the removal of biorecalcitrant and ECs Small foot print	High energy consumption and fouling, control of heat and mass transfer High aeration cost and roughness of membrane Pharmaceutical pollutants have low efficiencies Ineffective micropollutants removal	[2-21], [2-17], [2-26]
Chemical process Coagulation	Reduced turbidity arising from suspended inorganic and organic particles Increased sedimentation rate through suspended solid particles formation	Ineffective micropollutants removal Large amount of sludge Introduction of coagulant slats in the aqueous phase	[2-17], [2-24]
Ozonation	Strong affinity to ECs in the presence of H ₂ O ₂	High energy consumption, formation of oxidative by-products Interference of radical scavengers	[2-17], [2-19], [2-27]
AOPs	Selective oxidant favoring disinfection and sterilization properties Major ancillary effects on removal of ECs such as EDCs, pharmaceuticals, PCPs, and pesticides Short degradation rate	Energy consumption issues, operational and maintenance costs Formation of toxic disinfection by-products Interference of radical scavengers	[2-17], [2-19]
Fenton and photo-Fenton	Degradation and mineralization of ECs	Decrease of OH· forming chloro and Ferric sulfate complexes or due to scavenge of OH· forming Cl ₂ · and SO ₄ · ⁻ in the presence of chloride and sulphate ions	[2-17], [2-28], [2-29]
Photocatalysis (TiO₂)	Sunlight can be used by avoiding UV light Degrading persistent organic compounds High reaction rates upon using catalyst	Difficult to treat large volume of wastewater Cost associated with artificial UV lamps and electricity	[2-30]
Reverse osmosis	Can remove dye and pesticides Useful for treating saline water and WWTP influents Can remove PCPs, EDCs, and pharmaceuticals	High energy demand, membrane fouling, and disposal issue Corrosive nature of finished water and lower pharmaceutical removal	[2-17], [2-21], [2-31]
Physical process Micro- or ultra-filtration	Can remove pathogens	Not fully effective in removing ECs as not fully effective in removing some ECs as pore sizes vary from 100 to 1000 times larger than micropollutants	[2-21]
Nanofiltration	Applicable for heavy metal removal Useful for treating saline water and WWTP influents	High cost of operation High energy demand, membrane fouling, and disposal issue	[2-17], [2-31]

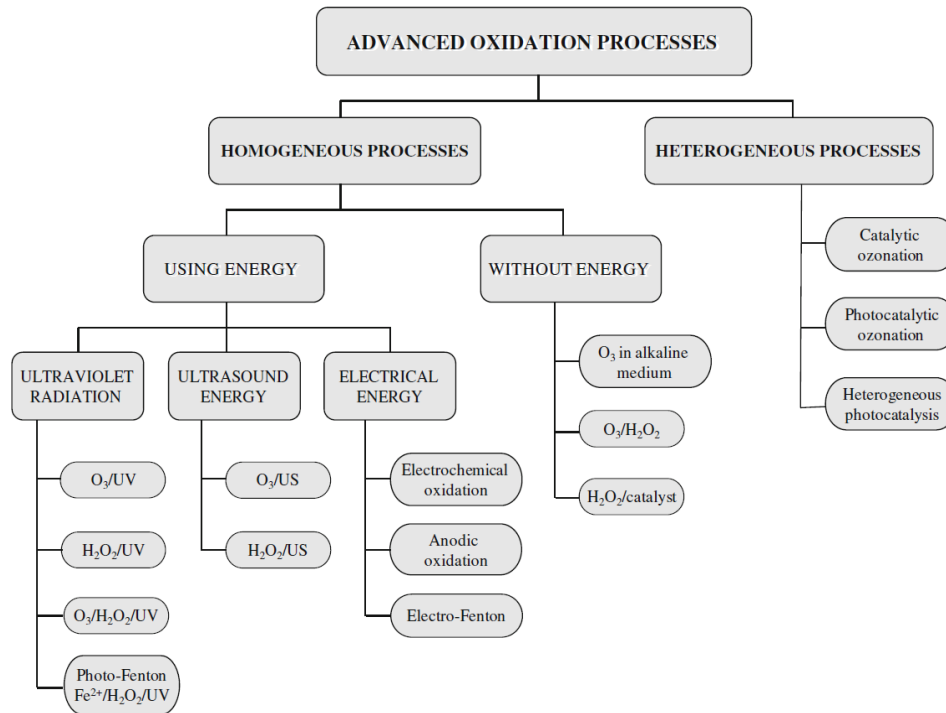
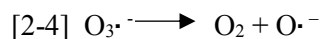
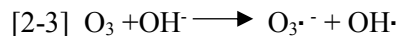


Figure 2- 7 Advanced oxidation process classification; applied abbreviations: O₃ ozonation; H₂O₂ hydrogen peroxide; UV ultraviolet radiation; US ultrasound energy; Fe²⁺ ferrous ion [2-32]

2-3-1. Ozonation in an alkaline medium

Ozone is a very selective oxidant with standard potentials of 2.07 V (vs. NHE) in acidic solution and 1.25 V (vs. NHE) in basic solution [2-35]. Due to instability of ozonation in an aqueous medium, spontaneous recompositing is expected to take place in a way which results in production of hydroxyl radicals. The degradation is proceeded by functionalization of both ozonation and generated hydroxyl radicals in an alkaline medium. The production of hydroxyl radicals is strongly dependent to pH of the medium and it will remarkably enhance once pH increases. The involved reactions are as follows [2-36].

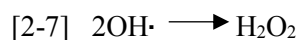
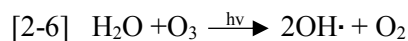




Although ozonation in alkaline medium is classified as without energy methods among AOPs, the conducted research on ozonation efficiency demonstrates that a very limited mineralization of organic compounds is obtained. The reason is relatively low solubility and stability of ozone in water and also the slow reaction with some organic compounds [2-38].

2-3-2. Ozone and ultraviolet radiation (O₃/UV)

The mechanism of O₃/UV is producing hydroxyl radicals by radiating ultraviolet through the aqueous medium which is saturated with ozone. The appropriate wavelength is 253.7 nm. At the mentioned wavelength, the extinction coefficient for gas-phase ozone is 3300 M⁻¹cm⁻¹ [2-37]. For each mole of hydroxyl formed, 0.5 mol (photons) of UV radiation, 0.5 mol of H₂O₂ (formed in situ), and 1.5 mol of ozone are consumed [2-39]. The photolysis reactions of ozone and production of hydroxyl radicals are described as followed:



One of the compound which is used as an industrial solvent is N- methyl -2- pyrrolidone (NMP). Due to presence of C=O bond, it is probably reactive toward ozone. Murugandham et al. [2-40] utilized ozone and ultraviolet radiation with the following experimental conditions: UV intensity of 5.5 mW/cm², a temperature of 25 °C, and pH equals to 10. The results indicated that the rate of TOC reduction was 56.2 %. In addition, the applied ozone concentration is 44.5 mg/L and applied ozone dosage is 184.5 mg/ (L min). Since the NMP initial concentrations were very low (500 mg/L), the total removal is obtained after 5 hours of exposure. The challenges which are

interrelated for all ozone based treatment processes are formation of some oxidative by-products, energy consumption, and interference of radical scavenger [2-16], [2-17], [2-19].

2-3-3. Ozone, hydrogen peroxide, and ultraviolet radiation (O₃/H₂O₂/UV)

The function of hydrogen peroxide is accelerating the decomposition of ozone and increasing the generation of hydroxyl radicals (OH·). The main concerns of using O₃/H₂O₂/UV is the high cost of utilizing two types of reagents. Based on Yonor et al. [2-41] cost estimation, the expected costs per one cubic meter for ozone, ozone/UV, H₂O₂ /UV, and O₃/H₂O₂/UV are presented in Table 2-4. The resulting action in the combination of two binary system (O₃/UV and O₃/H₂O₂) is:

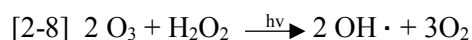


Table 2- 4 Operating cost of advanced oxidation processes ^a [2-41]

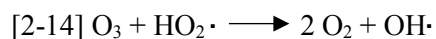
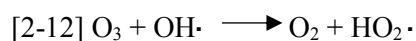
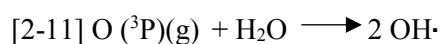
Process	Treatment cost (\$/m ³)
Ozone	5.35
Ozone/UV ^b	8.68
Ozone/H ₂ O ₂ /UV ^b	4.56
H ₂ O ₂ /UV ^b	11.25

^a Cost of labor not included; ^b Optimum lamp life: 2000. Operating costs calculated based on 90% COD removal

Peternel et al. [2-42] found out that the highest mineralization of organic pollutant is achieved by UV/H₂O₂/O₃. A comparison among ultraviolet, ultraviolet and hydrogen peroxide, ultraviolet and ozone, and finally ultraviolet, hydrogen peroxide and ozone is also conducted on organic dyes C.I. reactive Red 45 by Peternel et al. [2-42], and the following order with respect to removal efficiency is obtained: UV < UV/H₂O₂ < UV/O₃ < UV/H₂O₂/O₃.

2-3-4. Ozonation and ultrasound

Based on He et al. [2-43] study, once ozone and ultrasound are present in the treatment process, eight distinctive reactions took place in the medium which are described below (“))” is representative of ultrasound):



p-Aminophenol (PAP) is an environmental pollutant compound which is widely used as an intermediate in the production of certain medicines such as paracetamol. Due to its applicability as a photograph developer and relevancy to scope of this research, studying the efficiency of the degradation mechanism come into consideration. He et al. [2-43] studied the mechanism once the initial concentration of PAP is 10 mmol/L, and the operating conditions are 5.3 g/h ozone dosage, pH is equal to 11, and ultrasonic energy density of 0.3 W/mL at temperature of 25° C.. The achieved efficiency is 99% throughout 30 min exposure time. TOC removal efficacy also resulted in 77% in the same time interval. The parameters which strongly impact on the efficiency of the mechanism are pH and ozone dosage. Once the pH changes toward a strong basic condition, the efficiency will significantly boost. The increase in ozone dosage shows the same influence on

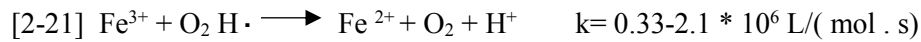
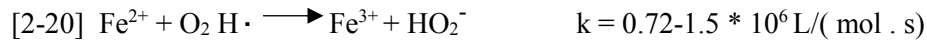
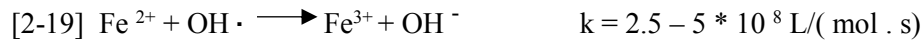
enhancement of removal efficiency, however the increase in ultrasound energy density does not result in the improvement to the efficiency. At last, n-butanol (a hydroxyl radical scavenger) with 100 mmol/L dropped the removal efficiency for 10% which shows the strong dependency of mechanism due to the presence of hydroxyl radicals.

Because of significant reduction in cost due to elimination of radiation, there is a potential to combine with oxidation processes, however the technology of ultrasonic requires the development and it is in an initial phase [2-32]. pH adjustment is also always required to obtain the best performance of degradation which limits its application in high sulphate contained wastewater. The studied wastewater in this research contains 4190 mg/L sulphate which shows the potential acidic condition that might occur after the initiation of treatment.

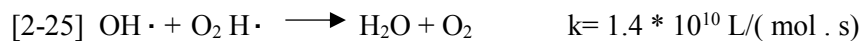
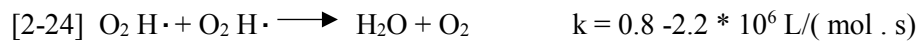
2-3-5. Fenton process

The Fenton process was found by H.J.H Fenton (in 1894) who reported that hydrogen peroxide could be activated by ferrous salts to oxidize tartaric acid [2-44]. Sychev and Isak [2-45] determined the mechanism of Fenton and presented 9 distinctive reactions. The first reaction (Eq. 2-17) could be considered as a core reaction in Fenton process which decomposes hydrogen peroxide to hydroxyl radical and converts ferrous ions to ferric ions. The regeneration of ferrous ions is carried out by the second reaction (Eq. 2-18) which is transferring ferric to ferrous by reduction reaction. The kinetics of regeneration of ferrous ions is relatively slower than the first reaction and is called Fenton-like reaction. One of the products of Fenton –like reaction is hydroperoxyl radicals ($O_2H\cdot$) which also attacks organic contaminants, however the observed sensitiveness is less than hydroxyl radicals. An external source of ferrous is added to the Fenton system to act as a catalyst for the consumption reaction of hydrogen peroxide to enhance the production of hydroxyl radicals. The

reaction of ferrous with hydroxyl and hydroperoxyl radicals are given in the third and fourth reactions (Eq. 2-19, Eq. 2-20) correspondingly. The reaction of ferric (Fe^{3+}) with hydroperoxyl is also presented in the fifth reaction (Eq. 2-21). The regeneration of ferrous ions results in the four last presented reactions, and they are considered as rate limiting steps in Fenton chemistry.



Four reactions are determined to provide the possible radicals for radical reactions or hydrogen peroxide-radical reactions which are presented below:

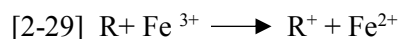
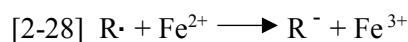


The decomposition of hydrogen peroxide to molecular oxygen and water is presented in Eq. 2-26 in the absence or presence of organic molecules. The side effect of the described reaction is exploitation of bulk oxidants which reduce the amount of oxidant and necessitates a pointless increase on treatment cost ^[2-46].



Hydroxyl radicals could be scavenged by ferrous ions (Eq. 2-19), hydrogen peroxide (Eq. 2-23), and/or hydroperoxyl radicals (Eq. 2-24) can even be auto scavenged by Eq.2-22^[2-47]. Babuponnusami and Muthukumar ^[2-48] state that hydroxyl radicals can act as radical generator (Eq. 2-17) and scavengers (Eq. 2-23).

It is possible that the hydroxyl radicals attack the organic radicals resulting in organics which are present in the wastewater. The mentioned radicals from organic matter can form dimmers or react with ferric and ferrous ions. All three scenarios are presented in Eq. 2-27 to Eq. 2-29.



The operating pH is strongly dependent on the iron and hydrogen peroxide specie factor. The optimal p regardless of type of the target substrate is around 3 ^{[2-49], [2-50], [2-51], [2-52]}. At very low pH values, iron complex species $[Fe (H_2O)_6]^{2+}$ are detected which react more slowly with hydrogen peroxide. It should be mentioned that increasing the concentration of ferrous ions will usually enhance the rate of degradation. The side effect of increasing ferrous ions is raising the amount of total dissolved solids content of the effluent which is not in accordance with environmental regulations. Thereby, optimising the loading of ferrous ions is crucial in laboratory scale studies ^[2-53]. The role of hydrogen peroxide concentration is crucial in the Fenton process. Regularly, the major impact of increasing hydrogen peroxide dosage is on the improvement of the pollutant removal efficiency, however exceeding appropriate dosage will lead to serious problems. First of all, COD will increase due to the contribution of unused hydrogen peroxide. Secondly, high dosage of hydrogen peroxide is harmful to many organisms which participate in biological oxidation ^{[2-}

^{54]}. Finally, the scavenging of hydroxyl radicals is expected to intensify once the over dosage of hydrogen peroxide is introduced to the system. As well as ferrous ion concentration, it is important to optimize hydrogen peroxide dosage in laboratory scale studies. Overview of the work conducted on Fenton oxidation is provided in Table 2-5.

The advantages of using Fenton process as a predominant method of treatment are: applicability in room temperature and atmospheric pressure; accessibility of required reagents and chemicals, furthermore, they do not cause environmental damage ^[2-46]. Three main drawbacks are scavenging of hydroxyl radicals due to wastage of oxidant, continuous loss of iron ions, and the formation of solids sludge ^[2-55].

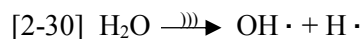
Table 2- 5 Overview of research works conducted on Fenton treatment in recent years

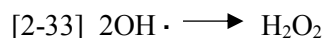
Wastewater/organic compound used	Experimental conditions	Remarks	Reference
2-6-dimethyl-aniline	2,6-DMA, n,n-dimethyl-aniline (n,n-DMA), aniline (AN), 2,6-dimethyl-phenol (2,6-DMP), 2,6-dimethyl-nitrobenzene (2,6-DMN), 2,6-dimethyl-benzoquinone (2,6-DMB), FeSO ₄ ·7H ₂ O, and H ₂ O ₂ are target pollutants ; FeSO ₄ ·7H ₂ O as a source of ferrous ions ; exposure time 20 minutes; the studied was carried out on both batch and continuous systems	Nearly complete degradation was obtained after 10 min Hydroxyl radical mechanism is assessed by using homogenous Fenton process	[2-56]
Phenol, 2 chlorophenol (2-CP) and 2-nitrophenol (2-NP)	Batch reactor (2 L) open to atmosphere was used. Initial concentration of phenol, 2-chlorophenol and 2-nitrophenol were 2.66mM, 1.95mM and 1.8mM, respectively. H ₂ O ₂ concentration: 0.2–3.5mM/mM of phenolic compounds. Fe ²⁺ /phenol compounds: 0.01/1, treatment time: 24 h	Presence of chloride and sulfate anions influenced the phenol, 2-CP, and 2-NP degradation. Higher resistance of formed intermediates was observed. Biodegradability of phenol was enhanced by the presence of chlorides	[2-57]
Poly hydroxyl benzoic acid	1 L capacity Fenton reactor was used. Fe ²⁺ concentration range used: 0–0.01 M, H ₂ O ₂ operating range used: 0–4 M, temperature: 20.8 °C and pH 3.2	Increase in Fe ²⁺ and H ₂ O ₂ concentration increases the pollutant removal and optimum Fe ²⁺ dosage was found to be 5mM. H ₂ O ₂ was completely utilized and found to be a limiting reactant. Increase in pH from 3 to 7 decreased the rate appreciably. Increase in temperature from 0 to 40.8 °C showed a variation in extent of degradation	[2-49]
Surfactant wastewater containing alkyl benzene sulfonate and linear alkyl sulfonate	Reactor with 2 L capacity was used. Fe ²⁺ range: 30–180 mg/L, H ₂ O ₂ concentration range: 20–80 mg/L, treatment time: 3 h	Optimum pH was observed as 3 and optimum FeSO ₄ and H ₂ O ₂ concentrations were found to be 90 and 60 mg/L, respectively. Subsequent treatment with coagulation is recommended to improve settling. Reaction followed first order with respect to reactants and rate constants depend on concentration of Fe ²⁺ and H ₂ O ₂	[2-58]
Landfill leachate	Batch 1-l double jacket spherical plastic reactor with four baffles. Mixing speed was about 1750 rpm. Its characteristics were pH 6.65–6.69, COD 8298–8894 mg L ⁻¹ , TOC 2040–2207 mg L ⁻¹ , and alkalinity as CaCO ₃ 3500–4600 mg L ⁻¹ . pH is adjusted throughout the treatment process	The oxidation of organic materials by Fenton's reagent was so fast that it was complete in 30 min with batch experiments. The oxidation of organic materials in the leachate revealed a pH dependence and was most efficient in the pH range of 2–3. A favorable H ₂ O ₂ /Fe ²⁺ molar ratio was 1.5, and organic removal increased as dosage increased at the favorable H ₂ O ₂ /Fe ²⁺ molar ratio.	[2-59]
Real effluent with COD: 1500 mg/L	Reaction was carried out in a 2 L Fenton reactor at a constant temperature of 25 8C and the contents were mixed with magnetic stirrer. Fe ²⁺ range used: 250–2250 mg/L; H ₂ O ₂ range used: 0–1600 mg/L; pH range studied: 2–9	The maximum COD removal efficiency was observed at a pH of 3.5 and it was drastically reduced when pH increased above 6. COD removal efficiency increased when Fe ²⁺ dosage increased up to 500 mg/L, beyond which removal efficiency becomes constant. Similar trends were observed in H ₂ O ₂ dosage	[2-60]

2-3-6. Sono-Fenton process

The oxidation of organics by ultrasound draws attention due to rapid degradation of chemical contaminants [2-61]. To define ultrasound phenomenon, it should be mentioned that it is a sound wave with a frequency greater than 20 kHz. The medium range frequency of ultrasound (300-1000 kHz) is utilized for sonochemical effects [2-62].

The mechanism of ultrasound waves is described by expansion and compression cycles. Meanwhile the expansion cycle, the pressure of the liquid reduced. In the case, the amplitude of ultrasound pressure is adequately large, acoustic cavitation will take place. The process includes formation, growth, and implosion of bubbles filled with vapor and/or gas. The parameters which affected the growth and implosion of bubbles are considered as ultrasound frequency and intensity, initial size of gaseous nuclei present in liquid, and physical properties of gas and liquid. Prior to implosion, the size of bubbles is oscillating. Once the cavitation bubbles explosively collapse, the pressure, and temperature will be able to reach several hundred atmospheres and several thousand Kelvin [2-63], [2-64], [2-65]. At several hundred atmospheres and several thousand Kelvin, organic compounds are decomposed directly by pyrolytic cleavage. The resulting hydroxyl radicals from pyrolysis also facilitate the degradation of organics. Thereby, three potential reaction sites are expected: 1) inside of cavitation bubbles, 2) interfacial region between the cavitation bubble and liquid phase, and 3) bulk region. The formation of hydroxyl radicals by water pyrolysis is provided in Eq. 2-30. The formed radical can undergo a variety of chemical reactions in the bulk solution and/or in a gas bubble which are presented in E.2-31, Eq.2-32, and Eq.2-33, respectively [2-66], [2-67].





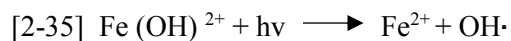
The mechanism of decomposition is strongly dependent on the wettability of chemicals. To support the statement, hydrophobic chemicals with high vapor pressure go through predominantly thermal decomposition inside the cavitation bubbles [2-68], [2-69]. While on the other hand, hydrophilic compounds with low vapor pressures mostly show the tendency to persist in the bulk region. Therefore, the destruction of hydrophilic chemicals is much easier due to oxidative degradation in the bulk solution.

The combination of Fenton, and sonolysis provides remarkable results. Nam et al. [2-70] applied sono-Fenton process on degradation of non-volatile organic compounds. A cylindrical reactor which was equipped with a titanium probe (dia: 1.3 cm, 20 kHz), was used. The temperature was preserved at 25 ± 2 °C using a water bath. Power intensity of $14.3\text{W}/\text{cm}^2$ was used. Fe^{2+} ions were added in the range from 0–20 mM. The pH was adjusted to 3.5 using phosphate buffer. Based on the achieved results, the hydroxyl radical production rate enhanced by 70% in comparison with sono ultrasound process alone. In addition, the degradation rate was increased by 2.8- and 3.6-fold at 10 and 20mM Fe^{2+} , respectively.

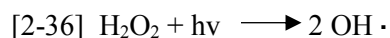
The drawbacks of the sono-Fenton process are: 1) Sensitivity of ultrasonic performance to the geometry of the reactor, 2) Significant influence of position of ultrasonic probe on propagation of sound waves, 3) The practicability of sono-Fenton at pilot scale is open to debate.

2-3-7. Photo-Fenton process

A combination of hydrogen peroxide UV radiation with ferrous or ferric oxalate ion is called the photo-Fenton process. The outcome would be an increase in production of hydroxyl radicals and in turn increases the rate of degradation of organic compounds ^{[1-10], [2-71], [2-72]}. Due to accumulation of ferric ions and consumption of all ferrous ions, the Fenton reaction does not proceed, however, photochemical regeneration of ferrous ions by photo-reduction (Eq. 2-35) of ferric ions takes place in photo-Fenton reactions.



Based on conducted research on photo-Fenton degradation of organic pollutants, the combination of Fenton reaction with conventional radiation zone of visible and near ultraviolet leads to better degradation. The investigated organic pollutants are 4-chlorophenol ^[1-12], nitrobenzene, and anisole ^[2-73], herbicides ^[2-71], and ethyleneglycol ^[2-74] respectively. Direct photolysis of hydrogen peroxide (Eq.2-36) contributes only to a lesser extent for photo-degradation of organic contaminants once iron complexes are present and the reason is strong adsorption of radiation by iron complexes ^{[2-75], [2-76]}.



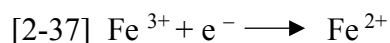
The optimal performance of photo-Fenton degradation is achieved by pH 3 when the hydroxyl-ferric complexes are more soluble and Fe (OH)^{2+} are more photoactive ^[2-77].

Amat et al. ^[2-78] juxtaposed the degradation of two commercial anionic surfactants which are sodium dodecyl sulfate and dodecylbenzenesulfonate. The experimental conditions were determined based on three scenarios. The first scenario was using a Fenton reagent with hydrogen peroxide in the presence or absence of solar radiation. The second scenario was utilizing photo

catalysis (TiO₂) with solar irradiation and the final scenario was carrying out photo-degradation using solar sensitizer (pyrylium salt). The results revealed that addition of a solar sensitizer would not give acceptable degradation efficiency and their further studies concluded that the photo-Fenton processes using solar radiation (0.1 mM of Fe²⁺ or Fe³⁺, and 1 mM H₂O₂) had a higher rate of surfactant degradation than that of solar-TiO₂ treatment.

2-3-8. Electro-Fenton process

Fenton process reactions are fully described in Section 2-3-5. To add further information on the appropriate oxidant in Fenton reactions, it should be noted that HClO is also able to react with ferrous in a Fenton-type reaction and the results would be in production of large amounts of hydroxyl radicals in the bulk solution [2-79]. Furthermore, the direct decomposition of hydrogen peroxide to hydroxyl radicals can be assessed by utilizing catalytic metal ions such as chromium, cerium, copper, cobalt, manganese, and ruthenium through conventional Fenton-like pathways [2-80]. The electro-Fenton process is introduced to overcome some of the drawbacks of the Fenton process (See Section 2-3-4). Brillas' and Oturan's group developed the electro-Fenton process during the last 15 years [2-81],[2-82]. The developments which was conveyed by the Brillas' and Oturan's group are summarized in three approaches: 1) the in situ and continuous electrogeneration of hydrogen peroxide at a carbonaceous cathode was fed with pure oxygen or air, 2) the addition of a ferrous catalyst to the solution, and 3) the cathodic reduction of ferric and ferrous which is described in Eq. 2-37, with consequent continuous production of Fenton reagents.

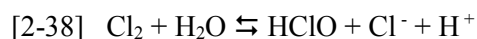


The best anode material which significantly enhances the electro-Fenton oxidation is boron doped diamond (BDD) [2-83]. The reason is production of reactive oxygen species (ROS) specifically M

(OH•). Platinum also gives enhanced electro-Fenton oxidation because of having relatively small energy gap between valance and conductive band with the value of 1.4 eV [2-84]. Due to high cost of BDD and platinum, the alternatives would be using graphite electrode which has high corrosion resistance and remarkable electro Fenton oxidation efficiency [2-84].

Several cathode materials which are carbon-polytetrafluoroethylene (PTFE) gas (O₂ or air), carbon felt (CF), carbon sponage, and reticulated vitreous carbon (RVC) have been investigated [2-81], [2-82], [2-85], [2-86]. According to efficiencies, two materials are placed on the top of list that are EF with carbon-PTFE air-diffusion electrode and EF with CF. Utilizing the first one leads to accumulation of high amounts of hydrogen peroxide in the medium with low ferrous regeneration through Eq. 2-37. While on the other hand, EF with CF provided the condition for the continuous transformation of ferric to ferrous due to low hydrogen peroxide electrogeneration at the CF cathode [2-87].

Kishimoto et al. [2-88],[2-89] developed an electro-Fenton type process using HClO as an oxidant and ferrous as a Fenton agent in which HClO is generated at the anode following Eq.2-38 and Eq.2-39. In addition, iron is added to the solution and the regeneration of ferric to ferrous is carried out via Eq.2-37.



Several operational parameters affect electro advanced oxidation processes (EAOPs) which are:

- 1) initial organic concentration,
- 2) current density (or applied current or potential),
- 3) temperature,
- 4) pH,
- 5) supporting electrolyte nature and concentration,
- 6) O₂ or air feeding flow rate, and finally

7) initial total dissolved iron concentration. The main electrochemical advanced oxidation processes parameters and impact on degradation efficacy are provided in Table 2-6.

The electro-Fenton process is applied to treat synthetic and real wastewater mostly at laboratory bench scale. The obtained results prove the high efficiency of EF once the pollutant concentrations are relatively high where most conventional methods are ineffective to reach the desired remained concentration. Some case studies conducted on synthetic and real wastewater are provided in Table 2-7.

Table 2- 6 The impacts of operating parameters on pollutants degradation efficiencies [2-125]

Parameter	Influence on degradation efficiency	References
Initial organic concentration	Higher initial organic concentrations require longer exposure times which lead to higher pollutant removal rates. The reason is faster oxidation of organics with hydroxyl radicals and inhibition of parasitic reactions. Also, lower pseudo-first-order kinetic constants are expected.	[2-90],[2-91],[2-92],[2-93],[2-94],[2-95], [2-96],[2-97]
Current density (or applied current or potential)	Higher generation of oxidizing species and consequent higher pollutant degradation efficiency is observed once j (or I or E) is increased. For higher j (or I or E) up to value that parasitic reactions occur in a high extent that leads to the degradation efficiency to be constant or even to decrease.	[2-98],[2-99],[2-100],[2-101],[2-102],[2-103]
Temperature	Diverse impact depending on the pH and wastewater composition due to its influence on the rate of ferrous generation and ferric regeneration through Eq.2-18, Eq.2-21, and Eq.2-39 which is followed: $\text{Fe}^{3+} + \text{O}_2 \longrightarrow \text{Fe}^{2+} + \text{O}_2$ (higher rate for higher temperature). Also, the amount of precipitated $\text{Fe}(\text{OH})_3$ is affected by increasing temperature	[2-100], [2-101], [2-102], [2-104],[2-105],[2-106]
pH	Frequently the highest degradation of pollutants is achieved by pH around 3 due to predominance of Fenton reactions. The addition of carboxylic acids can permit using higher pH values with higher degradation efficiency. Some studies found that pH 2.0 -4.0 will also give similar process efficiency.	[2-97], [2-107], [2-108], [2-109]
Supporting electrolyte nature and concentration	Contentious results: (i) $\text{NaCl} > \text{Na}_2\text{SO}_4$ due to degradation of pollutants with active chlorine species in the presence of chloride, scavenging of $\text{OH} \cdot$ by sulfate at higher rate than by chloride and/or formation of sulfate-iron complexes; (ii) $\text{Na}_2\text{SO}_4 > \text{NaCl}$ due to H_2O_2 consumption by reaction with HClO and/or formation of recalcitrant chloroderivatives; (iii) $\text{NaClO}_4 > \text{NaCl}$ due to non-reactivity of ClO_4^- toward iron and $\text{OH} \cdot$; or (iv) $\text{NaCl} > \text{NaClO}_4$.	[2-29],[2-110],[2-111],[2-112],[2-113]
O_2 or air feeding flow rate	High flow rates of oxygen (pure or air) guarantee maximum hydrogen peroxide electrogeneration	[2-99],[2-114],[2-115],[2-116],[2-117]
Initial total dissolved iron concentration	Higher degradation efficiency once the initial total dissolved iron concentration is increased. The limit is set based on the equilibrium between positive effect coming from Fenton reaction enhancement and negative impact from the growth of parasitic reaction.	[2-107]
Stirring rate or liquid flow rate	High stirring rate leads to prevention of solid deposition, fast solution homogenization and enhancement in mass transfer of pollutants towards electrodes and catalyst.	[2-118]

Table 2- 7 Overview of the conducted researches on pollutant degradation efficiency using electro-Fenton process

Wastewater/organic compound used	Experimental conditions	Remarks	Reference
Land fill leachate	A rectangular glass reactor containing 200mL solution was used for batch experiments. Constant current supply of 1–3 A using DC power supply was used. Two anode (Ti/RuO ₂ –IrO ₂) and cathode at different distances like 0.7, 1.3, 2.1, and 2.8 cm were placed into leachate solution. pH was adjusted to 3 utilizing sulfuric acid. H ₂ O ₂ range of 0.1–0.44 mol/L and Fe ²⁺ range of 0.1–0.12 mol/L was studied	The COD removal of 65% was obtained when H ₂ O ₂ alone used in the reactor. Presence of Fe ²⁺ greatly improved the COD removal up to 83.4% at a dosage of 0.038 mol/L Fe ²⁺ . Further increase in Fe ²⁺ concentration decreased the COD removal. The optimum electrode distance obtained was 2.1 cm. The step wise or continuous addition of H ₂ O ₂ was more efficient than addition of H ₂ O ₂ in a single step.	[2-119]
Nitro phenols	Undivided glass cell of 250 mL capacity containing graphite cathode and platinum black anode was used. The pH was kept constant at 3 using H ₂ SO ₄ . Also, Na ₂ SO ₄ was used to maintain the conductivity. All experiments were carried out at room temperature. Constant current of 0.05 A was maintained and 0.5 mmol/L of Fe ²⁺ was used	Degradation of 4-nitrophenol was significantly enhanced by the introduction of aeration and Fe ²⁺ . The results showed 98% removal of 4-NP and 13% removal of TOC. Electro-Fenton process eliminates the toxicity and improved the biodegradability of 4-Nitrophenols. Intermediates such as hydroquinone and benzoquinone were detected by GC/MS analysis	[2-120]
Synthetic wastewater Formic, glyoxylic, oxalic, acetic, glycolic, pyruvic, malonic, maleic, fumaric, succinic, malic acids	The synthetic wastewater contained 4.6–23 mg formic L ⁻¹ , 7.4–37 mg glyoxylic L ⁻¹ , 9.0–45 mg oxalic L ⁻¹ , 6.0–30 mg acetic L ⁻¹ , 7.6–38 mg glycolic L ⁻¹ , 8.8–44 mg pyruvic L ⁻¹ , 10–52 mg malonic L ⁻¹ , 12–58 mg maleic L ⁻¹ , 12–58 mg fumaric L ⁻¹ , 12–59 mg succinic L ⁻¹ or 13–67 mg malic L ⁻¹ in 5.6 g KCl L ⁻¹ . The experimental exposure volume is 200 mL in an undivided cell. The utilized material for anode and cathode are platinum mesh and carbon felt respectively. The applied current densities is varied based on the surface area of utilized cathode. For 56 cm ² and 112 cm ² the current densities are 1.1 - 5.4 mA/cm ² and 1.8-2.7 mA/cm ² respectively. The pH is maintained at 3. Also the initial total dissolved iron is 5.6 m L ⁻¹ .	Dissolved organic carbon is completely removed from the system.	[2-121]

Table 2-7 Continued- overview of the conducted researches on pollutant degradation efficiency using electro-Fenton process

Wastewater/organic compound used	Experimental conditions	Remarks	Reference
Synthetic wastewater Phenol	<p>The synthetic wastewater contained 31 or 99 mg phenol L⁻¹ in 7.0 g Na₂SO₄ L⁻¹. The exposure volume is 150 – 400 mL. Anode and cathode materials are platinum grid and carbon felt respectively. The practical current densities is varied based on the surface area of utilized cathode. For 48 cm² and 102 cm² the current densities are 2.1 mA/cm² and 0.98 mA/cm² respectively. The operational temperature is ambient and the pH is maintained at 3. Three different dosage of initial dissolved iron concentrations are assessed with three distinctive types of metals. 2.8–56 mg L⁻¹ or 2.9–59 Co²⁺ or 5.5–55 mg Mn²⁺ L⁻¹ or 64–635 mg Cu²⁺ L⁻¹.</p>	Dissolved organic carbon is completely removed from the system.	[2-122]
Mixture of 8 municipal sanitary landfill leachate	<p>The characteristics of studied real wastewater are as follows ([Cl⁻]₀ = 1420–8570 mg L⁻¹) Mixture of 8 municipal sanitary landfill leachate DOC (mg L⁻¹) = 1600–3100 TSS (mg L⁻¹) = 15310–17602 pH = 8.0–9.0 [SO₄²⁻] (mg L⁻¹) = 60–240 [Cl⁻] (mg L⁻¹) = 5000–6200 [NH₄⁺] (mg L⁻¹) = 1900–3200 [NO₂⁻] (mg L⁻¹) = 0 [NO₃⁻] (mg L⁻¹) = 0 Undivided cell with the volume of 250 mL. Anode and cathode type and the dimensions are as followed: BDD or Pt (24 cm²) Cathode: CF (70 cm²) The applied current density is 7.1–14 mA cm⁻², The operation of temperature is ambient. pH is adjusted to 3.0. Initial total dissolved iron concentration is 11 mg L⁻¹</p>	The maximum achieved dissolved oxygen decay is 93%.	[2-123]
Aniline	<p>The exposure volume is 10-30 L. The pollutant concentration is 1000 ppm aniline solution in 0.05 M Na₂ SO₄ + H₂ SO₄. A pilot flow reactor in recirculation mode with a filter-press cell containing an anode and an oxygen diffusion cathode, both of 100 cm² area. The total dissolved iron is 1 mM Fe²⁺ and a Ti/Pt or DSA anode is utilized.</p>	<p>Various configurations are considered and the maximal degradation for each type of anode is: 61% TOC removal in 2 hours while applying 20 A current with Ti/Pt anode. 63% TOC removal in 2 hours while applying 20 A current with Dimensionally Stable Anode (DSA). During this process energy demand was 3.8 kWh/g COD removal. The results showed 100% sulfide removal in 10 min. The results gave moderate energy costs.</p>	[2-124]

Table 2-7 Continued- overview of the conducted researches on pollutant degradation efficiency using electro-Fenton process

Wastewater/organic compound used	Experimental conditions	Remarks	Reference
Winery wastewater	The properties of wastewater contaminants are: DOC = 4298 mg L ⁻¹ , COD = 12000 mg L ⁻¹ , BOD ₅ = 7950 mg L ⁻¹ , C = 3178 μS cm ⁻¹ , TSS = 81 mg L ⁻¹ , pH = 3.7, TDI < 0.1 mg L ⁻¹ , SO ₄ ²⁻ = 30 mg L ⁻¹ , Cl ⁻ = 20 mg L ⁻¹ , NH ₄ ⁺ = 9.9 mg L ⁻¹ , NO ₂ ⁻ = 1.4 mg L ⁻¹ , NO ₃ ⁻ = 0.89 mg L ⁻¹ , PO ₄ ³⁻ < 0.02. Flow plant with undivided filter-press cell with exposure volume of 1.25 L. The utilized anode and cathode are BDD and Carbon-PTFE air-diffusion respectively. The applied current density is 10-100 mA cm ⁻² . The flow rate is 0.67 L min ⁻¹ with magnetic stirring. The operational temperature is 25 °C. The pH is maintained at 2.8 while the total dissolved iron concentration is 20 -70 mg L ⁻¹ .	No fitting of a pseudo-first-order kinetic model to experimental data. 82% removal efficiency is achieved with respect to DOC after 240 minutes.	[2-125]
Textile wastewater	The properties of wastewater compounds are : : DOC = 395 mg L ⁻¹ , COD = 1224 mg L ⁻¹ , C = 2914 μS cm ⁻¹ , TSS = 81 mg L ⁻¹ , pH = 4.8, SO ₄ ²⁻ = 38 mg L ⁻¹ , Cl ⁻ = 234 mg L ⁻¹ . An undivided cell is utilized to treat 500 mL wastewater. The utilized anode and cathode are Pt wire and PAN based-ACF with exposure surface area of 63 cm ² for cathode. The applied current density is 0.8-4.8 mA cm ⁻² . The operational temperature is in the range of 20 to 40 °C. Also the pH is varied in the range of 2 to 5. The initial dissolved iron concentration is 18-147 mg L ⁻¹ .	77% COD removal efficiency is achieved once 20 °C is obtained as operating temperature. COD removal percentage decreased from 75.2% to 68.1% as the temperature increased from 20 °C to 40 °C.	[2-126]
Leather tanning industry wastewater	A glass reactor with the volume of 500 mL is configured with the same type of material for anode and cathode which is iron and the distance between electrode is equal to 6 cm. Effective working area of electrodes was 45cm ² . The contents were stirred using a magnetic stirrer and pH was maintained at 3, 5, and 7.2. H ₂ O ₂ range used: 840–5010 mg/L and current used: 0.35–1.5A	The COD removal obtained at pH 3 and at neutral pH was 70% and 60%, respectively. Throughout this process energy demand was 3.8kWh/g COD removal. The results presented 100% sulfide removal in 10 min	[2-127]

Photo electro-Fenton (PEF) or solar photo electro-Fenton (SPEF) also showed influential results with respect to removal efficiency of hardly degradable pollutants in experimental bench scale. However, due to challenges in upscaling cost and design, it is not obtained as governing method

in this study. The use of artificial lamps in PEF technique is commonly responsible for high electrical costs^[2-118].

To briefly describe PEF or SPEF it should be mentioned that the mechanism of the reactions is similar to the photo-Fenton process while direct photolysis is employed by ligand-to metal-charge transfer extinction of complexes made between ferric and some organics, namely carboxylic acids. The described reaction is presented by Eq. 2-39. Eq. 2-39 facilitates the regeneration of ferrous ions parallel with the formation of weak oxidizing species such as superoxide anion radical, carbon dioxide anion radical, and hydrogen peroxide^[2-118].



The intensity and wavelength of artificial lamps determines the mechanism of degradation pathway of the pollutants. Due to higher wave intensity of solar mechanism (wavelength larger than 400 nm) higher pollutant degradation is expected to achieve and the cost would be significantly reduced.

The studies relating to the application of PEF process are very limited and most studies are associated to the treatment of herbicide^[2-48]. However, one of the successful results is obtained by Brillas et al.^[2-128] for degradation of aniline. A glass reactor is used as electrochemical reactor while platinum anode and carbon PTFE cathode is utilized to provide constant current with the magnitude of 0.1 A. A 125W mercury lamp with a releasing wavelength of 360nm is used as the irradiation source. Fe^{2+} concentration is maintained at 1mM. The aniline mineralization is increased by UV irradiation. The photo-electro-Fenton process allows 92% of TOC removal after 6 h. Whereas in the electro- Fenton, only 68% of mineralization was achieved. Reaction pathway

for aniline mineralization to CO₂ involving intermediates was proposed which is illustrated in Figure 2-7.

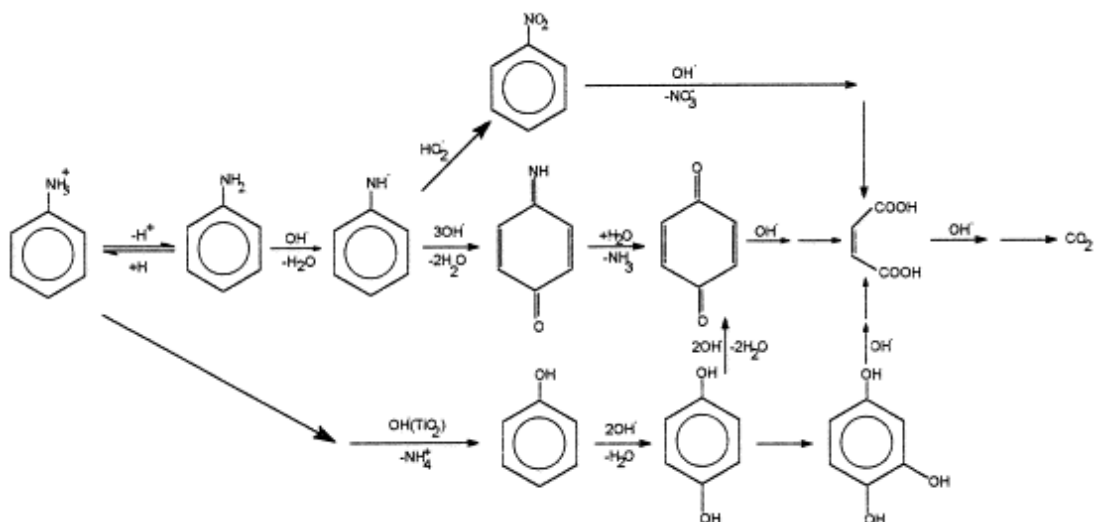


Figure 2- 8 Proposed reaction pathways for mineralization of aniline at pH 3 following photoelectro-Fenton processes (adopted from Brillas et al. ; 1998)

2-3-9. Cost comparison of Fenton, ozonation, and conductive-diamond electrochemical oxidation (CDEO)

To date, there is no comprehensive research on the cost estimation of electro-Fenton and photo Electro Fenton process and most research conducts a qualitative comparison among different methods of AOPs and EAOPs. The most completed comparison is provided by Cañizares et al. [2-129]. In the mentioned research, the economic feasibilities of three Advanced Oxidation Processes (AOPs) have been studied: conductive-diamond electrochemical oxidation (CDEO), ozonation, and Fenton oxidation.

Only CDEO could achieve complete mineralization of the pollutants for all wastes. A comparison with respect to COD mineralization, elimination is provided in Table 2-8. Furthermore, comparison of operation cost and capital investment are given in Table 2-9. Based on the

comparison, CDEO gives the lowest cost in both operation cost and capital investment except for eriochrome black T. Due to the fact that CDEO can be considered as one of the most expensive EAOPs, it can be extended that applying electro-Fenton would be an economical approach. Consequently, the author employed electro-Fenton as governing approach for two reasons: 1) excellent mineralization of organics, 2) economically feasible to assess for upscaling.

Table 2- 8 Operation cost of CDEO, ozonation, and Fenton process for 85% COD removal [2-129]

Compound	Operation cost (€ m ⁻³)		
	CDEO	Ozonation	Fenton
Butyric acid	11	205	35
2-Propanol	9	110	71
4-Chlorophenol	13	114	2
2-Naphthol	13	72	7
Eriochrome Black T	35	99	46
Olive oil	11	181	5

Table 2- 9 Capital investment of CDEO, ozonation, and Fenton process for 85% COD removal [2-129]

Compound	Capital investment			
	(€ m ⁻³)			
	CDEO 15000 € m ⁻²	CDEO 8000 € m ⁻²	Ozonation	Fenton
Butyric acid	23314	18939	123431	16575
2-Propanol	20564	16772	83986	18184
4-Chlorophenol	27811	22464	86303	10226
2-Naphthol	27811	22464	61076	14953
Eriochrome Black T	104910	81090	70798	15205
Olive oil	34400	27594	106244	16848

Chapter 3 Methodology

Chapter 3 describes the research road map and strategy (Section 3-1), reactor and experimental design (Section 3-2), experimental analysis methods (Section 3-3), and finally electrochemical reactions (Section 3-4) to provide a comprehensive view of research methodology.

3-1. Methodological approach

The major objectives of the research were designing and upscaling an Electro-Oxidation fed batch reactor to enhance the removal of target pollutants, which are Total Kjeldahl Nitrogen (TKN), ammonia (NH_3), and organic nitrogen (ON). The feed flow of the reactor (Influent) initially consists of 14000 mg/L of TKN, 11000 mg/L of ammonia, and 3000 mg/L of organic nitrogen.

Table 3-1 demonstrates the characteristics of the studied wastewater.

Table 3- 1 Characteristics of the industrial wastewater

Characteristics of the wastewater	Value
Ammonia (NH_3) [mg/L]	11000.0
Total kjeldahl nitrogen (TKN) [mg/L]	14000.0
Organic nitrogen (ON) [mg/L]	3000.0
Nitrate (NO_3^-) [mg/L]	485.0
Nitrite (NO_2^-) [mg/L]	34.0
Total nitrogen (TN) [mg/L]	14500.0
Sulfate (SO_4^{2-}) [mg/L]	4190.0
Ferrous (Fe^{2+}) [mg/L]	2760.0
Total suspended solids [g]	14.3
pH	6.8
Conductivity [mS/cm]	62.0
Oxidation reduction potential (ORP) [mV]	-10.7

No dilution factor is also implemented for the described influent. Determining objectives are considered as: a) defining apposite operating conditions, b) experimental investigating of upscaling parameters in three distinct reactor scales (small, medium, and large lab scales as 0.5 L, 2.2 L, and 5.8 L, respectively), c) reducing exposure time for one day and d) Validating an innovative electro Fenton sequential batch reactor (EF-SBR) for medium and large lab scales. Four distinct phases are investigated, and each of them consists of the three major categories (reactor design, matrix, and interrelated matrix and reactor design parameters). The four phases of the research are illustrated in Figure 3-1 and listed as follows:

- Phase 1 - Experimental parametric study of a small scale electrokinetic batch reactor
- Phase 2 - Experimental parametric study of a medium scale electrokinetic batch reactor
- Phase 3 - Experimental parametric study of a large scale electrokinetic batch reactor
- Phase 4 - Experimental parametric study of an electro-Fenton-sequential batch reactor (EF-SBR)

Phase 1 operating volume is 0.5 L which is called small scale. In addition, the defined stages mainly investigate all primary impacts related to the pollutant removal efficiency. Fig 3-2 illustrates the milestones of first phase stages. Phase 1 is one of the most important phases of study dealing with all preliminary and primary aspects which are related to reactor configuration and electrochemical reactions. Furthermore, it emerges as the first step of upscaling by using a small scale reactor with 0.5 L volume. The first phase of study delves into seven different stages that are classified in the following order:

- Reactor design parameters (Stage 1-1: Impact of anode to cathode surface area ratio and the electrodes configuration)

- Matrix parameters (Stage 1-2: Impact of time intervals of adding hydrogen peroxide; Stage 1-3: Impact of pretreatment of the present sulfate in the influent; Stage 1-4: Impact of adding Fenton agent)

- Interrelated reactor design and matrix parameters (Stage 1-5: Impact of current density variation; Stage 1-6: Impact of continuous airflow diffusion)

The second phase of study is proposed based on the Phase 1 results and conclusions. Therefore, the main approach is avoiding the previous phase failure scenarios and defining new stages for Phase 2. Fig 3-3 illustrates the research strategy of the second phase stages. The main purpose of the second phase is investigating the parameters influence on the effluent quality in order to find an optimal experimental upscaling pattern. All experiments run in the fixed 2.2 L volume reactors defined as a medium scale. The second phase of study follows the same classification (Reactor design, interrelated reactor design and matrix parameters) and it consists of the following four stages:

- Reactor design parameters (Stage 2-1: Impact of anode to cathode surface area ratio; Stage 2-2: Impact of a distance between electrodes)

- Interrelated reactor design and matrix parameters (Stage 2-3: Impact of current density variation; Stage 2-4: Impact of continuous airflow diffusion)

The third phase of the research follows the aim of the Phase 2 which is determining an optimal experimental upscaling trend while the main purpose is finding the suitable operating conditions utilizing EF-SBR. The exposure volume of wastewater is 5.8 L which is considered as a large scale test. Fig 3-4a illustrates the third phase stages related road map. The stages of Phase 3 are listed below:

- Reactor design parameters (Stage 3-1: Impact of electrode configuration)
- Matrix parameters (Stage 3-2: Impact of hydrogen peroxide purity; Stage 3-3: Impact of hydrogen peroxide molar ratio)

The fourth phase of study is contributed with novel utilization of electro-Fenton sequential batch reactor (EF-SBR) at both medium and large scales. Sequential batch reactor (SBR) is widely known because of its efficiency in aerobic biological wastewater treatment^[3-1]. At the end of each cycles of the process, specified volume of the effluent (usually less than 30%) is maintained in the reactor and the remained volume is substituted with influent (untreated wastewater). Combination of electro Fenton and SBR is mainly investigated in the fourth phase and the major aims are considered as optimizing experimental upscaling pattern, reducing reaction exposure time, and enhancement of energy consumption. Fig 3-4b illustrates the pertinent research plan for the fourth phase's stages. The fourth phase determined stages are the same in both medium and large scale EF-SBR, and they are listed as followed:

- Matrix parameters (Stage 4-1: Impact of hydrogen peroxide purity)
- Interrelated reactor design and matrix parameters (Stage 4-2: Impact of EF-SBR cycles)

3-2. Experimental configuration and reactor design

The research strategy stages, which belong to reactor design or interrelated reactor design and experimental configuration categories, require specific experimental configuration and reactor design. Therefore, attaining research objectives specifically finding experimental upscaling trend is severely depended on apposite experimental setup configuration and design. Except for one of the Phase 1 experiments, all remaining experiments were run in the cuboid reactor. In addition, the mentioned different experimental setup runs in cylindrical batch reactor.

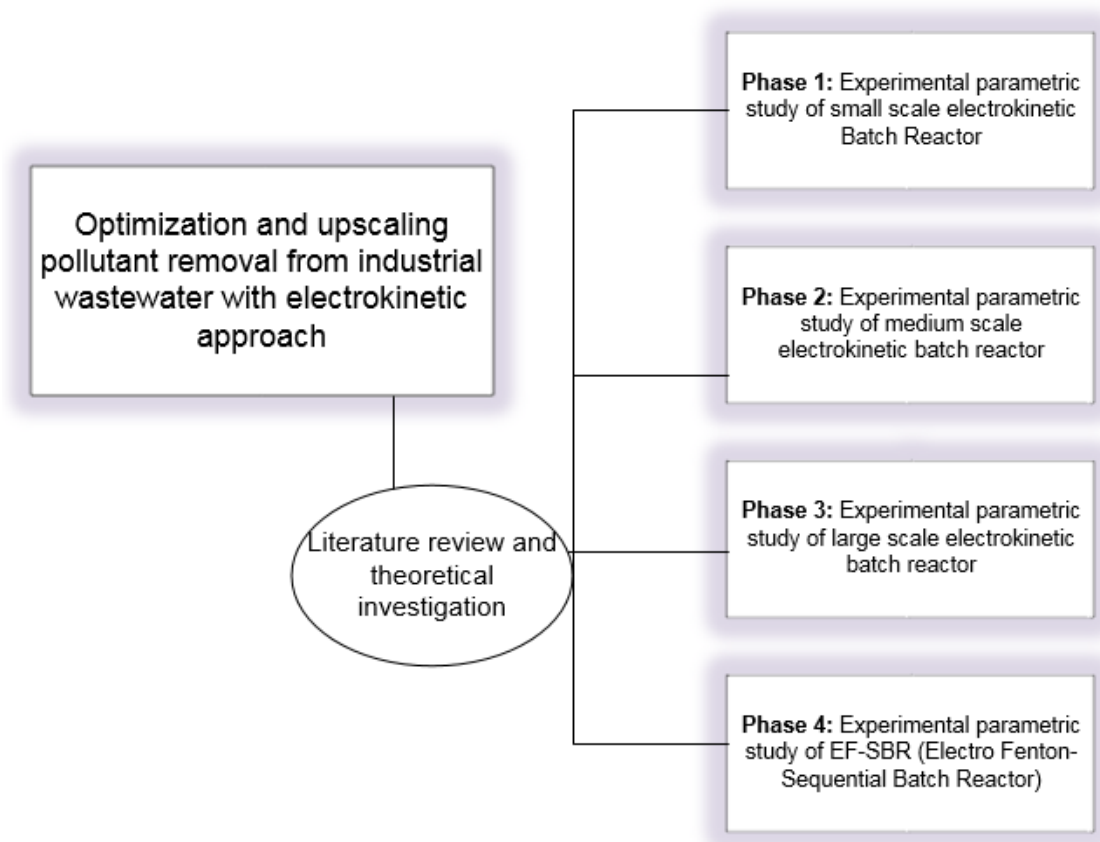


Figure 3- 1 Overview of the research flowchart of parametric study

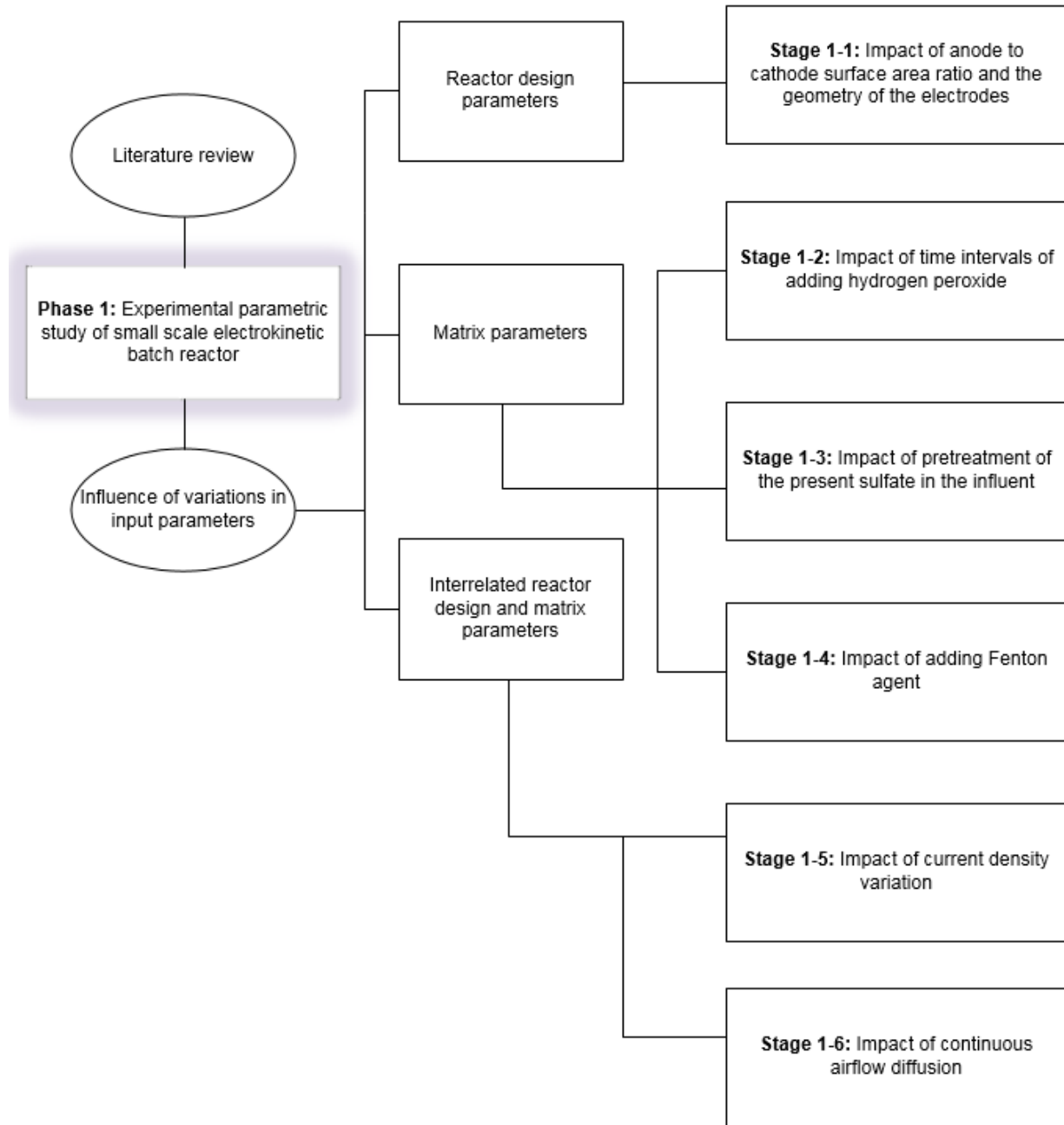


Figure 3- 2 Research flowchart for Phase 1: small scale which consider reactor design, matrix, and interrelated parameters

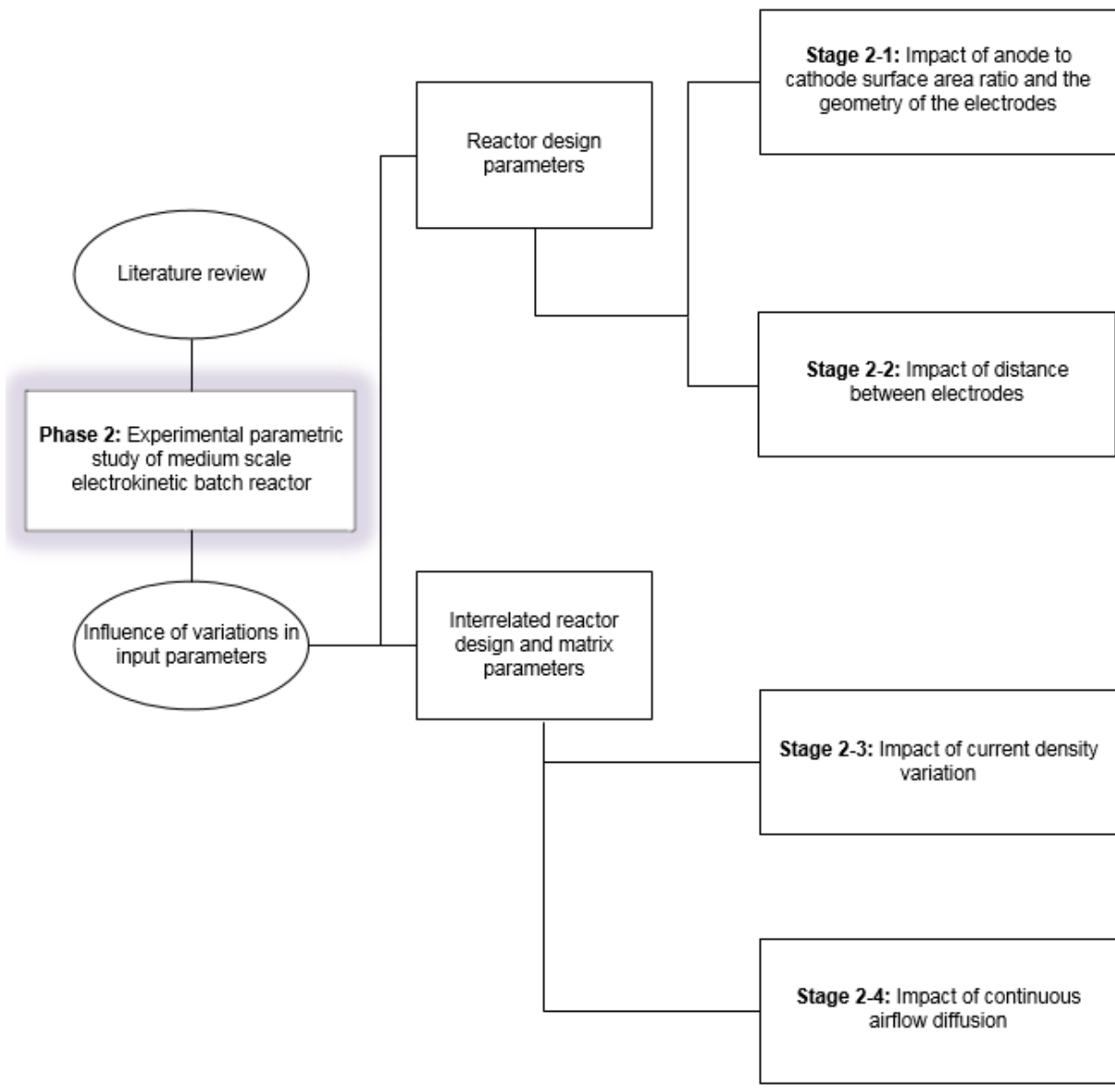
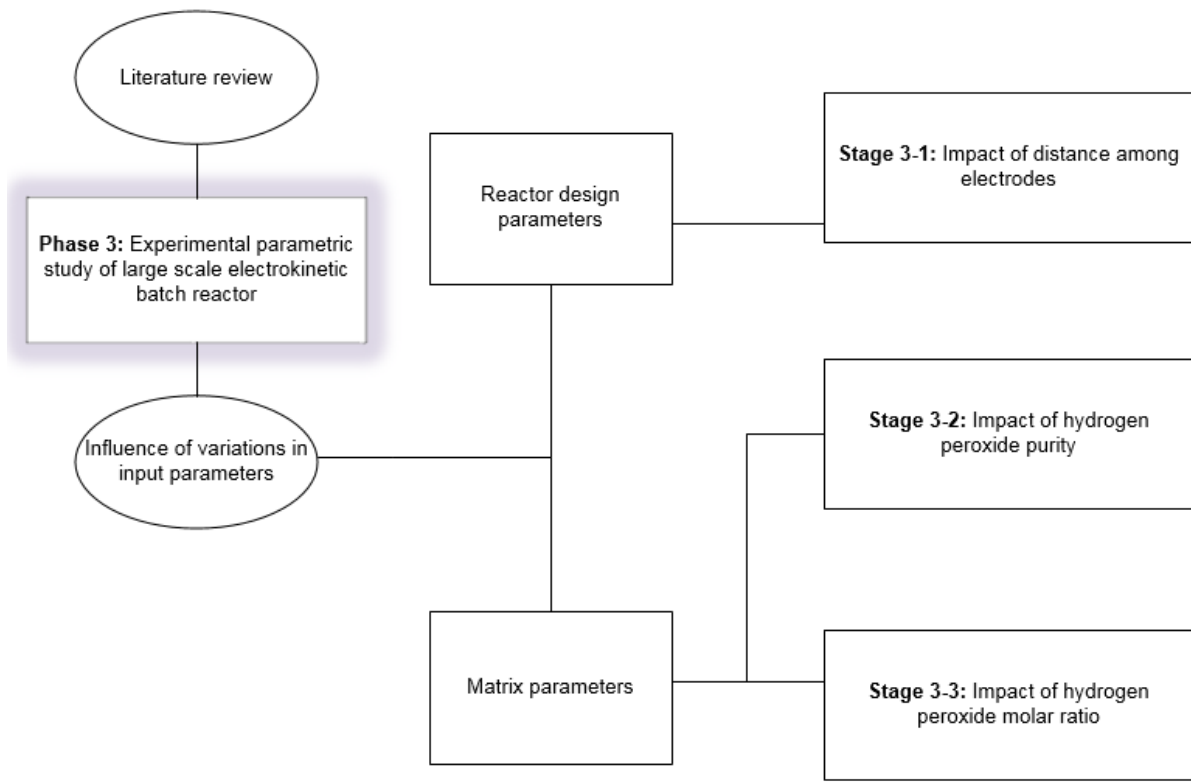


Figure 3- 3 Research flowchart for Phase 2: medium scale which consider reactor design and interrelated parameters



a)-Research flowchart for Phase 3: large scale which consider reactor design and matrix parameter

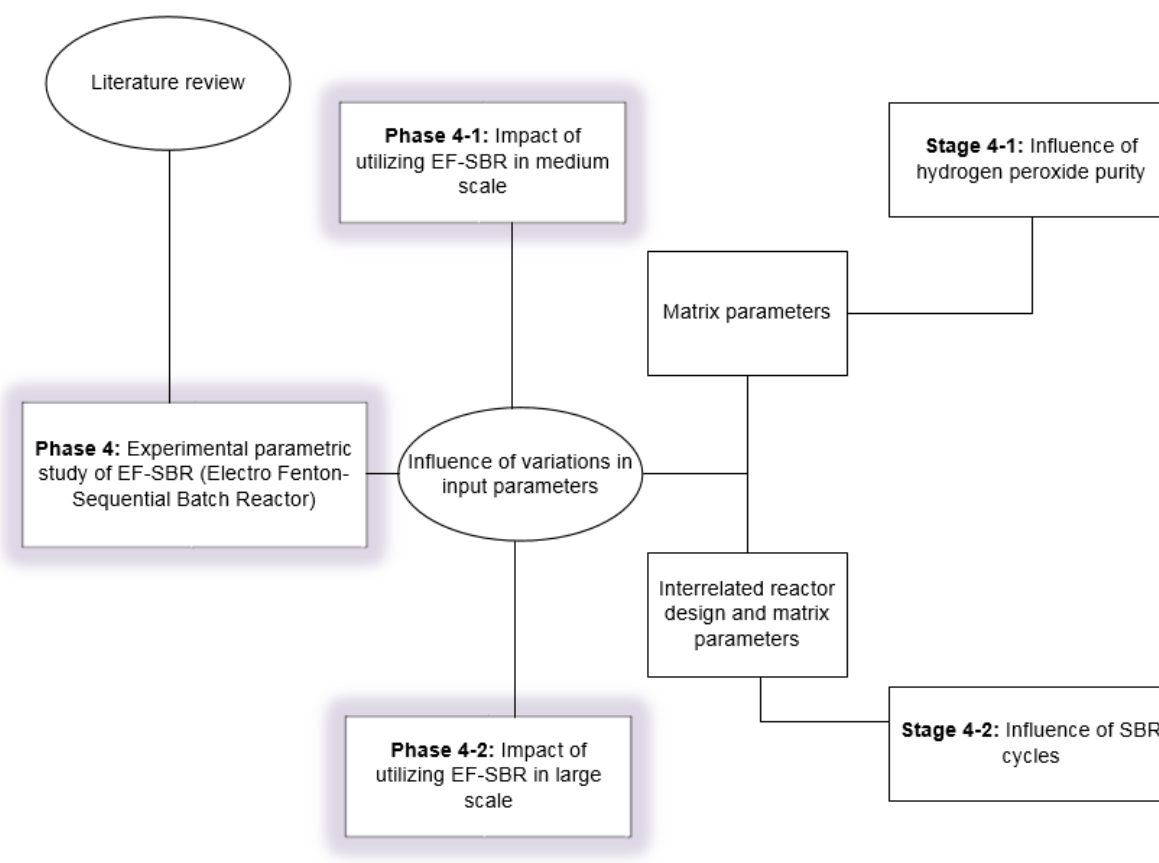


Figure 3- 4 b) Research flowchart for Phase 4: EF-SBR which consider matrix and interrelated parameters in both medium and large scale

3-2-1. Reactor and experimental design of Phase 1

Thirty-three experiments were run to investigate the impact of the small scale associated parameters (discussed in Fig.3-1) and 24 of the mentioned experiments are described in Section 3-2-1 to find a trend for process upscaling. Two reactor designs have been obtained for Phase 1 to investigate the response of the electrokinetic system while considering the constant initial volume as 0.5 L for running. The schemes of cuboid reactors are demonstrated in Fig 3.5a (all phase 1 stages), the scheme of the cylindrical reactor is also illustrated in Fig 3.5b (Stage 1-1).

The two cuboid batch reactors differ from each other with respect to the oxidizing agent input. Consequently, the first reactor has an uptake fed manual system for introducing hydrogen peroxide discretely in defined time intervals whereas the second reactor has side extension for air input. The cylindrical batch reactor is a PVC fabrication cell in which the anode is fixed centrally while the cathode is covered the internal side surface of the cylinder.

The constant direct current is applied. Both current and voltage are measured with multimeter built-in DC power supply Abra AB-5300-1 and the recorded error is $\pm 0.001\text{A}$ ($\pm 1\text{mA}$). The distance between electrodes are maintained on 5cm in all small-scale experiments.

Based on previous research ^[1-13], the best removal efficiency was achieved by using graphite as the anode and stainless steel as the cathode for the same studied type of influent. Therefore, the same type of electrodes is used in this research and graphite is selected as anode's material and stainless steel is chosen for being cathode.

The objectives of the Stage 1-1 that are experimentally studied are: a) impact of anode to cathode surface area ratio and dimensions b) impact of using different geometries of cathode (e.g. flat, mesh and perforated stainless steel), and c) impact of the geometry of the reactor and position of the anode.

It should be mentioned that the time interval of adding hydrogen peroxide is fixed at 24 hours for all experiments of Stage 1-1. To investigate the first objective of Stage 1-1, the surface area of the cathode (mesh stainless steel) is fixed at constant value of 25 cm^2 while the anode surface area is changed in each experiment, and its values are in the range of 10.35 up to 86.25 cm^2 . In addition, all experiments have been run in the cuboid batch reactor. The logics underlie the selection of constant surface area of cathode are associated with one main considerations which is analyzing

the experimental results while the number of variables are reduced (Tab. 3-2). Moreover, a dimensionless number is defined in order to follow the influence of dimensions of electrodes as well as the anode to cathode surface ratio simultaneously. The mentioned dimensionless number is the quotient of the ratio of anode to cathode height and the ratio of the anode to cathode width

$\left(\frac{H_a}{H_c} / \frac{W_a}{W_c}\right)$, which is called “Dimensional Quotient”. The experimental design of the first objective

is described in Table 3-2 considering all associated aspects of the reactor configuration.

The second objective of the Stage 1-1 is defining an impact of the cathode perforation (circular perforation, square mesh, and no void space) on the removal efficiency of the pollutants (e.g. ammonia, TKN and organic nitrogen). The dimensional quotient is selected stand on optimum achieved anode to cathode surface area ratio (Stage 1-1; 1st objective). The same flat graphite sheet with the thickness of 0.5 cm is utilized for the whole second objective experiments while three distinct types of cathode with the same alloy metallurgy (stainless steel) are used for each distinct experiment respectively. The three types are a perforated sheet (38.8% void space), a mesh stainless steel (68.25% void space), and a flat sheet (no void space). The experimental design of the second objective is explained in Table 3-3 providing all required details and operating conditions.

The last objective of Stage 1-1 is contributed with the geometry of the reactor. Two different batch reactors: cylindrical and cuboid are designed to investigate an impact of the anode position and array of the electrical field while all operating conditions for both reactors are the same. According to Figure 3.5b and described configuration for cylindrical batch reactor (Section 3.2.1), the graphite anode is placed in the center and stainless steel cathode is covered the inner surface area of the cell. The promising current density (resulted from primary current density study) for cuboid

batch reactor is also applied to make the results comparable to rectangular batch reactor experiments. Experimental design of the third objective is explained in Table 3-4 specifically.

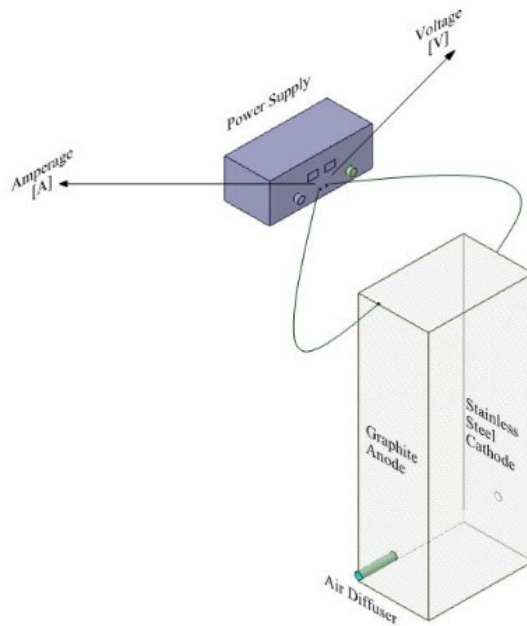
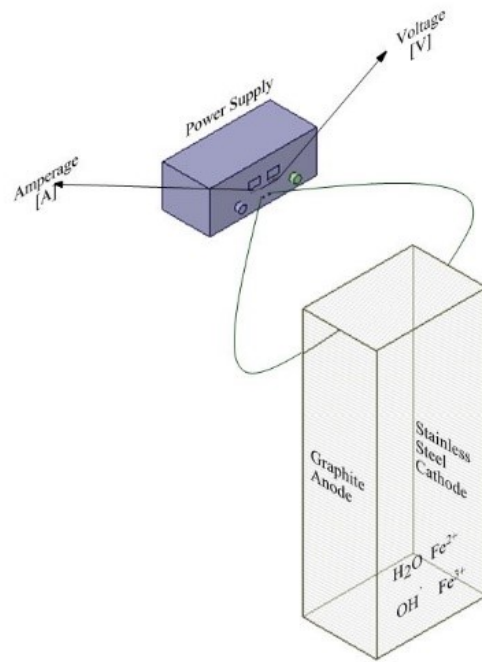


Figure3-5 a1) Schematic of the small scale reactor with hydrogen peroxide input; a2) Schematic of small scale reactor with air diffuser;

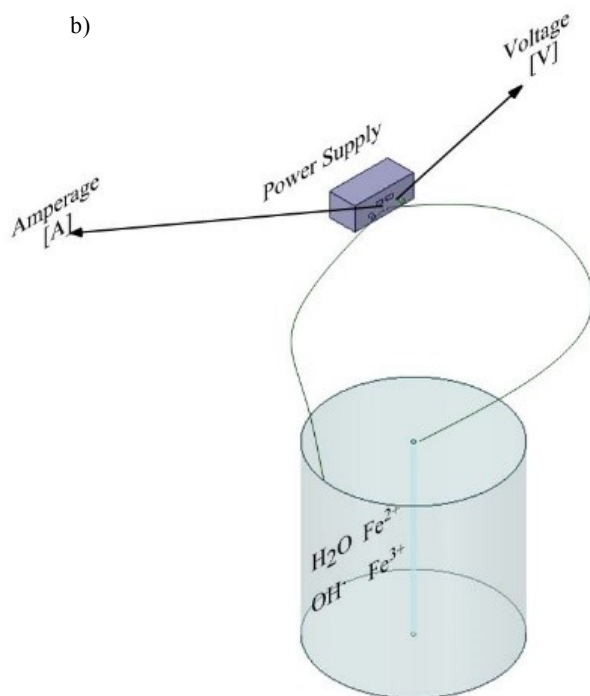


Figure 3- 5 b) Schematic of small scale cylindrical reactor considering associated electro-Fenton reactions

Table 3- 2 Experimental design and operating conditions of the Phase 1, Stage 1-1, 1st objective using mesh stainless steel as cathode; impact of anode to cathode surface area ratio and dimensions

No. of experiment	Distance between electrodes [cm]	Applied current density [mA/cm ²]	Exposure surface area of anode [cm ²]	Exposure surface area of cathode [cm ²]	Anode to cathode area ratio	$\left(\frac{Ha}{Hc} / \frac{Wa}{Wc}\right)$	Exposure time [h]
13	5.00	33.33	9.45	25.00	0.38	8.33	72.00
14			17.85		0.71	4.41	
15			30.45		1.22	2.59	
16			38.85		1.55	2.03	
17			50.40		2.02	1.56	
1			57.75		2.31	1.31	
18			70.35		2.81	1.12	
19			78.75		3.15	1.00	

Table 3- 3 Experimental design and operating conditions of the Phase 1, Stage 1-1, 2nd objective; impact of using different geometries of cathode

No. of experiment	Applied current density [mA/cm ²]	Distance between electrodes [cm]	Cathode type [Stainless Steel]	Exposure surface area of anode [cm ²]	Exposure surface area of cathode [cm ²]	Anode to cathode area ratio	$\left(\frac{H_a}{H_c} / \frac{W_a}{W_c}\right)$	Exposure time [h]
31	33.33	5.00	Perforated (38.8%)	78.75	48.20	1.63	1.00	72.00
32			Mesh (68.25%)		25	3.15		
23			Flat Plate (no void)		78.75	1.00		

Table 3- 4 Experimental design and operating conditions of the Phase 1, Stage 1-1, 3rd objective; impact of the geometry of the reactor and position of the anode

No. of experiment	Distance between electrodes [cm]	Cathode type [Stainless Steel]	Exposure surface area of anode [cm ²]	Exposure surface area of cathode [cm ²]	Anode to cathode area ratio	$\ln(r_c/r_a)$	$\left(\frac{H_a}{H_c} / \frac{W_a}{W_c}\right)$	Exposure time [h]
11	5.00	Flat Plate (no void)	22.00	208.9	0.11	2.30	N/A	72.00
13		Mesh (68.25%)	9.45	25	0.38	N/A	8.33	

The second stage of the Phase 1 is placed in matrix parameters category. Hydrogen peroxide which acts as an oxidizing agent, provides hydroxyl radicals in order to oxidize the pollutants and transmute them to easily degradable products. Therefore, the demands of finding the proper time interval of adding hydrogen peroxide come into consideration. Two sets of experiments have been determined. The logic of experimental design is based on the best achieved current density in primary experiments, and the surface area is set with respect to the mentioned current density experimental operating conditions (57.75 cm² for CD equal to 33.33 mA/cm².) The dimensional

quotient is considered as one to observe the intensity of the dimensional quotient in compared with the anode to cathode surface ratio. Three different experiments are considered with the same surface area of anode in order to prove the efficiency of time intervals for adding hydrogen peroxide in moderate values of the pollutant removal efficiencies which are achieved in Stage 1-1, 1st objective. The reason of choosing moderate experimental condition is providing the worst possible scenario to eliminate other possible enhancement and allocate significant consideration on the time intervals of adding hydrogen peroxide effectiveness. The experiments are designed considering the anode surface area as 57.75 cm². In addition, three distinct time intervals of adding hydrogen peroxide are implemented such as 24, 12, and 6 hours, respectively. Also, the same type of cathode is utilized (mesh stainless steel with 68.25% void space) with the same dimensional quotient (DQ=1). The experimental design parameters for Stage 1-2 are described in Table 3-5.

Table 3- 5 Experimental design and operating conditions of the Phase 1, Stage 1-2; impact of time intervals for hydrogen peroxide supply

No. of experiment	Distance between electrodes [cm]	Cathode type [Stainless Steel]	Exposure surface area of anode [cm ²]	Exposure surface area of cathode [cm ²]	Anode to cathode area ratio	Time interval of adding hydrogen peroxide [h]	$\left(\frac{H_a}{H_c} / \frac{W_a}{W_c}\right)$	Exposure time [h]
24	5.00	Mesh (68.25%)	57.75	18.48	3.125	24	1.00	72.00
29						12		
30						6		

The second matrix parameter of the first phase is associated with impact of pretreatment of the present sulfate in the influent, Stage 1-3. Two different molar ratios of barium hydroxide (Ba(OH)₂) to volume of the influent are introduced to the system by pretreating the influent for removing sulfate (See Tab. 3-1). The two mentioned molar ratios are 1:1 and 2:1 respectively. Moreover, the best experimental operating condition regarding promising attained removal

efficiency of the pollutant (Exp. 19) is utilized in two experiments and the results are compared with the pointed reference experiment (Exp. 19). The final remaining concentrations of sulfate are analyzed [3-2] and the results indicate the presence of 365 mg/L sulfate for 1/1 molar ratio and 169 mg/L sulfate for 2/1 molar ratio, respectively. In addition, all experiments are operated with the same surface area of anode (78.75 cm²) while the dimensional quotient is set as 1 and the same cathode type (mesh stainless steel with 68.25 % void space) is utilized. The operating conditions and associated experimental design parameters are explained in Tab 3.5. The time interval of adding hydrogen peroxide is fixed at 24 hours and the distance between electrodes is fixed at 5 cm while the current density is 33.33 mA/cm².

Table 3- 6 Experimental design and operating conditions of the Phase 1, Stage 1-3; impact of pretreatment of the present sulfate in the influent

No. of experiment	Cathode type [Stainless Steel]	Exposure surface area of anode [cm ²]	Exposure surface area of cathode [cm ²]	Anode to cathode area ratio	Barium hydroxide molar ratio	Mass of added barium hydroxide [g]	$\left(\frac{Ha}{Hc} / \frac{Wa}{Wc}\right)$	Exposure time [h]
19	Mesh (68.25%)	78.75	25	3.15	0/1	0	1.00	72.00
20					1/1	6.88		
21					2/1	13.76		

The last matrix parameter is the impact of adding the Fenton agent, Stage 1-4. Due to the presence of a relatively high concentration of ferrous ions in the influent (4190 mg/L Fe²⁺), no Fenton agent is added to the process in previous experiments; while, the approach of the Stage 1-4 showed the combined effect of adding Fenton and hydrogen peroxide. In addition, applied Fenton agent is in the form of ferrous sulfate (FeSO₄). The optimal molar ratio of added ferrous ions to hydrogen Peroxide (Fe²⁺/H₂O₂) is equal to 0.05 which is achieved in the previous research on the same influent [1-13].

The best experimental design is related to Exp.19 in which all reactor design parameters of the first phase demonstrate the best interaction expected effects. The Fenton agent (ferrous sulfate) is mixed with the influent by mixing with a magnetic stirrer at room temperature (20 °C) and it is added for one time before the experimental run is started. In contrast, the hydrogen peroxide is added daily (each 24 hours).

The current density and distance between electrodes are fixed at 33.33 mA/cm² and 5 cm respectively. In addition, the same cathode type of mesh stainless steel (68.25 % void space) is used for both Exp.19 and Exp.37. The experimental design and operating conditions of the Stage 1-4 is described in Table 3-7.

Table 3- 7 Experimental design and operating conditions of the Phase 1, Stage 1-4; impact of adding Fenton agent

No. of experiment	Exposure surface area of anode [cm ²]	Exposure surface area of cathode [cm ²]	Anode to cathode area ratio	Ferrous ions to hydrogen peroxide molar ratio	Mass of added ferrous sulfate [g]	$\left(\frac{Ha}{Hc} / \frac{Wa}{Wc}\right)$	Exposure time [h]
19	78.75	25	3.15	0/1	0	1.00	72.00
37				0.05/1	3.01		

Stage 1-5, impact of current density variation is placed in the interrelated reactor design and matrix parameters. It is crucial to mention that all previous described experiments in section 3-2-1 have been determined based on the optimal results for current density which is achieved in Stage 1-5.

The main approach is considering the same surface area of anode and cathode while the current density is varied among four distinct values to set the optimal one for further experimental design. The four values are 33.33, 37.70, 22.22, and 27.77 mA/cm², respectively. The logic underlies

selecting the mentioned values for the current density follows the research on the electrochemical treatment of the leather industry wastewater with the relatively similar pollutants [3-3]. The initial concentration of TKN and ammonia in the cited research are 180 mg/L and 30 mg/L respectively. The mentioned values are around 78 and 367 times lower than the concentration of TKN and ammonia of influent which is studied in this research. The improvement of TKN removal efficiency is observed while the applied current density is 20 mA/cm², and the optimal removal efficiency is achieved in 50 mA/cm² [3-3]. Therefore, four values were selected in 20 to 50 mA/cm² ranges considering also the limitation of equipment and energy consumption costs. The exposure surface area of anode and cathode are considered as constant values while the current density was varied among four different numbers. The details of experimental design and specifications of stage 1-5 are described in Table 3-8.

Table 3- 8 Experimental design and operating conditions of the Phase 1, Stage 1-5; impact of current density variation

No. of experiment	Current density [mA/cm ²]	Exposure surface area of anode [cm ²]	Exposure surface area of cathode [cm ²]	Anode to cathode area ratio	Applied current [A]	$\left(\frac{H_a}{H_c} / \frac{W_a}{W_c}\right)$	Exposure time [h]
1	33.33	57.75	25	2.31	1.92	1.31	72
2	37.7				2.17		
3	22.22				1.28		
4	27.77				1.60		

The air diffusion introduces the oxygen to the reaction to act as an oxidizing agent. Stage 1-6 is the last stage of the small scale which fits in the interrelated reactor design and matrix parameters. The previous research on the same wastewater proved that using air diffusion does not improve the removal efficiency [1-13]. However, the anode type of the above cited thesis was platinum and there was no experimental result on implementing air diffusion while the anode type is graphite.

Two different air flowrate which has been classified as high (152.6 mL/min) and low rate (83.4 mL/min.) are diffused from a perforated plastic pipe. The array of the holes is distributed on the top side of the pipe (ID 8 in and OD 16 in) while they have been placed in two parallel line with the 0.5 cm distance from the downward hole and the hole diameter of 1 mm. In addition, the phase angle of each hole is π radians. The surface area of anode has been chosen based on the optimal current density (33.33 mA/cm²). The corresponded surface exposure area of anode is 57.75 cm² and the cathode one is 25 cm². The experimental design parameters of Stage 1-6 are described in Table 3-9.

Table 3- 9 Experimental design and operating conditions of the Phase 1, Stage 1-6; impact of continuous airflow diffusion

No. of experiment	Current density [mA/cm ²]	Exposure surface area of anode [cm ²]	Exposure surface area of cathode [cm ²]	Anode to cathode area ratio	Air flow rate [mL/min]	$\left(\frac{Ha}{Hc} / \frac{Wa}{Wc}\right)$	Exposure time [h]
1	33.33	57.75	25	2.31	N/A	1.31	72
7					152.6		
10					83.4		

3-2-2. Reactor and experimental design of Phase 2

The medium scale experiments in Phase 2 are classified in to two main subcategories such as i) reactor design; ii) relationship between reactor design and matrix parameters. The exposure volume of the designed reactor for medium scale runs (Figure 3-6) is 2.2 L. In addition, time interval of adding hydrogen peroxide is 24 hours for all Phase 2 related experiments.

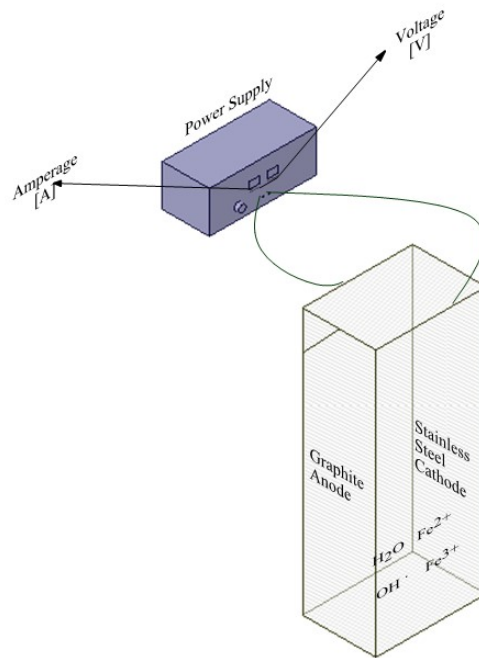


Figure 3- 6 Schematic of medium scale electrokinetic cell with 2.2 L volume

The first subcategory of study of reactor design parameters, involves two stages and both have been investigated in an integrated experimental configuration. The first stage, Stage 2-1, is mainly discussed about the impact of anode to cathode surface area ratio and the geometry of the electrodes. Preliminary experiments of the medium scale, proves that using mesh stainless steel as a cathode material would not be suitable. The reason is related to upscaling the reactor dimensions, which provide a higher surface area of anode. As a result, the product of current density and surface area of anode will lead to achieve higher applied current. The mesh stainless steel cathode could not stand the higher DC current due to significant amount of corrosion. Therefore, the alternative electrode would be stainless steel plate. As a result, the determined dimensionless number of “Dimensional Quotient” which have been discussed in Section 3-2-1, come into consideration. The fact that the best results are achieved with $DQ=1$ in small scale, leads the research to involve the higher exposure area by using graphite rods with the diameter of 2.54 cm (Exp.28) to keep the

DQ constant and investigate the impact of higher surface area ratio. Graphite plate is applied for anode in the second experiment (Exp.42). Due to the fact that dissimilar gravity forces may result because of different masses for both graphite rods and graphite plate, the height of exposure will be differed. Therefore, different exposure surface areas of cathodes are also expected. The experimental design and the specification of experiments are explained in Table 3-8.

Stage 2-2 is also categorized as reactor design parameters in which the “distance between electrodes” have been discussed. The reason is using carbon rods as the anode (Exp.28) increases the thickness of the anode, while a distance between electrodes is affected. However, the mentioned influence has been considered in the design and the width of the reactor is 7.54 cm which fixed the distance between electrodes on 5 cm value (the optimal distance between electrodes of the small scale study). The second experiment (Exp.42) that is also regarded as Stage 2-1 experiments, is using a graphite plate as anode. The thickness of utilized graphite plate is 1.27 cm ($\frac{1}{2}$ in). As a result, the distance between electrodes would be 6.27 cm. The variation of the distance is considered to determine different current density. The mentioned scenario will be discussed in Stage 2-3. Since both Stage 2-1 and Stage 2-2 objectives have been investigated by the same experimental design, the specifications and details of the relevant experiments for both stages are described in Table 3-10.

Table 3- 10 Experimental design and operating Conditions of the Phase 2, Stage 2-1 and 2-2; impact of anode to cathode surface ratio, the geometry of electrodes and distance between electrodes

No. of experiment	Distance between electrodes [cm]	Applied current density [mA/cm ²]	Exposure surface area of anode [cm ²]	Exposure surface area of cathode [cm ²]	Anode to cathode area ratio	$\left(\frac{Ha}{Hc} / \frac{Wa}{Wc}\right)$	Exposure time [h]
28	5	21.37	490.75	315.18	1.56	1	72
42	6.27	33.33	358.75	358.75	1		

The impact of current density variation, Stage 2-3, fits to the interrelated reactor design and matrix parameters subcategory. Three values have been set for current density. The first value is attributed to Exp,28 which is 21.37 mA/cm^2 . The logic beyond selecting the mentioned value is related to reverse search techniques in which the new optimal value will be set based on neighbor counter [3-4]. The Stage 2-3 experimental configuration is adapted from the cited article. The previous small scale optimal current density is 33.33 mA/cm^2 . The trend is considering a plate with the same height and width like the six carbon rods, calculating the tantamount surface area and finding the compensate applied current amperage based on 33.33 mA/cm^2 . The current will be set as the calculated value. Thereafter, the new current density will be calculated based on the real surface area of six carbon rods. The resultant value will be the true current density and the amount is 21.37 mA/cm^2 . The achieved removal efficiency shows significant improvement that proves the validity of experimental design logic. The second attempt is trying to reduce the current density in order to minimize the energy consumption as much as possible. Therefore, the similar approach is applied, however the input current density is set as the optimal value of current density gained in Exp.28 (21.37 mA/cm^2). The applied current will be 6.73 A. Therefore, the calculated true current density for actual surface area of six carbon rods with diameter of 2.54 cm (1 in) would be 13.72 mA/cm^2 . The last related experiment (Exp.42) in which the optimal current density of small scale (33.33 mA/cm^2) is applied, is associated with using graphite plate at a thickness of 1.27 cm ($1/2$ in). Since two parameters (distance between electrodes and current density) are changed at the same time, investigating the impacts of both parameters becomes complex. According to sensitivity analysis of distance between electrode that has been done in previous research on the same wastewater utilizing similar electrodes [1-13], the removal efficiency of TKN decreased once the distance exceeds more than 5 cm. Therefore, the increase in distance between electrodes would be expected

to cause negative influence on removal efficiency. The experimental configuration of the Stage 2-3, the impact of current density variation, are described in Table 3-11

Table 3- 11 Experimental design and operating conditions of the Phase 2, Stage 2-3; impact of current density variation

No. of experiment	Current density [mA/cm ²]	Exposure surface area of anode [cm ²]	Exposure surface area of cathode [cm ²]	Anode to cathode area ratio	Applied current [A]	$\left(\frac{Ha}{Hc} / \frac{Wa}{Wc}\right)$	Exposure time [h]
28	21.37	490.75	315.18	1.56	10.49	1	72
41	13.72				6.73		
42	33.33	358.75	358.75	1	11.96		

The last stage of the medium scale experiment which is classified as interrelated design and matrix parameters, is the impact of continuous airflow diffusion. The experimental design of the best achieved removal efficiency (Exp.28) is considered for Exp.38. The installed air diffuser provides air bubbles with the flowrate of 4416 ml/min and no hydrogen peroxide is added. The experimental design and configuration of the Stage 2-4, the impact of continuous airflow diffusion, are described in Table 3-12.

Table 3- 12 Experimental design and operating conditions of the Phase 2, Stage 2-4; impact of continuous air flow diffusion

No. of experiment	Current density [mA/cm ²]	Exposure surface area of anode [cm ²]	Exposure surface area of cathode [cm ²]	Anode to cathode area ratio	Air flow rate [mL/min]	$\left(\frac{Ha}{Hc} / \frac{Wa}{Wc}\right)$	Exposure time [h]
28	21.37	490.75	315.18	1.56	N/A	1	72
38					4416		

3-2-3. Reactor and Experimental Design of Phase Three

The large scale experiments are mainly focused on Phase 4, sequential batch reactor (SBR) rather than conventional batch one (Phase 3). Considering a sharp border between conventional large scale experiments and SBR large scale experiment is also complex in this research. However, primary experiments can be classified as conventional large scale experiments which will be discussed in Section 3-2-3. In addition, the first SBR cycle of the commensurate experiments of the Phase 4 can be considered as a comparison of results for Phase 3 experiments. The electrode configuration is illustrated in Figure 3-7 in which two graphite plate are utilized as anode and the sidewall anode has 1.27 cm ($\frac{1}{2}$ in) thickness and the middle one thickness is 1.59 cm ($\frac{5}{8}$ in). Two stainless steel plates are placed at a determined distance (5 or 7.5 cm) from the anode. Due to the fact that the middle electrode is fully exposed to the influent, the involved surface area is considered as the summation of two exposed front sides surface areas (height*width) and the exposed edge surface areas (thickness*height). As a fixed matrix parameter, the hydrogen peroxide adding time interval is 12 hours in all large and EF-SBR large scale experiments. Finally, due to the optimal achieved value for current density in medium scale experiments, 21.37 mA/cm², is fixed as the current density in all large and EF-SBR large scale experiments.

The optimal dimensional quotient (DQ) is achieved in both small and medium scale experimental investigation once it is set as one. The distance among electrodes, (Stage 3-1) is the only parameter which is investigated as the reactor design parameter for the large scale experiments. Two different distances among electrodes were considered. The first obtained distance is 7.5 cm for 6.4 L influent and the second one is 5cm for 5.8 L influent.

A different acquisition of the initial influent volume may cause inaccuracy for the comparative study. However, three regions of study are expected in each reactor which will appease the

intensity of influence in the final remained pollutant concentration. It means that the 600 mL extra volume is divided in three regions when 5.8 L which is considered as a reference one. Therefore, each region will contain extra 200 mL; the resultant volume of each region surges from 1933 to 2133 mL. A safety margin of 5 cm height of vacant space is essentially needed to avoid overflow of gaseous and resultant foam production in the first day of the reaction. So, considering the varied volume of influent in different electrode configurations is unavoidable. The experimental design of Stage 3-1 experiments is described specifically in Table 3-13.

Table 3- 13 Experimental design and operating conditions of the Phase 3, Stage 3-1; Impact of distance among electrodes

No. of experiment	Distance among electrodes [cm]	Applied current density [mA/cm ²]	Exposure surface area of NA* and TA**[cm ²]	Exposure surface area of cathode [cm ²]	Applied current for NA* and TA** [A]	Anode to cathode area ratio of NA and TA	Exposure time [h]
34	7.5	21.37	305.92;687.36	305.92;305.92	6.84;14.54	1/1;	72
40	5.0		345.60;776.52	345.6;345.60	7.38;16.59	2.24/1	

* NA: Narrow anode; **TA: Thick anode

The impact of hydrogen peroxide purity, Stage 3-2, is categorized as matrix parameters. The implemented purities are 30% and 50% respectively. The fact that hydroxyl radicals act as oxidizing agent, which predominantly control the oxidation reduction potential, mineralization and the rate of oxidation, makes the hydrogen peroxide purity role so vital in understanding the mechanism of reactions. The higher purity will strength the influence of hydroxyl radicals and the presence of mass unit in each unit of volume (mg/L) will increase in compared with 30% purity standard solution. Therefore, investigating the response of the occurred reactions in the system by providing higher purity of hydrogen peroxide comes into consideration. The distance between electrodes is fixed at 5 cm and the current density is 21.37 mA/cm². The molar ratio of adding

hydrogen peroxide is also fixed at $3.81/1 \frac{H_2O_2}{Fe^{2+}}$ to eliminate the influence of its molar ratio variation on the experimental results. The present ferrous ions in the raw wastewater is considered as the reference moles. It should be mentioned that all the experiments of Stage 3-2 and 3-3 have the same initial exposure volume of 5.8 L. The experimental design and specifications of operation of Stage 3-2 are described in Table 3-14.

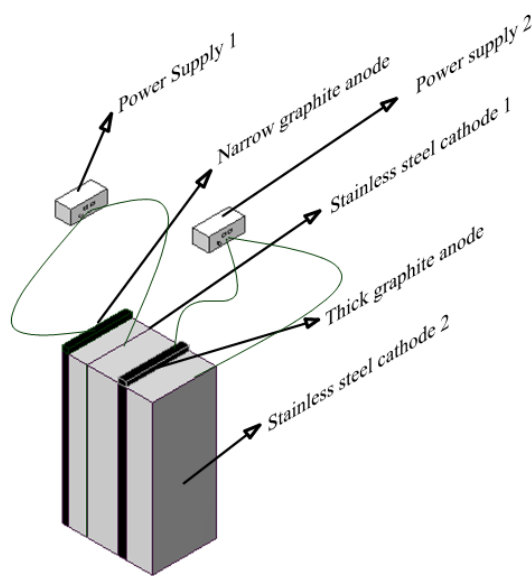


Figure 3- 7 Schematic of large scale electrokinetic cell with 5.8 L volume; the exposure areas of the electrodes are from the side of width* height of the exposure

Table 3- 14 Experimental design and operating conditions of Phase 3, Stage 3-2; impact of hydrogen peroxide purity

No. of experiment	Initial exposure surface area of NA* and TA** [cm ²]	Initial exposure surface area of cathode of cathode [cm ²]	Anode to cathode area ratio of NA and TA	Hydrogen peroxide purity [%]	Time interval of adding hydrogen peroxide [h]	Molar ratio of $\frac{H_2O_2}{Fe^{2+}}$	Exposure time [h]
40	345.60;776.52	345.6;345.60	1/1; 2.24/1	50	12	3.81/1	72
47				30			

* NA: Narrow anode**TA: Thick anode

The molar ratio of hydrogen peroxide to the exposure volume is investigated in Stage 3-3. The fact that the process upscaling faces the nonlinearity, setting the molar ratio of hydrogen peroxide 1:1 will not be a practical approach. To make a juxtaposition of applying two different molar ratios feasible, two different experiments are designed. The hydrogen Peroxide molar ratio of the first experiment (Exp. 36) is set as 3.44:1 ratio and the second one (Exp.40) molar ratio is 1.11/1. The distance between electrodes is fixed at 5 cm and the applied current density is 21.37 mA/cm². The time interval of adding hydrogen peroxide and its purity is also set as 12h and 50 % respectively. As it is expected for all experiments of large scale phase, the dimensional quotient (DQ) is set as 1. The specified details of experimental design and operating conditions of Stage 3-3 are described in Table 3-15.

Table 3- 15 Experimental design and operating conditions of Phase 3, Stage 3-3; Impact of hydrogen peroxide molar ratio

No. of experiment	Initial exposure surface area of NA* and TA** [cm ²]	Initial exposure surface area of cathode [cm ²]	Anode to cathode area ratio of NA and TA	Hydrogen peroxide purity [%]	Time interval of adding hydrogen peroxide [h]	Molar ratio of $\frac{H_2O_2}{Fe^{2+}}$	Exposure time [h]
36	345.60;776.52	345.6;345.60	1/1; 2.24/1	50	12	3.44/1	72
40						3.81/1	

* NA: Narrow anode**TA: Thick anode

3-2-4. Reactor and experimental design of Phase 4

The fourth phase of study is constituted from two subdivisions. The first subdivision is allocated for investigation of using the electro-Fenton sequential batch reactor (EF-SBR) at medium scale and the second one is contributed to applying EF-SBR at large scale. Conventional SBR is widely used for biological treatment of wastewater, dye, and landfill leachate; it might be applicable in both aerobic and anaerobic setups. SBR process consists of five stages: 1. Fill, 2. React, 3. Settle,

4. Decant, 5. Idle. No electrokinetic sequential batch reactor was designed so far to my knowledge. The proposed process for an electro-Fenton sequential batch reactor consists of several cycles, each of them has 3 stages: 1. Fill, 2. React, 3. Decant. The first cycle of the EF-SBR is designed for 72 hours and the remaining cycles (cycle 2 and cycle 3) are defined for 48 hours. Conclusions from Phases 1, 2, and 3 with respect to best technological parameters were applied to design the EF-SBR in order to remove TKN, ammonia, and organic nitrogen.

The 5.8 liters of influent is the exposure volume of the first cycle for large scale and 2.2 L is initial volume of the medium scale. After 72 hours, once the first cycle is finished, 75% of volume is decanted and 25% of effluent remains in reactor, then, 75% of free space is filled with fresh wastewater. It is important to mention that the remained volume in the reactor is calculated based on the final cycle 1's volume, not initial one. In fact, due to liquid to vapor phase exchange which takes place during the treatment, makes the remained volume be differ from initial influent one. Therefore, if the reference volume is considered as initial influent volume of the large scale EF-SBR, the remained effluent volume will be varied between 13.2% to 17 %. Thus, it is expected to reduce the residence time for one day (24 hours) by keeping a specific volume of effluent for initiating the proper reaction condition of the removal of the pollutants. The schematics of the reactors are illustrated in Figure 3-8 m which two complete cycles of EF-SBR are described.

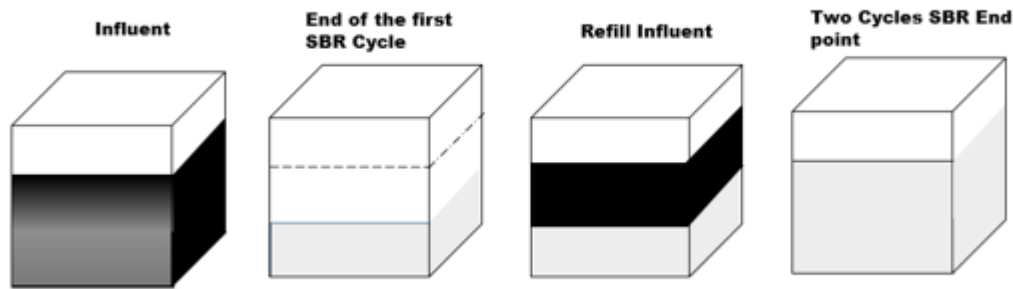


Figure 3- 8 Schematic concept of electro Fenton sequential batch reactor (EF-SBR); the reactor is refilled after the first 72 hours (end of the first cycle) and the second cycle of SBR is ended after 48 hours

The electrode configuration and initial experimental design of both medium and large scale EF-SBR are the same as described in concept designs in Sections 3-2-2 and 3-2-1, respectively. For the medium scale, the graphite plate has been used as the anode and the distance between electrodes is set as 6.27 cm.

The impact of hydrogen peroxide purity, Stage 4-1, is one of the determining concerns which directly addresses the appropriate reaction initiating condition. The mentioned parameter is fully investigated for both medium and large scale EF-SBR while two distinct purity percentages of 30 and 50 are considered respectively. Experimental design of the medium scale EF-SBR investigating the impact of hydrogen peroxide purity is described in Table 3-16. In addition, the full detailed explanation of experimental design of the large scale EF-SBR considering the same objective is provided in Table 3-17. It should be mentioned that two cycles of EF-SBR (Exp.45) are compared with Exp.42 at medium scale.

The last parameter that is experimentally investigated in the Phase 4 is the impact of SBR cycles, Stage 4-2. The expected objectives are reducing the time exposure for 24 hours and observing the

removal efficiency enhancement of the reaction in each specific cycle of the SBR. 4 cycles of SBR proceeded for the medium scale in which the volume of remaining effluent is varied based on the last observed volume prior to the new SBR cycle start point. Also, 3 cycles of SBR were applied at large scale. The EF-SBR objectives are expected to result in a significant decline in energy consumption as a direct impact of the exposure time decrease. The experimental designs of Stage 4-2 are completely described in Tables 3-18 and 3-19 for medium and large scales, respectively.

Table 3- 16 Experimental design and operating conditions of the Phase 4, Stage 4-1; impact of hydrogen peroxide purity on medium-scale EF-SBR removal efficiency

No. of experiment	Applied current Density [mA/cm ²]	Exposure surface area of anode [cm ²]	Exposure surface area of cathode [cm ²]	Anode to cathode area ratio	Hydrogen peroxide purity [%]	No. of cycles	$\left(\frac{Ha}{Hc} / \frac{Wa}{Wc}\right)$	Exposure time [h]
42	33.33	358.75	358.75	1/1	30	4	1	72+48
45					50	2		

* NA: Narrow anode; **TA: Thick anode

Table 3- 17 Experimental design and operating conditions of the Phase 4, Stage 4-2; impact of hydrogen peroxide on large-scale EF-SBR removal efficiency

No. of experiment	Applied current density [mA/cm ²]	Initial exposure surface area of NA [*] and TA ^{**} [cm ²]	Initial exposure surface area of cathode [cm ²]	Anode to cathode area ratio of NA and TA	Hydrogen peroxide purity [%]	No. of cycles	$\left(\frac{Ha}{Hc} / \frac{Wa}{Wc}\right)$	Exposure time [h]
44	21.37	345.60;776.	345.6;345.6	1/1;	50	2	1	72+48
46		52		2.24/1	30			

* NA: Narrow anode; **TA: Thick anode

Table 3- 18 Experimental design and operating conditions of the Phase 4, Stage 4-2; impact of SBR cycles on medium-scale EF-SBR removal efficiency

No. of experiment	Applied current density [mA/cm ²]	Exposure surface area of anode [cm ²]	Exposure surface area of cathode [cm ²]	Anode to cathode area ratio	Hydrogen peroxide purity [%]	No. of cycles	$\left(\frac{Ha}{Hc} / \frac{Wa}{Wc}\right)$	Exposure time [h]
42	33.33	358.75	358.75	1:1	30	2	1	72+48
42*						4		72+48+48+48

* NA: Narrow anode; **TA: Thick anode

Table 3- 19 Experimental design and operating conditions of the Phase 4, Stage 4-2; impact of SBR cycles on large-scale EF-SBR removal efficiency

No. of experiment	Applied current density [mA/cm ²]	Initial exposure surface area of NA* and TA** [cm ²]	Initial exposure surface area of cathode [cm ²]	Anode to cathode area ratio of NA and TA	Hydrogen peroxide purity [%]	No. of cycles	$\left(\frac{Ha}{Hc} / \frac{Wa}{Wc}\right)$	Exposure time [h]
46	21.37	345.60;	345.6; 345.6	1/1;	30	2	1	72+48
46*		776.52		2.24/1		3		72+48+48

* NA: Narrow anode; **TA: Thick anode

3-3. Experimental Analysis Methods

Due to the high required precision for measuring pollutants concentration, appropriate methods of analysis are required. The TKN, ammonia, nitrate, sulfate, and total nitrogen methods of analysis are presented in Table 3-20 while the principles of measurement for each specific method are described. Measuring pH, oxidation reduction potential (ORP), temperature and conductivity also helps to resolve and capture the reactions that have taken place during of the process. The Hach CDC40101 IntelliCAL lab conductivity probe was used for conductivity measurement and Hach MCT10101 IntelliCAL ORP lab probe for ORP. The temperature and pH are measured with built-

in ACT probe at the same time in order to minimize the possible error which originated from temperature fluctuations.

Table 3- 20 Analysis methods of measuring pollutant concentration

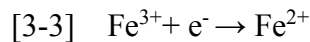
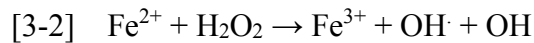
Method Name	Principles of the Measurements	Measurable Components	References
Nitrogen, Simplified TKN (s-TKN™), Method 10242	Total Kjeldahl Nitrogen (TKN) is the sum of organic nitrogen and ammonia. In the simplified TKN method, inorganic and organic nitrogen are oxidized to nitrate by digestion with peroxydisulfate. The nitrate ions react with 2,6-dimethylphenol in a solution of sulfuric and phosphoric acid to form a nitrophenol. Oxidized forms of nitrogen in the original sample (nitrite + nitrate due to sample preservation) are determined in the second test vial and then subtracted, which results in TKN.	TKN, Summation of Nitrate and Nitrite, Total Nitrogen	[3-5]
Nitrogen, Ammonia-Salicylate HR Method 10205	Ammonium ions react at pH 12.6 with hypochlorite ions and salicylate ions in the presence of sodium nitroprusside as a catalyst to form indophenol. The amount of color formed is directly proportional to the ammonia nitrogen present in the sample.	Ammonia (Ammoniacal Nitrogen)	[3-6]
Nitrate, Dimethylphenol HR Method 10206	Nitrate ions in solutions that contains sulfuric and phosphoric acids react with 2,6-dimethylphenol to form 4-nitro-2,6-dimethylphenol.	Nitrate	[3-7]
Sulfate, Turbidimetric HR Method 10227	Sulfate ions in the sample react with barium chloride in aqueous solution and form a precipitate of barium sulfate. The resulting turbidity is measured photometrically at 880 nm.	Sulfate	[3-8]

3-4. Electrochemical reactions

The governing process of organic and inorganic pollutants removal of this study is electro-Fenton/oxidation. Due to the fact that the wastewater of the research contains iron and the system provide conditions where iron is in ionic form, the homogenous catalytic reactions are expected to take place while the demand of adding Fenton agent is removed from the initial conditions required. The kinetics of pollutants removal reactions will be discussed while the diffusion will be investigated theoretically.

3-4-1. Electro-Fenton Reactions

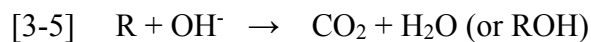
The Electro-Fenton is an indirect oxidation that generates hydrogen peroxide by the reduction of oxygen at electrode surface (Eq.3-1). Then, the oxidizing power is improved by the production of OH radicals in bulk solution through Fenton reaction (Eq.3-2). This reaction is catalyzed from the electrochemical regeneration of ferrous ions (Eq. 3-3).

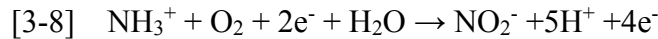
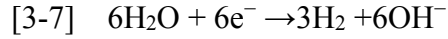


Hydroxyl radicals lead the process to a higher oxidation potential level, and ferric ions are produced in the result of potential oxidation increase (Eq. 3-4). Effective destruction of wastewater contaminants is due to generation of highly reactive radicals (HO·), a powerful oxidizing agent.



Hydroxyl radicals react with persistent organics and may mineralize into inorganic ions. Electro-Fenton process removes organic nitrogen (Eq.3-5)^[2-118], ammonia (Eq. 3-6 and 3-7)^[3-10], and TKN (Eq. 3-8)^[3-9] in the following equations:





If TKN contains derivatives of amides, Fenton process makes more complex. The amides oxidation needs a high oxidation-reduction potential (ORP) to initiate its degradation [3-11]. The proposed method of treatment should provide conditions adjusted to amide (or their derivatives) degradation. Sun and Pignatello [2-71] showed that Fenton's reaction can be well applied in acidic pH 2.8–3.0.

3-4-2. Mass Transfer

Based on the time dependent (TD) Fickian diffusion, if it is considered that diffusing species k passing through a rectangular volume element as it is illustrated in Figure 3-9, the diffusion equation would be described as follows [3-12]:

$$[3-9] \quad f_k(x) = -D_k \frac{\partial c_k(x)}{\partial x} \quad \text{Inward flux}$$

$$[3-10] \quad f_k(x+dx) = -D_k \frac{\partial c_k(x+dx)}{\partial x} \quad \text{Outward flux}$$

$$[3-11] \quad c_k(x+dx) \cong c_k(x) + \frac{\partial c_k(x)}{\partial x} dx \quad \text{Taylor theorem expansion for concentration}$$

$$[3-12] \quad f_k \cong f_k(x) - f_k(x+dx) \quad \text{Fickian Diffusion}$$

After substitution Eq.3-11 in Eq.3-10, the derived equation for Fickian diffusion equations (Eq.3-13a, Eq.3-13b) based on Eq.11 would be as follows:

$$[3-13a] \quad f_k = -D_k \frac{\partial c_k(x)}{\partial x} - \left\{ -D_k \frac{\partial}{\partial x} \left(c_k + \frac{\partial c_k(x)}{\partial x} dx \right) \right\} .$$

$$[3-13b] \quad f_k = -D_k \frac{\partial^2 c_k(x)}{\partial x^2} dx$$

And finally, the derived equation is:

$$[3-14] \quad \frac{\partial f_k}{\partial x} = -D_k \frac{\partial^2 c_k(x)}{\partial x^2}$$

Based on the continuity equation it can be interpreted that:

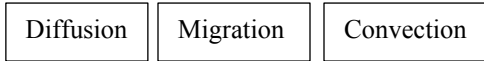
$$[3-15] \quad \frac{\partial f_k}{\partial x} = \frac{\partial c_k}{\partial t}$$

So, the one dimensional and three dimensional time dependent Fickian diffusion will have the following equations respectively:

$$[3-16a] \quad \frac{\partial c_k}{\partial t} = -D_k \frac{\partial^2 c_k}{\partial x^2} \quad \text{1-D TD Fickian diffusion}$$

$$[3-16b] \quad \frac{\partial c_k}{\partial t} = -D_k \nabla^2 c_k \quad \text{3-D TD Fickian diffusion}$$

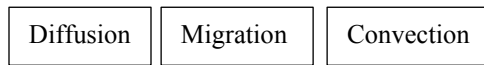
There are three terms which are associated with the fluxes that appeared in the electrochemical reactions which are specified in Eq.3-17. The first term is completely derived through above equation which is stand for diffusion term. The second term is migration and it appears once charged species move under the influence of a gradient in electrochemical potential with a driving force F . Finally, the third term is strongly dependent on fluid dynamics associated with parameters (like mixing and solution velocity) or emerges in importance once the electrodes are rotating. The full equations of fluxes are provided as followed ^[3-13]:



$$[3-17a] \bar{f}_j = -D\nabla c_j - \frac{z_j F}{RT} D_j c_j \nabla \varphi + c_j \bar{\vartheta} = f_{j,D} + f_{j,M} + f_{j,C}$$

Continuity equation relates time rate of change of species concentration with the divergence of the material flux.

$$[3-17b] \frac{\partial c_j}{\partial t} = -\nabla \cdot \bar{f}_j$$



$$[3-17c] \frac{\partial c_j}{\partial t} = D_j \nabla^2 c_j + D_j \frac{z_j F}{RT} \nabla \cdot (c_j \nabla \varphi) - \nabla \cdot (c_j \bar{\vartheta})$$

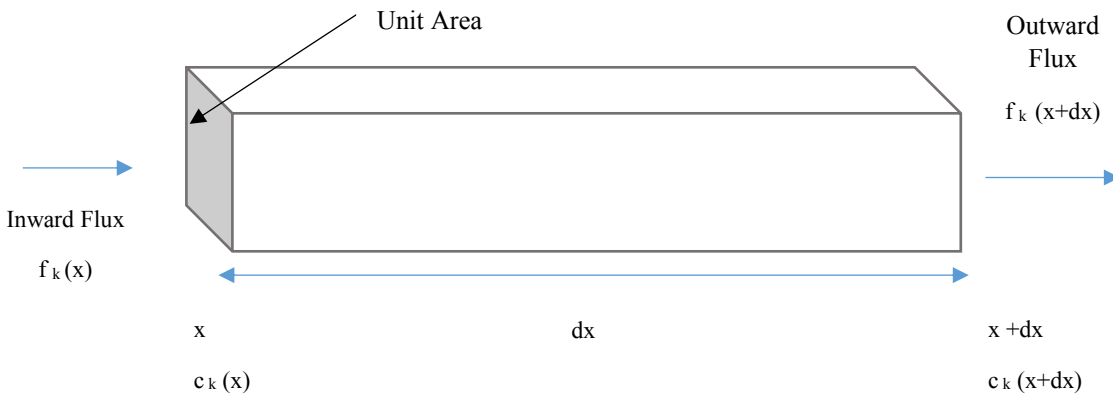


Figure 3- 9 Schematic of time dependent Fickian diffusion volume element

However, it is possible that the diffusion coefficient is time dependent and considering it as constant would not be a practical right approach. Due to the fact that diffusion coefficient is strongly dependent on kinetics of the reactions, once kinetics become nonlinear, the diffusion coefficient will also vary with respect to time.

Wu and Berland [3-14] fully described the method of determining time dependent diffusion as “In systems where particles or molecules diffuse without restrictions via Brownian dynamics, the mean-square displacement (MSD) of the particles in n-dimensional space is proportional to time, written as $\langle \Delta r^2 \rangle = 2nDt$; where D and t signify the diffusion coefficient and time, respectively. In the case of anomalous diffusion, the MSD does not increase linearly with time.

The fluorescence correlation spectroscopy (FCS) can directly measure the anomalous diffusion experimentally. The model which is widely used for FCS anomalous diffusion measuring is considering MSD versus time as a power law scaling. The applied model is as follows:

$$[3-18] \langle \Delta r^2 \rangle = \Gamma t^\alpha$$

Where α is an anomalous exponent and it determines whether the mobility is called anomalous subdiffusion ($\alpha < 1$) or superdiffusion ($\alpha > 1$). The constant prefactor Γ is usually considered as transport factor and it has the dimensions of length-squared per fractional time. The physical properties of diffusive motion are designated by a density distribution function as followed which is called propagator, $f(\hat{r}, (t + \tau) | r, t)$.

The propagator solves the diffusion equation and specifies the probability that a particle located at position r at time t , will be found at position \hat{r} at time $t + \tau$. For normal Brownian motion, the propagator is a Gaussian distribution. In general, the standard diffusion coefficient defined by Fick's law, and the corresponding diffusion equation cannot describe the nonlinear time dependent MSD, and there is no simple comparable propagator for anomalous diffusion, although many sophisticated approaches have been introduced to model anomalous dynamics.

A mathematically simplified approach that is commonly used to model anomalous diffusion defines a time-dependent diffusion coefficient $D(t)$ based on the partial power-law dependence of

the MSD as in Eq. 16. Assuming no spatial heterogeneity in $D(t)$, one can then obtain an extended diffusion equation from Fick's first law and the continuity equation as follows ^{[3-15],[3-16]}:

$$[3-19] \frac{\partial}{\partial t} f(\hat{r}, (t + \tau)|r, t) = D(t)\nabla^2 f(\hat{r}, (t + \tau)|r, t)$$

The most accurate physically correct pathway to solve the above equation is determining the instantaneous diffusion coefficient defined in terms of the time-dependent slope of MSD versus time following the equation 3-20 ^[3-17]:

$$[3-20] D_{\text{ins}}(t) = \frac{1}{2n} \frac{\partial \langle \Delta r^2 \rangle}{\partial t} = \frac{\alpha}{2n} \Gamma t^{\alpha-1}$$

If Eq.3-18 is used for $D(t)$ in Eq.3-17, the anomalous diffusion propagator is easily obtained by standard methods, yielding

$$[3-21] f(\hat{r}, (t + \tau)|r, t) = \frac{1}{\left(\frac{2n\Gamma\tau^\alpha}{n}\right)^{n/2}} \exp\left(\frac{-|r-\hat{r}^2|}{\frac{2\Gamma\tau^\alpha}{n}}\right)$$

The above mentioned equation solves the extended diffusion equation and produces the correct power law scaling of MSD versus time (τ), removing widespread confusion regarding whether or not this propagator can be used legitimately for data analysis. Furthermore, this exact solution to the extended diffusion equation allows precise clarification of the definition of the FCS diffusion time and its relation to the anomalous exponent and transport factor. Furthermore, with this exact solution, the correct constant factors for diffusion in two ($n=2$) or three ($n=3$) dimensions can be easily determined.

The validity of the propagator is proven; however, it is crucial to investigate its compatibility and physical dynamics corresponding for applying FCS. It is required to define an observation volume which appropriate representation of the underlying molecular dynamics. In FCS with one- or two-

photon excitation, the volume profile is typically modeled as a three-dimensional Gaussian function of the form as follows:

$$[3-22] O_{3DG}(r) = \exp\left(-\frac{2mx^2}{\omega_0^2} - \frac{2my^2}{\omega_0^2} - \frac{2mz^2}{z_0^2}\right)$$

With the radial and axial beam waists ω_0 and z_0 , respectively. The index m specifies one ($m=1$) or two-photon ($m=2$) excitation. The autocorrelation equation for anomalous diffusion is provided as follows [3-18],[3-19].

$$[3-23] G(\tau) = \frac{\gamma_{nDG}}{C V_{nDG}} \left(1 + \left(\frac{\tau}{\tau_D}\right)^\alpha\right)^{-1} \left(1 + \left(\frac{1}{x^2}\right) \left(\frac{\tau}{\tau_D}\right)^\alpha\right)^{-(n-2)/2}$$

$$[3-24] \tau_D = \left(\frac{\omega_0^2}{4m\Gamma}\right)^{\frac{1}{2n}} = \frac{\alpha\omega_0^2}{4mD_{ins}(\tau_D)}$$

The volume and gamma factors are $\gamma_{nDG} = 2^{-n/2}$, $V_{2DG} = 2^{-m}\pi\omega_0$, and $V_{3DG} = 2^{-\frac{3m}{2}}\pi^2\omega_0^2 z_0$.

The structure factor, is defined as $x = \frac{z_0}{\omega_0}$. The variable C specifies the molecular concentration.

FCS curves and the MSD reports only on low-order properties of the propagator; therefore, as noted above, it is unlikely that curve fitting alone will generally be capable of resolving the applicability of different physical models. Instead it will be important to measure the anomalous dynamics on different length scales or timescales and to couple the analysis of how experimental parameters change with predictions from different mechanistic models. With imprecise parameter definitions, this type of analysis is not possible, and the clarifications introduced above can be of significant importance for future investigations of anomalous dynamics.”

It is expected that fluxes determination equations (Eq 3-15a to 3-15c) can be simplified by considering fair assumptions. The convective term will be negligible in this study due to unstirred

experimental condition and batch reactor utilizing. The migration term is the second term which is strongly dependent on a limiting molar ionic conductivity of ions in the microscopic scale and is also interrelated with the supporting amount of electrolyte in the mesoscale [3-12].”

Table 3-21 provides the limiting conductivity of selected multivalent and monovalent ions [3-12]. The limiting molar conductivity is determined by considering the resulting molar ionic conductivities of anions and cations corresponding to the electrolyte once the current passes through it. It can be calculated as follows:

$$[3-25] \Lambda_m^\circ = \nu_+ \lambda_+^\circ + \nu_- \lambda_-^\circ$$

Where ν demonstrates the number of associated electrons (valent) in forming the ionic compound. In case the electrolyte is considered as parallel circuit, conductance would be apposite terminology to consider for interpretation of the phenomena. Since the total conductance of a circuit of resistors in parallel can be easily defined as the sum of the conductance comprising the circuit [3-12]. For dilute solutions, each ion transports current in its division of the circuit without interacting with the movement of the other ions and the cation’s transport number can be defined as shown in Eq. 3-26 [3-12].

$$[3-26] t_+ = \frac{j_+}{j} = \frac{\sigma_+}{\sigma} = \frac{\nu_+ \lambda_+}{\Lambda_m}$$

Where σ is defined as the conductivity (inverse of the resistivity). The majority of current is expected to be transported by protons once the target compound consists of hydrogen bonds. Eq.3-4 manifests one of the determining contributions of H^+ in limiting molar conductivity which is corresponding with this study (adding hydroxyl agent as oxidizing agent). The reason for limiting the ionic molar conductivity of the proton is that the high stems from the proton mobility

mechanism is ionic movement by successive jumps, taking with them part of their hydration layer. In 1806, de Grotthus proposed a mechanism which considers that “protons move rather in ‘chain reactions’, breaking covalent bonds and reforming in their place hydrogen bonds. This transport mechanism is also called structural diffusion.” [3-21]. The schematic of structural diffusion mechanism is illustrated in Figure 3-10.

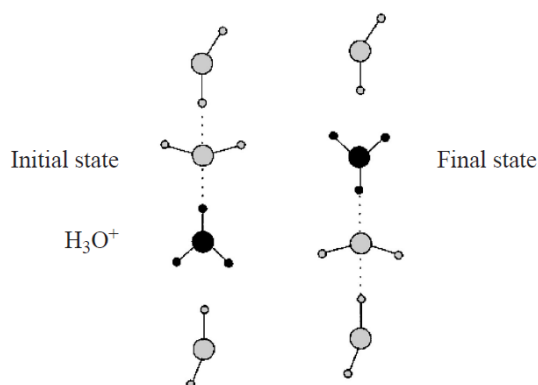


Figure 3- 10 Schematic of proton mobility in structural diffusion phenomenon (Adapted from n Kornyshev et al;2003)

Considering H_3O^+ (oxonium) as proton is significant simplification which affects the physics of process. Since isolated proton cannot exist in solution and two different stable complex compounds is proposed in aqueous form. The first form is called “Eigen Cation” which consists of an H_3O^+ core strongly hydrogen-bonded to three H_2O molecules. Another proposed structure is one where a proton is shared by two H_2O molecules to form the “Zundel cation” H_5O_2^+ . The topic of proton mobility is an open debate which is associated with interpretation of the several hydrogen bonds [3-12].

However, it is not practical to consider the non-diluted wastewater (the scope of the study) as the appropriate electrolyte for certain assumptions of limiting molar conductivities which are

determined for diluted or in some cases very diluted electrolyte. Therefore, justifying the negligence of migration term by considering supporting electrolyte is not acceptable for this study.

In a mesoscale point of view, the supporting electrolyte is defined based on IUPAC as “An electrolyte solution, whose constituents are not electroactive in the range of applied potentials being studied, and whose ionic strength (subsequently, contribution to the conductivity) is usually much larger than the concentration of an electroactive substance to be dissolved in it [3-22]. “Due to detecting 113 mS/cm conductivity as initial value without applying current, the electrolyte of the study is promisingly electroactive. Therefore, supporting electrolyte phenomenon cannot justify the negligence of the migration term.

Table 3- 21 Limiting molar conductivity of the different ions in dilute solutions (ion-ion interactions can be neglected)

Cation	$\lambda_i^0/cm^2\Omega^{-1}mol^{-1}$	Anion	$\lambda_i^0/cm^2\Omega^{-1}mol^{-1}$
H ⁺	349.8	OH ⁻	198.3
Li ⁺	38.7	F ⁻	55.4
Na ⁺	50.1	Cl ⁻	76.4
K ⁺	73.5	Br ⁻	78.1
Rb ⁺	77.8	I ⁻	76.4
Cs ⁺	77.3	NO ₃ ⁻	71.5
NH ₄ ⁺	73.6	ClO ₄ ⁻	67.4
Me ₄ N ⁺	44.9	SCN ⁻	66.0
Mg ²⁺	106.1	SO ₄ ²⁻	160.0
Ca ²⁺	119.0	Fe (CN) ₆ ³⁻	302.7
Fe ³⁺	204.0	Fe (CN) ₆ ⁴⁻	442.0

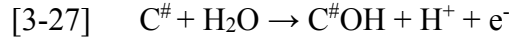
When current passes through an electrochemical reactor, it must overcome the equilibrium potential difference, anode overpotential, cathode overpotential, and ohmic potential drop of the solution [3-20]. The anode overpotential includes the activation overpotential and concentration

overpotential, as well as the possible passive overpotential caused from the passive film at the anode surface, while the cathode overpotential is principally constituted of the activation, and concentration overpotential.

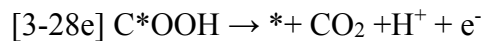
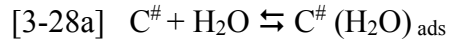
Investigating the migration term associated mechanisms requires defining major reactions in the electrochemical reactor which are a) oxidation reaction at the anode, b) oxidation reactions at the anode side, c) reduction reaction at the cathode zone, and d) the hydrolysis reactions.

a) Oxidation reaction at the anode

Gallagher and Fuller ^[3-24] presented an appropriate kinetics for electrochemical oxidation of graphite carbon in acidic environments which can be implemented in our study. The justification is explained by the target oxidation processes which is predominantly taken place in low pH (lower than pH=3) and it is experimentally observed in this study. Gallagher and Fuller ^[3-24] considered two types of sites on the carbon surface which are illustrated by # and *. The # sites are the active sites for the rate determining step of CO₂ formation. In the mentioned sites, the water is reversibly adsorbed and initial oxides are formed. The * sites are the location of both CO₂ loss and simultaneous oxide formation. The reasons for considering two-site assumption are allowing to produce an oxide that does not consume sites involved in the rate determining step and proposing the gas-phase oxidation of carbon. The first reaction, Eq.27 is the growth of a catalytic oxide necessary to represent the CO₂ behavior observed in graphitized carbons ^[3-25]. The term of “catalytic” refers to constancy of mentioned oxide during CO₂ formation. Although initial presence of equilibrium surface concentration of the oxide may or may not physically correct but allows for semi-empirical approach to modelling the observed reaction. Considering the mentioned assumption is valid for non-graphitized carbons and it just provide the condition in which the model can be defined ^[3-24].



The actual mechanism of graphite oxidation can be defined as 5 steps reactions (Eq. 3-28a to 3-28e) which are determined and described as followed:

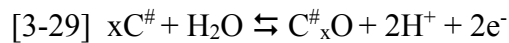


The first reaction (Eq. 3-28a) is reversible adsorption of water into the reaction site #, the second reaction (Eq. 3-28b) is rate determining step (RDS) because of its slow kinetics. The reason of considering the mentioned reaction as RDS is the first order reaction dependence on water partial pressure. $C^\#OH$ is the only surface oxide which is experimentally proved to be in RDS reaction. Considering later steps as RDS requires additional oxides and more complicated dependence on partial pressure of water. Due to the fact that, there is limiting experimental investigation for the existence of intermediate reactants in the literature, they assumed to be negligible in the site balance.

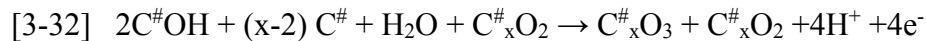
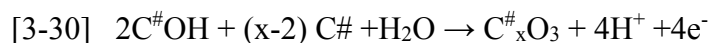
The described mechanism by Gallagher and Fuller^[3-24] also considers the sources of current decay descriptively. The first source is due to mass loss suffered during the gasification of CO_2 . The experimental measurements based on Brunauer-Emmett-Teller did not show a significant change in specific surface area after persistent prolonged oxidation. Due to the fact that the observations show CO_2 production is proportional to the total sites available, it is not expected to see significant

contribution in current decay which is caused by CO₂ origin mass loss. It merges its significance under conditions of elevated potential and temperature for long times or many cycles.

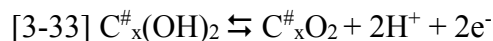
The second source of time decay originated from the reversible formation of passive surface oxide as presented in Eq.3-29. The observed power-law decay of $i = kt^{-n}$ is interpreted by the oxide, C[#]_xO. Based on an ideal system (no other transients are expected to take place) that is presented by Gallagher and Fuller [3-24], x is considered as 3 and the CO₂ current decaying is investigated at n=1/2. The results of the described ideal system show that the oxidation current from the growth of this oxide typically dominates the total current at short times. Gallagher and Fuller [3-24] found out that 2.6 electrons were required per oxygen atom removed in their system.



Based on Gallagher and Fuller [3-24] research, the third and final source of time decay is irreversible and results from reduction of the oxidized carbon surface. The three expected reaction which are physically followed the chemistry of the phenomena are represented in Eq. 3-30 to Eq.3-32. The first equation, Eq.3-30, takes place as a consumption of the catalytic oxide to establish an equilibrium concentration on the # sites. It is suggested that the presented reaction is affected by the production of another surface oxide. Once the exposure to potentials of 1 V or greater, the C[#]_xO and C^{*}O will be produced on the carbon surface. Gallagher and Fuller [3-24] proposed that a reduction of C^{*}O oxide, Eq.31, is resulted in the formation of specie that further decrease in the equilibrium concentration of the catalytic C[#]O₂.



The final electrochemical equation, Eq. 33, which is presented by Gallagher and Fuller [3-24] is the redox couple of the quinone/hydroquinone group (Q/HQ). This oxidation reduction reaction is prominent in the cyclic voltammetry studies of oxidized graphene-based carbons [3-24],[3-25],[3-26],[3-27],[3-28].



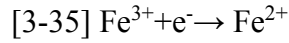
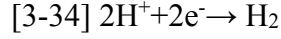
Therefore, it is a fair simplification to analyze migration term based on the last Equation (Eq.3-33) due to the fact that it governs the process of graphite oxidation.

b) Oxidation reactions at the anode side

As it is described in subsection 3-4-1, the anode side reactions are directed to removal of ammonia, organic nitrogen, and TKN. The attributed reactions for organic nitrogen (Eq.3-5) [3-10], ammonia (Eq. 3-6 and 3-7) [3-10], and TKN (Eq. 3-8) [3-9] removal are described. Except for ammonia, the rest of the pollutants are removed by one oxidation reaction. However, ammonia removal is followed by two reactions which are oxidation and reduction reactions respectively. Therefore Eq.3-6 can be classified as one of the oxidation reactions at the anode side. (Eq.3-5), (Eq.3-6) and (Eq.3-8) are expected oxidation reactions at the anode side.

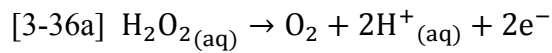
c) Reduction reactions at the cathode zone

The hydrogen gas production is one of the main reactions of electrochemical cells. The second reaction is allocated to oxygen reduction that leads to production of hydrogen peroxide (Eq.3-1). The associated reaction for hydrogen gas production is Eq.3-34. The next reaction (Eq.3-35) which is classified as one of the catalyzed reactions is the regeneration of ferrous ions (Fe^{2+}) through the reduction of ferric ions (Fe^{3+}) on the cathode [2-119],[3-29].



d) The hydrolysis reactions

The associated hydrolysis reactions are related to catalytic assisted hydrogen peroxide hydrolysis (Eq.3-4) and graphite active site hydrolysis (Eq.3-29). The hydrolysis mechanism is evaluated by K_h which is called the hydrolysis constant. In the other words, it is considered as an equilibrium constant for hydrolysis reaction. Finally, the equilibrium potential difference between cathode and anode is affected by introduced hydrolysis reactions (Eq.3-36a). The K_{h1} is presented in Eq. 3-36b and K_{h2} which is associated with Eq.27 is equal to $\frac{C_{H^+}^*}{C_{C\#}^*}$ while C_j^* represents the bulk concentration of species j [mol/L]. According to Chen et al. [3-23], pH does not affect the equilibrium potential. The overall associated terms of equilibrium potential are explained in Eq.3-37 and simplified in Eq.3-38.



$$[3-36b] K_{h1} = \frac{C_{H^+}^{*2}}{C_{H_2O_2(aq)}^*}$$

$$[3-37] E_q = \varphi^o_{Fe^{3+}/Fe} - \varphi^o_{\frac{H^+}{H_2}} + \frac{RT}{F} \left(\ln \frac{(p_{H_2})^{\frac{1}{2}}}{K_{h1}} + \ln \frac{(p_{H_2})^{\frac{1}{2}}}{K_{h2}} \right)$$

Or

$$[3-38] E_q = \varphi^o_{Fe^{3+}/Fe} - \varphi^o_{\frac{H^+}{H_2}} + \frac{RT}{F} \left(\ln \frac{p_{H_2}}{K_{h1}K_{h2}} \right)$$

Based on Scott ^[3-20] research and Chen et al. ^[3-23], the mass transfer which is associated with migration term is determined by the Nernst-Plank equation ^[3-30] for constant diffusion coefficient is presented in Eq.3-39 (expanded Eq.17-1) and Eq.3-40 respectively:

$$[3-39] \quad J_j(x) = \underbrace{-D \frac{\partial C_j(x)}{\partial x}}_{\text{Diffusion}} - \underbrace{z_j F D_j \frac{C_j(x)}{RT} \frac{\partial \varphi(x)}{\partial x}}_{\text{Migration}} + \underbrace{C_j(x) u(x)}_{\text{Convection}}$$

$$[3-40] \quad J_j(x) = -D \frac{\partial C_j(x)}{\partial x} + u_j C_j(x) \frac{\partial \varphi(x)}{\partial x} + C_j(x) u(x)$$

Notations of the Eq [32] and Eq [33] are as follows:

$J_j(x)$ flux of species j at distance x, mol/m²s

$C_j(x)$ concentration of species j at distance x, mol/l

R gas constant, J/mol K

F Faraday Constant, C/mol

z_j charge number of species j

D_j diffusion of coefficient of species j, m²/s

$u(x)$ convective velocity of water flow in the current direction at distance x, m/s

$\varphi(x)$ potential at distance x, V

u_j mobility of species j, m²/V s

The total current is calculated by Eq.3-41 ^[3-23] while considering all ions existing in the wastewater.

Once Eq.3-42 is expanded by importing Eq.3-40, the new driven equation is generated as Eq.3-42.

The migration term can be considered as number of species multiplied by current density, Therefore Eq. 3-43 is introduced while “ t_{jj} ” is represented as equivalent of migration term in Eq. 3-40.

$$[3-41] \quad j = F \sum z_j j$$

$$[3-42] \quad j = \sum z_j \left[-D \frac{\partial C_j(x)}{\partial x} + u_j C_j(x) \frac{\partial \phi(x)}{\partial x} + C_j(x) v(x) \right]$$

$$[3-43] \quad j = \sum \{ z_j F \left[-D \frac{\partial C_j(x)}{\partial x} + C_j(x) v(x) \right] + t_{jj} \}$$

t_j transport number of species j

j current density, A/m²

As it is described in subsection 3-4-2, nonlinear change of the kinetics of the reactions leads the process to face time-dependent diffusion. Experimental and theoretical determination of time-dependent diffusion is also described. However, considering the time-dependent diffusion in diffusion-migration electrochemical system is still an open debate. Valuable research of Bieniasz [3-31] leads the determination of time-dependent diffusion be facile by considering fair simplification while using 1D dynamically adaptive grid techniques for the solution of electrochemical kinetic equations. The mentioned simplification is introduced because of occurred discontinuity of model parameters at the membrane/electrolyte interference, which prevents the meaningful application of finite-difference spatial discretisation.

In order to solve this problem, the discontinuities of the diffusion coefficients and of the fixed spatial charge distribution have been approximated by continuous functions $dA(x)$, $dC(x)$, and $\chi(x)$ of coordinate x , using the hyperbolic tangents. Therefore, the unit step function of $H(x)$ (Eq.3-44):

$$[3-44] H(x) = \begin{cases} 0 & \text{for } x \leq 0 \\ 1 & \text{for } x > 0 \end{cases}$$

is approximated by the “smoothed” step function (Eq 3-45):

$$[3-45] H^*(x, \sigma) = [1 + \tanh(x/\sigma)]/2$$

Where σ is a positive parameter. When σ is sufficiently small, solution of the problem formulated using function $H^*(x, \sigma)$ in the place of $H(x)$, approximates well the solution corresponding to $H(x)$. Table 3-22 is adopted from Moya and Horno ^[3-32] model while introducing the simplification and modification of Bieniasz ^[3-33] for diffusion coefficients.

Table 3- 22 Initial boundary value problem describing chronopotentiometry for an electrolyte| membrane | electrolyte system (Bieniasz;2003)

Model Parameters	z_A, z_C = charge numbers $d_{AS}, d_{AM}, d_{CS}, d_{CM}$ = dimensionless diffusion coefficients ϵ = dimensionless dielectric permittivity Δ = membrane thickness χ^0 = fixed charge parameter σ = parameter of the smoothed unit step function $H^*(x, \sigma)$ t_{step} = current pulse duration i_{step} =current pulse amplitude $d_A(x) = d_{AS} + (d_{AM} - d_{AS})[H^*(x, \sigma) - H^*(x - \Delta, \sigma)]$
Distributions of diffusion coefficients	$d_C(x) = d_{CS} + (d_{CM} - d_{CS})[H^*(x, \sigma) - H^*(x - \Delta, \sigma)]$
Fixed charge distribution	$\chi(x) = \chi^0[H^*(x, \sigma) - H^*(x - \Delta, \sigma)]$
Applied current pulse	$i(t) = i_{step}[H(t) - H(t_{step})]$
Distributed unknowns	$c_A(x, t) = c_c(x, t)$ = concentrations $\varphi(x, t)$ = electric potential
Governing equations	$\frac{\partial c_A(x,t)}{\partial t} = \frac{\partial [d_A(x) \frac{\partial c_A(x,t)}{\partial x}]}{\partial x} + z_C \frac{\partial [d_A(x) c_A(x,t) \frac{\partial \varphi(x,t)}{\partial x}]}{\partial x}$ $\frac{\partial c_C(x,t)}{\partial t} = \frac{\partial [d_C(x) \frac{\partial c_C(x,t)}{\partial x}]}{\partial x} + z_C \frac{\partial [d_C(x) c_C(x,t) \frac{\partial \varphi(x,t)}{\partial x}]}{\partial x}$ $0 = \frac{\epsilon \partial^2 \varphi(x,t)}{\partial x^2} + z_A c_A(x, t) + z_C c_C(x, t) - \chi(x)$
Starting approximations to steady-state initial conditions	$c_A(x, t_{min}) = c^0 [H(-x) - H(x - \Delta)]$ $c_C(x, t_{min}) = \{\chi^0 - (z_A c^0 + \chi^0) [H(-x) - H(x - \Delta)]\}$ $\varphi(x, t_{min}) = 0$ (arbitrary value) $c_A(x_{min}, t) = c^0$
Boundary conditions at $x = x_{min}$	$c_C(x_{min}, t) = -\left(\frac{z_A}{z_C}\right) c^0 - \epsilon \frac{\partial^2 \varphi(x_{min}, t)}{\partial x \partial t} = i(t) +$ $z_A d_{AS} \left[\frac{\partial c_A(x_{min}, t)}{\partial x} + \frac{z_A c_A(x_{min}, t)}{\partial x} \frac{\partial \varphi(x_{min}, t)}{\partial x} \right] + z_C d_{CS} \left[\frac{\partial c_C(x_{min}, t)}{\partial x} + \frac{z_C c_C(x_{min}, t)}{\partial x} \frac{\partial \varphi(x_{min}, t)}{\partial x} \right]$
Boundary conditions at $x = x_{max}$	$c_A(x_{max}, t) = c^0$ $c_C(x_{max}, t) = -\left(\frac{z_A}{z_C}\right) c^0$ $\varphi(x_{max}, t) = 0$ (arbitrary value)
Displacement current	$i_D(t) = \frac{-\epsilon \partial^2 \varphi(x_{min}, t)}{\partial x \partial t}$

3-4-3. Kinetics

The determination of kinetics order is achieved by finding the trends of substrate concentration variation versus time. The expected trends are zeroth order, first order, pseudo first order, and second order. Fogler (2016) considers method of excess, integral method, differential method of analysis, and nonlinear regression to investigate the order of kinetics based on experimental data.

[3-33]

The logic beyond obtaining the differential method of analysis is the different kinetics behavior of ammonia and organic nitrogen oxidation in the presence of different organic compounds. Usually, the kinetics of the oxidation reactions between organic compounds and oxidants (HClO, H₂O₂, H₂S₂O₈) is considered to be second order: i.e., first order with respect to the concentration of the electro-generated oxidants ([Ox]) and first order with respect to the concentration of the organic compounds (COD)^[3-34]. However, Li and Liu ^[3-35] claim that ammonia oxidation follows zeroth order or pseudo zeroth order reaction in the presence of chloride. Therefore, considering research reviews as reference to determine an order of the reactions would not be an appropriate approach.

One of the assumptions of using an integral method is assuring that the order of the reaction is known. Its application is mostly desired for investigating specific reaction rate constant at different temperatures to determine the activation energy. ^[3-33] Therefore, an integral method is not applicable in the condition of high uncertainty.

This research is focused on determination of kinetics order by implementing finite difference for differential method of analysis. In the differential method, the reaction order, α , is obtained by plotting of $\ln(-\frac{dC_A}{dt})$ versus $\ln(C_A)$. The general equation and the neutral logarithmic form of it

are described in Eq.3-46a and Eq.3-46b considering a batch reactor with concentration of A while the mole balance is combined with the rate law. [3-33]

$$[3-46a] -\frac{dC_A}{dt} = k_A C_A^\alpha$$

$$[3-46b] \ln\left(-\frac{dC_A}{dt}\right) = \ln k_A + \alpha \ln C_A$$

The graphical pathway of determining k_A (rate constant with respect to A) and α is illustrated in Figure 3-11. “ α ” will be calculated based on the slope of linear regression line while k_A is obtained by dividing the desired value of the selected concentration derivative to the concentration of the desired point in the power of the reaction order. All described values are considered from the \ln - \ln graph. [3-33]

In order to apply the finite difference method, it is essential to define the numerical differential equation for the initial, interior and last point. Fogler determine the derivatives by using Eq. 47a, Eq.47b, and Eq.47c respectively. Table 3-23 is provided the required equations to determine numerically the concentration derivatives values. [3-33]

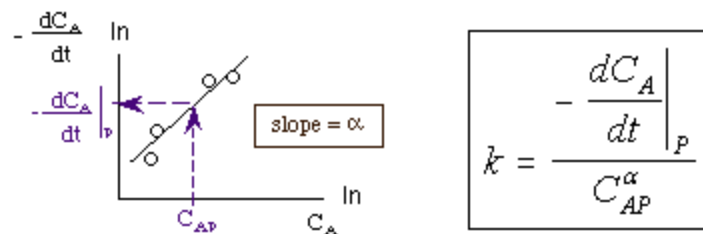


Figure 3- 11 The graphical determination of rate constant of the substrate A and the order of the reaction (adopted from <http://www.umich.edu/~elements/fogler&gurmen/html/course/lectures/five/index.htm>)

Table 3- 23 The finite difference equations applied for determining the concentration derivatives values versus time in initial, interior, and last point locations

Location of point	Equation	Number of Equation
Initial point	$\left(\frac{dC_A}{dt}\right)_{t_0} = \frac{-3C_{A0} + 4C_{A1} - C_{A2}}{2\Delta t}$	3-47a
Interior point	$\left(\frac{dC_A}{dt}\right)_{t_i} = \frac{1}{2\Delta t} [C_{A(i+1)} - C_{A(i-1)}]$ $\left(\frac{dC_A}{dt}\right)_{t_i} = \frac{1}{2\Delta t} [C_{A(i+1)} - C_{A(i-1)}]$	3-47b
Last point	$\left(\frac{dC_A}{dt}\right)_{t_5} = \frac{C_{A3} - 4C_{A4} + 3C_{A5}}{2\Delta t}$	3-47c

The described experimental plan for experimental upscaling would be followed in Chapter 4 to observe the variations of monitoring parameters (e.g. voltage, pH, ORP, conductivity, and temperature) and analyze the responds of objective parameters (removal efficiency values of ammonia, TKN, total nitrogen, and organic nitrogen, respectively). EF-SBR would be designed based on the best experimental conditions investigated by Phase 1, Phase 2, and Phase 3.

Chapter 4 Results and Discussion

4-1. Phase 1 results and discussion

4-1-1. Stage 1-1 analysis

The first phase of study (small scale) consists of 6 distinctive stages which are described in Chapter 3, Methodology. The experimental parametric study of small scale electrochemical batch reactor requires specified quantitative parameters to assess a better understanding of the process mechanism. The monitored parameters are voltage, pH, conductivity, oxidation-reduction potential (ORP), and temperature. Removal efficiency of ammonia, TKN, organic nitrogen (ON), and total nitrogen (TN) are also an objective of the parametric study. Since the first stage of Phase 1 includes 3 distinct objectives (Section 3-2-1), each objective will be investigated individually. The changes of voltage, pH, conductivity, oxidation-reduction potential (ORP) and temperature for the entire process in a small scale of the first objective of Stage 1-1 are illustrated in Figure 4-1a, Figure 4-1b, Figure 4-1c, Figure 4-1d and Figure 4-1e, respectively.

Figure 4-2a, Figure 4-2b, Figure 4-2c and, Figure 4-3d show the removal efficiency of ammonia, TKN, organic nitrogen, and total nitrogen, respectively.

Figure 4-1a illustrates that an impact of the anode to cathode surface area ratio (A:C). In the other words, dimensional quotient (DQ) on voltage variation follows certain trend which is the increase of endpoint voltage of each experiment in comparison with the previous experiment endpoint. Due to the higher surface area of anode, higher initial current will be achieved, and it might affect electrolysis of water.

The investigation of the impact of the A:C on pH through entire exposure time requires grouped and individual analyses. Following a group analysis, a sharp drop is expected after 24 hour for all

experiments. However, experiments with lower than 2.04 value of dimensional quotient (but higher than 1.54 A:C) faced severe pH decrease in juxtaposition with the out-range experiments and the pH of the endpoint might reach lower value than 1.

Following an individual analysis, the Exp.13 (A:C =0.38 or DQ=8.33) showed a distinct behavior after the sharp decrease at 24 hours. pH (Fig. 4.1b) surged in the remained 48 hour exposure time (from 24 hours to 72 hours). To construe the pH surge for the Exp.13, it is crucial to investigate the ORP state, relevant current, and voltage value. Being in reduction state meanwhile the process, limits the production of hydroxyl radicals for the Exp.13. Subsequently, adequate oxidation state would not be provided to have ferrous ions involved in electro-Fenton reaction. It is also speculated that the available current of 0.31 A provided lower voltage that required overpotential to initiate Tafel reactions (Section 3-4-2).

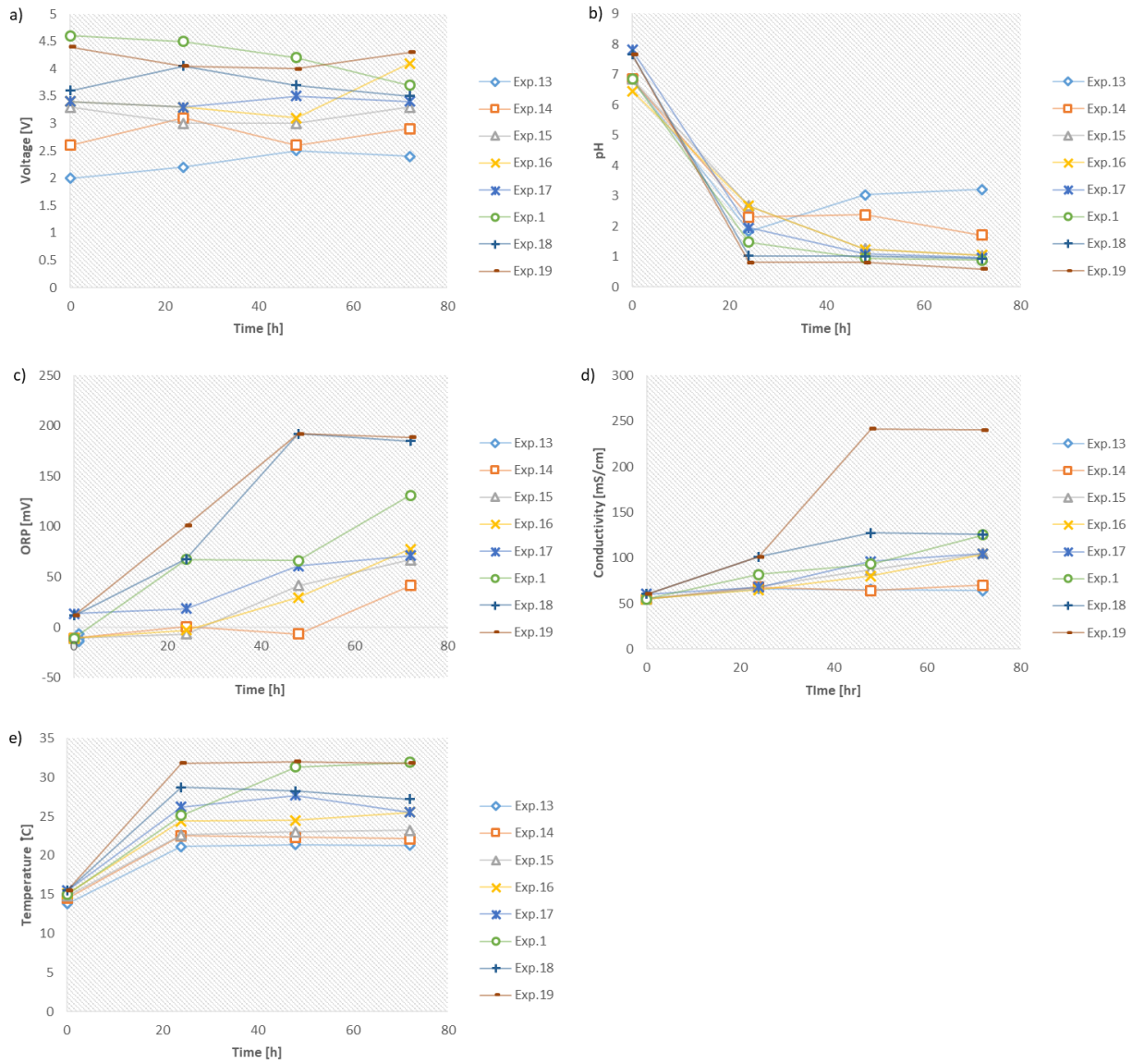


Figure 4- 1 Variations of relevant parameters for experiments of the Stage 1-1; a) voltage versus time; b) pH versus time; c) ORP versus time; d) conductivity versus time; e) temperature versus time

The tendency of the ORP variation (Fig. 4.1c) versus time showed a sharp increase in the first and second day of the exposure time. The Exp.13, Exp.14, Exp.15 and Exp.16 were in the reduction state during the first 24 hour exposure time. However, the Exp.14 and Exp.15 continued to be in reduction state up to 48 hour exposure time. The only experiment, which preserved reduction state was the Exp.13. When a dimensional quotient decreased, the slope of the ORP increase sharpened. Based on the achieved results, it is speculated that the available surface of graphite anode significantly affected the oxidation kinetics and reaction rate, which resulted in higher intensification on ORP. It can be related to higher active surface for carbon to involve in oxidation reactions.

The conductivity increased meanwhile 48 hour exposure time once the A:C ratio increased, and dimensional quotient decreased (Fig. 4.1d). When the dimensional quotient was less than 2.60, the slope of the conductivity sharply increased. It can be construed by considering the increase in constant applied current while the anode surface area increased. Consequently, the voltage increased by applying higher amperage based on the recorded values for voltage.

The temperature changes (Fig.4.1e) are caused by the applied electrical power and thermodynamics concepts of occurred oxidation/reduction reactions (e.g. enthalpy and activation energy). The similar trend of increase in the first 24 hour period observed for the relevant experiments of the first objective of the Stage 1-1. No significant change was also detected during the last 48 hour exposure time for all experiments. As much as the dimensional quotient decreased, the temperature value increased. Subsequently, the maximum temperature was recorded for the lowest dimensional quotient.

The ammonia removal efficiency significantly increased once the dimensional quotient decreased whereas the A: C increase (Fig. 4-2a). However, the Exp.17 (DQ = 1.56) had better ammonia removal efficiency in comparison with the Exp.1 (DQ = 1.31). The reason might be the deficiency of spontaneous diffusion, which is possible to be initiated by significant increase of total solids (TS). The recorded amount of TS for the Exp. 17 was 4.7 g/L while the Exp.1's TS was 5.5 g/L. Based on Abbassi-Guendouz et al. research, total solids content drove high solid anaerobic digestion via mass transfer limitation and hydrolysis rate constants slightly decreased with increase of TS ^[4-1]. The minimum and maximum ammonia removal efficiency were achieved for the Exp.19 and Exp.13 with 32.2% ± 0.018% and 99.4% ± 0.018%, respectively.

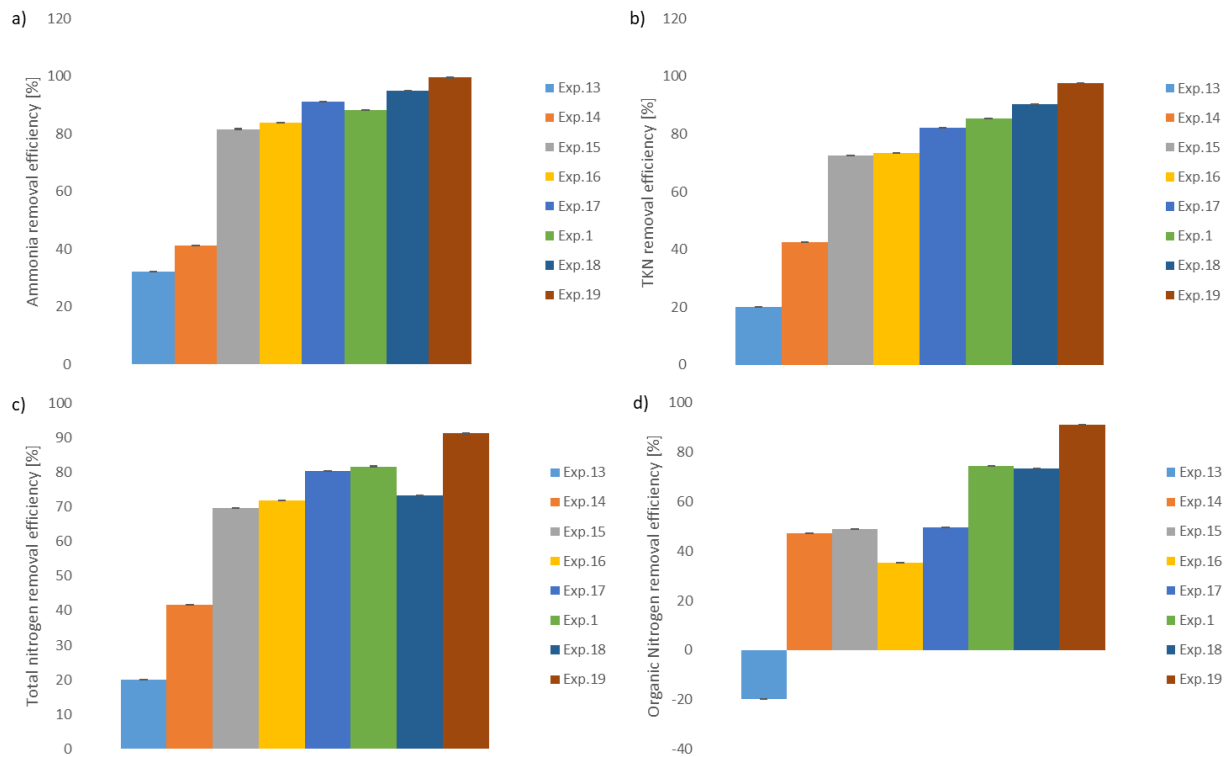


Figure 4- 2 Removal efficiency for Stage 1-1 a) ammonia removal; b) TKN removal; c) organic nitrogen removal; d) total nitrogen removal

TKN represents total concentration of ammonia and organic nitrogen, thus, the degradation of TKN is hardly proceeded because of both organic and inorganic compounds. The TKN removal efficiency (Fig 4.2b) was pointedly improved once the dimensional quotient decreased or the A:C surface area ratio increased. The sharpest increase belonged to the Exp.15 (DQ= 2.59; A:C=1.22) in which the removal efficiency increased for 30.2% in comparison with the previous experiment (Exp.14). The minimum and maximum TKN removal efficiency were achieved for the Exp.19 and Exp.13 by $20\% \pm 0.011\%$ and $97.6\% \pm 0.011\%$, respectively.

The organic nitrogen removal efficiency (Fig. 4-2d) can be assessed by considering the maximum removal efficiency which is achieved in dimensional quotient equal to 1. Organic nitrogen is computed by subtracting ammonia concentration from TKN concentration. Consequently, the differential nature of organic nitrogen leads to obtaining random results.

For instance, the outcomes of the Exp.16 showed that the removal efficiency of TKN and ammonia were improved for 1.07% and 2.27% in comparison with the results of the Exp.15. However, the removal efficacy of organic nitrogen showed a decrease of 13.7%.

The negative removal efficiency value of the Exp.13 can be explained by deficiency of TKN removal rate. The rate of TKN removal was 38.88 mg/L.h in the entire 72 hour exposure time while the ammonia removal rate was 49.16 mg/L.h . Having higher removal rate of ammonia in comparison with TKN removal rate resulted an increase in the subtraction of ammonia from TKN. Therefore, the concentration of organic nitrogen (subtraction of ammonia from TKN) would increase in the system and exceed from initial concentration of organic nitrogen (3000 mg/L). So, negative value of the removal efficiency of the organic nitrogen would be achieved while the described phenomenon (higher removal rate of ammonia in comparison with TKN) is taken place.

The total nitrogen is defined as the summation of TKN, nitrite, and nitrate. According to Eq.3-8, one of the products of TKN oxidation might be nitrite and the mentioned product is unstable in aqueous state. It was expected that the nitrate and nitrite concentrations vary meanwhile the process. The tendency of total nitrogen (Fig.4-2c) removal efficiency was likewise of the TKN and the sharpest increase was achieved for the Exp.15. The difference between total nitrogen removal efficiency of the Exp.14 and Exp.15 was 28%. Furthermore, the minimum and maximum detected removal efficiency were found to be $20\% \pm 0.038\%$ (Exp.13) and $96.91\% \pm 0.038\%$ (Exp. 19).

Assessing an impact of different geometries of cathode was the second objective of Stage 1-1. The perforated or mesh geometry facilitated the hydrogen gas transfer to the surface electrolyte. Since the present gas was expected to affect the conductivity of the electrolyte due to its high electrical resistivity. Therefore, permitting the produced gas to transport to the surface was crucial^[4-2]. Three different cathode geometries were implemented and an optimal dimensional quotient (DQ=1) was considered. The effectiveness of using the optimal dimensional quotient (DQ =1) was validated in the Exp.19 by giving the highest removal efficiency among all relevant experiments of the first objective of Stage 1-1.

However, the exposure surface area of cathode was expected to be different from each other. Perforated stainless steel had 38.8% void space while the mesh one had 68.2% void space; therefore, anode to cathode surface area ratio (A:C) varied.

The voltage changes versus time (Fig.4-3a) showed that the initial and final achieved voltage value for mesh stainless steel cathode was higher than the perforated and flat plate one. The lowest initial and final voltage was resulted by implementing flat plate stainless steel cathode. The only

descending trend among all three scenarios (using perforated, mesh, and flat plate stainless steel) an optimal dimensional quotient (DQ=1) was also related to using perforated stainless steel.

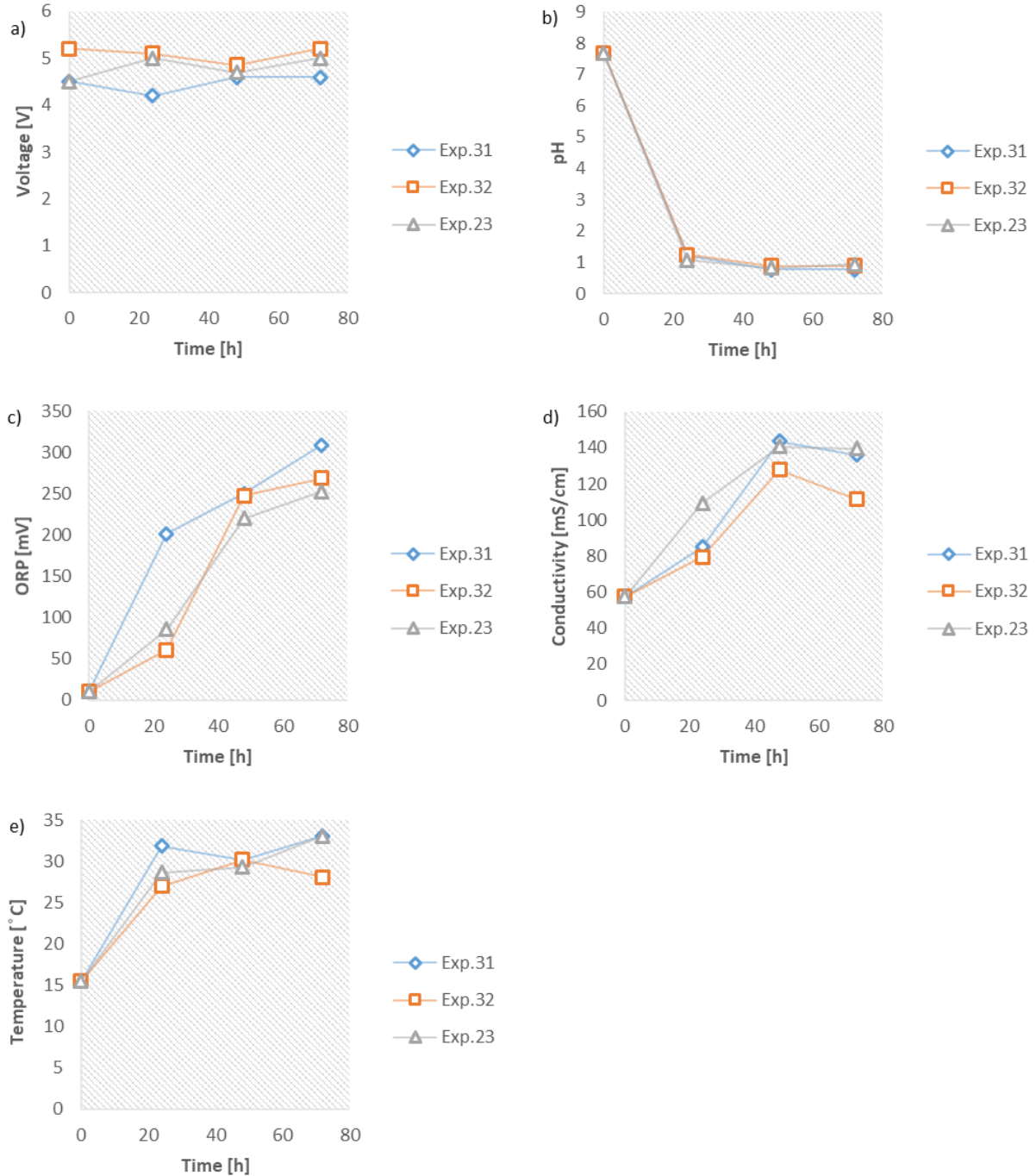


Figure 4- 3 Variations of monitored parameters for the relevant experiments of the 2nd objective of Stage 1-1; a) voltage versus time; b) pH versus time c) ORP versus time; d) conductivity versus time; e) temperature versus time

Based on Anglada et al. research [4-3], for a certain current density, the higher electrolyte concentration would result the higher conductivity, and consequently the lower voltage was required [4-3]. Therefore, the voltage descending behavior of the the Exp.31 (perforated stainless steel cathode) for the last 24 hour exposure time can be interpreted by considering the related conductivity at the same time segment (48 hours to 72 hours). Based on Fig. 4-3d, the maximum conductivity at 48 hours belonged to the Exp.31 with 143.3 mS/cm. Consequently, the required voltage for the Exp.31 would be lower than other comparative experiments (Exp.23 and Exp.32).

The pH variation versus time (Fig.4-3b) showed minor difference among three experiments which proved that the geometry of cathode did not directly impact on pH variation. A sharp decrease was observed during the first 24 hour period. However, a slight increase of pH was detected for the Exp.23 during last 24 hour exposure time (flat stainless steel electrode) and it increased from 0.83 to 0.95. The interpretation of the observed variation required further investigation. Due to expected deficiency in hydrogen phase exchange for flat plate stainless steel electrode, the concentration of hydrogen ions exceeded close to cathode side. Consequently, the formation of hydroxyl radicals was accelerated due to increase in available reactants. Therefore, the pH slightly increased during the last 24 hour period. These speculations require further experimental work.

ORP changes versus time (Fig.4-3c) showed that the maximum amount was achieved for perforated stainless steel cathode (Exp.31). The ORP of both perforated and mesh stainless electrodes were also reached 250.1 mV and 247.4 mV after 48 hours which were very similar. Based on the results, it can be concluded that the highest ORP would not guarantee that a high removal efficiency would be achieved. Since the Exp.23 (flat plate stainless steel cathode) with the lowest final ORP reaches the best removal efficiency of ammonia, TKN, and TN, in comparison with other experiments (Exp.31 and Exp.32). However, the upward tendency of ORP

changes and being higher than 150 mV might be an appropriate indicator for achieving a high removal efficiency.

Conductivity variation versus time (Fig.4-3d) showed sharp a decrease for the Exp.32 (mesh stainless steel cathode) and leads the mentioned experiment to reach the minimal value of conductivity among all three experiments. The dependency of voltage variation to conductivity is fully described in explanations related to voltage changes versus time (Interpretation of Fig. 4-3a).

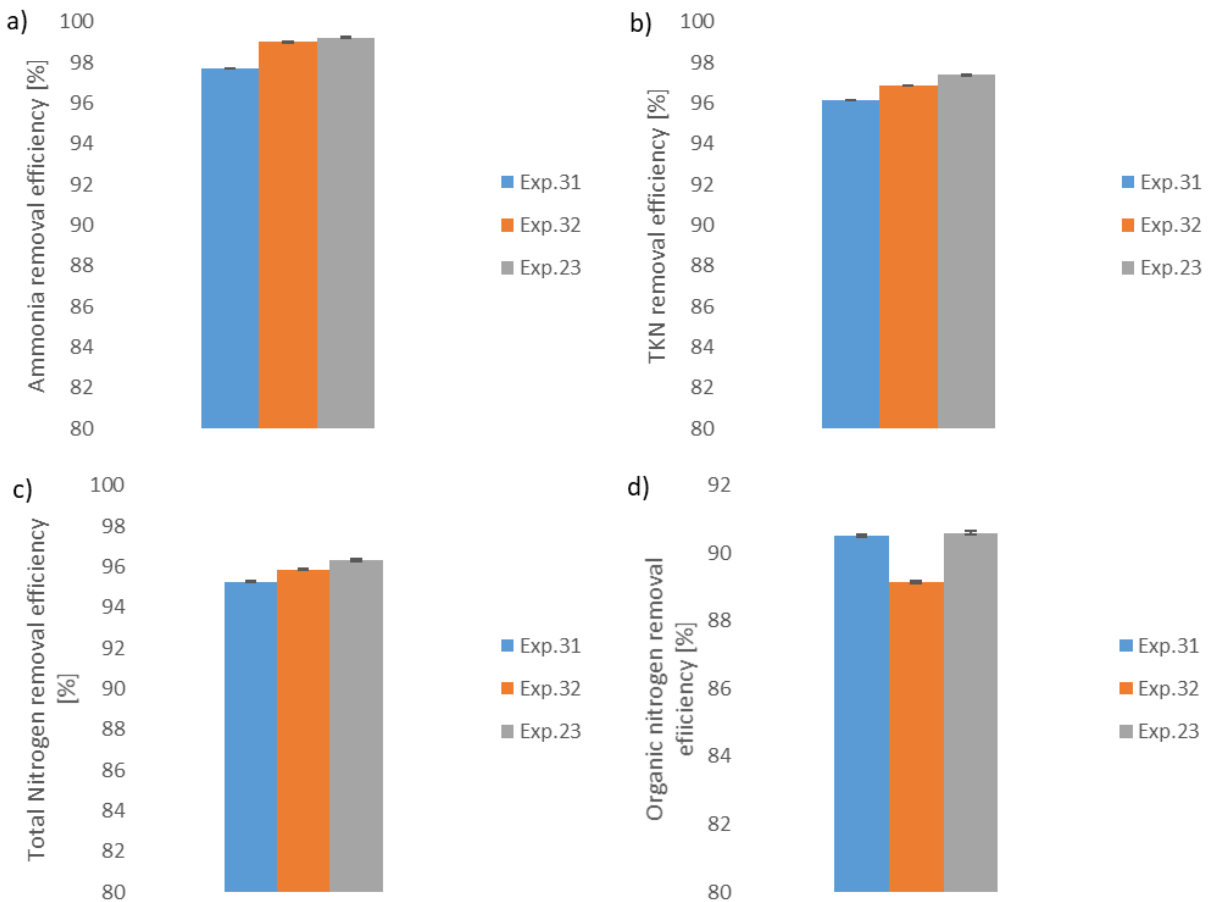


Figure 4- 4 Removal efficiency versus time for the 2nd objective of Stage 1-1 considering: a) ammonia; b) TKN; c) organic nitrogen; d) total nitrogen

The temperature changes versus time (Fig.4-3e) showed totally different behavior in comparison with the results generated by the experiments of the first objective, particularly for the last 24 hour. The only non significant changes for temperature behavior were observed for the second 24 hours of exposure time in the Exp.23 (flat plate cathode). Both Exp.31 and Exp.32 temperatures (perforated and flat plate stainless steel, respectively) showed an increase in ascending order for the last 24 hour period while the temperature of the Exp.32 decreased sharply. The temperature variation results showed that the generated heat of the system depends on enthalpy of the oxidation reactions rather than ohmic heat. For instance, the lowest final voltage belonged to the Exp.32 (mesh stainless steel cathode) while the highest final temperature was also measured in the Exp.32. Since the small scale reactor was covered with parafilm, it would be a fair assumption that the heat transfer through surface of the liquid to the ambient was minimized. In addition, the experimental conditions and the materials of the designed reactors were considered the same to eliminate the impact of designing parameters on heat transfer. It is crucial to mention that the associated sources of heat generation were electricity and reactions.

The best removal efficiency values were achieved for ammonia, TKN, total nitrogen, and organic nitrogen with the values of $99.23\% \pm 0.018\%$, $97.38\% \pm 0.011\%$, $96.32\% \pm 0.038\%$, and $90.6\% \pm 0.04\%$ respectively by implementing the flat plate stainless steel cathode (Exp.23). The lowest removal efficiency values were obtained for ammonia, TKN, and total nitrogen with the magnitude of $97.7\% \pm 0.018\%$, $96.16\% \pm 0.011\%$, and $95.26\% \pm 0.038\%$, respectively by using perforated stainless steel cathode (Exp.31). One of the notable reasons to construe the excellency of flat plate stainless steel cathode was the distribution of the electrical field. Since graphite anode was used as plate geometry and even distribution of electrical field might have an impact on better mineralization of the pollutants.

The third objective of Stage 1-1 was investigating the impact of the reactor configuration and position of the anode on removal efficiency of the target pollutants. Two types of configurations were considered which were cuboid and cylindrical. Figure 3-5a1 and Fig.3-5a2 illustrates the design of the cuboid and cylindrical reactors. A detail of the designs of the reactors were described in Section 3-2-1. The major difference between a cylindrical and a cuboid one was the anode to cathode exposure surface area ratio (A:C ratio). A:C ratio of cylindrical reactor was 0.11 whereas the A:C ratio of cuboid reactor was 0.38.

Voltage changes versus time (Fig.4-5a) showed a distinctive behavior in the Exp.13 (cuboid reactor) while the Exp.11 followed the expected response that was discussed in voltage changes of the second objective of Stage 1-1. The mentioned behavior of the Exp.13 was the decrease of voltage while the conductivity increased.

The typical behavior of the Exp.11 might be interpreted by considering the results of Gabrielli et al. research ^[4-4]. Their model presented the stochastic behavior of the electrochemical interface when reactions were limited by diffusion of reacting species ensued on the electrode surface. The source of random fluctuations of the voltage and the concentration were a Poisson elementary noise sources equation which were acted on both reactive and diffusive fluxes. In order to evolve the state variables, they implemented Langevin equations which were obtained from linearization of electrochemical equations that originated from heterogenous electrochemical kinetics. The time dependent equation of voltage changes which was derived from their study is described in Eq.4-1. The described equation is just valid for small amplitudes. The Exp.13's 48 hour voltage value was 2.5 V and its final voltage value was 2.4 V. Therefore, applying Eq.4-1 is the appropriate solution.

$$[4-1] \Delta V(t) = \Delta E(t) + R_e \Delta I(t) + \vartheta_{Re}(t)$$

$V(t)$ variation of voltage with respect to time [V]

$E(t)$ variation of electrochemical potential across the electrochemical interface [V]

$I(t)$ variation of amperage with respect to time [A]

R_e the resistance of the electrolyte between a working and a reference electrode [Ω]

ϑ_{Re} voltage noise generated by the electrolyte resistance [V]

Therefore, due to the limited diffusion of the reactions which might happen in the last 48 hour period, the voltage noise might cause voltage drop and construe the observed phenomena.

pH variations of the Exp.13 (Fig.4-5b) are fully described in the first objective of the Stage 1-1; in pH changes section. The pH change of the Exp.11 showed a steady decline as expected. The final achieved pH after 72 hours is 1.54.

The ORP results (Fig.4-5c) showed an upward tendency for the Exp.11 (cylindrical reactor). In the last 48 hour exposure time of the Exp.11, the ORP value was positive which indicated that the reactions were in an oxidation state. However, ORP of the Exp.13 (cubic reactor) decreased meanwhile the first 24 hour exposure time and it kept a negative value during the entire exposure time. Due to the central position of the graphite anode in cylindrical reactor, the active surface area of graphite was twice larger than that graphite anode which was placed in the cuboid reactor (Exp.13). The reason was the one-side exposure surface area of the electrode due to its fixed position close to wall of the reactor.

The conductivity changes versus time (Fig.4-5d) showed its increase for both experiments meanwhile the first 24 hour exposure time. The conductivity also kept increasing in the entire exposure time of 72 hours in the Exp.11 (cylindrical reactor). In contrast, the conductivity of the Exp.13 decreased meanwhile the last 48 hour period. It can be speculated that the electrolyte resistance increased during the last 48 hour exposure time due to an increase in non-electro-conductive compounds, maybe due to deposition on electrodes. The specified determination of ions type requires analytical chemistry experiments and amperometry analysis ^[4-5].

The temperature changes versus time (Fig.4-5e) showed an expected surge during the first 24 hour exposure time and the non significant variations were observed for the subsequent 24 hours. The Exp.13 (cubic reactor) kept the tendency of non significant changes meanwhile the last 24 hour exposure time whereas the Exp.11 experienced a sharp drop during the last 24 hour period.

In the Exp.11, the removal efficiency of the ammonia and TKN is higher than the obtained value in the Exp.13. Due to being in an oxidation state for the last 36 hours of exposure time, the Exp. 11 demonstrated better removal efficiency than the Exp.13 with respect to ammonia and TKN. (Fig, 4-6a and Fig.4-6b)

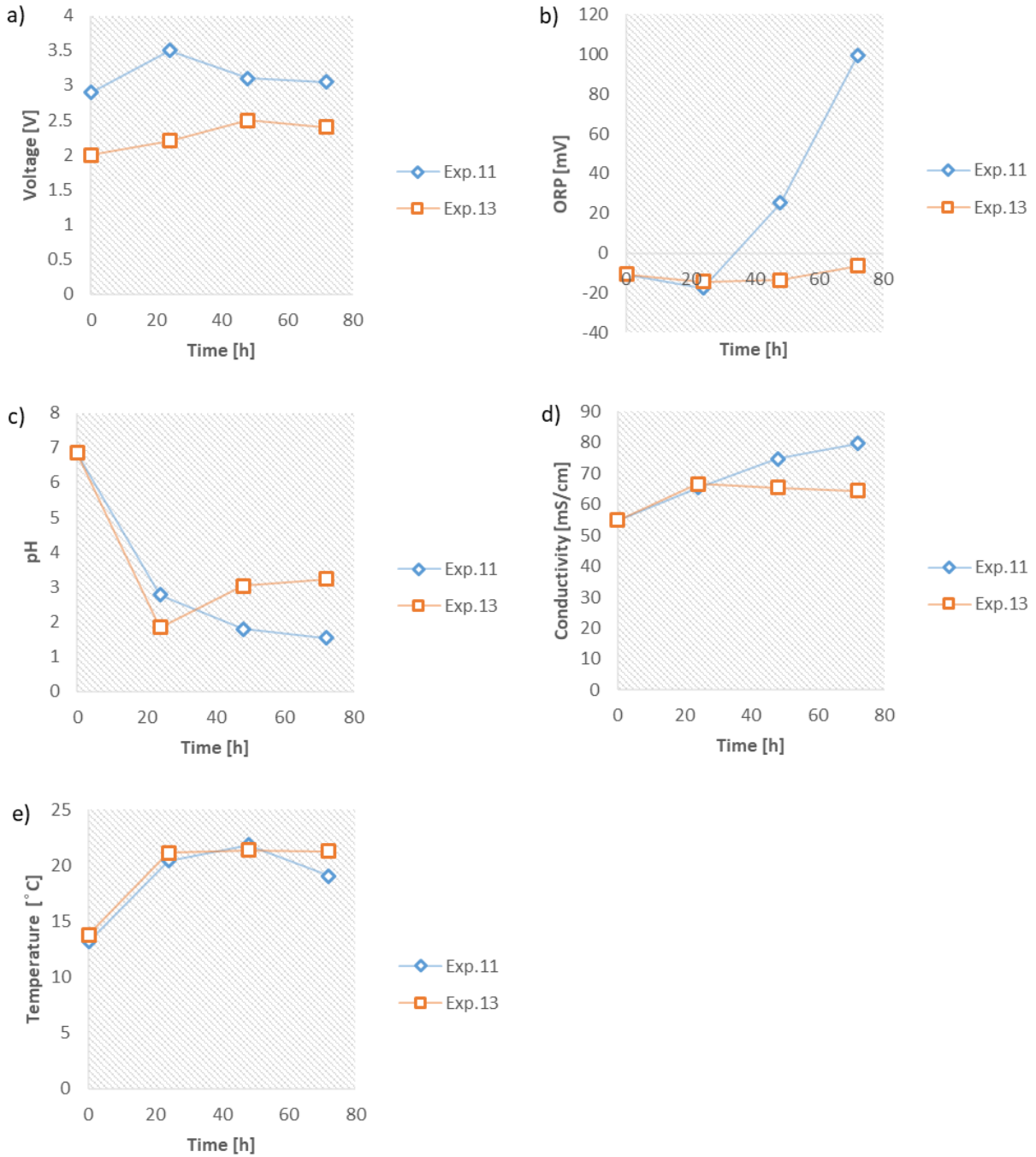


Figure 4- 5 Variations of monitored parameters for the relevant experiments of the 3rd objective of Stage 1-1: a) voltage versus time; b) pH versus time; c) ORP versus time; d) conductivity versus time; e) temperature versus time

The total nitrogen results (Fig.4-6c) surprisingly showed the equal removal efficiency for both experiments. It can be interpreted by the nature of the total nitrogen. Since the total nitrogen is a resultant of TKN, nitrate, and nitrite, the portion of nitrate and nitrite summation was significantly higher for Exp.13. Organic nitrogen removal efficiency (Fig.4-6d) showed a higher increase for the Exp.11. Based on previous discussion regarding the reason of achieving negative value for removal of organic nitrogen for the Exp.13, the rate of TKN removal was $38.88 \text{ mg/L}\cdot\text{h}$ throughout the entire exposure time while the ammonia removal rate was $49.16 \text{ mg/L}\cdot\text{h}$. In addition, the rates of TKN and ammonia removal during the entire exposure time were $41.66 \text{ mg/L}\cdot\text{h}$ and $54.16 \text{ mg/L}\cdot\text{h}$, respectively. The difference between removal rates of ammonia and TKN was $-10.28 \text{ mg/L}\cdot\text{h}$ for the Exp.13 while the mentioned difference was $-12.5 \text{ mg/L}\cdot\text{h}$ for the Exp.11. Therefore, it was expected to have a higher organic nitrogen formation in the cylindrical cell (Exp.11).

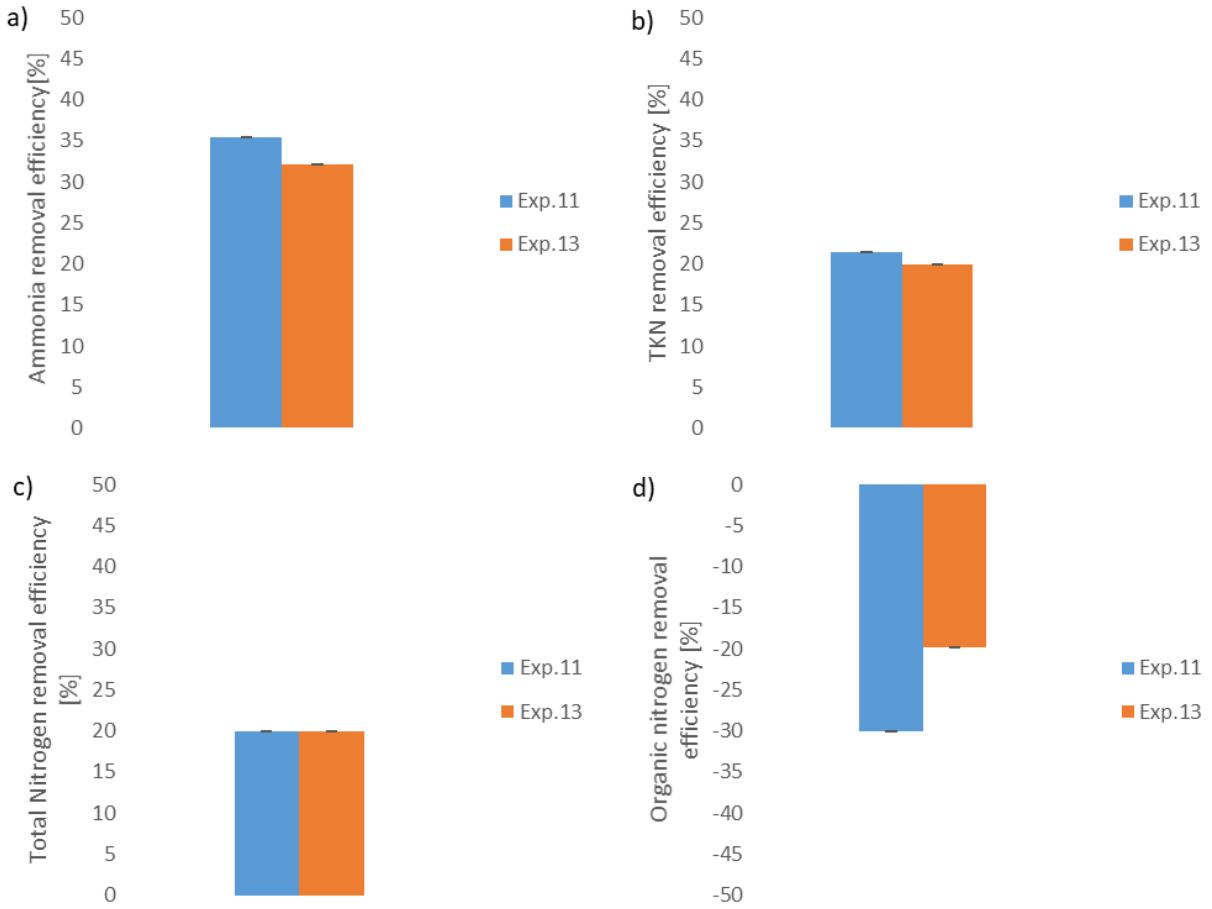


Figure 4- 6 Removal efficiency versus time for the 3rd objective of stage 1-1 considering: a) ammonia; b) TKN; c) organic nitrogen; d) total nitrogen

4-1-2. Stage 1-2 analysis

Stage 1-2 is determined to investigate the impacts of time intervals of adding hydrogen peroxide as one of the predominant parameters of upscaling on removal efficiency of target pollutants. In addition, the appropriate selection of time interval significantly affects the process efficiency in small scale. The function of hydrogen peroxide is providing sufficient hydroxyl radicals to proceed the electro-Fenton reactions. Therefore, the time interval of adding hydrogen peroxide is directly influenced on the mineralization of target compounds and the variations of monitoring parameters (e.g. ORP, conductivity, pH, and voltage). Three intervals of 24, 12, and 6 hours are considered for the Exp.24, Exp.29, and Exp.30, respectively.

The voltage changes versus time (Fig.4-7a) were the smoothest for the Exp.29 (12 hour interval) in comparison with other experiments. The voltage also increased to 3.9 V at the final 12 hour exposure time while the conductivity decreased to 112.43 mS/cm. The corresponding changes of voltage with respect to conductivity followed an expected behavior which was an increase in the voltage as a subsequent of decrease in conductivity^[4-3]. The Exp.30 (6 hour interval) showed high voltage changes due to a frequent addition of the hydrogen peroxide. The sharpest decrease took place in the first 6 hour period and the sharpest increase was detected after 18 hours. The increase of voltage during the last 6 hour exposure time (3.95 to 4.4 V) can be justified by a conductivity decrease (108.9 to 112.43 mS/cm).

However, the Exp.24 (24 hour interval) demonstrated an unexpected increase of voltage (3.6 to 3.9 V) while conductivity also increased (from 133.37 mS/cm to 140.23 mS/cm). Since an increase of 0.3 V cannot be considered as an insignificant change, justification of the mentioned unexpected behavior requires further assessment. It can be speculated that the exposure surface area of the

electrodes was exposed to a significant precipitation which interfered with the performance of the electrodes, conductivity, and subsequently voltage.

The pH changes curves (Fig.4-7b) showed a sharp decrease for all experiments during the first 24 hour period. The Exp.29 (12 hour interval) showed a lower pH (3.27) value at the first 12 hour exposure time in comparison with the Exp.30 (6 hour interval) which reached pH equals to 4.25. The highest final pH was also measured in the Exp.24 (24-hour interval) with the value of 0.96. A minimal pH (0.32) was found in the Exp.29 (12-hour interval) which was almost the same (0.34) as in Exp.30.

For the first 24 hour interval, the highest ORP (Fig.4-7c) belonged to Exp.24 (24 hour exposure time) with 107.45 mV while the Exp.29 (12 hour interval) and the Exp.30 (6 hour interval) stood on second and third rank, respectively. However, the significant increase was observed during the second 24 hour period for the Exp.29 and Exp.30. The detected ORP values for the Exp.24, Exp.29, and the Exp.30 were 223.47 mV, 360.2 mV, and 393.57 mV, respectively.

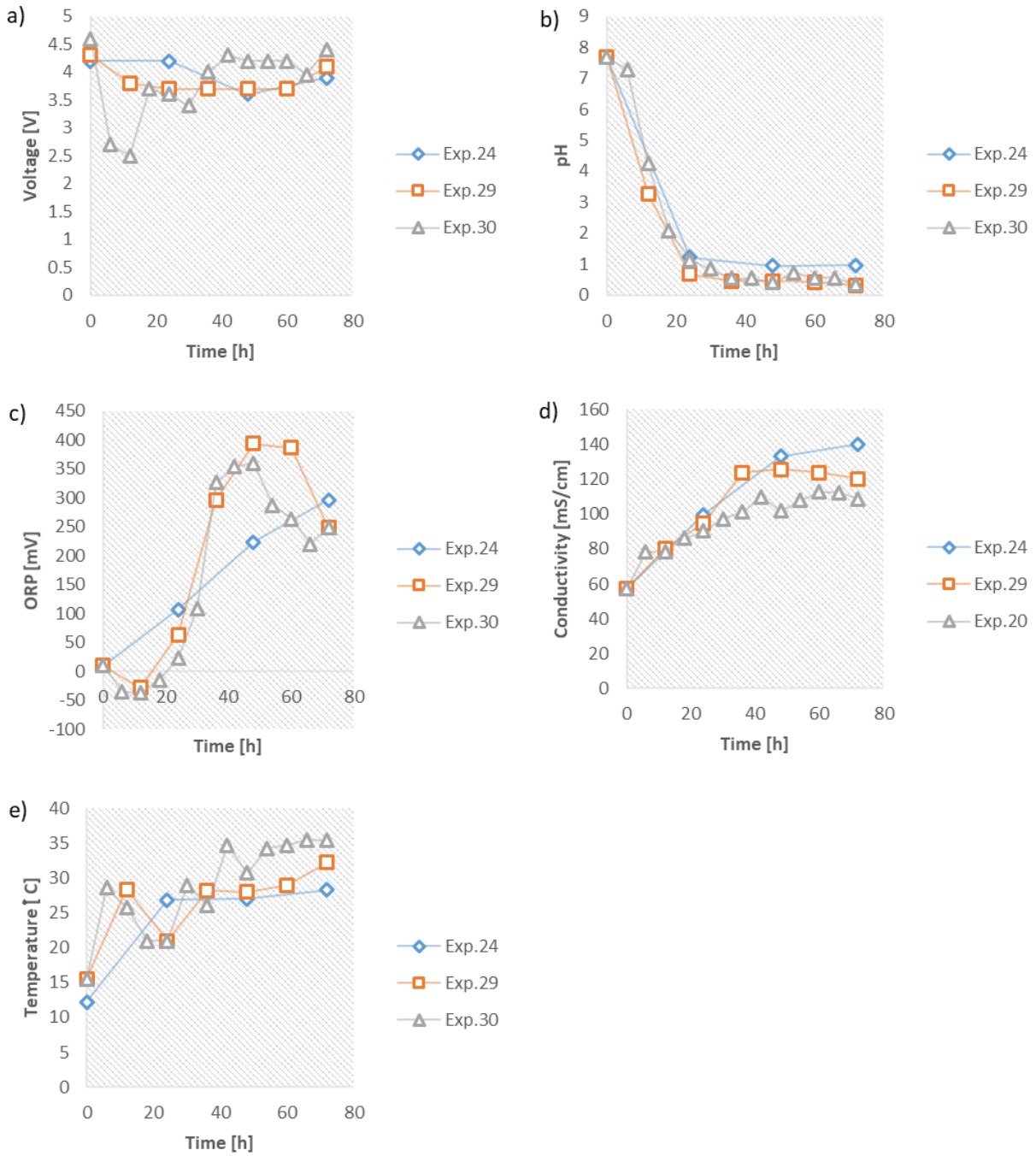


Figure 4- 7 Variations of monitored parameters for the relevant experiments of Stage 1-2; a) voltage versus time; b) pH versus time c) ORP versus time; d) conductivity versus time; e) temperature versus time

Experiments demonstrated unlike trends during the last 24 hour period. The Exp.24 (24 hour interval) provided the highest ORP among all experiments with the value of 296.87 mV. The Exp.29 (12 hour interval) experienced a slow decrease during the fifth 12 hour interval from 393.57 mV to 386.33 mV. However, the last 12 hour period demonstrated the sharpest reduction among all experiments, which lessened from 386.33 mV to 248.63 mV.

Remarkable decrease was observed for the Exp. 30 at 54 hours which kept its descending trend up to 60 hours. The Exp.30 experienced a significant increase during the last 6 hours. The value of ORP was 220.56 mV at 54 hours while the ORP at 60 hours was 249.03 mV.

The conductivity changes (Fig.4-7d) showed a congruous trend for all experiments during the first 24 hour exposure time, and the Exp.24 kept ascending tendency meanwhile the entire process time. However, the Exp.30 showed a gradual increase in conductivity from 24 hours to 42 hours and a sudden decrease from 42 hours to 48 hours. Again, the conductivity increased from 101.97 mS/cm to 112.43 mS/cm from 48 h to 60 h. The last 6 hours of exposure time of the Exp.30 proceeded with a gradual decrease in conductivity which ended up giving 108.9 mS/cm.

The Exp.29 (12-hour time interval) showed a sharp increase from 90.43 mS/cm to 123.73 mS/cm during the third 12-hour time interval. However, the mentioned experiment experienced a continuous gradual decline from 36 h to 72 h, while the final achieved conductivity was 120.25 mS/cm. The minimal achieved conductivity belonged to the Exp.30 with the value of 108.9 mS/cm and the maximal one belonged to the Exp.24 (24 hour interval) which was equal to 140.23 mS/cm.

The temperature variation of the Exp. 24 (Fig.4-7e) followed an expected behavior which was an initial surge, being slightly constant in the second 24 hour period, and a gradual increase in the last 24 hour exposure time. However, temperature variation was significantly distinctive in the Exp.29

(12-hour time interval). It experienced a sharp increase in the first 12 hour exposure time while sharp decrease was detected in the second 12 hour period. The second sharp increase was recorded at the third 12 hour interval which proceeded with ascending trend up to the end. The final temperature of Exp.29 was 32.2 °C.

The distinctive behavior of the Exp.30 (6 hour time interval) showed several sharp both increases and decreases meanwhile the process. The maximal final temperature among all experiments also belonged to the Exp.30 with the value of 35.4 °C. Four sharp increases took place at 6, 30, 42, and 54 hour exposure time, respectively. On the other hand, four sharp decreases occurred at 12, 18, 36, and 48 hours, respectively.

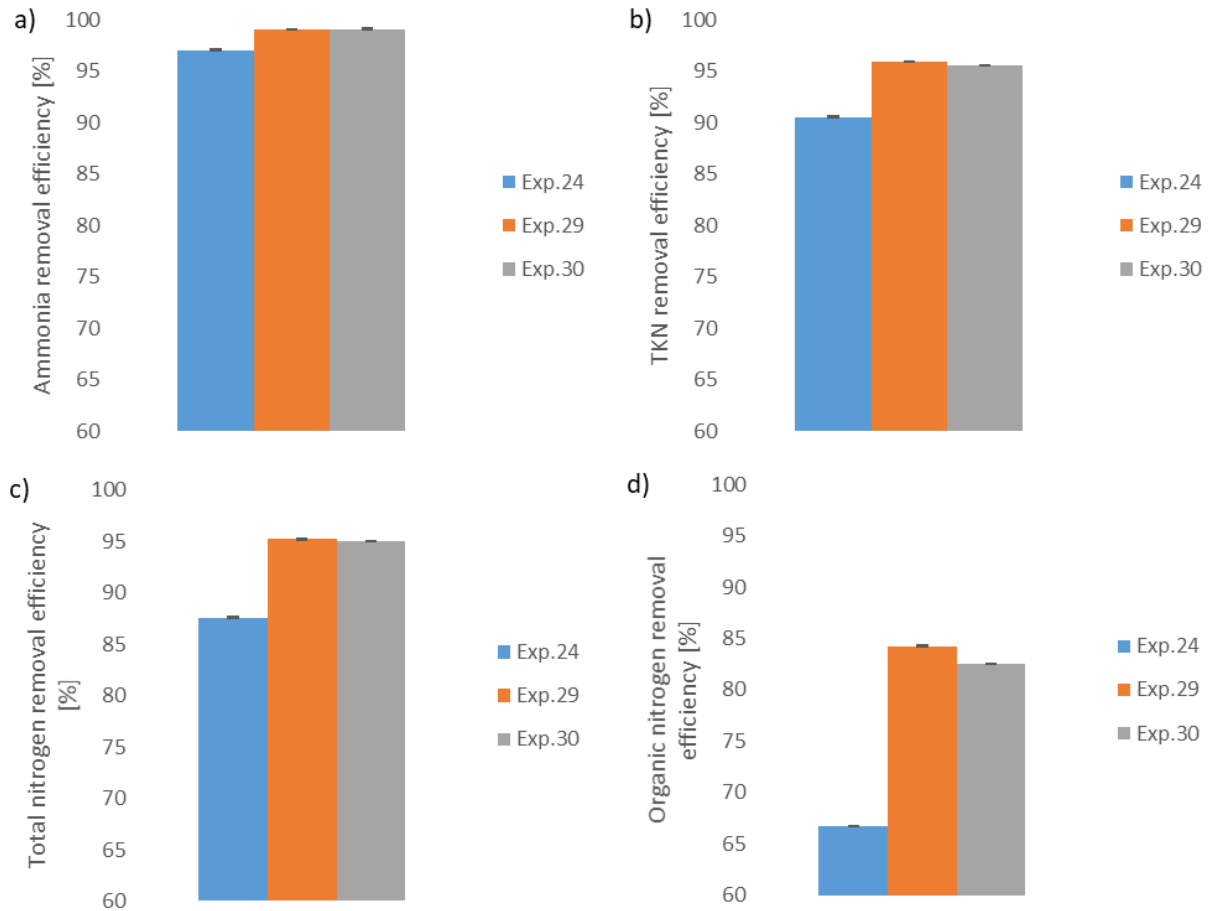


Figure 4- 8 Removal efficiencies of the pollutants for stage 1-2 a) ammonia removal efficiency; b) TKN removal efficiency; c) organic nitrogen removal efficiency; d) total nitrogen removal efficiency

Removal efficiency of ammonia was $99.08\% \pm 0.018\%$ for the Exp.29 (Fig.4-8a), which was approximately like achieved removal in the Exp.30 with $99.13\% \pm 0.018\%$. For TKN (Fig.4-8b), total nitrogen (Fig.4-8c), and organic nitrogen (Fig.4-8d), the best achieved removal efficiency was obtained with adding hydrogen peroxide each 12 hours meanwhile the process. In addition, the removal efficiency for TKN, total nitrogen, and organic nitrogen were $95.9\% \pm 0.011\%$, $84.26\% \pm 0.038\%$, and $95.23\% \pm 0.04\%$, respectively. It might be questionable that why adding hydrogen peroxide in the 6 hour time interval did not give superior results in comparison with 12 hours. The answer could be related to the demand of sufficient retention time for the expected

oxidation reactions. Therefore, one of the upscaling experimental parameters would be time interval of adding hydrogen which is set as 12 hour for large scale.

4-1-3. Stage 1-3 analysis

Stage 1-3 investigates the impact of pretreatment of the present sulfate in the influent. Due to expected problems originated from the sulfate presence in the system (e.g. enormous sludge generation, very low pH evolution and a possibility of hydrogen sulfide emission); then, removing sulfate came into consideration. Barium hydroxide ($\text{Ba}(\text{OH})_2$) was used to precipitate present sulfate in the form of barium sulfate (BaSO_4). Two distinctive molar ratios of 1/1 and 2/1 were applied. The obtained results were compared with the Exp.19, where no barium hydroxide was added.

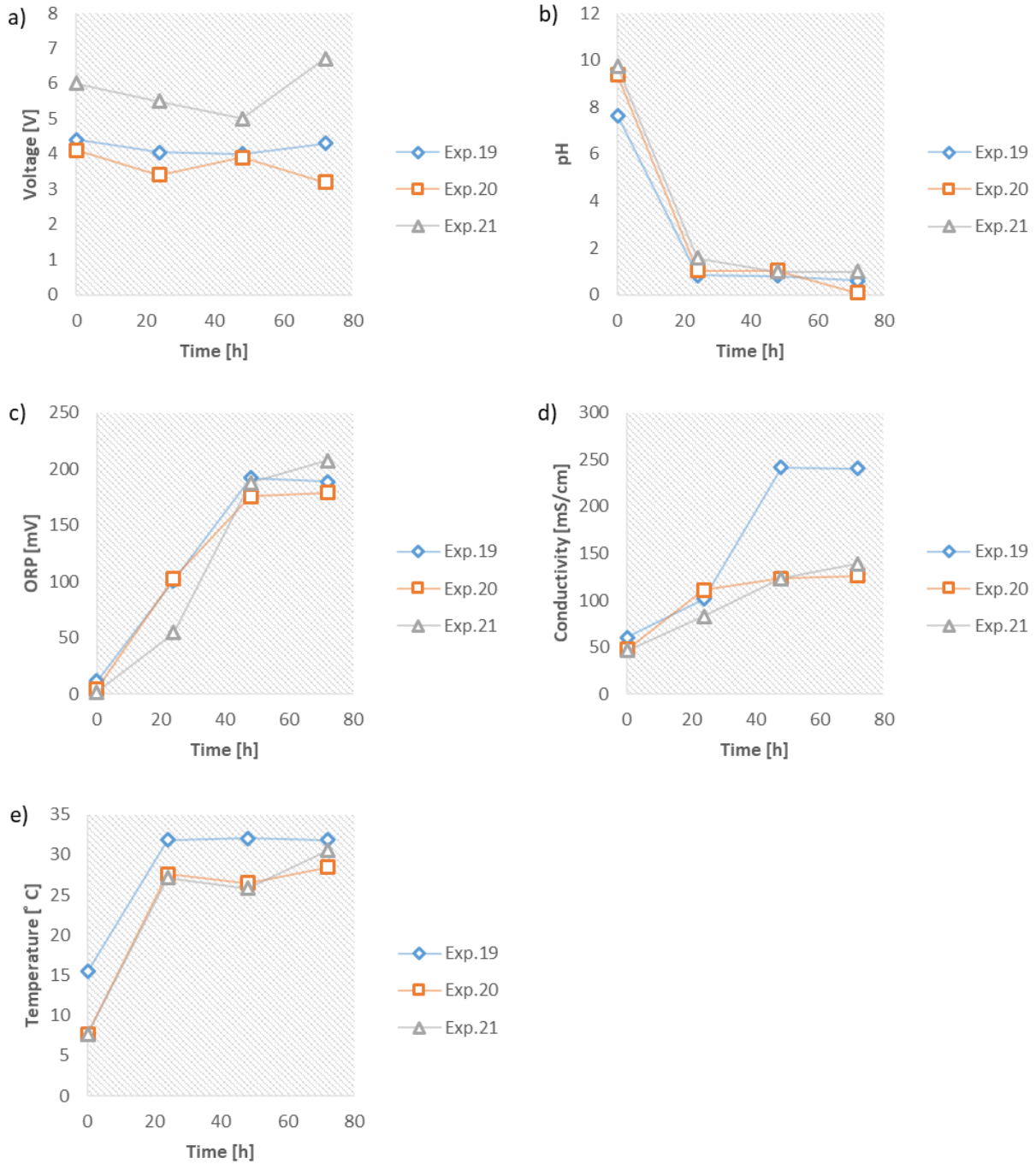


Figure 4- 9 Variations of monitored parameters for the relevant experiments of Stage 1-3; a) voltage versus time; b) pH versus time c) ORP versus time; conductivity versus time e) temperature versus time

The voltage variations (Fig.4-9a) of the Exp.19 (without barium hydroxide) showed a descending tendency from the beginning up to 48 hours, and it was congruous with a sharp increase of

conductivity. However, the voltage increased from 4 V to 4.3 V during the last 24 hour period while conductivity decreased from 241.73 mS/cm to 240.2 mS/cm. The Exp.20 showed an expected behavior for the first 24 hour exposure time. In the other words, voltage decreased from 4.1 V to 3.4 V while the conductivity increased from 47.9 mS/cm to 111.1 mS/cm. The voltage changed from 3.9 V to 3.2 V matched with the conductivity variations which increased from 123.6 mS/cm to 125.9 mS/cm. The distinctive behavior was observed for The Exp.21 (with 2/1 barium hydroxide) with an initial voltage of 6 V and the final voltage of 6.7 V. The initial and final voltage were the highest values that were recorded among all experiments of Phase 1. The tendency of the voltage changes was declining from the beginning up to 48 hours and the value of voltage was 5 V at 48 hours. However, the voltage change in the Exp.21 did not correspond expected conductivity changes during the last 24 hour exposure time and both curves were ascending. The voltage increased from 5 V to 6.7 V and conductivity surged from 123.6 mS/cm to 138.9 mS/cm. The reason is justified by the barium compounds ability to enhance the performance of the electrochemical cell. Based on Patent WO2000030198A1 ^[4-6], using barium hydroxide as an additive significantly improves the cathode performance, which leads to increase the electrode potential at the cathode side. In addition, the conductivity significantly increases due to introducing electroactive compounds.

pH changes showed a sharp decrease (Fig.4-9b) in the first 24 hour period. The Exp.19 (no additives) showed stabilized change in the range of 0.82 to 0.81 during the second 24 hour exposure time. In addition, Exp.20 (1/1 molar ratio of barium hydroxide) showed the same behavior as the Exp.19 with a variation within the range between 1.09 and 0.99 during the second period of 24 hours. The Exp.19 (no additives) and the Exp.21 (2/1 molar ratio of barium hydroxide) demonstrated a slight change during the last 24 hour period. In contrast, Exp.20 showed a sharp

decrease from 1.04 to 0.1 during the last 24 hour exposure time. It can be concluded that the molar ratio of 2/1 was effective in stabilizing the pH around 1.

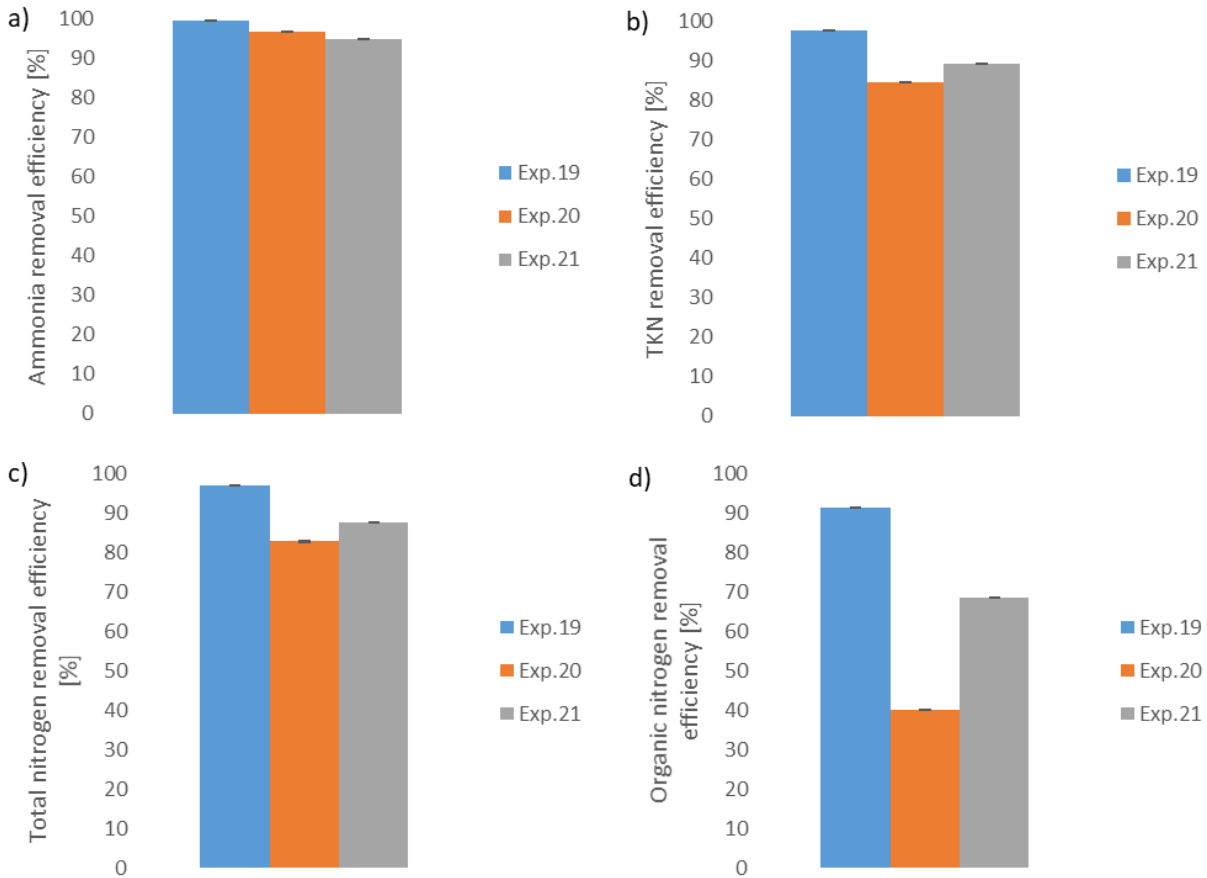


Figure 4- 10 Removal efficiencies of the pollutants for Stage 1-3; a) ammonia removal efficiency; b) TKN removal efficiency; c) organic nitrogen removal efficiency; d) total nitrogen removal efficiency

The trends of ORP changes (Fig.4-9c) were ascending while the lowest conductivity was achieved in the Exp.21 (2/1 molar ratio of barium hydroxide) during the first 24 hour period. During the second 24 hour exposure time (from 24 hours to 48 hours), the intensity of increase was relatively stronger for the Exp.21 and the maximum attained ORP was 187.9 mV at the end of the second 24 hour exposure time. The Exp.19 (no additives) showed descending behavior during the last 24 hour exposure time (from 48 hours to 72 hours) and the final ORP was 188.53 mV. However, the

lowest ORP was achieved by the Exp.20 (1/1 molar ratio of barium hydroxide) with the value of 178.93 mV. However, the observed tendency was ascending for the Exp.20. The maximum ORP (207.26 mV) was achieved by the Exp.21. The reason of ascending behavior in both Exp.20 and Exp.21 is the presence of hydroxyl ions which can participate in oxidation reactions.

Conductivity variations (Fig.4-9d) showed that the Exp.20 (1/1 molar ratio of barium hydroxide) and Exp.21 (2/1 molar ratio of barium hydroxide) have lower final value in comparison with the Exp.19 (no additives). The tendencies of all experiments were ascending during the initial 48 hour exposure time (from 0 to 48 hours). In addition, the maximum conductivity was achieved by the Exp.19 with the value of 241.73 mS/cm at 48 hours. The ascending tendency of the Exp.20 and Exp.21 continued during the last 24 hour exposure time (from 48 hours to 72 hours), while the Exp.19 faced a gradual decrease. The significant difference between final conductivity values of the Exp.20 (125.9 mS/cm) and the Exp.21 (138.9 mS/cm) with the Exp.19 (240.2 mS/cm) was observed. In the other words, the difference between the final conductivity of both Exp.19 and Exp.20 was 114.3 mS/cm and measured difference between the final conductivity of Exp.19 and Exp.21 was 101.3 mS/cm. The observed significant difference can be justified by the solution of barium hydroxide increased the resistivity of the cell due to the introduced total solid content. As a result, the conductivity significantly decreased in comparison with the experiments with additives.

Then, temperature variations (Fig.4-9e) of the Exp.19 was ascending during the first 24 hour exposure time. It also continued with slightly constant changes from 24 hours to 72 hours. However, the tendency of variations for the Exp.20 and Exp.21 did not show the same behavior as Exp.19. Furthermore, the decrease and increase of the temperature were observed for the Exp.20 and Exp.21 during the second and third 24 hour period, respectively. The maximum temperature

was obtained by the Exp.19 with the value of 31.8 °C and the minimum one was achieved by Exp.20 with the amount of 28.4 °C.

According to Figure 4-10, the best ammonia removal efficiency ($99.4\% \pm 0.018\%$) was achieved by the Exp.19 (no additives) while the minimum ($94.76\% \pm 0.018\%$) by the Exp.21. The highest removal efficiency for TKN, TN, and organic nitrogen was also obtained in the experiment without additives (Exp.19) at the levels of $97.66\% \pm 0.011\%$, $96.91\% \pm 0.038\%$, and $91.15\% \pm 0.04\%$, respectively. The minimum removal efficiency of TKN was obtained in the Exp.20 (1/1 barium hydroxide molar ratio) with the value of $84.57\% \pm 0.011\%$. In addition, the minimum removal of total nitrogen, and organic nitrogen resulted in the Exp.20 which were 82.69% and 40.16%, respectively. It can be concluded that adding barium hydroxide did not improve the removal efficiency of ammonia, TKN, total nitrogen, and organic nitrogen, correspondingly.

4-1-4. Stage 1-4 analysis

Stage 1-4 investigates the impact of adding the Fenton agent. Fenton agent which acts as heterogeneous catalyst was added to the electrokinetic (EK) reactor in the form of ferrous sulfate (FeSO_4). A major material which was used as a source of ferrous (Fe^{2+}) was ferrous sulfate heptahydrate ($\text{FeSO}_4 \cdot 7\text{H}_2\text{O}$)^[4-7]. Based on Zhukovskaya's research^[1-13] on the same wastewater, the optimal ratio of ferrous ions to hydrogen peroxide ($\text{Fe}^{2+}/\text{H}_2\text{O}_2$) was 0.05. Therefore 3.01 g of ferrous sulfate was added to a raw wastewater.

The voltage changes (Fig.4-11a) demonstrated that the initial voltage (5 V) of the Exp.37 (with adding Fenton agent) was significantly higher than the initial voltage (4.4 V) of the Exp.19 (no addition of Fenton agent). The tendencies of both experiments were descending during the first 24 hour exposure time. The voltage of the Exp.19 decreased slightly from 4.05 V to 4 V. In contrast,

the Exp.37 experienced a sharp increase from 4.4 V to 5.9 V meanwhile the second 24 hour exposure time (from 24 hours to 48 hours). During the last 24 hour period, both experiments showed an increasing tendency. However, the Exp.37's voltage slightly increased from 5.9 V to 6 V. On the other hand, the Exp.19's voltage increased sharply from 4 V to 4.3 V.

pH changes (Fig.4-11b) showed that the Exp.37 (with adding Fenton agent) experienced a sharper decrease in comparison with the Exp.19 in which reached 0.28 from the initial value of 6.45 meanwhile the first 24 hour exposure time. It is notable that adding Fenton agent decreased the initial pH from 7.65 to 6.45. The reason was an increase in available sulfate ions after adding Fenton agent. The pH of the Exp.37 continued decreasing to 0.18 during the second 24 hour exposure time (from 24 hours to 48 hours). Distinctively, pH changes showed an ascending behavior and pH increased from 0.18 to 0.78 meanwhile the third 24 hour exposure time (from 48 hours to 72 hours).

ORP variations (Fig.4-11c) of the Exp.37 (with adding Fenton agent) demonstrated an exclusive trend in which the final ORP was remarkably higher than the Exp.19 one. During the first 24 hour period, the ORP of the Exp.37 increased from initial 9.9 mV to 181.53 mV. Then, it kept increasing to 426.53 mV meanwhile the second 24 hour exposure time until the final ORP of 442.1 mV which is the highest among all experiments of Phase 1. The reason was availability of a higher mass of catalyst which accelerated the production of hydroxyl radicals.

Conductivity changes (Fig.4-11d) in the Exp.37 (with adding Fenton agent) showed that it can be significantly decreased meanwhile the process. The initial conductivity of the Exp.37 was 57.4 mS/cm while the Exp.19's initial conductivity was 60.6 mS/cm. The Exp.37 conductivity increased to 110.46 mS/cm after 24 hours which was close to the value of obtained in the Exp.19

(101.3 mS/cm). However, the slope of increase was much larger for the Exp.19 in comparison with the Exp.37 for the second 24 hour exposure time (from 24 hours to 48 hours). For instance, the conductivity of the Exp.37 increased from 110.46 mS/cm to 123.3 mS/cm while the Exp.19's conductivity reached 241.73 mS/cm from 101.3 mS/cm. During the last 24 hour exposure time (from 48 hours to 72 hours), the conductivity of the Exp.37 decreased to 103.2 mS/cm and the observed behavior was descending. In contrast, the Exp.19 experienced a negligible decrease in which the conductivity reached 240.2 mS/cm from 241.73 mS/cm.

Temperature variations (Fig.4-11e) of the Exp.37 (with Fenton agent) demonstrated that a significant difference between the final temperature of the Exp.19 and Exp.37. In fact, the final temperature of the Exp.37 was 40.5 °C while the ultimate temperature of the Exp.19 was 31.8 °C. The tendency of changes of the Exp.37 was ascending during 48 hour exposure time (0 to 48 hours) and the achieved temperature was 40.4 °C at 48 hours. During the last 24 hour period, the temperature of the Exp.37 was almost constant and reached 40.5 °C at 72 hours.

According to Fig.4-12a, once Fenton agent was introduced to the electrokinetic reactor, the removal efficiency of the target pollutants enhanced except for ammonia. The Exp.37 (with adding Fenton agent) reached 98.82% ± 0.018% ammonia removal while the corresponding value for the Exp.19 (no addition of Fenton agent) was 99.44% ± 0.018%. TKN removal efficiency (Fig.4-12b) was improved after adding the heterogeneous Fenton agent and it increased for 0.71%. The TKN removal efficiency of the Exp.37 was 98.37% ± 0.011%.

Total nitrogen removal efficiency (Fig.4-12c) was also improved by 0.49% and it reached 97.4% ± 0.038%. The result of the organic nitrogen removal efficiency can be considered as the best achieved results in the Exp.37 among all experiments of Phase 1. The organic nitrogen removal

efficiency (Fig.4-12d) enhanced by 5.58% and the observed efficiency was $96.73\% \pm 0.04\%$. Therefore, it can be speculated that adding heterogeneous Fenton agent will significantly increase the organic nitrogen mineralization. However, obtaining the heterogeneous Fenton agent as governing method was avoided due to detection of 2 ppm hydrogen sulfide gas emission.

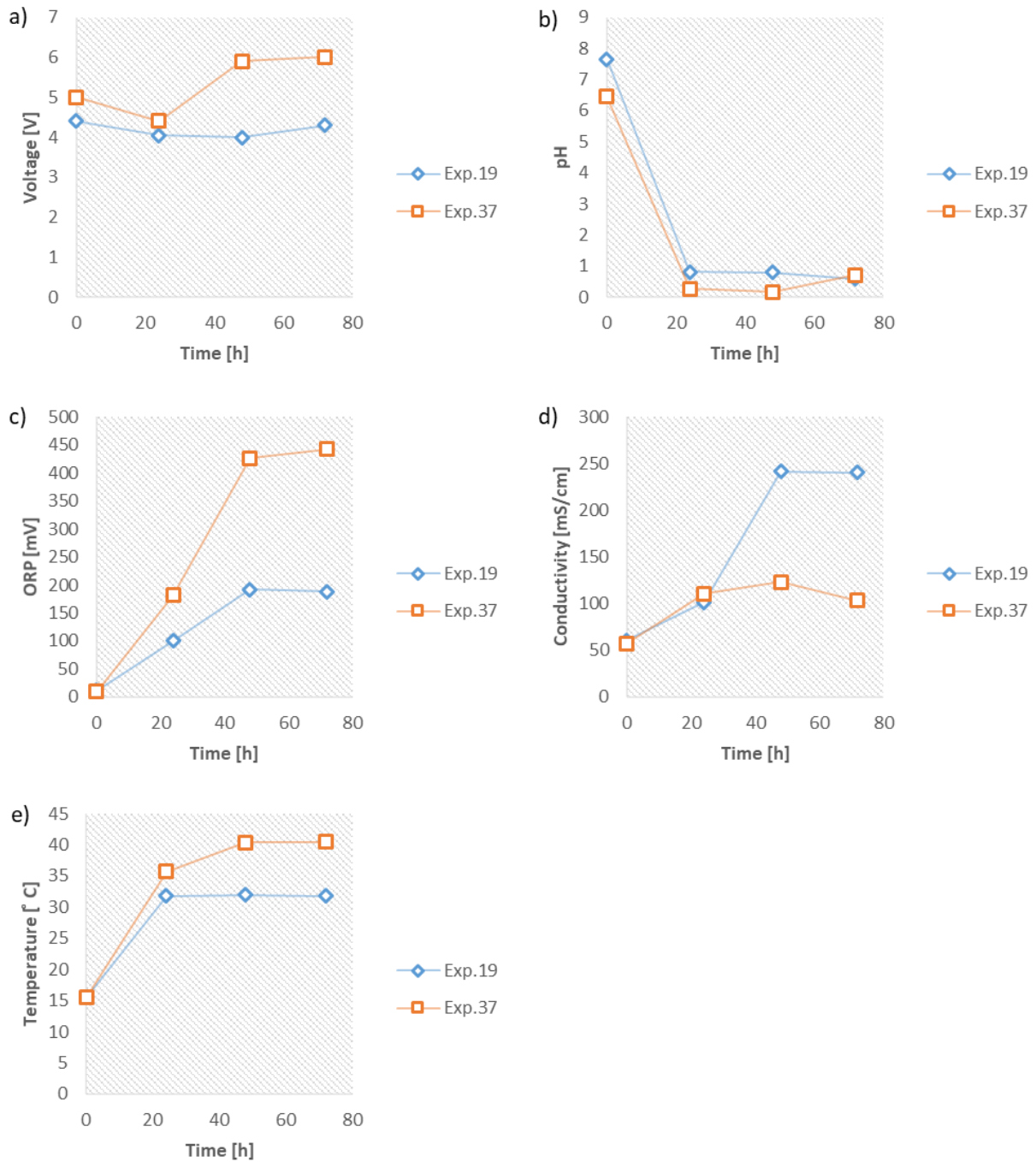


Figure 4- 11 Variations of monitored parameters for the relevant experiments of Stage 1-4; a) voltage versus time; b) pH versus time c) ORP versus time; d) conductivity versus time e) temperature versus time

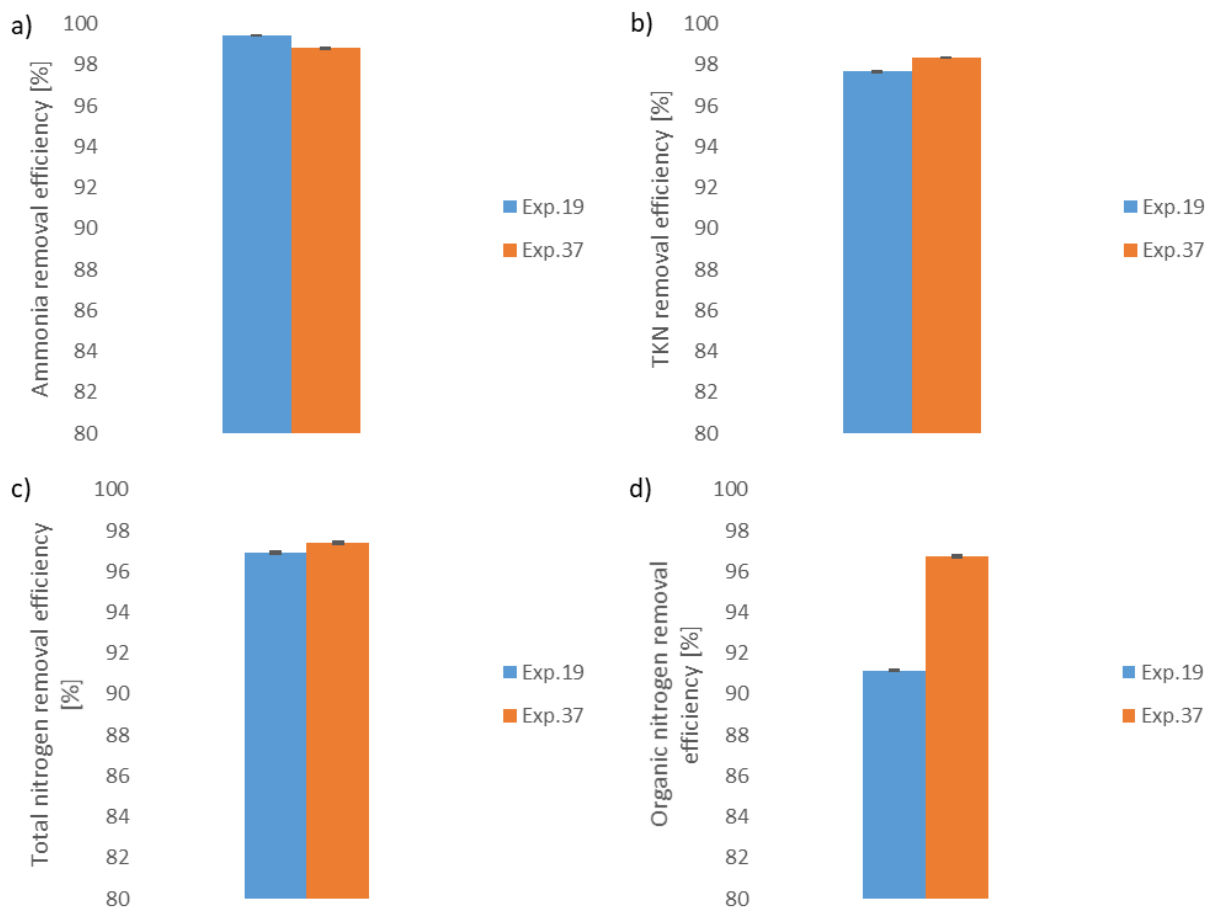


Figure 4- 12 Removal efficiencies of the pollutants for Stage 1-4; a) ammonia removal efficiency; b) TKN removal efficiency; c) organic nitrogen removal efficiency; d) total nitrogen removal efficiency

4-1-5. Stage 1-5 analysis

The impact of current density variation is investigated in Stage 1-5. Four distinctive current densities (33.33 mA/cm^2 , 37.7 mA/cm^2 , 22.22 mA/cm^2 , and 27.77 mA/cm^2) were considered and the logic of the current density selection was described in Section 3-2-1. The applied current density was strongly dependent on an exposure surface of the anode. In order to eliminate the impact of the anode surface area on the applied current, the constant value of 57.75 cm^2 was considered as the exposure surface area of anode.

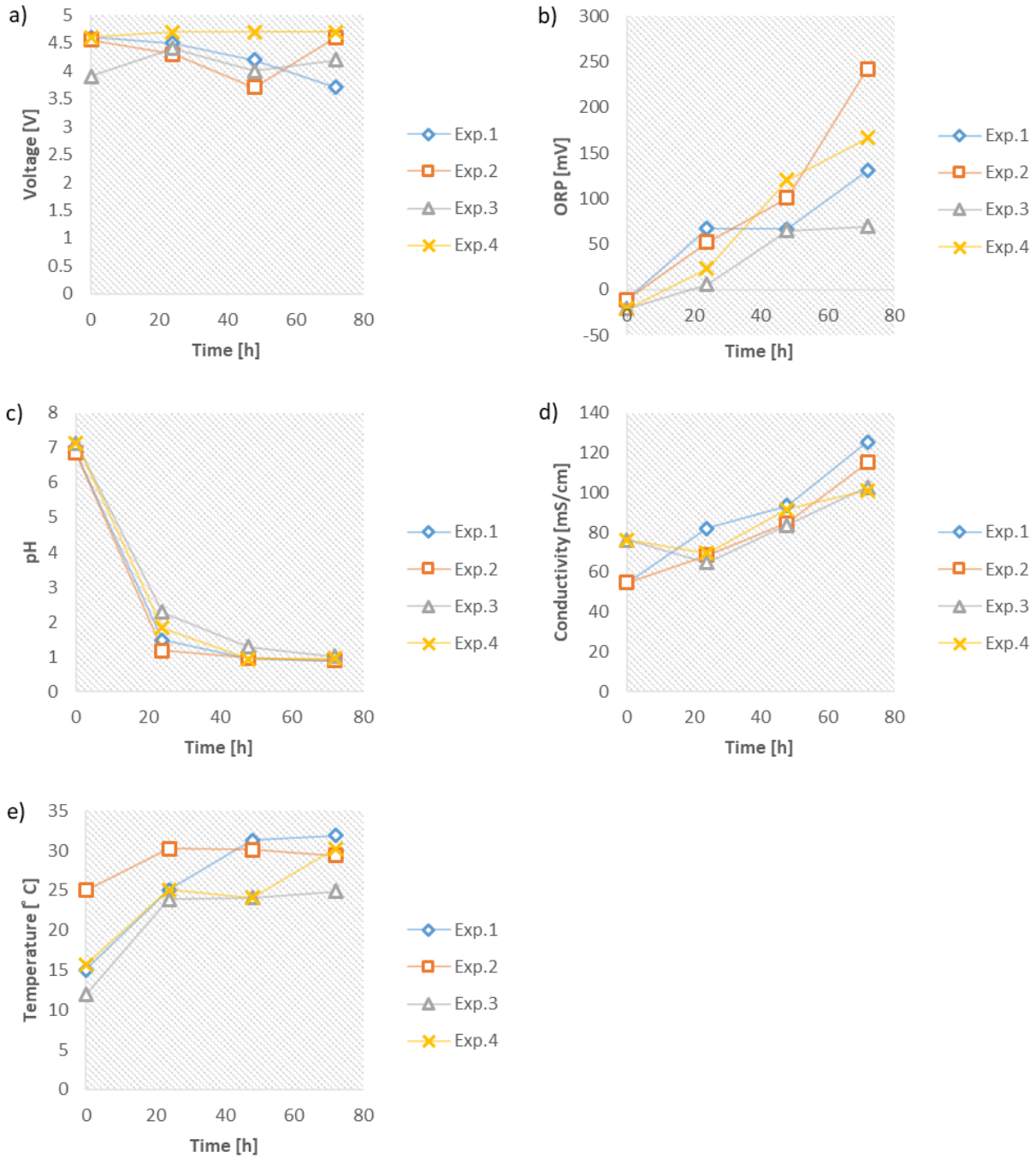


Figure 4- 13 Variations of monitored parameters for the relevant experiments of Stage 1-5; a) voltage versus time; b) pH versus time c) ORP versus time; d) conductivity versus time e) temperature versus time

The voltage changes curves (Fig.4-13a) showed that the Exp.1 (current density of 33.33 mA/cm²) obtained a descending trend, in which the initial voltage of 4.6 V reached 3.7 V after 72 hours.

The conductivity measurements demonstrated an ascending trend which was expected. Over the first 48 hour period, the voltage of the Exp.2 (current density of 37.7 mA/cm^2) decreased continuously from 4.55 V to 3.7 V, while it experienced a sharp increase meanwhile the last 24 hour exposure time (from 48 hours to 72 hours) and reached 4.6 V. The voltage of the Exp.3 (current density of 22.22 mA/cm^2) showed a sharp increase during the first 24 hour exposure time (from initial to 24 hours) reaching 4.4 V from initial value of 3.9 V. Afterwards, the Exp.3 obtained a descending trend and the cell potential reached 4 V. Meanwhile the last 24 hour exposure time, the Exp.3 faced a gradual increase and the final potential was 4.2 V after 72 hour exposure time. The Exp.4 (current density of 27.7 mA/cm^2) demonstrated a distinctive behavior, where no significant variation was observed during the entire exposure time. The only variation occurred during the first 24 hour period and the voltage reached 4.7 V from initial 4.6 V. The cell potential remained constant during the remaining 48 hour exposure time (from 24 hours to 72 hours).

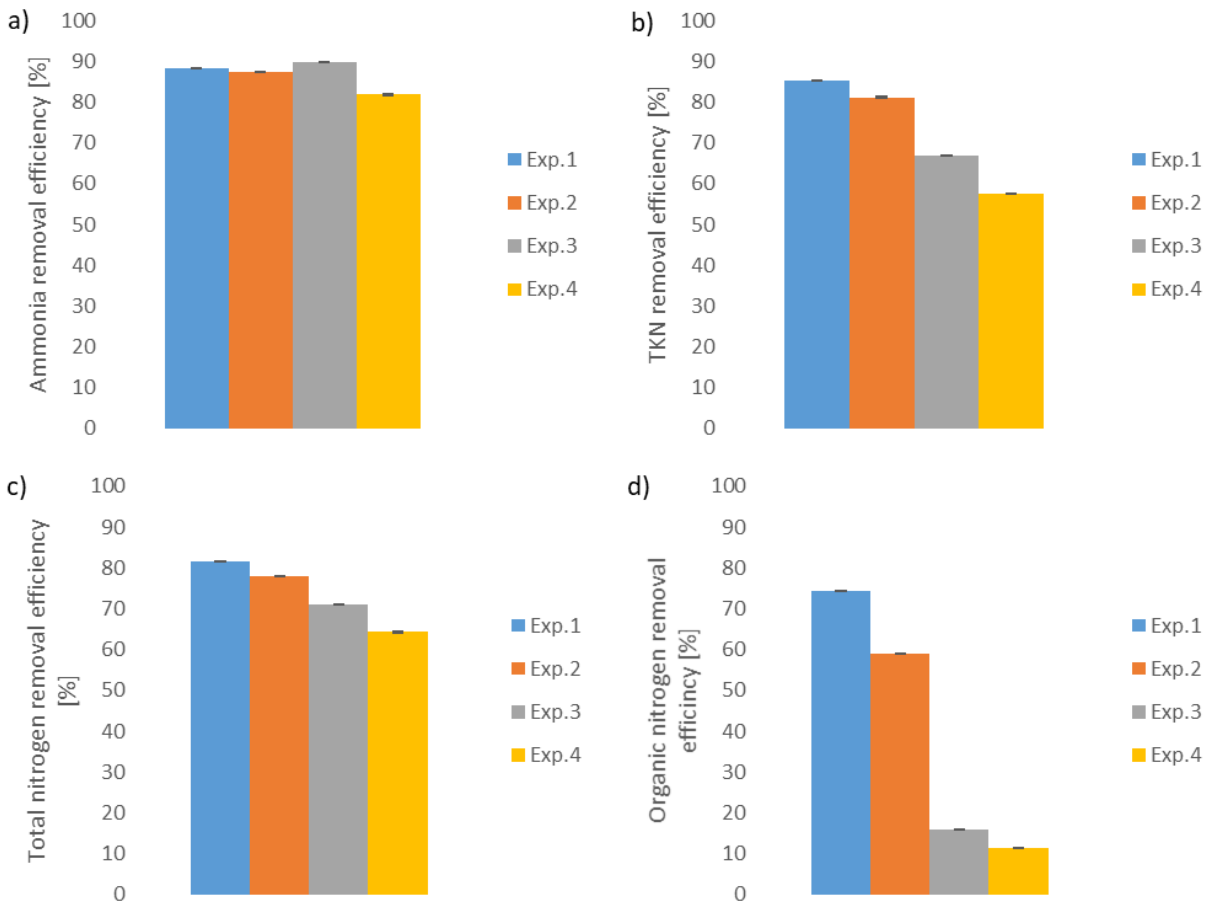


Figure 4- 14 Removal efficiencies of the pollutant for Stage 1-5; a) ammonia removal efficiency; b) TKN removal efficiency; c) organic nitrogen removal efficiency; d) total nitrogen removal efficiency

After 24 hours of treatment, the Exp.3 (current density of 22.22 mA/cm^2) reached the highest pH (2.28) value while the lowest pH (1.18) was observed in the Exp.2 (current density of 37.7 mA/cm^2). In addition, the Exp.3 showed the highest pH (1.29) at 48 hours whereas the lowest pH (0.94) was achieved by the Exp.4 (current density of 27.77 mA/cm^2). The final pH values of all experiments were in the range between 0.89 to 1.01, while both Exp.1 (current density of 33.33 mA/cm^2) and Exp.2 reached the pH minimal value of 0.89 (Fig.4-13b).

ORP changes (Fig.4-13c) demonstrated that the Exp.1 (current density of 33.33 mA/cm²) provided the highest ORP (67.23 mV) at 24 hours while the lowest ORP was reached by the Exp.3 (current density of 22.22 mA/cm²). Meanwhile the second 24 hour exposure time (from 48 hours to 72 hours), the sharpest increase and the highest value were obtained by the Exp.4 (27.77 mA/cm²) when ORP increased from 23 mV to 120.23 mV. Whereas the lowest recorded ORP was 64 mV (Exp.3) at 48 hours. The maximum ORP (242.46 mV) was achieved by the Exp.2 (current density of 37.7 mA/cm²) at the third 24 hour exposure time (from 48 hours to 72 hours). The minimum ORP value was achieved by Exp.3 with the value of 69.43 mV. The gradual and non-significant increase of ORP in Exp.3 showed that the occurred reactions were not capable of providing a strong oxidation state while the current density was minimal (22.22 mA/cm²). In contrast, the highest ORP was provided by applying the highest current density equals 37.7 mA/cm².

Conductivity variations (Fig.4-13d) showed that the Exp.1 (current density of 33.33 mA/cm²) and the Exp.2 (current density of 37.7 mA/cm²) had ascending trends meanwhile the first 24 hour exposure time (initial to 24 hours). Whereas, both Exp.3 (current density of 22.22 mA/cm²) and Exp.4 (current density of 27.77 mA/cm²) obtained descending trend. During the remaining 48 hour exposure time (from 24 hours to 72 hours), all experiments demonstrated an ascending behavior and the maximum conductivity of 125.53 mS/cm was achieved by the Exp.1 (current density of 33.33 mA/cm²) at the end point (72 hours). In addition, the minimum conductivity was achieved by the Exp.4 which was equal to 101.2 mS/cm. It was expected to observe the maximum conductivity in the Exp.2 due to having the highest current density; however, the observations did not follow the expectation. To construe the observed behavior, it was crucial to consider the associated parameters in the conductivity equation (Eq.4-2)

$$[4-2] \sigma = \frac{1}{\rho} = \frac{J}{E}$$

σ conductivity S/m,

ρ electrical resistivity [Ωm],

J magnitude of current density [A/m^2],

E electric field [V/m], where distance between electrodes and their surface are constant,

Since the electric field was varied due to the change of the voltage, the final point of electric field was considered to investigate the reason of the maximum conductivity in the Exp.1. The expected conductivity of the Exp.1 based on observed voltage and implementing the values into Eq.4-2 was 4.5 S/m (45 mS/cm) while 4.1 S/m (41 mS/cm) was obtained for the Exp.2. Although the calculated results were different from observed conductivity, it can fairly show that the Exp.1 should obtain a higher conductivity than the Exp.2.

Results showed that the temperature increased in all experiments during the first 24 hour exposure time (from initial to 24 hours), while the maximum temperature (30.2 °C) was achieved in Exp.2 (current density of 37.7 mA/cm²). During the remained 48 hour exposure time (from 24 hours to 72 hours), the Exp.2 presented a descending behavior with a final temperature of 29.4 °C. In contrast, Exp.1 (conductivity of 33.33 mA/cm²) and the Exp.4 (conductivity of 27.77 mA/cm²) demonstrated an ascending trend during the remained 48 hour exposure time. Furthermore, the maximum temperature of 31.9 °C was achieved in the Exp.1. The Exp.3 (22.22 mA/cm²) showed an insignificant decrease in temperature (from 25.1 °C to 24.9 °C) during the remaining 48 hours.

According to Fig.4-14a, the highest ammonia removal efficiency (89.91% ± 0.018%) was obtained by implementing CD equals to 22.22 mA/cm² (Exp.3) while the lowest one was achieved by

introducing CD equals to 27.7 mA/cm². The Exp.1 (current density of 33.33 mA/cm²) reached a better efficiency in comparison with the Exp.2 (current density of 37.7 mA/cm²), when a difference between the obtained removals was 1%.

TKN removal efficiency (Fig.4-14b) of Exp.1 (current density of 33.33 mA/cm²) found to be superior among all experiments of Stage 1-5. The achieved TKN removal efficiency was 85.28% ± 0.011% for the Exp.1. In contrast, the lowest removal efficiency (57.63 % ± 0.011%) was obtained once CD equals to 27.77 mA/cm² (Exp.4) was applied. In addition, total nitrogen removal efficiency (Fig.4-14c) faced the same standings. An excellent removal efficiency was observed for the Exp.1 (current density of 33.33 mA/cm²) while the worst one (64.27% ± 0.038 %) was obtained for the Exp.4.

The significant difference was recorded for the organic removal efficiency (Fig.4-14d) among all experiments of Stage 1-5. The Exp.1 (current density of 33.33 mA/cm²) and Exp.2 (current density of 37.7 mA/cm²) provided 74.33% ± 0.04% and 59% ± 0.04% removal efficiency, respectively. Whereas, the Exp.3 (current density of 22.22 mA/cm²) and Exp.4 (current density of 27.77 mA/cm²) reached 16% and 11.33% removal efficiency, correspondingly.

Based on the achieved removal efficiency, the current density equals to 33.33 mA/cm² was considered for further tests in the small-scale experiments. Particularly, the highest removal efficiency resulted in applying CD equals to 33.33 mA/cm².

4-1-6. Stage 1-6 analysis

Stage 1-6 is focused on the impact of continuous airflow diffusion. Two ranges of air flowrate were introduced which are categorized as relatively high and low flowrate. The Exp.7 (high air flow rate) had the flow rate in the range of 115.78 mL/min to 200 mL/min, while the Exp.10 (low

air flow rate) had the air feed rate in the range between 48 mL/min and 136.19 mL/min. It is essential to mention that airflow takes over the role of oxidizing agent (hydrogen peroxide) for the electro-Fenton oxidation in Stage 1-6.

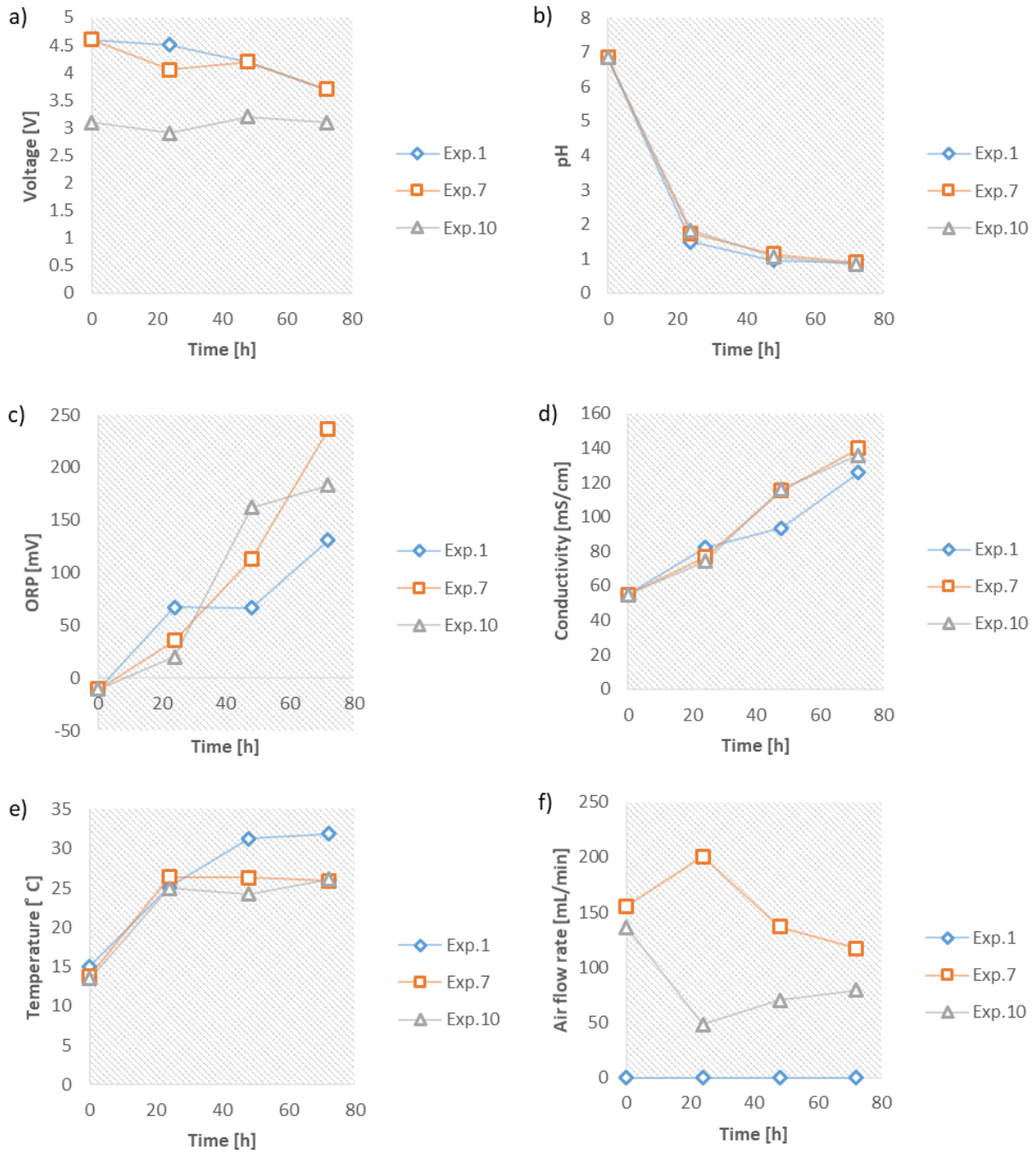


Figure 4- 15 Variation of monitored parameters for the relevant experiments of the Stage 1-6; a) voltage versus time; b) pH versus time c) ORP versus time; d) conductivity versus time e) temperature versus time; f) air flow versus time

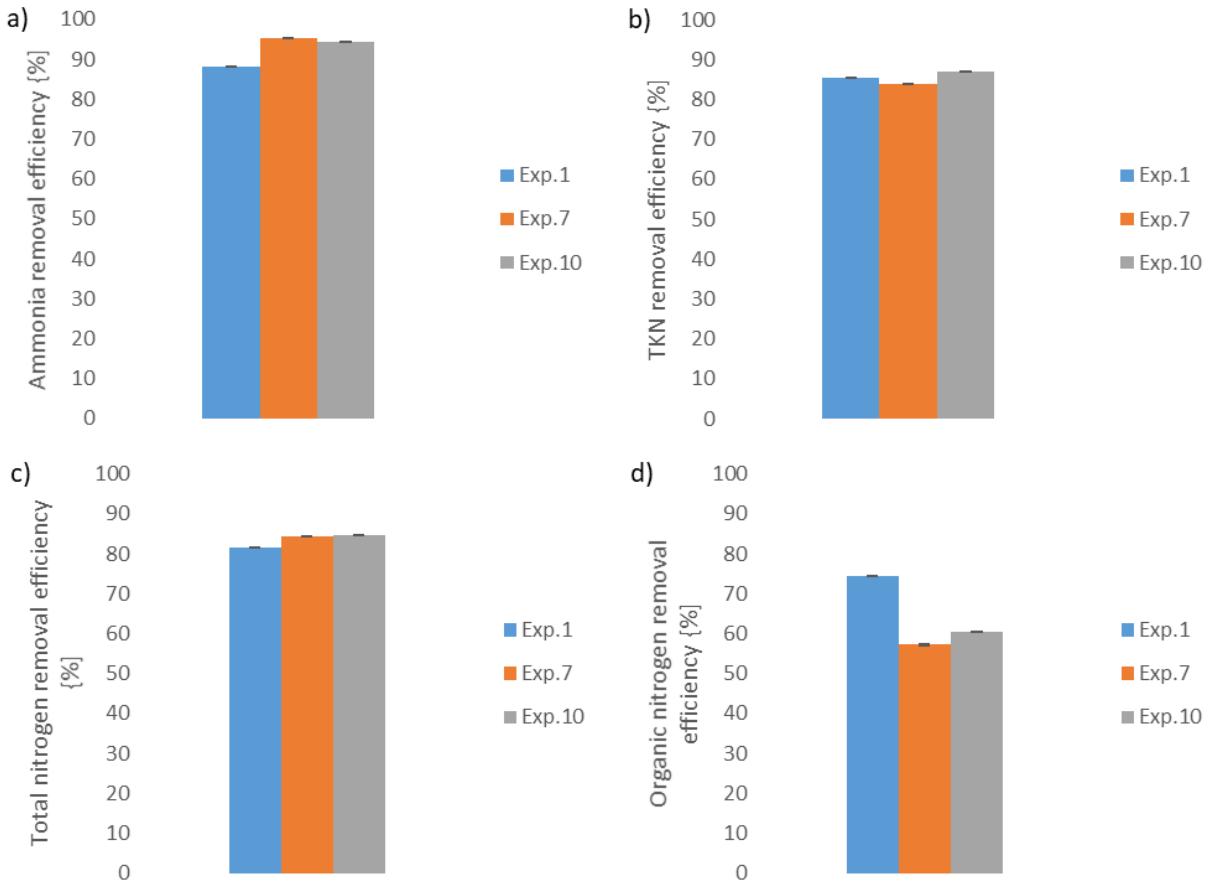


Figure 4- 16 Removal efficiencies of the pollutants for stage 1-6; a) ammonia removal efficiency; b) TKN removal efficiency; c) organic nitrogen removal efficiency; d) total nitrogen removal efficiency

The air flowrate graphs (Fig. 4-15f) demonstrated that the Exp.10's rate (low flowrate) fell significantly throughout the first 24 hour period, on the other hand, the Exp.7 (high flowrate) reached a peak of 200.63 mL/min after 24 hours. During the second 24 hour-period, the Exp.10 recovered and reached 70 mL/min from 24 mL/min. In contrast, the air flow rate of the Exp.7 decreased steadily, and was reached 136.85 mL/min. Meanwhile the third 24 hour exposure time (from 48 hours to 72 hours), the air flowrate of the Exp.10 increased, and the final recorded flowrate was 79.36 mL/min. In addition, the Exp.7 continued decreasing and its final value was 117.05 mL/min.

The voltage variations (Fig.4-15a) demonstrated that in the first 24 hour exposure time, all experiments faced a decrease. The Exp.1 (no air flow) kept decreasing for the remaining 48 hours and its final value was 3.7 V. In contrast, both Exp.7 (high air flow rate) and Exp.10 (low air flowrate) faced a gradual increase during the second 24 hour-period (from 24 hours to 48 hours); however, the observed trends were descending meanwhile the third 24 hour-period (from 48 hours to 72 hours). A remarkable difference between voltage curves of the Exp.7 and Exp.10 showed that airflow rate was directly influenced the cell potential and lower air flowrate provided lower electrical potential.

The pH changes (Fig.4-15b) in all three experiments showed the similar tendency where the final achieved pH value was in the range between 0.82 and 0.89 after 72 hour exposure time. In addition, the Exp.7 (high flow rate) and Exp.10 (low flow rate) had the same final pH value equals to 0.89. The results proved that pH changes were independent on the airflow rates when the applied flow rate was in the range between 48 mL/min to 200 mL/min.

The ORP variations (Fig.4-15c) showed that during the first 24 hour period, the highest ORP (67.2 mV) was achieved in the Exp.1 (no air flowrate), while the lowest ORP was obtained (20.2 mV) in the Exp.10 (low air flowrate). Meanwhile the second 24 hour-period, the trend of ORP changed to be strongly ascending in the Exp.7 and Exp.10. The ORP increased from 35.7 mV to 112.95 mV in the Exp.7 and built up from 20.2 mV to 162.2 mV in the Exp.10 at 24 hours. During the last 24 hour exposure time, all experiments showed a strong ascending behavior and the maximum ORP was obtained by the Exp.7 (high air flowrate) which was 237 mV. In addition, an interesting intermediate value of 183.2 mV was obtained in the Exp.10. The results showed that the air diffusion will significantly enhance the oxidation potential and would enable the electrokinetic reactor to remain in a high continuous oxidation state.

Conductivity changes (Fig.4-15d) showed that the difference in the air flowrate did not significantly affect the conductivity although the overall conductivity increased when the air flow substituted the hydrogen peroxide. The maximum conductivity was achieved by the Exp.7 (high airflow rate) with the value of 139.9 mS/cm after 72 hours while the minimum one was obtained by the Exp.1 (no air flowrate) with the value of 125.53 mS/cm.

The behavior of temperature variations (Fig.4-15e) were similar for all experiments of Stage 1-6 during the first 24 hour exposure time (from initial to . The obtained temperatures of the Exp.1 (no airflow), Exp.7 (high airflow rate) and Exp.10 (low airflow rate) were 25.1 °C, 26.4 °C, and 24.9 °C, respectively. The results revealed that the air diffusion would significantly decrease the temperature in comparison with the process in which the hydrogen peroxide was used as an oxidizing agent. The final temperature of the Exp.7 and Exp.10 were 25.9 °C and 26.1 °C, respectively. In contrast, the final temperature of the Exp.1 was 31.9 °C.

High airflow rate demonstrated the influential alteration in enhancement of the ammonia removal efficiency (Fig.4-16a) since the highest removal efficiency of ammonia was achieved by the Exp.7 (high air flowrate) with the value of $95.4\% \pm 0.018\%$ in Stage 1-6. The low air flowrate in the Exp.10 also reached a good ammonia removal equals to $94.35\% \pm 0.018\%$. Whereas, the lowest removal of ammonia ($88.27\% \pm 0.018\%$) was achieved in the Exp.1 where no air flowrate was applied. The results indicated that the air diffusion could be effective to enhance the ammonia oxidation in EK cell.

TKN removal efficiency (Fig.4-16b) was enhanced by applying the low air flowrate (Exp.10) as an oxidizing agent in comparison with using hydrogen peroxide ($85.28\% \pm 0.011\%$) in the Exp.1. The highest removal efficiency ($87.07\% \pm 0.011\%$) of TKN was obtained by Exp.10 (low flowrate)

in Stage 1-6. Exp.7 (high air flow) demonstrated the lowest ($83.72\% \pm 0.011\%$) removal efficiency among all experiments of Stage 1-6. It can be concluded that the rate of airflow played an important role in the TKN removal. Based on the achieved results in Stage 1-6, the TKN removal can be enhanced in a small EK cell, as far as the air flow rate maintains the range between 48 mL/min and 136.19 mL/min.

Total nitrogen (TN) removal efficiency (Fig.4-16c) followed the trends of TKN removal for the same experimental conditions since the low air flowrate provided the best TN removal efficiency by $84.76\% \pm 0.038\%$. However, the Exp.1 (No air flow) resulted in the lowest TN removal of $81.65\% \pm 0.038\%$ and the high air flowrate (Exp.7) gave the TN removal by $84.28\% \pm 0.038\%$. It can be concluded that the total nitrogen removal efficiency was enhanced by applying an air flow. In addition, total nitrogen removal efficiency slightly depends on the rate of applied air flow since a difference between the results of two scenarios (low and high air flowrate) was only 0.48%.

Introducing the airflow to the reactor did not provide any acceptable results for the organic nitrogen removal efficiency (Fig.4-16d). The achieved results with applying the airflow were $57.2\% \pm 0.04\%$ and $60.37\% \pm 0.04\%$. On the other hand, no air flow associated experiments (Exp.1) gave $74.33\% \pm 0.04\%$ organic nitrogen removal efficiency. Based on the achieved results, no airflow was applied in further investigations.

Table 4-1 provides the obtained removal efficiency for all significant experiments of Phase 1. Additional experiments were also run to investigate the interaction of Phase 1's parameters or the impact of an intermittent DC. The objective of the Exp.26 was investigating the interaction of parameters while the objective of the Exp.35 was applying an intermittent current. The removal efficiency of ammonia, TKN, total nitrogen, and organic nitrogen of the Exp.19 were provided in

each 24 hour-period. These data were also represented in relevant sections of Stage 1-1, Stage 1-3, and Stage 1-4, respectively. Furthermore, Exp.13 is also presented in the discussions of the results of Stage 1-1 (the first and third objective). Likewise, Exp.1, used for comparison, also appears in Stage 1-1, Stage 1-5, and Stage 1-6.

The results of Exp.26 (99.68%, 98.14%, 97.05% and 92.55% removal efficiency for ammonia, TKN, total nitrogen, and organic nitrogen, respectively) proved that adding hydrogen peroxide each 12 hour interval and considering dimensional quotient equals to 1 would provide the best experimental design parameters to follow in the upscaling process. In addition, it would be feasible to reduce the exposure time to be exposed to DC to 60 hours for the proposed electro-Fenton process. Furthermore, based on the Exp.26, the time of exposure can be reduced even up to 24 hours, if the ammonia removal is the main objective.

On the other hand, unsatisfactory results of the Exp.35 showed that implementing an intermittent current with 5 min on/5 min off to a high strength wastewater did not enhance the removal efficiency of pollutants, and it required additional studies with other operation modes.

Table 4- 1 Removal efficiencies of ammonia, TKN, total nitrogen, and organic nitrogen for all experiments of Phase 1

Stage	No. of Exp.	Ammonia removal [%] ±0.018%	TKN removal [%] ±0.011%	Total nitrogen removal [%] ±0.038%	Organic nitrogen removal [%] ±0.04%	Remarks
1-1;1 st objective	13	32.18	20	20	-19.8	DQ* =8.33
	14	41.3	42.6	41.65	47.33	DQ* =4.41
	15	81.64	2.43	69.65	49	DQ* =2.59
	16	83.91	73.5	71.8	35.3	DQ* =2.03
	17	91.1	82.21	80.34	49.63	DQ* =1.56
	1	88.27	85.28	81.65	74.33	DQ* =1.31
	18	95	90.36	88.14	73.33	DQ* =1.12
	19-1	75.45	61.28	61.52	9.33	24h analysis DQ* = 1
	19-2	97.82	92.28	89.65	71.96	48h analysis
	19-3	99.44	97.66	96.91	91.15	72h analysis
1-1;2 nd objective	31	97.7	96.16	95.26	90.5	Perforated SS** cathode
	32	99	96.87	95.85	89.13	Mesh SS** cathode
	23	99.23	97.38	96.32	90.6	Flat SS** cathode
1-1,3 rd objective	11	35.45	21.42	20	-30	Cylindrical cell
	13	32.18	20	20	-19.8	Cuboid cell

DQ*: Dimensional Quotient; SS**: Stainless Steel ; CD***: Current Density

Table 4-1 Continued- removal efficiencies of ammonia, TKN, total nitrogen, and organic nitrogen for all experiments of Phase 1

1-2	24	97.08	90.57	87.58	66.7	24 h time interval of adding H ₂ O ₂
	29	99.08	95.9	95.23	84.26	12 h time interval of adding H ₂ O ₂
	30	99.13	95.57	95.01	85.52	6 h time interval of adding H ₂ O ₂
1-3	19	99.44	97.66	96.91	91.15	No barium hydroxide
	20	96.68	84.57	82.69	40.16	1/1 molar ratio of barium hydroxide
	21	94.76	89.14	87.44	68.53	2/1 molar ratio of barium hydroxide
1-4	19	99.44	97.66	96.91	91.15	No Fenton agent
	37	98.82	98.37	97.4	96.73	$0.05/1 \frac{Fe^{2+}}{H_2O_2}$
1-5	1	88.27	85.28	81.65	74.33	CD*** equal to 33.33 mA/cm ²
	2	87.27	81.21	78.07	59	CD*** equal to 37.7 mA/cm ²
	3	89.91	67	71.1	16	CD*** equal to 22.22 mA/cm ²
	4	81.82	57.63	64.27	11.33	CD*** equal to 27.77 mA/cm ²
1-6	1	88.27	85.28	81.65	74.33	No air flow
	7	95.4	83.72	84.28	57.2	High flowrate
	10	94.35	87.07	84.76	60.37	Low flowrate

DQ*: Dimensional Quotient; SS**: Stainless Steel ; CD***: Current Density

Table 4-1 Continued- removal efficiencies of ammonia, TKN, total nitrogen, and organic nitrogen for all experiments of Phase 1

Additional experiments	26-1	97.06	81.64	49.44	25.1	36 h analysis DQ =1 12 h time interval of adding H ₂ O ₂
	26-2	99.59	95.89	95.01	82.34	48 h analysis DQ =1 (Exp.19's experimental design) 12 h time interval of adding H ₂ O ₂
	26-3	99.69	97.5	96.57	89.47	60 h analysis DQ =1 (Exp.19's experimental design) 12 h time interval of adding H ₂ O ₂
	26-4	99.68	98.14	97.05	92.55	72 h analysis DQ =1 (Exp.19's experimental design) 12 h time interval of adding H ₂ O ₂
	35	73.45	68.57	66.07	49.33	Intermittent DC 5'on/5' off

DQ*: Dimensional Quotient; SS**: Stainless Steel; CD***: Current Density

4-2. Phase 2 results and discussion

Phase 2 of the research focuses on the experimental upscaling of the EK electro-Fenton reactor. The optimal experimental configuration of Phase 1 are also considered to determine the experimental design of Phase 2. In addition, the outcomes of Phase 2 (medium scale experiments) was expected to provide the necessary information for the tests at a bigger scale (Phase 3) and develop the electro-Fenton sequential batch reactor (EF-SBR) in Phase 4. The Initial and operating conditions as well as a reason for choosing them were discussed in detail in Section 3-2-2.

4-2-1. Stage 2-1 and Stage 2-2 analysis

An increase of the anode surface area is feasible by using the graphite rods while keeping the dimensional quotient constant. Consequently, the distance between electrode will be determined considering the diameter of the rods. Therefore, two parameters: 1) distance between electrodes and 2) surface area of anode are changed concurrently. As a result, two individual experiments are run with graphite rods and graphite plate. Based on the described experimental condition, assessing Stage 2-1 (impact of the anode to cathode surface area ratio and the geometry of the electrodes) and Stage 2-2 (impact of distance between electrodes) requires the same set of experiments.

As far as the discretization length (indicator of curvature) is increasing, the current distribution is affected ^[4-8]. Therefore, it is expected to have a significant difference between the actual potential and the actual current density with expected ones (theoretical values). So, it is anticipated to have a better electrode functionality with a graphite plate ^[4-8].

The voltage changes (Fig.4-17a) demonstrated that the Exp.28 (graphite rods anode) faced a steady decrease during the first 24 hour exposure time, and it reached 5.54 V from the initial value of 6.42 V. The Exp.42 (graphite plate) also experienced a fall in value. However, the slope of the decline was higher in comparison with the Exp.28. The initial voltage of the Exp.42 was 6.18 V while it decreased to 4.34 V. Meanwhile the remained 48 hours, the Exp.28 increased steadily and its final achieved voltage was 6.11 V. It is notable to mention that the slope of variation was increased by 0.47 V during the last 24 hour period (from 48 hours to 72 hours). For the remaining 48 hours, the voltage decreased slightly in the Exp.42 and reached 4.18 V at 72 hours. Therefore, it can be speculated that a higher cell potential can be reached by using the graphite rods.

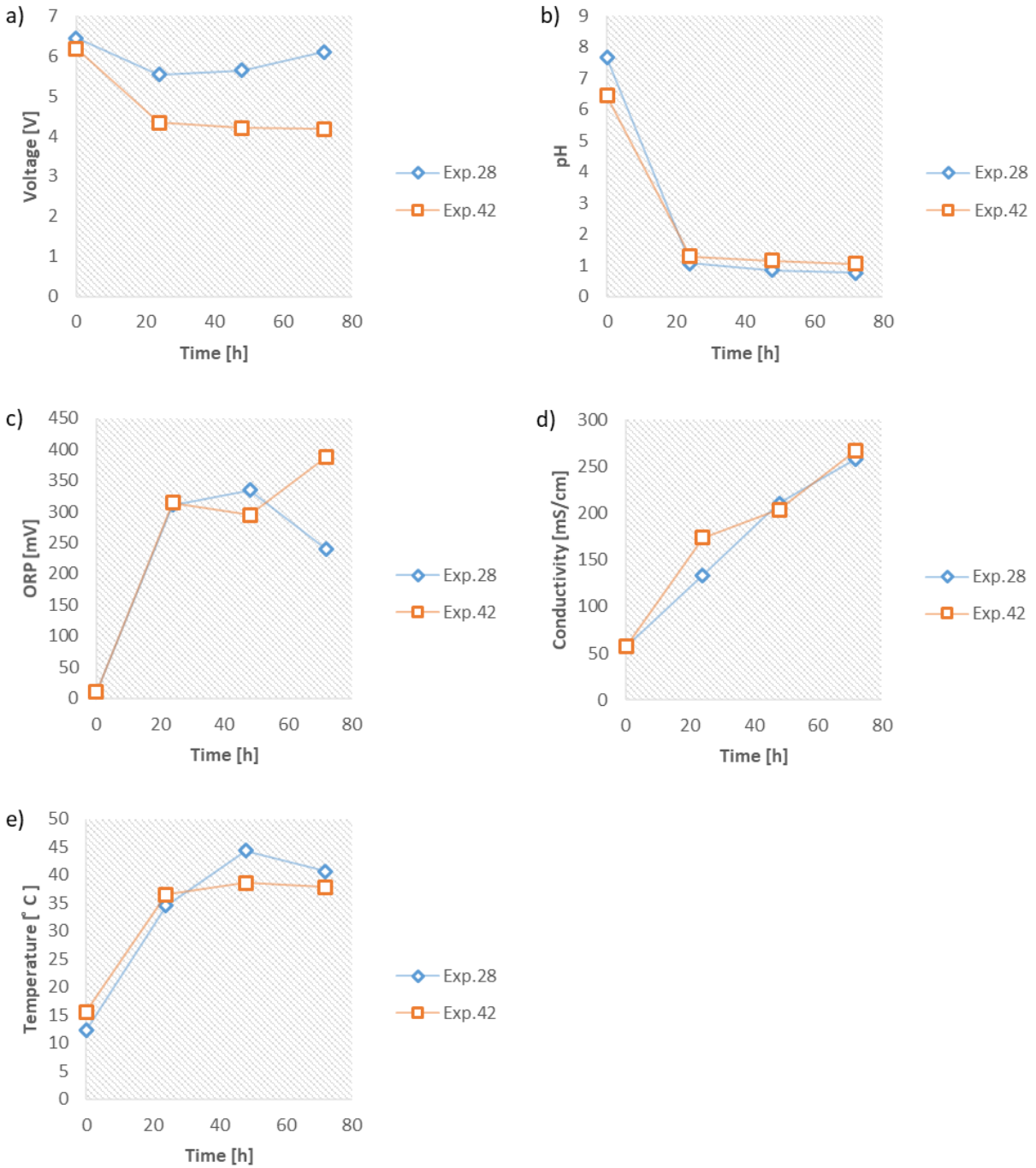


Figure 4- 17 Variations of monitored parameters for the relevant experiments of Stage 2-1 and Stage 2-2; a) voltage versus time; b) pH variation versus time c) ORP versus time; d) conductivity versus time e) temperature versus time

The graphs of pH variations (Fig.4-17b) showed a sharp decrease for both experiments meanwhile the first 24 hour-period. However, the intensity of the pH decrease (graphite rods anode) was higher in the Exp.28 in comparison with the Exp.42 (graphite plate). During the second 24 hour exposure time (from 24 hours to 48 hours), the Exp.28 and Exp.42 obtained pH equal to 1.06 and 1.28, respectively. pH values of both experiments kept decreasing gradually and the final obtained value were 0.76 and 1.05 for Exp.28 and Exp.42 correspondingly.

The graphs of ORP variations (Fig.4-17c) demonstrated the similar behavior meanwhile the first 24 hour exposure time. The Exp.28 (graphite rods) and Exp.42 (graphite plate) reached 239.5 mV and 245.4 mV, respectively. During the second 24 hour-period, the Exp.42 experienced a slight decrease and ORP reached 294.8 mV, while the Exp.28 faced a steady increase during the same time interval. During the last 24 hour exposure time (from 48 hours to 72 hours), the ORP of the Exp.28 decreased, whereas, the ORP of Exp.42 increased. The final recorded ORPs for both Exp.28 and Exp.42 were 239.6 mV and 388 mV, respectively. The oxidation state could be an indicator in the Exp.42 for evaluating the anode oxidation. The observed anode oxidation was superior in comparison with the graphite rods anode in the Exp.28.

Conductivity changes (Fig.4-17d) showed that for both experiments, the tendency of changes was totally ascending during the total exposure time. The final achieved conductivities were 258 mS/cm and 267 mS/cm for the Exp.28 and Exp.42, respectively. During the first 24 hour period, the Exp.28's conductivity reached 173 mS/cm while the Exp.42's conductivity was 133.7 mS/cm. The representative slope of the increase of conductivity for Exp.28 was higher than Exp.42's slope during the first 24 hour exposure time. Although the Exp.42 maintained the same slope of increase during the second 24 hour exposure time, the Exp.28 faced a remarkable decrease with respect to slope in the same time interval. Exp.28's conductivity was 210.8 mS/cm at 48 hours and Exp.42's

one was 204 mS/cm. It is obvious that the difference between the monitored conductivity at 48 hours for both experiments was momentarily decreased and both representative values converged. To clarify the observed behavior, it should be mentioned that the measured difference at 24 hours was 39.3 mV while the difference was reduced to less than 3 mS/cm. The conductivity of both experiments increased steadily during the last 24 hour period, and the highest conductivity was achieved by the Exp.42.

Temperature changes (Fig.4-17e) in both experiments showed a similar tendency during the first 24 hour exposure time. The achieved results were 34.5 °C and 36.5 °C for the Exp.28 (graphite rods) and Exp.42 (graphite plate). The Exp.28 faced an intensive increase during the second 24 hour exposure time (from 24 hours to 48 hours). While the Exp.42 experienced a gradual increase in the same period. Meanwhile the last 24 hour period, the Exp.28's temperature decreased significantly. In addition, the Exp.42's temperature faced a gradual decrease. The final achieved temperature values were 40.6 °C and 37.8 °C for the Exp.28 and Exp.42, respectively.

Ammonia removal efficiency (Fig.4-18a) of the Exp.28 (Graphite rods) was insignificantly higher than the Exp.42 (Graphite plate) with a difference of 0.11%. The obtained efficiencies were 99.35% ± 0.018 and 99.24 % ± 0.1% for the Exp.28 and Exp.42, respectively. However, the graphite plate (Exp.42) as an anode led to obtain a significant higher TKN removal (Fig.4-18b) in comparison with the graphite rods. The measured difference was 0.87% and the Exp.42's removal efficiency was equal to 98.63% ± 0.12%. In addition, the total nitrogen removal efficiency (Fig.4-18c) of Exp.42 was slightly higher (by 0.4%) than the Exp.28. The maximal removal efficiency was achieved by the Exp.42 with the value of 96.55% ± 0.15%. The most remarkable enhancement was observed for the organic nitrogen removal efficiency (Fig.4-18d) while graphite plate was

used as anode. The achieved efficiency was $96.4\% \pm 0.26\%$ while Exp.28's removal efficiency was $91.96\% \pm 0.04\%$.

Therefore, based on Stage 2-1 and Stage 2-2 results, using graphite plate would be preferable due to higher TKN, total nitrogen and organic nitrogen removal efficiency.

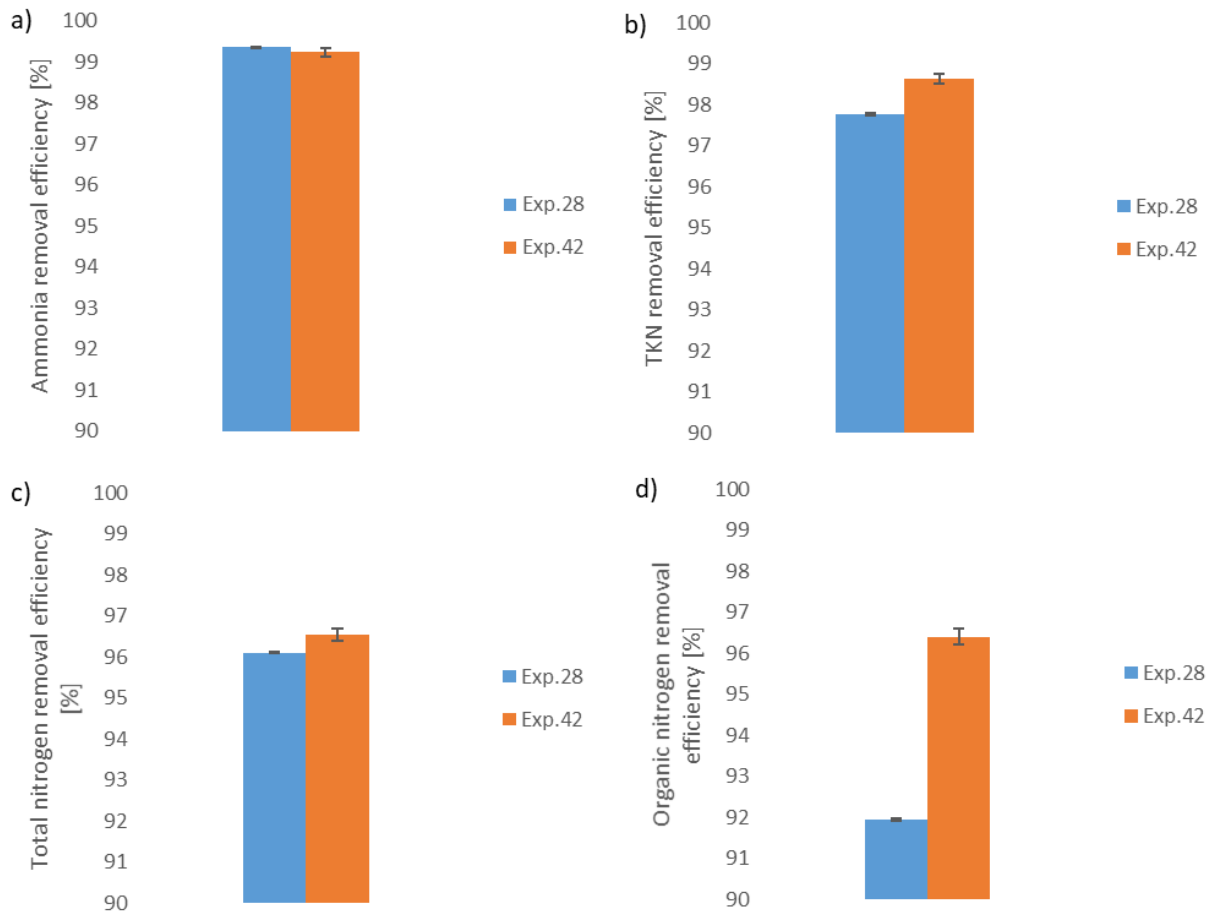


Figure 4- 18 Removal efficiencies of the pollutants for stage 2-1 and 2-2; a) ammonia removal efficiency; b) TKN removal efficiency; c) organic nitrogen removal efficiency; d) total nitrogen removal efficiency

4-2-2. Stage 2-3 analysis

One of the challenges of upscaling of the electrochemical wastewater treatment process is a high energy consumption. To overcome the described challenge, it is crucial to introduce solutions

which are providing solutions to adjust the current and voltage of the electrokinetic reactor. Since the input of the system is constant current, the only direct way to lessen energy consumption is reduction of applied current. So, three distinctive current densities were considered: 21.37 mA/cm², 13.72 mA/cm², and 33.33 mA/cm². To consider a higher anode surface area, the Exp.28 (current density of 21.37 mA/cm²) and Exp.41 (current density of 13.72 mA/cm²) were run by using graphite rods as anode and the provided constant current were 10.48 A and 6.73 A, respectively. Also, the Exp.42 (33.33 mA/cm²) was run by using graphite plate and the provided current was 11.96 A.

The voltage variations (Fig.4-19a) showed that voltage was slightly increased in the Exp.41 (current density of 13.72 mA/cm²) during the first 24 hour period, and it reached 5.24 V from the initial 5.14 V. While the Exp.41's voltage was gradually decreased during the second 24 hour exposure time and the obtained value was 5.08 V at 48 hours. During the third 24 hour-period (from 48 hours to 72 hours), the voltage was stabilized for the Exp.42. The final voltage was 5.10 V and the difference was 0.02 V throughout the entire 72-hour exposure time. The fluctuations of voltage was less than 0.1 V in the Exp.41. Therefore, the Exp.41's voltage was stable. The highest final voltage among all experiments of Stage 2-3 belonged to the Exp.28 (current density of 21.37 mA/cm²). The variation of voltage for the Exp.28 and Exp.42 were fully described in Section 4-2-1.

The pH changes (Fig.4-19b) of the Exp.41 (13.72 mA/cm²) was fit to variation curves of the other experiments. The difference was relatively small and the final achieved pH was 0.87 after 72 hours. The sharpest decrease was observed during the first 24 hour-period and pH reached 1.5. The recorded value for Exp.41 was the highest among all achieved results at 24 hours. However, the

final magnitude was not placed as the highest pH among all experiments and it can be considered as an intermediate one in comparison with other runs.

The ORP variations (Fig.4-19c) showed that the tendency of the Exp.41 (current density of 13.72 mA/cm²) was ascending throughout the exposure time. During the first 24 hour period, ORP increased notably and the reaction state was transmuted to oxidation state (52.7 mV) from the initial reduction state (-31.8 mV). The sharpest increase was observed meanwhile the second 24 hour exposure time (from 24 hours to 48 hours). The ORP of Exp.41 reached 232.2 mV from 52.7 mV. Exp.41 experienced a steady increase during the last 24 hour-period (from 48 hours to 72 hours) and its final ORP (264.2 mV) was placed in the second rank among all experiments of Stage 2-3. The ORP variations of the Exp.28 and Exp.42 were fully described in Stage 2-1 and Stage 2-2.

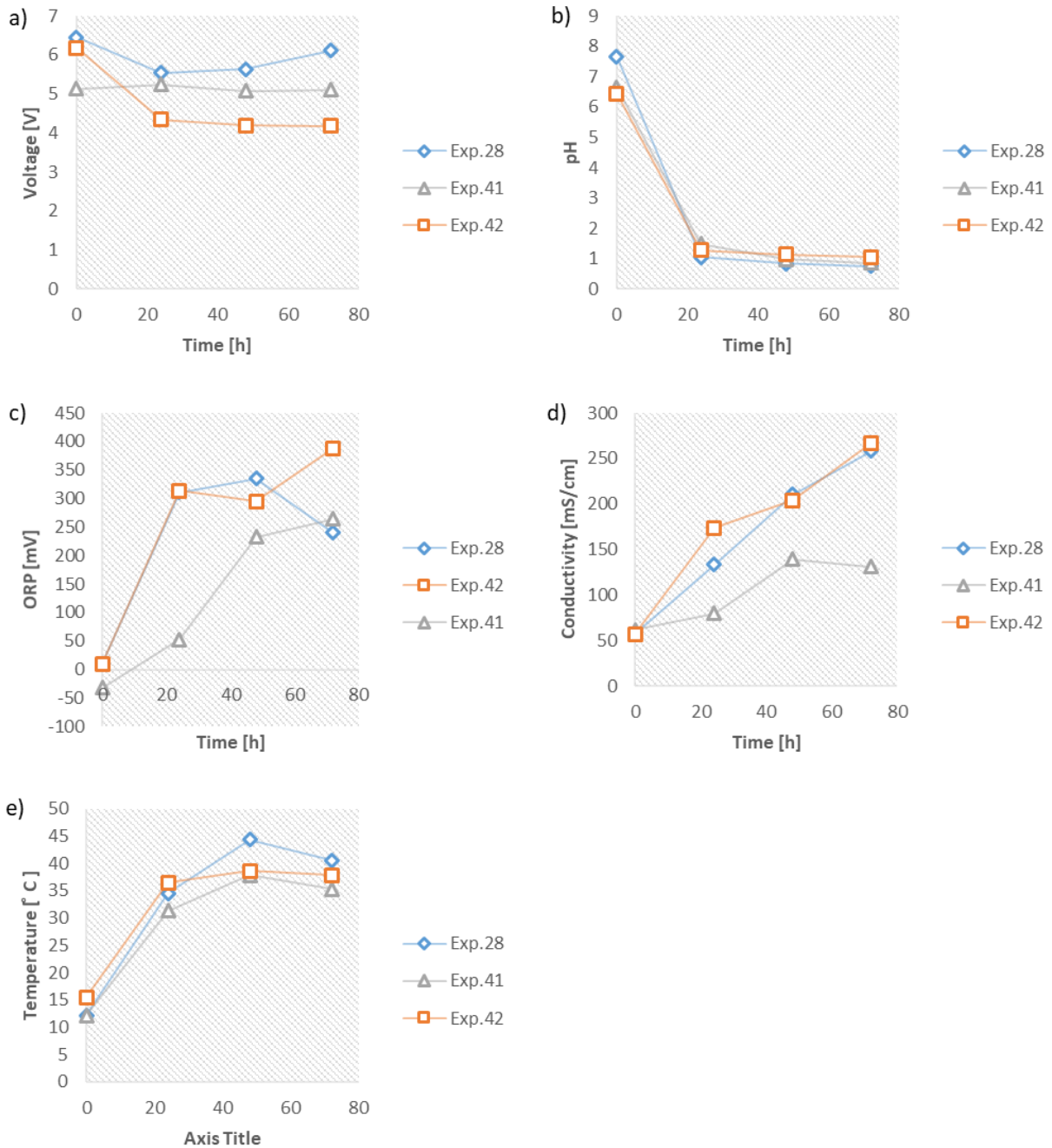


Figure 4- 19 Variations of monitored parameters for the relevant experiments of Stage 2-3; a) voltage versus time; b) pH versus time c) ORP versus time; d) conductivity versus time e) temperature versus time

The conductivity changes (Fig.4-19d) of the Exp.41 (current density of 13.72 mA/cm²) was the smoothest among all experiments of Stage 2-3. During the first 24 hour exposure time, Exp.41's

conductivity reached 80.23 mS/cm from the initial magnitude of 61.8 mS/cm. Throughout the second 24 hour-period, the Exp.41 experienced a sharp increase and the measured conductivity was 139.5 mS/cm. However, the Exp.41 faced a steady decrease meanwhile the last 24 hour exposure time (from 48 hours to 72 hours) and its final conductivity was recorded equals to 131.1 mS/cm. A significant difference was observed among the Exp.41's conductivity and the other experiments of Stage 2-3. For instance, the subtraction of the Exp.41's conductivity in 72 hours from Exp.28 resulted 135.9 mS/cm which showed that the conductivity of the Exp.28 in 72 hours was 2 times more than the conductivity of the Exp.41 at 72 hours.

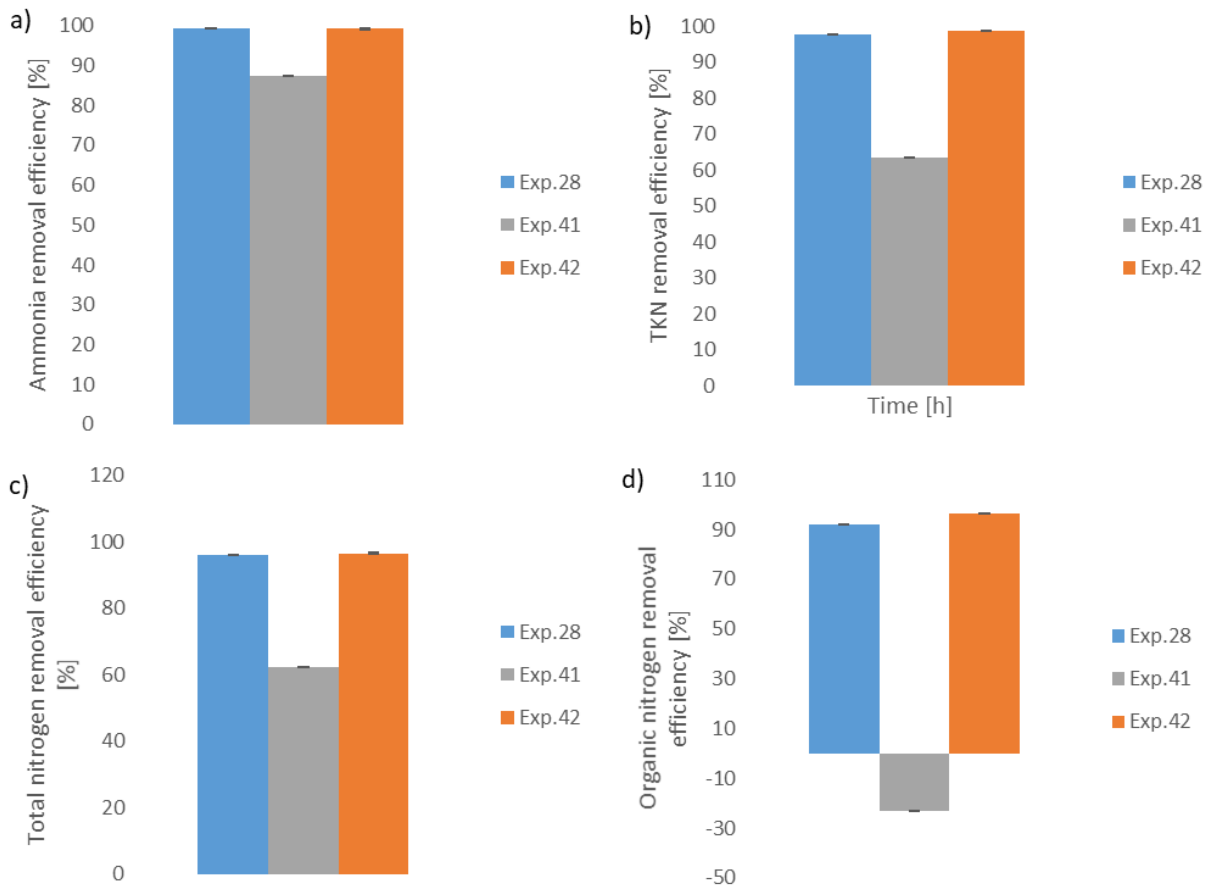


Figure 4- 20 Removal efficiencies of the pollutants for Stage 2-3; a) ammonia removal efficiency; b) TKN removal efficiency; c) organic nitrogen removal efficiency; d) total nitrogen removal efficiency

The temperature variations (Fig.4-19e) of the Exp.41 (current density of 13.72 mS/cm) showed the same trend as the Exp.28 (21.37 mA/cm²) although each point of the temperature curve of the Exp.28 had a higher magnitude than Exp.41's curve. The maximum temperature of Exp.41 was achieved at 48 hours which was equal to 37.8 °C. During the last 24 hour exposure time, Exp.41's temperature steadily decreased and reached the final value of 35.3 °C.

The ammonia removal efficiency (Fig.4-20a) of Exp.41 (current density of 13.72 mS/cm) was the lowest among all experiments of Stage 2-3 and it was equal to 87.36% ± 0.018%. In addition, the Exp.41's TKN (Fig.4-20b), and total nitrogen (Fig.4-20c) removal efficiency stood as the lowest one and the obtained results were 63.36 % ± 0.011% and 62.2% ± 0.038%, respectively. The organic nitrogen concentration exceeded throughout the process. Therefore, the removal percentage of the organic nitrogen (Fig.4-20d) provided the negative value (- 23.3% ± 0.04%) in Exp.41. The justification of obtaining negative removal efficiency of organic nitrogen was described in detail in Stage 1-1.

The results of Stage 2-3 proved that minimizing the applied current density would lead to a low removal efficiency of target pollutants. In addition, it is crucial to consider a lower limit for current density. In simple words, 21.37 mA/cm² would be an appropriate value to apply for the upscaling to minimize the energy consumption.

4-2-3. Stage 2-4 analysis

Substituting air flow as an oxidizing agent instead of adding hydrogen peroxide is the experimental configuration of Stage 2-4. This is the investigation of the impact of the air diffusion on the removal efficiency of the target pollutants. The applied air flow was 4416 mL/min which can be considered as a high airflow rate. Because of experimental design limitations, the only applicable flowrate

was the stated one. The achieved results were only capable to evaluate the impact of high airflow rate. So, it would be impossible to imply whether applying airflow led to a failure or success in medium scale. Complete assessment of the impact of the continuous airflow diffusion can be considered as one of the future work of this study. The experimental design of the Exp.38 (With high airflow rate) was the same as the Exp.28 and the only difference was related to the type of oxidizing agent.

The voltage changes (Fig.4-21a) demonstrated that the initial voltage of the Exp.38 (with a high airflow rate) increased to 8.06 V in the first 24 hour exposure time. During the second 24 hour-period (from 24 hours to 48 hours), the Exp.38 faced a gradual decrease and the voltage reached 7.8 V. Throughout the last 24 hour exposure time (from 48 hours to 72 hours), it was fair to consider the changes of the Exp.38's voltage as a stabilized variation. The final recorded voltage was 7.88 V. During the last 24 hour-period, the actual trend of the Exp.38 was gradually ascending. The important point was a significant difference between the recorded voltage values of the Exp.28 which showed that introducing a high airflow rate led to an increase in cell potential.

The pH changes (Fig.4-21b) of the Exp.38 (with a high airflow rate) showed a similar trend like the Exp.28 (no air flow) and its pH significantly decreased to 0.94 from 6.45. The Exp.38's pH decreased gradually meanwhile the second 24 hour-period (from 24 hours to 48 hours) and its obtained value was 0.46. The final measured pH was equal to 0.47 which showed that pH changes were stabilized during the last time interval. The comparison of the final achieved pH of the Exp.38 with the Exp.28 revealed that using the high airflow rate resulted noteworthy reduction in pH. To support the mentioned statement, it is essential to mention that the difference between final obtained pH magnitude of the Exp.28 and Exp.38 was 0.3. The changes were stabilized during the

last time interval. A comparison of the final achieved pH of the Exp.38 and Exp.28 revealed that using the high airflow rate resulted in the significant reduction in pH.

The ORP variations (Fig.4-21c) showed that Exp.38 (with high airflow rate) experienced a relatively sharp increase in comparison with the Exp.28 (no airflow) during the first 24 hour exposure time. The measured value was 423.1 mV at 24 hours and it stabilized meanwhile the second 24 hour- period (from 24 hours to 48 hours) and reached 424.1 mV. Throughout the last 24 hour exposure time (from 48 hours to 72 hours), the ORP gradually increased and the final recorded value was 432 mV. Based on observed variations of the ORP in both experiments, it can be interpreted that applying a high airflow rate would strongly affect the ORP increase while the final achieved ORP was 1.8 times higher than Exp.28 (no airflow).

The conductivity changes (Fig.4-21d) demonstrated that using a high airflow rate as an oxidizing agent would significantly improve the conductivity. For instance, the conductivity momentarily increased meanwhile the time interval from 24 hours to 72 hours and it reached 299 mS/cm at 48 hours from 111.1 mS/cm at 24 hours. In addition, the conductivity kept increasing sharply and the final measured conductivity was 432 mS/cm. It is crucial to mention that the final recorded conductivity of the Exp.38 was the highest among all experiments of all phases.

Temperature variations (Fig.4-21e) showed that during the first 24 hour-period, the temperature significantly increased in Exp.38 (with high airflow rate) and the measured value was 52.9°C. The mentioned value was the highest temperature that was detected among all experiments. However, the temperature of the Exp.38 steadily decreased throughout the second 24 hour exposure time and it reached 42.3°C. The final recorded value after 72 hours demonstrated that the tendency of changes was ascending in the third 24 hour-period and the final detected temperature was 50.2°C.

Ammonia removal efficiency (Fig.4-22a) significantly decreased once a high airflow rate was used in the cell and the analyzed removal efficiency was $68.18\% \pm 0.018\%$. Therefore, the removal efficiency of the Exp.38 levelled off for $31.17\% \pm 0.018\%$ in comparison with Exp.28 (using hydrogen peroxide). In addition, TKN removal efficiency (Fig.4-22b) of the Exp.38 fell to $75.59\% \pm 0.011\%$ that was 22.17% lower than the Exp.28's one. The total nitrogen efficiency (Fig.4-22c) also decreased for to 21.39% in comparison with the Exp.28 and the obtained removal efficiency of total nitrogen for Exp.38 was equal to $74.71\% \pm 0.038\%$. The obtained results of organic nitrogen (Fig.4-22d) removal efficiency were shown that implementing high airflow as an alternative input of oxidizing agent led to increase the organic nitrogen concentration. The reason was the higher rate of ammonia removal in comparison with TKN removal which led to observe an increase in the differential value. Although the initial value of ammonia concentration was less than TKN, ammonia removal was developed faster than TKN removal which did not show a removal but rather an accumulation of the compound. Then, percentage of organic nitrogen removal was $-35\% \pm 0.04\%$.

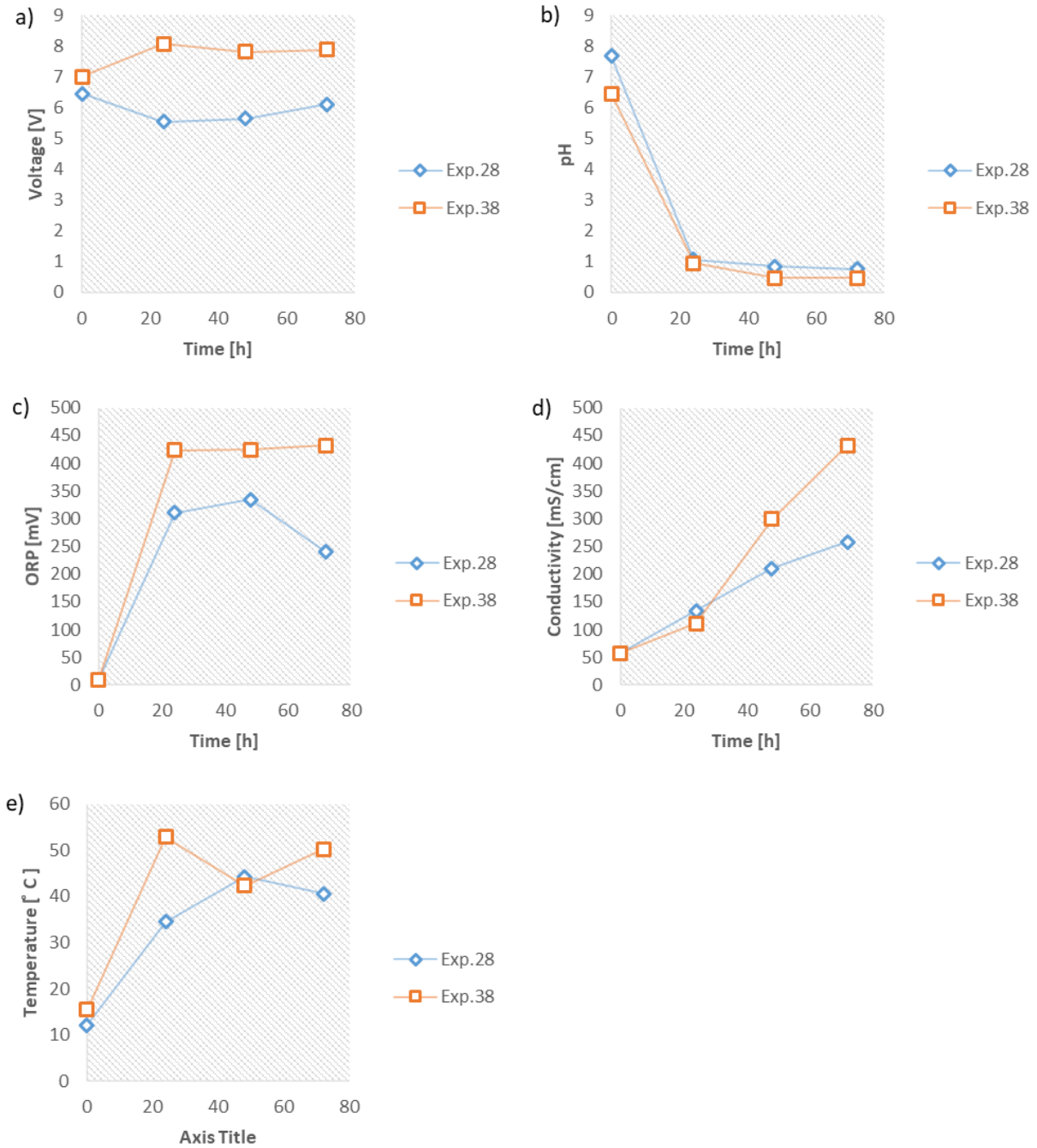


Figure 4- 21 Variations of monitored parameters for the relevant experiments of Stage 2-4; a) voltage versus time; b) pH versus time c) ORP versus time; conductivity versus time e) temperature versus time

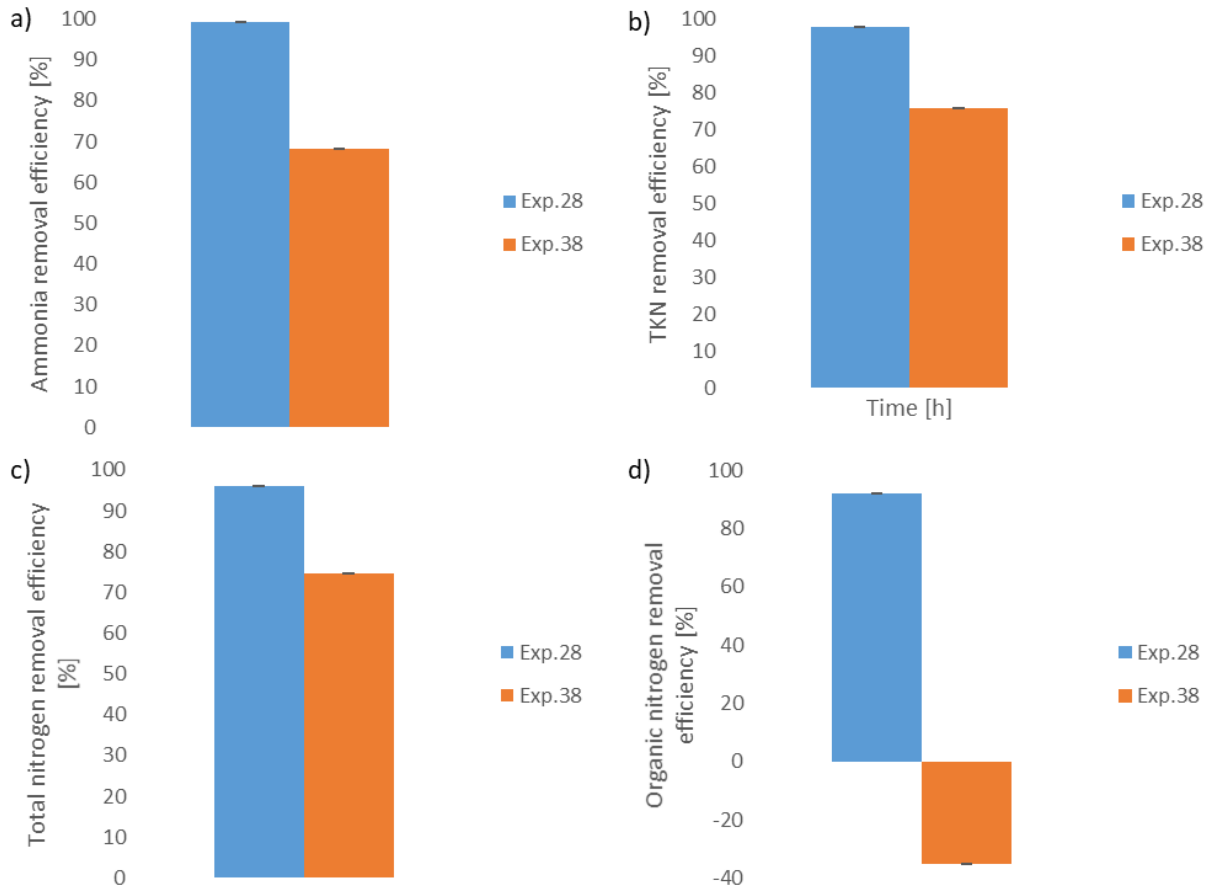


Figure 4- 22 Removal efficiencies of the pollutants for Stage 2-4; a) ammonia removal efficiency; b) TKN removal efficiency c) organic nitrogen removal efficiency; d) total nitrogen removal efficiency

Based on achieved results in Stage 2-4, applying the high airflow rate caused the poor removal efficiency of pollutants specifically for ammonia and organic nitrogen.

Table 4-2 describes the obtained removal efficiencies of the second phase experiments. It also provides the remarks of the experiments to describe the distinctive experimental configuration for each individual Stage. It is crucial to mention that the Exp.28 and Exp.42 belongs to three stages and the reason to duplicate the associated results is emerging the relevant remarks. Based on evaluation of achieved removal efficiencies and considering the main objective of the research, (removal of TKN) the Exp.42's experimental configuration is the best one and the approach of the upcoming phases will be optimizing the energy consumption of the described experiment. It might

be debatable that what is the reason of not implementing 12 h time interval of adding hydrogen peroxide in the experimental configuration of Phase 2. The justification is elimination of the demand of narrowing time interval of adding hydrogen peroxide due to achieving tenable removal efficiency with 24-hour time interval. Therefore, the demand of obtaining 12 h time interval would not be economically construed.

Table 4- 2 Removal efficiencies of ammonia, TKN, total nitrogen, and organic nitrogen for all experiments of Phase 2

Stage	No. of Exp.	Ammonia removal [%]	TKN removal [%]	Total nitrogen removal [%]	Organic nitrogen removal [%]	Remarks
2-1 & 2-2	28	99.35± 0.018	97.76± 0.011	96.1± 0.038	91.96± 0.04	Anode to cathode surface area ratio =1.56 Anode surface area = 490.75 cm ² Distance between electrode = 5 cm
	42	99.24± 0.1	98.63± 0.12	96.65± 0.15	96.4± 0.26	Anode to cathode surface area ratio =1.56 Anode surface area = 358.75 cm ² Distance between electrodes = 6.27 cm
2-3	28	99.35± 0.018	97.76± 0.011	96.1± 0.038	91.96± 0.04	CD* equal to 21.37 mA/cm ²
	41	87.36± 0.018	63.36± 0.011	62.2± 0.038	-23.3± 0.04	CD* equal to 13.72 mA/cm ²
	42	99.24± 0.1	98.63± 0.12	96.65± 0.15	91.96± 0.26	CD* equal to 33.33 mA/cm ²
2-4	28	99.35± 0.018	97.76± 0.011	96.1± 0.038	91.96± 0.04	No air flow
	38	68.18± 0.018	74.71± 0.011	75.59± 0.038	-35± 0.04	High airflow rate (4416 mL/min)

CD* : Current Density

4-3. Phase 3 results and discussion

The reactor configuration of large scale reactor was developed based on the best achieved results of Phase 1 and Phase 2. The optimal time interval of 12 hours was obtained from Phase 1 results to be introduced in Phase 3 experimental design. In addition, the dimensional quotient was set to be 1 (DQ=1) which was approved to be the optimal value based on Phase 1 and Phase 2. According to Stage 2-3 results (Exp.28), current density of 21.37 mA/cm² was considered while the anode to cathode surface area was set equal to 1 for the side electrodes. It might be questionable why the anode to cathode area ratio was changed to 1 from 1.56 which was considered in Phase 2 experimental design (medium scale). The justification was the attempt to optimize the energy consumption by considering the lower applied current and recompensing the lower current with obtaining higher present volume of hydrogen peroxide in narrower time interval. The designed three compartment large scale cell was illustrated in Fig. 3-8 and its configuration was completely described in Section 3-2-4.

4-3-1. Stage 3-1 analysis

Stage 3-1 focused on investigating the impact of distance among electrodes on removal efficiency and mineralization of the target compounds. Two different distances (5 cm and 7.5 cm) were considered and the applied current was set based on exposure surface area of anodes.

Voltage variations (Fig.4-23a) of the Exp.34 (7.5 cm gap) and the Exp.40 (5 cm gap) compartment 1 demonstrated that the tendency of both experiments was downwards meanwhile the first 12 hour period and the Exp.34's voltage reached 4.16 V from the initial value of 5.35 V and Exp.34's obtained 3.4 V from the initial value equals 4.7 V. It is notable to mention that the Exp.34's compartment 1 voltage was significantly higher than the Exp.40's one throughout the process. The

highest observed difference was 1.21 V which occurred at 36 hours. In the remained 60 hours, the overall trend of the Exp.40's voltage variations were stable, and the final voltage increased to 3.5 V from the recorded value which was equal to 3.4 V at 12 hours. However, the Exp.34's compartment 1 voltages showed an instable behavior and the peak was achieved at 36 hours which was equal to 4.24 V. The third compartment voltage changes showed a sharp decrease for the Exp.34 meanwhile the first 12 hour period in which voltage reached 5.83 V from the initial value of 8.03 V. Likewise, the Exp.40's voltage decreased to 4.77 V from the initial magnitude of 6.8 V. the Exp.34's voltage demonstrated remarkable smooth variation in which the final voltage was 4.85 V. However, the Exp.40's variation was not as smooth as the Exp.34's one while the difference between voltage at 12 hours and the final voltage was smaller (0.37 V) and the detected voltage was 4.3 V.

pH variations (Fig.4-23b) of compartment 1 of the Exp.34 and Exp.40 showed that a sharp decrease occurred in the first 12 hour exposure time. The measured pH at 12 hours were 2.01 and 1.86, respectively. In the period between 12 hours and 36 hours based on the Exp.34, the tendency of pH changes was unstable, and a peak was observed with the value of 1.34 at 36 hours. However, in the period from 36 hours to 72 hours, the variations of pH of the Exp.34 were smooth and the pH values steadily decreased, and the final observed pH was 0.58. On the other hand, the Exp.40 pH variations could be analyzed in 2 time-segments. The first segment was associated with the first 12 hour period which was completely described and the second one focused on the period between 12 hours and 72 hours. The Exp.40 experienced the smooth variations in which the final obtained pH was 0.99. Therefore, compartment 1 of the Exp.34 can be more acidic in comparison with the Exp.40's one. The results of

Compartment 2 demonstrated that except the first 24 hours, the curves of pH variations of both experiments were partially fitted, and from 24 hours to 72 hours, both experiments faced the smooth changes and the gradual decreases. In addition, the final achieved pH values were 0.58 and 0.54, respectively. Meanwhile the first 12 hour exposure time, both experiments faced the sharp decreases and the obtained pH were 2.44 and 1.91, respectively. However, the pH changes of the Exp.34 were sharper than the Exp.40's one meanwhile the second 12 hour period and the Exp.34's pH at 24 hours was equal to 1.19. On the other hand, Exp.40's pH was 1.29 at 24 hours.

pH changes of compartment 3 meanwhile the first 12 hour period are distinctive in comparison with other compartments. The Exp.34's pH reached 2.4 while the Exp.40's pH at 12 hours was equal to 1.26 (The most acidic pH in comparison with all compartments at 12 hours). The Exp.34's pH steadily decreased meanwhile the remained 60 hours and the final obtained pH was 0.55. On the other hand, the Exp.40's pH analysis required to define three periods. The first period was allocated to the first 12 hour period which has been already discussed completely. The second period was defined as the period between 12 hours to 48 hours, and the last period was started from 48 hours to 72 hours. Meanwhile the second time interval, the pH smoothly and gradually decreased from 1.26 at 12 hours to 0.68 at 48 hours. Throughout the third time segment, the pH changes curve experienced an increase at 60 hours and its value was equal to 0.95. While the pH decreased and reached 0.72 at 72 hours.

ORP variations (Fig.4-23c) of Stage 3-1 experiments (Exp.34 (7.5 cm gap) and Exp.40 (5 cm gap)) in compartment 1 demonstrated that the Exp.34's ORP gradually increased meanwhile the first 12 hour period and it reached 0.83 mV from the initial value of -21.7 mV. In contrast, the Exp'40's ORP experienced a sharp increase during the first 12 hour interval and obtained 92.2 mV ORP. It can be interpreted that the Exp.40 was shifted to oxidation state relatively quicker than the Exp.34

during the first 12 hour exposure time. The Exp.34's variations can be assessed by considering three distinctive time segments which are initial to 12 hours, 12 hours to 36 hours and finally 36 hours to 72 hours as the first, second, and third segment, respectively. The first time segment relevant ORP variations were described completely. Meanwhile the second time segment, the Exp.34's ORP steadily increased (65.1 mV) during the second 12 hour period, and gradually declined (57.67 mV) throughout the third 12 hour period. Meanwhile the third time segment ORP was increased in the period between the third 12 hour exposure time and fifth 12 period (36 hours to 60 hours) and it reached 352.37 mV. Then, the Exp.34 experienced a steady increase during the last 12 hour period and obtained 401 mV as final ORP. In addition, to assess the variation of ORP of the Exp.40, defining three time segments was required while they were the same as the Exp.34's time segments. Meanwhile the second time segment (12 hours to 36 hours), ORP value increased to 413.5 mV from 92.9 mV. When the third time segment changes were smoother in comparison with the second one in which the Exp.40 experienced an steady increase in the fourth 12 hour period (439.1 mV from 413.47 mV) while the ORP gradually decreased in the remained 24 hours (the fifth and sixth 12 hours). The final obtained ORP of the Exp.40 in compartment 1 was 418.53 mV.

In compartment 2, the tendency of ORP variations was upwards during the first 12 hour period for both experiments and the measured ORP values were 88.97 mV and 0.86 mV for the Exp.34 and Exp.40, respectively which increased from initial values of -21.7 mV. The ORP of the Exp.34 changed steadily during the second 12 hour exposure time, and reached 59.83 mV. In the period of 24 to 48 hours, the Exp.34's ORP increased to 308.63 mV from 59.83 mV. ORP variations of the Exp.34 increased steadily and the final obtained value was 399.23 mV. The Exp.40's ORP increased to 471.73 mV from 89.97 in the period of 12 hours to 48 hours. While throughout the

fifth and sixth 12 hour exposure time, the trend of variations was downwards, and the final obtained pH was 407.93 mV. The remarkable difference between the ORP values showed that except the final converged ORP, a difference between graphs was in the range of the lower limit of 88.11 mV (at 24 hours) and the upper limit of 250.77 mV (at 24 hours).

ORP changes of compartment 3 can be assessed by considering three time segments for the Exp.34 (initial to 24 hours as segment 1, 24 hours to 48 hours as segment 2 and 48 hours to 72 hours as segment 3) and two time sections (Initial to 48 hours as section 1 and 48 hours to 72 hours as section 2) for the Exp.40. Meanwhile the first time segment, the Exp.34 experienced an steady increase and the reactor is shifted to oxidation state with obtaining 0.13 mV at 12 hours. In addition, the measured pH at the end point of the first time segment (24 hours) was equal to 57.4 mV. Throughout the second time segment, ORP increased to 293.33 mV at 48 hours which showed that proceeding oxidizing reactions had high potential. ORP changes meanwhile the last time segment was sharp and the ORP increased to 400.33 mV from 293.33 mV. The Exp.40's ORP meanwhile the first time section (0 to 48 hours) increased to 473.33 mV from initial value of -21.7 mV. The results showed that the transmute of ORP to oxidation state was quicker than the Exp.34's ORP meanwhile the first 12 hour period. Throughout the second time section, the Exp.40 faced a steady decrease and ORP reached 400 mV which was approximately equal to the final ORP of the Exp.34. There was a significant offset between the Exp.34 and Exp.40 compartment 3 curves. The highest difference was observed at 36 hours which was equal to 241.1 mV while both curves converge at 72 hours.

The conductivity curve (Fig.4-23d) of the Exp.34 (7.5 cm gap) in compartment 1 showed that the tendency was instable and three time segments were required to provide precise analysis. The first, second, and third time segments was initially to 36 hours, 36 hours to 60 hours and 60 hours to 72

hours, respectively. In the first time segment, the Exp.34's conductivity increased steadily up to 88.8 mS/cm during the first 24 hour period and increased to 145.2 mS/cm meanwhile the third 12 hour period. Throughout the second time segment, the Exp.34 faced a significant decline and reached 114.2 mS/cm. In the other words, 34 mS/cm decrease was observed in the second time segment. In the third time segment, the conductivity increased to 199.47 mS/cm at 72 hours which showed a 85.27 mS/cm increase from measured conductivity at 60 hours. In contrast, the Exp.4's conductivity increased smoothly meanwhile the process and the final obtained conductivity was equal to 261 mS/cm at 72 hours. The significance difference was observed in conductivity in compartment 1 between Exp.34 and Exp.40 (approximately 61.2 mS/cm).

The results generated in compartment 2 indicated that the trends of variations were similar to compartment 1 except the conductivity variation in the Exp.34 meanwhile the fifth and sixth 12 hour period. The semi stabilized behavior was observed throughout the fifth 12 hour exposure time in which the conductivity increased to 114.13 at 60 hours from 108.27 mS/cm at 48 hours). In addition, throughout the sixth 12 hour period, conductivity increased to 208.87 mS/cm which was around 9 mS/cm higher than the final observed conductivity in compartment 1. The Exp.40 showed the similar smooth variations like compartment 1 and the final obtained conductivity was 260 mS/cm, which was almost the same as compartment 1 final conductivity.

The conductivity variations of the Exp.34 in the compartment 3 is distinctive in comparison with the other compartments. Three time segments should be defined (initial to 24 hours, 24 hour to 48 hours, 48 hours to 72 hours as segment 1, segment 2, and segment 3, respectively) to assess the variations analysis. Throughout the first time segment the conductivity increased steadily and reached 88.03 mS/cm at 24 hours from initial value of 61.4 mS/cm. Meanwhile the second time segment, the Exp.34 experienced a sharp increase during the third 12 hour period and attained

147.7 mS/cm. While it faced a significant decrease throughout the fourth 12 hours and obtains 114.23 mS/cm. Throughout the third time segment, conductivity increased to 199.47 mS/cm and fell back to 154.15 mS/cm at 72 hours. However, the Exp.40's conductivity curve in compartment 3 demonstrated an alike behavior like the compartment 1 and compartment 2 which smoothly increased meanwhile the process. The final achieved conductivity was 264 mS/cm.

The interpretation of conductivity results indicated that the conductivity magnitude which were obtained in each compartment of the Exp.34 were directly impacted by larger distance between electrodes (7.5 cm). In addition, the offset between curves were identical through the last 24 hour exposure time. The mentioned results construed that the increase in distance between electrodes led to nonlinearity of conductivity variations. The reason was the significant gradient in current intensity (the magnitude of an electric current as measured by the quantity of electricity crossing a specified area of equipotential surface per unit time), which was the consequence of an increase in distance between electrodes. In contrast, all compartments conductivity curves of the Exp.40 were fitted with maximum difference of 3 mS/cm between each two compartments.

Temperature variations (Fig.4-23e) of compartment 1 showed that temperature values of both experiments increased meanwhile the first 12 hour period and the Exp.34's and Exp.40's temperature values reached 44.5 °C and 47.8 °C from the initial 12.5 °C. Throughout the second 12 hour exposure time, the Exp.34's temperature increased to 46.9 °C while the Exp.40's temperature gradually decreased and obtained 46.9 °C. The Exp.34's temperature smoothly declined and the final obtained value at 72 hours was 43.5 °C. While on the other hand, the Exp.40's temperature declined to 40.3 °C meanwhile the third 12 hour period. Throughout the fourth 12 hour period, temperature slightly increased (43 °C at 48 hours). During the fifth and sixth 12 hour exposure time, the temperature smoothly decreased and obtained the final value of 39.7 °C.

The temperature variations in the compartment 2 were distinctive and the highest temperature among all compartments was achieved by the Exp.40 at 12 hours which increased to 48.9 °C from initial 12.5 °C. In addition, the Exp.34's temperature sharply increased to 46.8 °C. Throughout the second 12 hour period, Exp.34's temperature increased to 48.1 °C whereas the trend of variations smooth declined throughout the remained exposure time and obtained 44 °C. From 12 hours to 36 hours, the Exp.40's temperature smoothly declined during the second and third 12 hours. In the following time interval, a sharp decline reached 40.8 °C. Whereas temperature increased to 44.1 °C in the next 12 hours. The last recorded temperature which was obtained after a gradual decrease meanwhile the last 12 hour period was equal to 41.4 °C

Temperature variations in compartment 3 demonstrated that temperature of both experiments (Exp.34 and Exp.40) increased to 44.6 °C Also, both experiments (Exp.34 and Exp.40) kept an upward trend in the second 12 hour exposure time and obtain 49.4 °C and 51.6 °C, respectively. The Exp.40's temperature at 36 hours with the magnitude of 51.6 °C was the highest recorded temperature among all compartments. In the following time interval, the Exp.34's temperature steadily declined and reached 47.2 °C. Whereas, the Exp.34's temperature increased, and the measured value was 46.9 °C at 48 hours. For the last 24 hour period, the Exp.34 experienced a gradual decline led to the final temperature of 42.7 °C. the Exp.40's temperature smoothly decreased throughout the interval of 24 hours to 72 hours and reached 42.7 °C. As it was expected the highest temperature was obtained in compartment 3 which was under exposure of the highest current (14.54 A and 16.59 A for the Exp.34 and Exp.40, respectively). The reason was the significant heat generation in compartment 3 which was initiated by applying high .

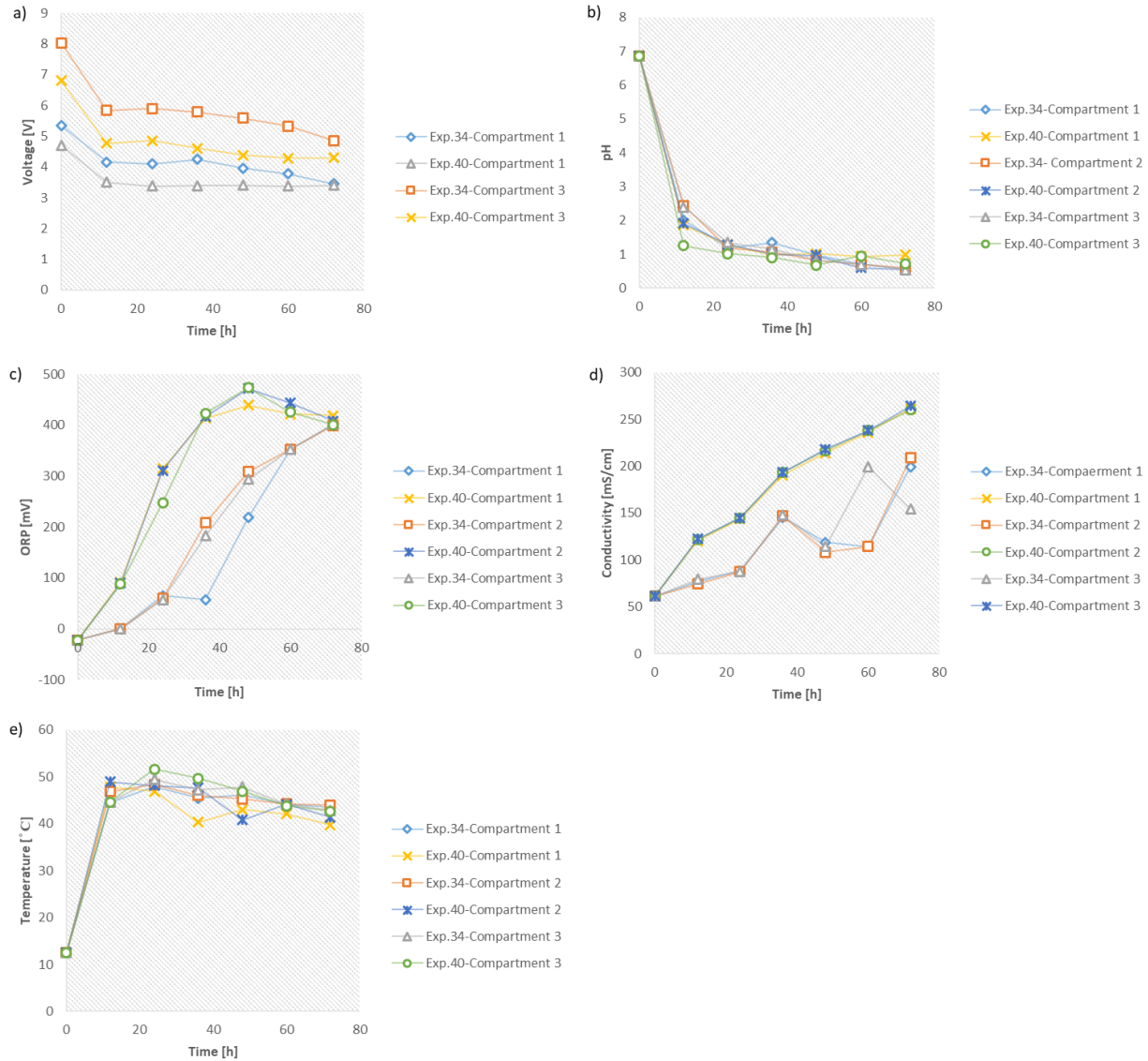


Figure 4- 23 Variations of monitored parameters for the relevant experiments of Stage 3-1; a) voltage versus time; b) pH versus time c) ORP versus time; d) conductivity versus time e) temperature versus time

The values of removal efficiency of the target pollutants were investigated in 60 and 72 hours for the Exp.34 (7.5 cm gap) and the Exp.40 (5 cm gap). According to Figure 4-24, the removal efficiency of ammonia, TKN, total nitrogen, and organic nitrogen in Exp.40 were significantly higher than the Exp.34's results. Ammonia removal efficiency (Fig.4-24a) of the Exp.34 (78.57 %

$\pm 0.018\%$) was significantly lower than the Exp.40's efficiency ($98.97\% \pm 0.018\%$). The Exp.34's efficiency enhanced at 72 hours and obtained $88.51\% \pm 0.018\%$. However, the ammonia removal efficiency of the Exp.40 gave better results and reached $99.45\% \pm 0.018\%$. TKN removal efficiency (Fig.4-24b) of the Exp.40 ($96.6\% \pm 0.011$) was 28.34% higher than the Exp.34 ($68.24\% \pm 0.011\%$) at 60 hours. Whereas the difference between the obtained values in the Exp.34 and Exp.40 decreased to 16.82% at 72 hours. The Exp.34 and Exp.40 achieved $81.59\% \pm 0.011\%$ and $98.41\% \pm 0.011\%$ efficiency, respectively.

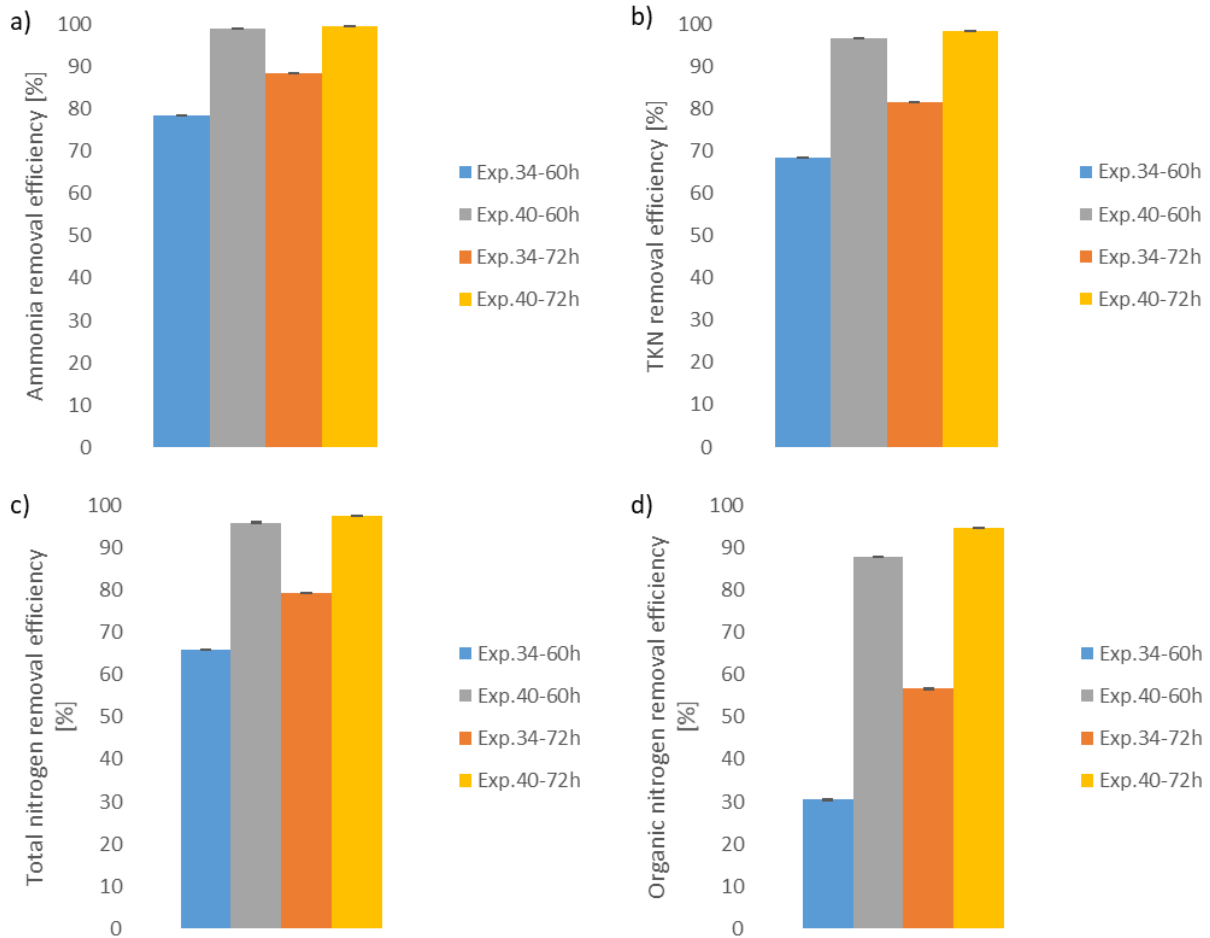


Figure 4- 24 Removal efficiencies of the pollutant for Stage 3-1; a) ammonia removal efficiency; b) TKN removal efficiency; c) organic nitrogen removal efficiency; d) total nitrogen removal efficiency

Total nitrogen (TN) removal efficiency (Fig.4-24c) in the Exp.34 and Exp.40 demonstrated that the difference between TN removal efficiency of Exp.34 and Exp.40 one was similar to TKN one. Furthermore, the obtained TN difference was 30.02%. In addition, the achieved removal efficiency values were $65.95\% \pm 0.038\%$ and 95.97% for the Exp.34 and Exp.40, respectively. The removal efficiency of the Exp.34 significantly boosted meanwhile the last 12 hour period and the final obtained removal efficiency was $79.33\% \pm 0.038\%$. It experienced $13.38\% \pm 0.038\%$ increase meanwhile the last 12 hour exposure time. However, the total nitrogen removal efficiency of the Exp.40 was far higher ($97.45\% \pm 0.038\%$) than the Exp.34.

Fig.4-24d illustrates the removal efficiency of the organic nitrogen. The results of the Exp.34 showed that $30.44\% \pm 0.04\%$ of organic nitrogen was removed after 60 hours. While the Exp. 40 the removal efficiency of organic nitrogen was $87.88\% \pm 0.04\%$ by considering 5 cm distance among electrodes and 60 hour treatment. Consequently, a difference equals to 57.44% was observed between Stage 3-1's experiments (Exp.34 and Exp.40). The Exp.34 experienced a remarkable increase (26.23%) in organic nitrogen removal efficiency during the last 12 hour interval and obtained $56.67\% \pm 0.04\%$. Whereas, the Exp.40 reached $94.63\% \pm 0.04\%$ efficiency which was 37.96% higher than in the Exp.36.

Based on the removal efficiency analysis, applying 5 cm would be an appropriate approach to follow in Phase 3 and Phase 4 of the research. Applying 7.5 cm distance required a higher current density due to the nonlinear changes in the resistivity of the cell once the distance among electrodes increased. Therefore, obtaining 21.37 mA/cm^2 (applied current density of 5 cm gap) would not lead to an acceptable removal efficiency once the distance between the electrode was 7.5 cm.

4-3-2. Stage 3-2 analysis

Stage 3-2 concentrated on the impact of hydrogen peroxide purity on removal efficiencies of the target pollutants. Due to the fact that the purity of hydrogen peroxide directly affects the available mass of hydrogen peroxide which is introduced to the system, investigating different purities come into consideration. The vision is reducing the exposure time for 12 hours (total time of 60 hours instead of 72 hours) by adding 50% purity hydrogen peroxide instead of 30% one.

In addition, using 50% hydrogen peroxide is expected to significantly decrease the cost consumption due to its low price and consequence reduction in process exposure time. The molar ratio of adding hydrogen peroxide to the bulk volume was 1.11/1 for both experiments (3.81/1 $\frac{\text{Fe}^{2+}}{\text{H}_2\text{O}_2}$).

The variations of the Exp.40 (50% purity H_2O_2) were discussed in Stage 3-1. So, the overall trend of the Exp.40 would be discussed in Stage 3-2 while the variations of the monitoring parameter in Exp.47 would be discussed in detail.

The results of compartment 1 in the Exp.47 demonstrated that voltage fluctuations (Fig.4-25a) were intense during the first 36 hour exposure time although the variations were stabilized throughout the remaining exposure time. Furthermore, the overall measured voltage of the Exp.47 was higher than the Exp.40's during 12 to 72 hours. No sharp decrease was observed during the process and the highest decline was detected in the first 12 hour exposure time (From 3.96 V to 3.63 V). While the voltage was recovered to 3.86 V during the second 12 hour period. In the remaining time, the voltage values fluctuated between 3.86 V and 3.72 V and the end point value was 3.75 V. Results of the Exp.40 determined that voltage significantly declined in the first 12

hour period. Next, the voltage gradually decreased during the second 12 hour period. Throughout the remained exposure time, voltage stabilized and the final value was 3.4 V.

The results in compartment 3 revealed that the Exp.47's voltage steadily decreased to 4.01 V from initial 5.39 V meanwhile the first and second 12 hour periods. Throughout the remaining 48 hours, voltage fluctuated between 4.01 V to 3.73 V and the final obtained value was 3.77 V. In contrast, the voltage values of the Exp.40 in compartment 1 were slightly higher than the Exp.47's ones. In addition, the averaged difference was 0.63 V. Using the hydrogen peroxide with 50% purity led to the stabilization of the voltage in compartment 1. On the other hand, a smooth trend was observed in compartment 3.

The pH results of the Exp.44 in compartment 1 (Fig.4-25b) demonstrated that pH fell sharply to 2.44 from initial 6.85 meanwhile the first 12 hour period. pH continued decreasing steadily throughout the second 12 hours and reached 1.27. Unexpectedly, pH smoothly increased meanwhile the remained 48 hour exposure time and the final measured pH was equal to 1.59. The averaged difference between Exp.40 and Exp.47 results was 0.38.

pH outcomes of the Exp.47 in compartment 2 showed that throughout the first 12 hour exposure time, pH significantly decreased to 2.68 and kept declining to 1.52 meanwhile the second 12 hour interval. However, during the remained 48 hours, pH smoothly increased to 1.59 which was equal to the final pH of compartment 1. In addition, the overall trend of the results of Exp.47 in compartment 2 was similar to compartment 1. The average difference between Exp.47 and Exp.40 results was 0.54 and the Exp.47's results demonstrated the higher values for pH in comparison with Exp.40's ones.

The last compartment results of the Exp.47 were distinctive in comparison with the Exp.40 considering the last 12 hour period results. A significant difference with the Exp.40's pH was observed at 12 hours which was 1.46 and the value of the Exp.47's pH was 2.69. pH steadily declined meanwhile the following 24 hours and measured pH at 36 hours was 1.33. From 36 hours to 60 hours, pH gradually increased to 1.65. During the last 12 hour period, pH surprisingly declined and the final pH was 1.47. The average difference between the Exp.40 and Exp.47 was 0.7 which showed the highest observed difference among all compartments. Furthermore, the Exp.47's pH was significantly higher than the results in Exp.40 .

Compartment 1 ORP results (Fig.4-25c) indicated that the Exp.47 (30% purity H₂O₂) experienced a gradual decrease from -21.7 mV to -26 mV meanwhile the first 12 hour period. While ORP value increased throughout the second 12 hour period and the measured pH was 276.8 mV at 24 hours. ORP magnitude gradually declined to 270.9 mV during the third 12 hour period. ORP steadily increased to 311.87 in the fourth 12 hour exposure time while the tendency of variations were downwards during the fifth 12 hour period. At last, ORP sharply increased throughout the last 12 hour exposure time and it reached 373.1 mV. The overall ORP of the Exp.40 was higher than the Exp.47's one, and the averaged considerable difference was 87.39 mV.

Compartment 2 showed similar tendency as compartment 1 with respect to on the Exp.47 variations in ORP. Meanwhile the first 12 hour period, ORP steadily decreased to -36.73 mV from initial -21.7 mV. However, the tendency changed during the second, and third 12 hour periods and ORP increased substantially to 348.17 mV while the measured ORP at 24 hours was 234.9 mV. The variations were stabilized throughout the fourth 12 hour period and the measured ORP at 48 hours was 355.48 mV. ORP steadily declined to 323.25 mV in the fifth 12 hour period and finally, the ORP tendency was upward throughout the last 12 hour period and the detected ORP at 72 hours

was 387 mV which was close to the Exp.40's final ORP (407.93 mV). The average difference between compartment 2 results was 64.46 mV which was significantly lower than compartment 1 one.

Compartment 3 results of the Exp.47 demonstrated the sharpest decrease among all compartments throughout the first 12 hour exposure time and the measured ORP was -39.77 mV. Following, ORP tendency was strongly upwards meanwhile the second and third 12 hour period and the measured ORP at 36 hours was equal to 291.47 mV. Through the fourth and fifth 12 hour period, ORP gradually decreased to 275.5 mV and the tendency of the last 12 hour exposure time was upwards and the final ORP was 359.23 mV. The average difference between Exp.40 and Exp.47 ORP was 100.62 mV which was the highest observed difference among all compartments and the Exp.40's ORP was higher than the Exp.47's one during the entire process time.

Analyzing the ORP results revealed that using hydrogen peroxide with 30% purity provides lower ORP in comparison with 50% purity hydrogen peroxide and the offset between curves was intensified meanwhile the third, fourth, and fifth 12 hour period for all three components.

Conductivity curves (Fig.4-25d) of the Exp.47 showed the similar values for three components and the curves were partially fitted with averaged 2.5 mS/cm offset. The same behavior was observed for the Exp.40 in which the conductivity curves had 2 mS/cm offset. Therefore, it would be logical to assess the analysis for one compartment and consider it as the representative of system behavior. Compartment 2 was selected as the representative regions. In the first 12 hour period, the Exp.47's conductivity increased sharply and reached 112.67 mS/cm and it was gradually increasing during the second 12 hour exposure time and the obtained value was 117.8 mS/cm at 24 hours. Through the third, fourth, and fifth 12 hours, the conductivity sharply increased to 237.5

mS/cm. The final measured conductivity was 261 mS/cm. The average difference between conductivity values of the Exp.40 and Exp.47 was 11.85 mS/cm while compartment 1 and compartment 2 average differences were 13.64 mS/cm and 15 mS/cm, respectively. Overall, the achieved conductivity of the Exp.40 was higher than the Exp.40's one and the results analysis proved that using 50% purity hydrogen peroxide as an oxidizing agent will provide higher conductivity.

Compartment 1 results of temperature (Fig.4-25e) demonstrated that both experiments (Exp.40 and Exp.47) experienced a sharp increase and reached 45.3 °C and 47.8 °C, respectively. The tendency of the Exp.47's temperature variations was steadily downwards throughout the interval of 12 hours to 60 hours and the obtained temperature at 60 hours was 40.4 °C. While the decreasing trend was intensified in the following 12 hour period (The last 12 hour exposure time) and the final obtained temperature was 31.6 °C. The variations of the Exp.40's temperature was fully discussed in Stage 3-2 relevant temperature results. It is notable to mention that the Exp.40's temperature was higher than Exp.47's one through the process time. The averaged difference between curves (offset) was 2.38 °C.

Compartment 2 results showed that the Exp.47 faced a sharp increase throughout the first 12 hour exposure time and the obtained temperature was 46.2 °C. While on the other hand, temperature decreased to 41.5 °C. Temperature was stabilized and gradually decreased meanwhile the second, third, and fourth 12 hour period and the measured temperature at 48 hours was 42.6 °C. Throughout the fifth and sixth 12 hour interval, temperature sharply declined and the final detected temperature was 31.7 °C. In compared with the Exp.40's results, the Exp.47's temperature magnitude were steadily lower and the averaged difference between two curves was 4.41 °C.

Compartment 3 results demonstrated a distinctive behaviour meanwhile the first 12 hour exposure time because of achieving the higher temperature for the Exp.47 (50.1 °C) in compared with Exp.40 (44.6 °C). Throughout the remained 60 hours, temperature of the Exp.47 was downward and the final measured temperature was 31 °C. The averaged difference between Exp.40 and Exp.47 cuves was 5.73 °C which was stand as the highest difference among all compartments.

Ammonia removal efficiencies (Fig.4-26a) of the Exp.40 (50% purity H₂O₂) and the Exp.47 (30% purity H₂O₂) were 98.97% ± 0.018% and 99.46% ± 0.018%, respectively at 60 hours. In addition, based on experimental anaysis the calcuated ammonia removal efficiencies of the Exp.40 and Exp.47 were 99.45% ± 0.018% and 99.48% ± 0.018% correspondigly. Therefore, using 30% purity hydrogen peroxide led to a higher ammonia removal efficiencies at 60 hours and 72 hours.

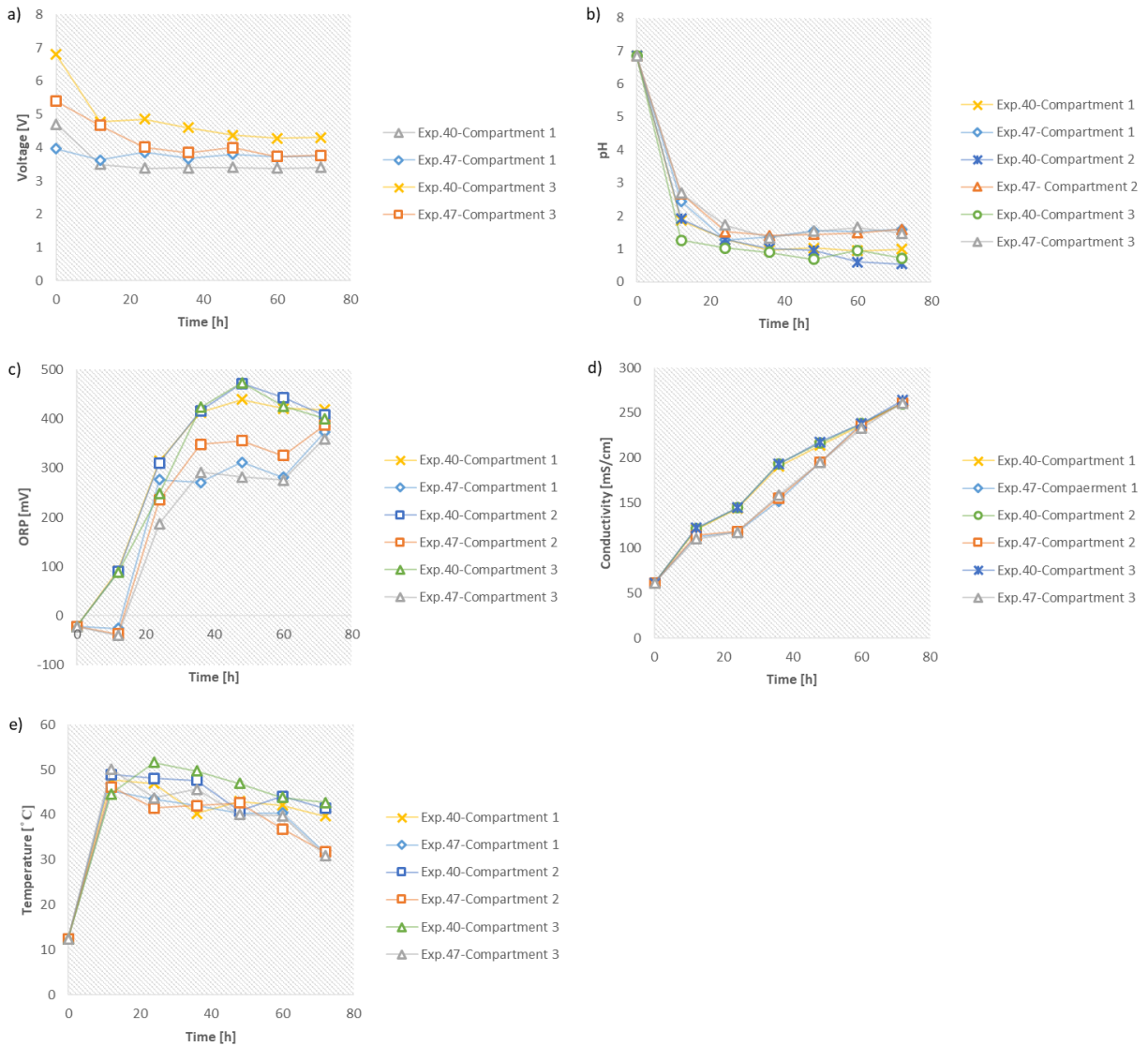


Figure 4- 25 Variations of monitored parameters for the relevant experiments of Stage 3-2; a) voltage versus time; b) pH versus time c) ORP versus time; d) conductivity time e) temperature versus time

TKN removal efficacy of the Exp.47 (Fig.4-26b) was superior in comparison with the Exp.40's one at 60 hours ($96.6\% \pm 0.011\%$ for the Exp.40 and $97.8\% \pm 0.011\%$ for Exp.47) which demonstrated 1.6% higher efficiency. In contrast, the Exp.40's efficiency at 72 hours ($98.41\% \pm 0.011\%$) was higher than the Exp.47's one ($97.18\% \pm 0.011\%$) and a slight decrease in efficiency of the Exp.47 was observed between 60 hours and 72 hours. The mentioned decline was initiated

from transformation of TKN to nitrite and subsequently nitrate which proved on consequence decrease in total nitrogen removal.

Total nitrogen removal efficiencies (Fig.4-25c) of the Exp.40 and Exp.47 were $95.97\% \pm 0.038\%$ and $95.76\% \pm 0.038\%$ respectively at 60 hours. In addition, at 72 hours, the Exp.40 gives $97.45\% \pm 0.038\%$ removal efficiency with respect to the total nitrogen while on the other hand, the achieved removal efficiency of the Exp.47 was $95.76\% \pm 0.038\%$. The higher removal efficiency of the Exp.40 compared with Exp.47 demonstrated the excellency of total nitrogen once 50% purity hydrogen peroxide was used.

The last response parameter which was analyzed was the organic nitrogen removal efficiency (Fig.4-26d). At 60 hours, the Exp.47 demonstrated a better removal efficiency in comparison with the Exp.40 and 4.34% difference was observed. The achieved removal efficiencies of the Exp.40 and Exp.47 were 87.88% and 92.22%. However, the Exp.40's efficiencies surprisingly boosted and reached 94.63% at 72 hours while its efficiency was 3.58% higher than the Exp.47 with removal efficiency of 91.05%.

Therefore, based on the achieved removal efficiencies, it was preferable to use the hydrogen peroxide with 50% purity. The reason was higher removal efficiencies of TKN, total nitrogen and organic nitrogen at 72 hours.

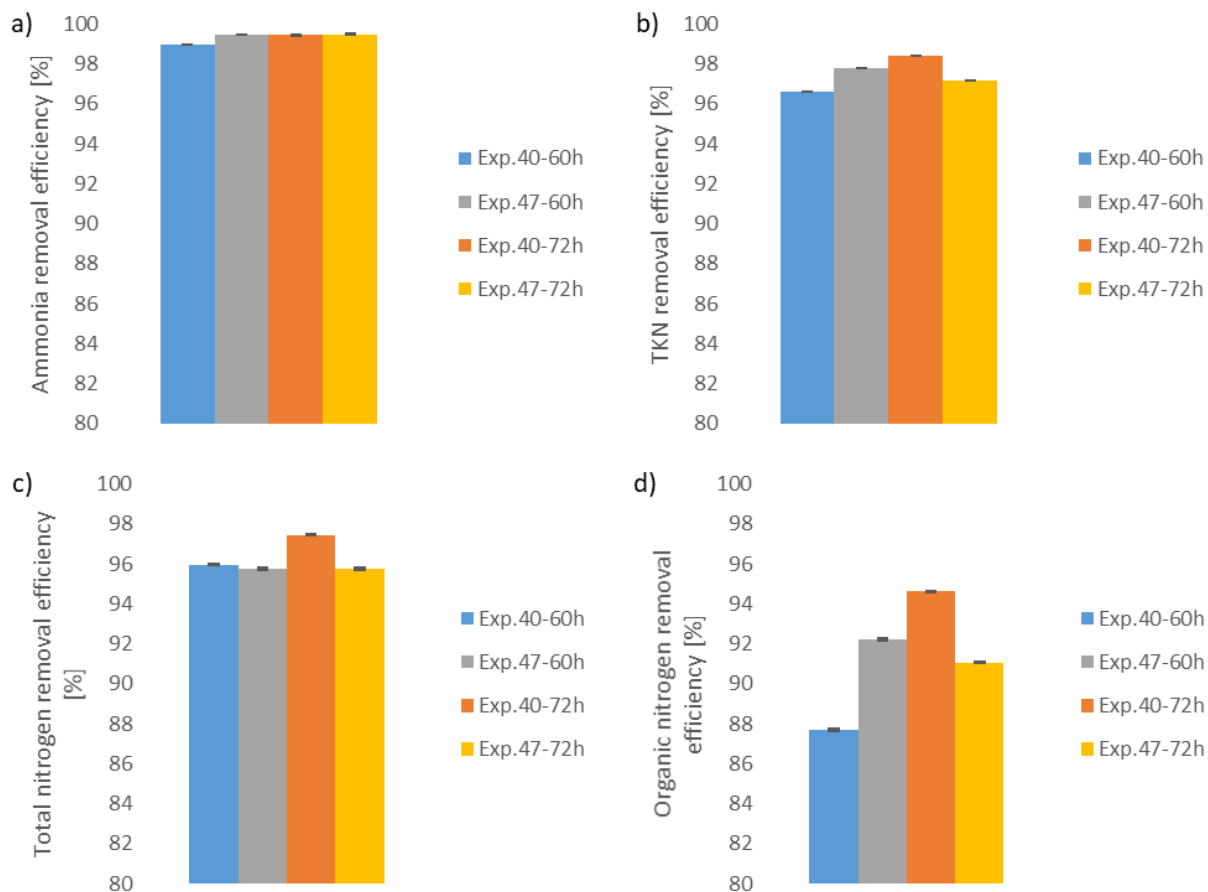


Figure 4- 26 Removal efficiencies of the pollutants for Stage 3-2; a) ammonia removal efficiency; b) TKN removal efficiency; c) organic nitrogen removal efficiency; d) total nitrogen removal efficiency

4-3-3. Stage 3-3 analysis

Stage 3-3 focused on the impact of molar ratio of adding hydrogen peroxide with respect to the present homogenous catalyst (Ferrous ions) in the raw wastewater. The obtained molar ratio of hydrogen peroxide and ferrous ions ($3.44/1 \frac{H_2O_2}{Fe^{2+}}$) in Phase 1 and Phase 2 followed in Phase 3, Exp.36. In addition, the molar ratio of $3.81/1 \frac{H_2O_2}{Fe^{2+}}$ was considered for the Exp.40 to investigate the influence of the increase in volume of hydrogen peroxide on response outcomes.

The Exp.40's (Molar ratio of $3.81/1 \frac{\text{H}_2\text{O}_2}{\text{Fe}^{2+}}$) variations were discussed in Stage 3-1 relevant results and focusing on overall trend in comparison with the Exp.44 (30% purity H_2O_2) was the approach of studying the Exp.40's results in Stage 3-3.

The voltage variations in compartment 1 (Fig.4-27a) demonstrated that the Exp.36 experienced a sharp decline in the first 12 hour period and reached 3.1 V from initial 4.5 V. Throughout the second and third 12 hour exposure time, voltage gradually decreased and the obtained voltage at 36 hours was 3.27 V. In contrast, the voltage declined steadily and reached 2.77 V in the fifth 12 hour exposure time. Throughout the last 12 hour period, the tendency of voltage variations was upwards and the detected voltage at 72 hours was 2.96 V. Comparing the Exp.40's voltage variations, the Exp.36's voltage fluctuated more specifically during the last 24 hour exposure time. The average offset between voltage curves of the Exp.36 and Exp.40 was 0.37 V.

The voltage variations in compartment 3 showed that the Exp.36's voltage significantly fell to 4.46 V from initial 7.73 V. Then, the voltage steadily increased to 5.4 V meanwhile the second 12 hour period. Throughout the interval of 24 hours to 48 hours, the voltage of the Exp.36 smoothly declined to 4.81 V. Unexpectedly, the Exp.36's voltage remained constant during the fifth 12 hour exposure time. The tendency of variations was downwards meanwhile the last 12 hour exposure time and the final measured value of voltage was 4.62 V. Comparing the Exp.36 and Exp.40 voltage curves reveals that the voltage of the Exp.36 in compartment 3 was majorly higher than the voltage of Exp.40. Furthermore, the averaged offset between voltage curves was 0.44 V.

pH curves in compartment 1 (Fig.4-27b) showed that the pH variations of the Exp.36 (molar ratio of $3.44/1 \frac{\text{H}_2\text{O}_2}{\text{Fe}^{2+}}$) and the Exp.40 (molar ratio of $3.81/1 \frac{\text{H}_2\text{O}_2}{\text{Fe}^{2+}}$) were fitted in the time interval of 36 hours from the beginning. In addition, the only minor offsets were observed throughout the fourth

and fifth 12 hour exposure time. The Exp.36 gave lower pH at 48 hours and 60 hours with the values of 0.68 and 0.7, respectively. In addition, throughout the last 12 hour exposure time, pH increased to 0.99. The averaged offset between Exp.36 and Exp.40 curves was 0.05 which can be considered as negligible offset.

The results of compartment 2 indicated that the Exp.36's pH significantly declined to 1.3 from initial 6.8 throughout the first 12 hour period. During the second and third 12 hour interval, pH steadily decreased to 1.4 and both curves of the Exp.36 and Exp.40 curves were fitted. However, an offset between the Exp.36 and Exp.40 was observed throughout the fourth 12 hour exposure time and the detected pH was 0.7 at 48 hours. Then, the pH stabilized at 0.69 in the fifth 12 hour period and the final detected pH was 0.32. it was the most acidic pH that was observed in compartment 1 of experiments in Phase 3. In addition, the average difference was equal to 0.13 which was stand as the highest offset among all three compartments of Stage 3-3.

pH curves of compartment 3 was fitted with the Exp.40 during the first 12 hour exposure time and reached 1.36. So, it can be considered as the sharpest decrease among all experiments of Phase 3 which occurred meanwhile the first 12 hour interval. During the second 12 hour period, pH declined and gave 1.28. Then, pH gradually fell to 0.94 and kept declining up to 0.8 at 48 hours. Throughout the fifth 12 hour period, pH slightly stabilized and declined to 0.78. However, pH steadily declined throughout the last 12 hour period and the measured pH was 0.66. In addition. the averaged difference was equal to 0.024 which was the half of compartment 1 relevant offset.

ORP changes (Fig.4-27c) of the Exp.36 (Molar ratio of $3.44/1 \frac{H_2O_2}{Fe^{2+}}$) in compartment 1 demonstrated that meanwhile the first 12 hour period, ORP steadily increased to 10.8 mV from initial -21.7 mV. Furthermore, ORP increased throughout the second and third 12 hour exposure

time and reached 400.63 mV at 36 hours. Based on the achieved results, it can be interpreted that the reactions taken place in the oxidation state and the evolution of organic compounds degradation in the second and third 12 hour period. Consequently, The observed phenomenon can be considered as an indicator for the occurrence of oxidation reactions. The ORP kept increasing meanwhile the fourth and fifth 12 hour exposure time and the measured ORP at 60 hours was equal to 482.23 mV. Unexpectedly, ORP fell to 356.7 mV during the last 12 hour period. The ORP of the Exp.40 (molar ratio of $3.81/1 \frac{\text{H}_2\text{O}_2}{\text{Fe}^{2+}}$) was higher than the Exp.36's one during the first 36 hour period. The reason was the higher volume of hydrogen peroxide input in Exp.40 which was added each 12 hour. However, the Exp.40' ORP was less than the Exp.36's one in the fourth and fifth 12 hour period. The reason was probably the formation of intermediates throughout oxidation that were more difficult to remove [4-9]. Therefore, the oxidation reactions could not be thoroughly developed and shift to oxidation state. The averaged offset between the Exp.36 and Exp.40 curves was 54.38 mV and Exp.40's ORP was higher than the Exp.36's one.

It was crucial to consider that a high oxidation state does not guarantee the high removal efficiencies of organic compounds. But, the high oxidation potential could be assessed as an indicator for progress of oxidation process.

Compartment 2 results of the Exp.36 demonstrated the same tendency as compartment 1 although the ORP values were slightly lower than compartment 1 results. For instance, the detected ORP at 36 hours (after a large increase throughout the second and third 12 hour exposure time) was 389.87 mV which was 10.76 mV lower than compartment 1 achieved ORP at the same monitoring point. Although the achieved ORP at 60 hours (482.3 mV) was approximately the same as compartment 1 ORP, the final obtained ORP (346.27 mV) was significantly lower than the compartment 1 final

ORP. The difference was 10.43 mV. The comparison of Exp.36 and Exp.40 results revealed that throughout the first and second 12 hour interval, the offset between curves was significant and the representative values were 76.94 mV, 191.97 mV. While on the other hand, the offset was minimized and truncated to 12.77 mV at 48 hours. Majorly, the Exp.40's obtained ORP was higher than the Exp.36's one and the only exception was related to 60 hours ORP which was 39.1 mV higher. In general, the average offset was 146.20 mV.

Compartment 3 and compartment 2 were identical. Moreover, the tendency of variations and achieved values were slightly similar with less than 5 mV difference throughout 60 hours from the beginning. The only significant difference was related to the final ORP (356.3 mV). The achieved ORP was identical to compartment 1 ORP with 0.03 mV difference. The average offset between the Exp.36 and Exp.40 curves was 40.35 mV. Comparing offset values among all three compartments showed that the highest offset belongs to compartment 2.

The variations of conductivity (Fig.4-27d) demonstrated the similar tendency in all compartments of the Exp.36 and all three curves were partially fitted. In addition, the difference between each compartment curve (e.g. difference between conductivity values compartment 1 and compartment 2; difference between conductivity values compartment 1 and compartment 3) would not exceed 4 mS/cm. So, considering compartment 2 as a representative compartment to analyze the variations would be a logical approach. Therefore, the Exp.40 would be selected for investigation. In the first 12 hour period, conductivity gradually increased and reached 78.8 mS/cm. A gradual increase was observed during the second 12 hour exposure time which led to 85.2 mS/cm at 24 hours. Then, the conductivity increased to 148.9 mS/cm throughout the third 12 hour interval. The tendency of changes was upwards, and the final obtained conductivity was 227 mS/cm. The averaged offset between compartment 2 conductivity curves of the Exp.36 and Exp.40 was 36.53 mS/cm and the

Exp.40's conductivity was consistently higher than the Exp.36's one. Therefore, the higher hydrogen peroxide to ferrous ions molar ratio led to obtain higher conductivity in the process. It would be probable that the oxidation reactions intensified by providing a higher number of hydroxyl radicals which led to increase in conductivity.

Compartment 1 temperature variations (Fig.4-27e) demonstrated that it would be impossible to assess to state which experiment provided the higher temperature entire the process. To specifically analyze the tendency, both experiments (Exp.36 and Exp.40) temperature magnitude increased meanwhile the first 12 hour exposure time and reached 45.6 °C and 47.8 °C, respectively. Therefore, the Exp.40 (Molar ratio of $3.81/1 \frac{H_2O_2}{Fe^{2+}}$) provided the higher temperature during the first 12 hour period. Then, Exp.36's temperature increased throughout the second 12 hour period and reached 46.4 °C (0.5 °C lower than Exp.40). In contrast, throughout the third and fourth 12 hour exposure time, the Exp.36's temperature outpaced the Exp.40's one and reached 44.6 °C at 48 hours. Although the Exp.40's temperature (42.1 °C) outpaced the Exp.36's one at 60 hours, the final recorded Exp.36's temperature (42.4 °C) was 2.7 °C higher than the Exp.40's one. Finally, the average difference between Exp.36 and Exp.40's temperature curves was -0.59 °C which was shown that the Exp.40's temperature was lower than the Exp.36 throughout the process

Compartment 2 temperature changes showed that the Exp.36's temperature was lower than the Exp.40's one and the exceptions were detected throughout the fourth and sixth 12 hour period. Furthermore, the Exp.36's temperature with exception at 44.2 °C and 42.1 °C which were higher than the Exp.40's temperature for 3.4 °C and 0.7 °C, respectively. To provide specific analysis on different time intervals, it should be mentioned that the Exp.36's temperature increased in the first 12 hour exposure time to 42.4 °C. Then, temperature steadily increased throughout the second and

third 12 hour period to 47.6° C at 36 hours. However, the tendency of variations was gradual downwards throughout the remained 36 hours. Lastly, the averaged offset between Exp.36 and Exp.40 temperature magnitude was 0.97° C.

Compartment 3 temperature variations provided the distinctive behavior in the first 12 hour interval in which the Exp.36's temperature (47.9° C) was higher than the Exp.40's one (44.6° C). While on the other hand, the Exp.36 reached the lower temperature in comparison with the Exp.40 throughout the remained 60 hours. The tendency of the Exp.36's variations was downwards and reached 45.9° C in the second and third 12 hour period. However, the Exp.36 faced a steady increase and provided 46.9° C at 48 hours. Then, the temperature significantly fell to 40.4° C and gradually declined throughout the last 12 hour exposure time to 39.8° C at 72 hours. In addition, the averaged offset of compartment 3 between Exp.36 and Exp.40 curves was equal to 1.68° C which demonstrated that the Exp.40's temperature was thoroughly higher than the Exp.36's one through the process. Therefore, based on achieved results it would not be feasible to conclude that exceeding hydrogen peroxide input volume will directly impact the compartments temperature variations in Stage 3-3.

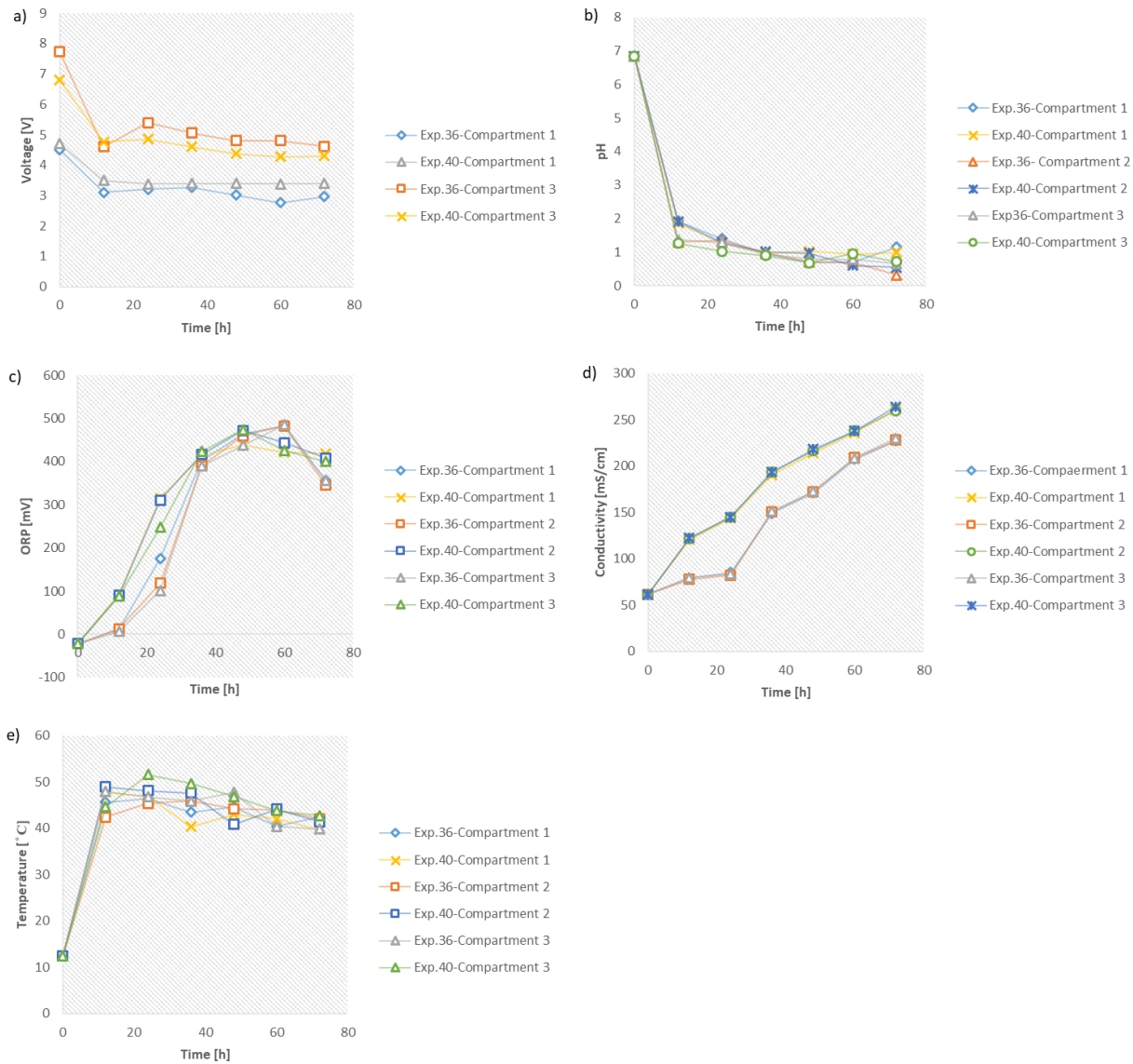


Figure 4- 27 Variations of monitored parameters for the relevant experiments of Stage 3-3; a) voltage versus time; b) pH versus time c) ORP versus time; d) conductivity versus time e) temperature versus time

Target pollutants removal efficiencies were investigated at 60 hours and 72 hours, respectively.

Ammonia removal efficiencies (Fig. 4-28a) of the Exp.36 (molar ratio of $3.44/1 \frac{H_2O_2}{Fe^{2+}}$) were significantly lower than the Exp.40 (molar ratio of $3.81/1 \frac{H_2O_2}{Fe^{2+}}$) at 60 hours and the provided efficacies were $95.1 \% \pm 0.018\%$ and $98.97\% \pm 0.018\%$, respectively. Although, the removal efficiency of the Exp.36 enhanced in the last 12 hour period for 2.3% at 72 hours, the Exp.40's

efficiency with the value of $99.45\% \pm 0.018\%$ was 2.04% higher than the Exp.36's one. The second compound which was analyzed with respect to removal efficiency was TKN (Fig.4-28b). The Exp.36's TKN efficiency was equal to $93.76\% \pm 0.011\%$ at 60 hours while the Exp.40's one was 96.6%. So, the Exp.40's experimental design provided 2.8% higher efficiency in comparison with the Exp.36's results. Then, the Exp.36's efficiency ($95.81\% \pm 0.011\%$) boosted for 2.05% during the last 12 hour period. However, the Exp.40 kept the excellency and reached $98.41\% \pm 0.011\%$ which was 2.6% higher than the Exp.36.

Total nitrogen removal efficiency (Fig.4-28c) of the Exp.36 was 93.14% while the Exp.40's one was 2.83% higher with the value of $95.97\% \pm 0.038\%$. Throughout the last 12 hour interval, the Exp.36's removal efficiency was improved by 1.39% and reached $94.53\% \pm 0.038\%$. However, the Exp.40's efficiency continued to be superior and provided $97.45\% \pm 0.038\%$ which was 2.93% higher than the Exp.36's one.

The last compound which was investigated was the organic nitrogen (Fig.4-28d). Surprisingly, the Exp.36's efficiency outpaced the Exp.40's one and reached $88.8\% \pm 0.04\%$ while the difference was 0.92%. However, the Exp.40's efficiency remarkably increased for 6.75% at 72 hours with the value of $94.63\% \pm 0.04\%$ while on the other hand, the analyzed removal efficiency of the Exp.36 was equal to $89.93\% \pm 0.04\%$ at 72 hours. So, it can be concluded that removal efficiency of the Exp.36 was not enhanced significantly in the last 12 hour period and it would be a reason for outpacing the Exp.40 throughout the sixth 12 hour exposure time.

Therefore, it can be construed that increasing hydrogen peroxide input volume will significantly enhance the removal efficiencies of ammonia, TKN, total nitrogen, and organic nitrogen, respectively. The obtaining molar ratio of $3.81/1 \frac{\text{H}_2\text{O}_2}{\text{Fe}^{2+}}$ would be a logical approach for Phase 4.

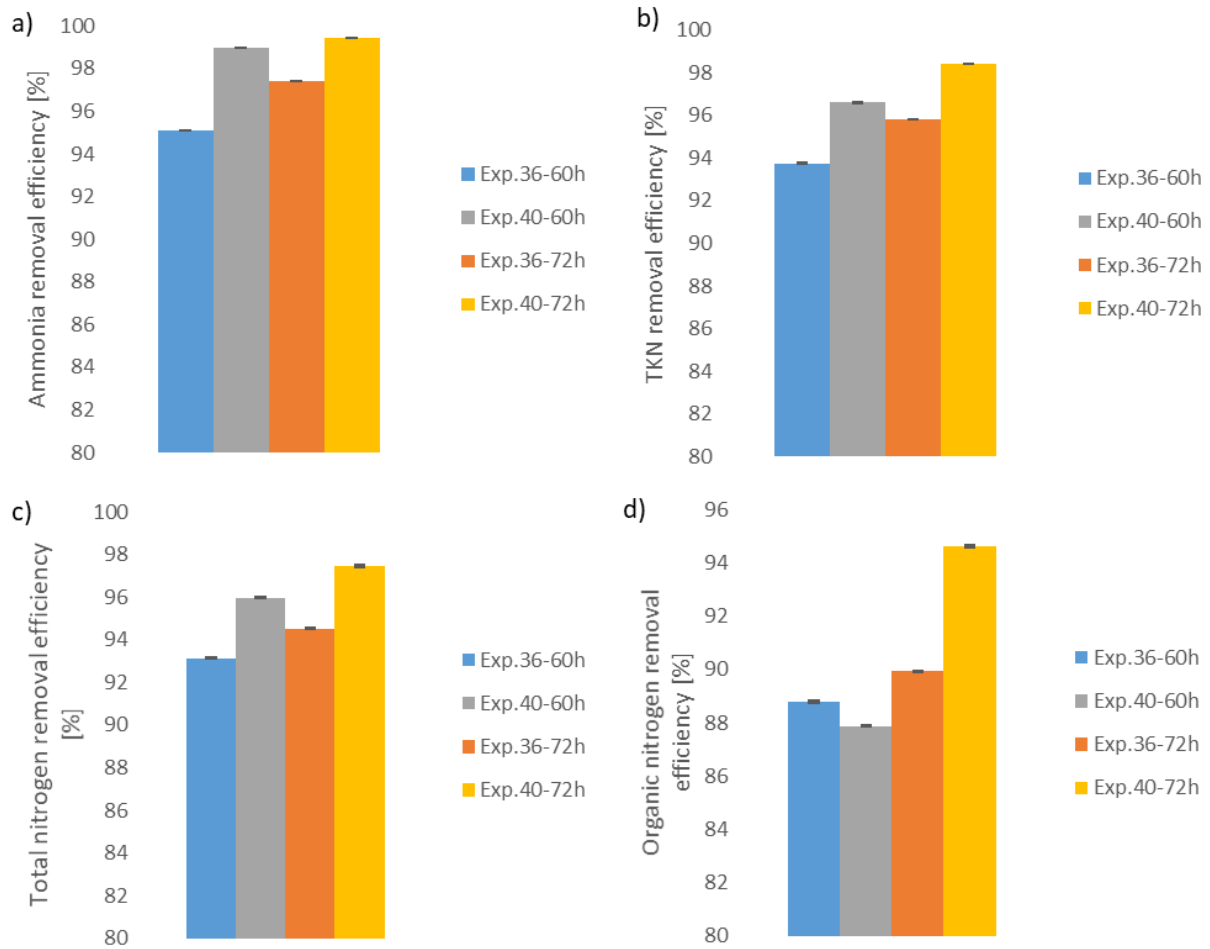


Figure 4- 28 Removal efficiencies of the pollutants for Stage 3-3; a) ammonia removal efficiency; b) TKN removal efficiency; c) organic nitrogen removal efficiency; d) total nitrogen removal efficiency

Table 4-3 illustrates the obtained removal efficiencies of the third phase experiments. It also provides the remarks of the experiments to show the experimental design. It is critical to mention that the Exp.40 belonged to all three stages of Phase 3 and its results are duplicated in each section of the table to provide experimental design considerations and facilitate tracking of the objectives for each individual stage.

Table 4- 3 Removal efficiencies of ammonia, TKN, total nitrogen, and organic nitrogen for all experiments of Phase 3

Stage	No. of Exp.	Ammonia removal [%] ± 0.018%	TKN removal [%] ± 0.011%	Total nitrogen removal [%] ± 0.038%	Organic nitrogen removal [%] ± 0.04%	Remarks
Stage 3-1	34-60 h	78.57	68.26	65.95	30.44	7.5 cm distance among electrodes
	40-60 h	98.97	96.6	95.97	87.89	5 cm distance among electrodes
	34-72 h	88.51	81.59	79.33	56.67	7.5 cm distance among electrodes
	40-72 h	99.45	98.41	97.45	94.63	5 cm distance among electrodes
Stage 3-2	40-60 h	98.97	96.6	95.97	87.89	50% purity H ₂ O ₂
	44-60 h	99.46	97.8	95.76	92.22	30% purity H ₂ O ₂
	40-72 h	99.45	98.41	97.45	94.63	50% purity H ₂ O ₂
	44-72 h	99.48	97.18	95.76	91.05	30% purity H ₂ O ₂
Stage 3-3	36-60 h	95.11	93.76	93.14	88.8	molar ratio of 3.44:1 $\frac{H_2O_2}{Fe^{2+}}$
	40-60 h	98.97	96.6	95.97	87.89	molar ratio of 3.81:1 $\frac{H_2O_2}{Fe^{2+}}$
	36-72 h	97.41	95.81	94.53	89.93	molar ratio of 3.44:1 $\frac{H_2O_2}{Fe^{2+}}$
	40-72 h	99.45	98.41	97.45	94.63	molar ratio of 3.81:1 $\frac{H_2O_2}{Fe^{2+}}$

4-4. Phase 4 results and discussion

The novelty of this research is specifically addressed in the objectives of Phase 4, experimental parametric study of EF-SBR. The first application of combined electro-Fenton sequential batch reactor was introduced in Lin and Chang (2000) research [4-10]. The objective of their study was treatment of an old-aged landfill leachate which was constituted of 150.9 mg NH₃-N/L. The concentration of ammoniacal nitrogen reached 28.2 mg NH₃-N/L after treating by electro-Fenton oxidation process. SBR phase was applied as a biological treatment and after 5 times 12 h cycles, the concentration of ammoniacal nitrogen met the allowable concentration to discharge to the waterbodies.

However, the mechanism which is introduced in this study is applying electro-Fenton oxidation mechanism by 2 different SBR cycles with the duration of 72 hours and 48 hours. In simple words, SBR and electro-Fenton oxidation mechanisms are functionalized at the same time. In addition, the novelty of this research is using the SBR to facilitate electro-Fenton oxidation.

The EF-SBR was conducted in both medium and large scales. Two parameters of the impact of hydrogen peroxide purity and the number of SBR cycles on removal efficiency of the target pollutants were investigated in this study.

4-4-1. Stage 4-1 analysis

4-4-1-1. Impact of hydrogen peroxide purity on medium scale EF-SBR efficiency

Stage 4-1 investigated the impact of the hydrogen peroxide purity on the removal efficiency of the target pollutants in the medium-scale (2.2 L) electrochemical reactor. Due to the fact that the hydrogen peroxide purity plays an important role in providing available hydroxyl radicals, Stage 4-1 is designed to investigate the contribution of hydrogen peroxide purity to enhancement of the

removal of efficiency of target pollutants. It is also probable that using high purity hydrogen peroxide aids in decreasing the exposure time for more than 1 day. Therefore, experimental design of Stage 4-1 is focused on utilizing two different hydrogen peroxide purities which are 30% and 50%, respectively. The analyzed medium scale experiments of Stage 4-1 are Exp.42 (30% purity H₂O₂) and the Exp.45 (50% purity H₂O₂) respectively.

To clarify the process, it is essential to mention that the exposure time of the first cycle and second cycle were 72 hours and 48 hours, respectively. The first cycle of SBR was set based on the experimental design of Phase 2 considering the optimal achieved results. Also, the similar experimental design was attained for the following cycles and the only difference was related to exposure time which was modified to 48 hours. So, Exp.42's cycle 1 was investigated in Phase 2 results and the approach would be considering the overall trend of Exp.42's cycle 1 as a reference to juxtapose with the results of the cycle 1 in Exp.45 (50% purity H₂O₂).

The voltage changes (Fig.4-29a) of the Exp.42 (30% purity H₂O₂) was strongly downwards during the first 24 hour exposure time. In addition, the voltage variation of the Exp.45 (50% purity H₂O₂) was obtained the same trend as the Exp.42 meanwhile the same time interval (the first 24 hour exposure time). Furthermore, the Exp.42's voltage fell to 4.34 V from the initial value of 6.18 V and the voltage of Exp.45 declined steadily to 5.32 V from the initial magnitude of 6.99 V. Throughout the remaining exposure time (from 24 hours to 72 hours), the Exp.42's voltage slightly stabilized and declined to 4.18 V at 72 hours (end of the first cycle). On the other hand, Exp.45 kept a downward tendency throughout the second and third 24 hour- period, and the final obtained voltage was 4.59 V at 72 hours.

Once the second cycle commenced the raw wastewater was substituted with the 75% of effluent (treated wastewater) and 25% of effluent would remain in the electrochemical reactor. Therefore, it is expected that the initial applied voltage of the second cycle would be different from the initial voltage of the first cycle. The results also showed that the initial voltage of the second cycle of the Exp.42 and Exp.45 were lower than the relevant values of cycle 1. In addition, the voltage values were 4.9 V and 6.19 V at 72.5 hours for Exp.42 and Exp.45, respectively that are 0.8 V and 1.28 V lower than cycle 1 voltage values. The reason was a significant increase in the initial conductivity of the second cycle in which the conductivity increased to 84.1 mS/cm and 84.5 mS/cm from initial 57.4 mS/cm, respectively. The increase in conductivity is often expected to result a decline in voltage. Meanwhile the fourth 24 hour-period ((from the cycle 2 start point to 24 hours), Exp.42's voltage steadily decreased to 4.11 V while Exp.45 experienced a significant decline and reached 4.46 V throughout the same time interval. However, both experiments demonstrated a distinctive behavior during the last 24 hour exposure time of the second cycle (from 96.5 hours to 120.5 hours). The Exp.42's voltage steadily increased to 4.71 V while the Exp.45's one slightly stabilized and decreased to 4.07 V. It is probable that due to remarkable increase in suspended solid concentration, the cell potential was increasing. The averaged offset between Exp.42 and Exp.45 voltage curves was 0.71 V.

Therefore, based on the results it can be interpreted that the hydrogen peroxide purity directly influenced the cell potential and resulted in a higher voltage once the higher purity of hydrogen peroxide was used.

The pH variations (Fig.4-29b) of Stage 4-1's experiments showed that both experiments faced a significant fall throughout the first 24 hour exposure time. The measured pH values were 2.16 and 1.28, respectively. Both experiments slightly stabilized in the second and third 24 hour- period,

and reached 1.9 and 1.05 at 72 hours, correspondingly. After mixing 75% raw wastewater and 25% of cycle 1 effluent, pH of the Exp.42 and Exp.45 increased to 1.97 and 1.99, respectively. Throughout the first 24 hour- period of the second cycle (from 72.5 hours to 96.5 hours) the Exp.42 experienced a steady decrease to 1.2; on the other hand, the Exp.45 faced a gradual increase and reached 2.15. However, the trend was reversed for each experiment throughout the last 24 hour exposure time and the Exp.42's voltage steadily raised to final value of 1.4 at 120.5 hours while Exp.45 gave 1.92 at the same end point. Consequently, the trends of experiments did not change after the start of the second cycle and the Exp.42's pH was consistently lower than Exp.45's one. It means that using 30% hydrogen peroxide leads to more acidic conditions. The reason can be construed by the number of hydrogen ions available after hydrogen peroxide electro-dissociation which is weakened the acidity of the effluent. The averaged offset between pH curves of the Exp.42 and Exp.45 is equal to 0.57.

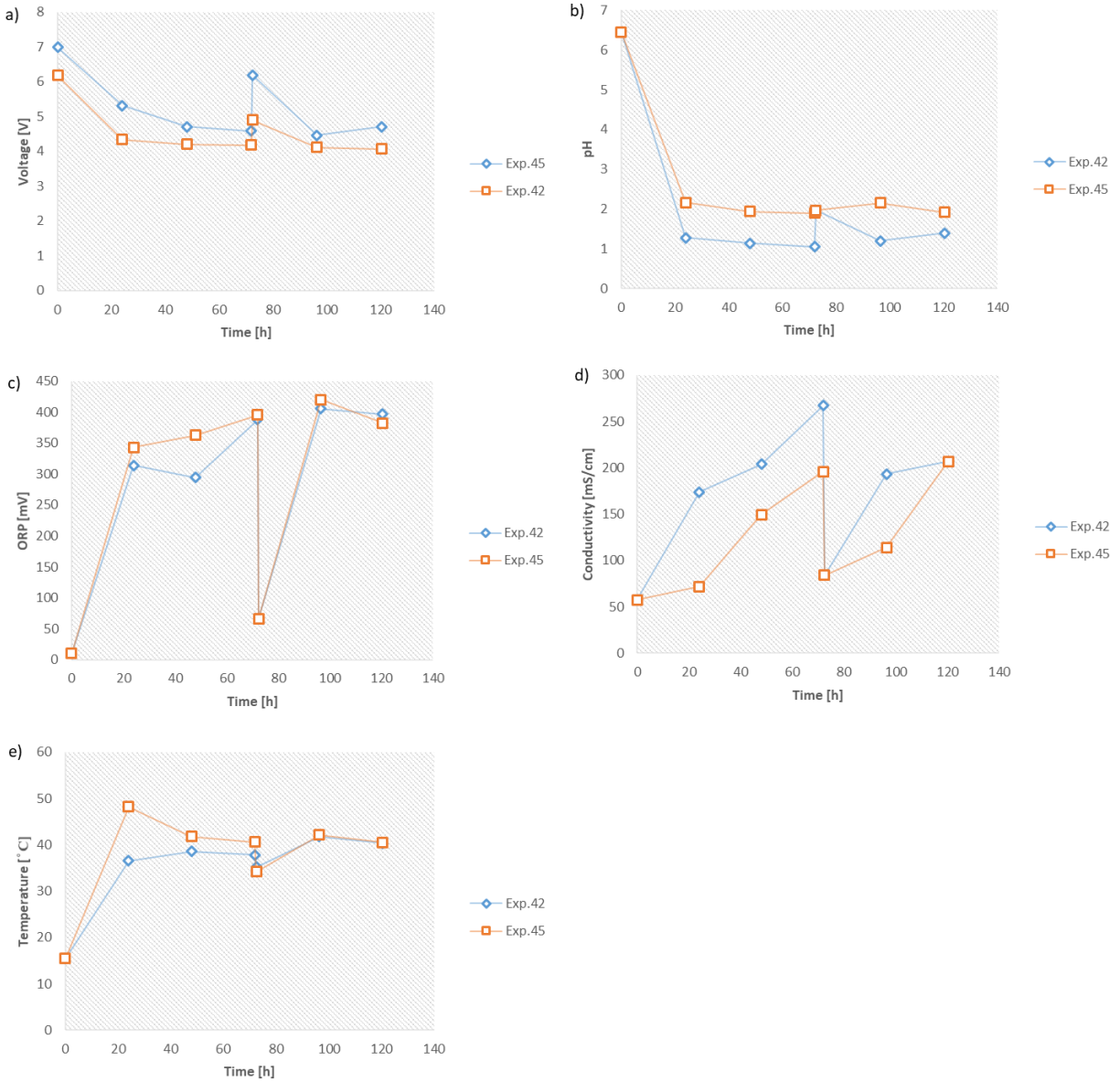


Figure 4- 29 Variations of monitored parameters for the relevant experiments of Stage 4-1 for medium scale EF-SBR; a) voltage versus time; b) pH versus time c) ORP versus time; d) conductivity versus time e) temperature versus time

The ORP variations (Fig.4-29c) demonstrated that Exp.42 (30% H₂O₂) and Exp.45 (50% H₂O₂) faced sharp increase in the first 24 hour period and the representative values increased to 313.8 mV and 343.1 mV, respectively. Therefore, reactions proceeded to a strong oxidation state in which organic compounds degradation was expected to be accelerated. However, the Exp.42 steadily decreased to 294.8 mV which might be the evidence of the intermediate compounds

existence. Then, the Exp.42's ORP sharply increased meanwhile the third 24 hour-period and obtained 388mV at 72 hours. In contrast, the Exp.45's ORP consistently increased throughout the second and the third day and the measured value was 395.6 mV at 72 hours. Once the second cycle of the Exp.42's SBR commenced, the measured ORP of the second cycle start point (66.16 mV) was significantly higher than initial raw wastewater water which was equal to 9.9 mV. The same improvement was experienced in ORP for the Exp.45 with 55.36 mV surge in ORP value in comparison with the initial value of 10.8 mV. The reason was influential partaking of the remaining 25% volume of the first cycle effluent in leading the initial state of the reactions to oxidation state. Throughout the first 24 hour- period of the second cycle (72.5 hours to 96.5 hours) the ORP of both experiments increased to 405.5 mV and 420.1 mV. Whereas, the Exp.45 faced a constant decline to 382.6 mV during the last 24 hour exposure time. The influence of the weakening of the oxidation state meanwhile the last 24 hour- period of the second cycle was reflected in resulting remarkable reduction with respect to target pollutant removal efficiency (See Fig. 4-30). Although, the intensity of the Exp.42's ORP decline was lower than the Exp.45's one (from 405.5 mV to 397.17 mV), the target pollutants removal efficiency was impacted thoroughly and faced a strong decrease except for Ammonia. At last, the averaged offset between Exp.42 and Exp.45 curves was 16.17 mV.

The conductivity results (Fig.4-29d) showed that the conductivity of the Exp.42 (30% H₂O₂) sharply increased to 173.9 mS/cm from initial 57.4 mS/cm. Also, the Exp.45's conductivity steadily increased to 71.7 mS/cm. Throughout the second 24 hour exposure time, the Exp.42's conductivity consistently increased and reached 204 mS/cm. Then, a sharp increase was measured for the third 24 hour exposure time and the Exp.42's conductivity reached a peak (267 mS/cm).

On the other hand, the Exp.45 showed a sharp increase throughout the second and third 24 hour period and obtained 196 mS/cm at 72 hours.

At the start point of the second SBR cycle, the initial conductivity values of both experiments reached 85.1 mS/cm and 84.1 mS/cm. The detected values were 27.7 mS/cm and 26.7 mS/cm higher than the initial conductivity of the raw wastewater. A similar justification as ORP surge could be implied for the observed increase in conductivity. In addition, it is essential to mention that close values of conductivity in SBR cycle 2 start point for both experiments revealed the governing influence of the raw wastewater's conductivity on overall achieved conductivity. Throughout the first 24 hour exposure time of the second cycle (from 72.5 hours to 96.5 hours), the Exp.42's conductivity increased to 193.5 mS/cm and steadily continued increasing to 206.8 mS/cm meanwhile the last 24 hour period. Whereas, the Exp.45's conductivity steadily increased to 114 mS/cm throughout the first 24 hour exposure time of SBR cycle 2 and faced a sharp increase to 207.1 mS/cm during the last 24 hour period. It might be questionable that why both experiments were reached an approximate similar value at the end of cycle 2. The justification is the sharper increase of the Exp.45's conductivity during the first and second 24 hour exposure time of the cycle 2 in comparison with the obtained values throughout the same time intervals of the first SBR cycle.

In the nutshell, adding 30% hydrogen peroxide led to have higher conductivity in the process and the tendency was unchanged throughout the second cycle. Finally, the average offset between conductivity curves was 44.78 mS/cm.

The temperature variations (Fig.4-29e) of the Exp.42 were smoother than the Exp.45 during the first 24 hour exposure time. The Exp.42's temperature steadily increased to 36.5 °C from 15.5 °C

while the Exp.45's temperature increased to 48.2 °C. In the second and the third 24 hour period, the Exp.42 showed a gradual increase and decrease and obtained 38.6 °C and 37.8 °C at 72 hours, respectively. On the other hand, the Exp.45's temperature declined sharply to 41.8 °C during the second 24 hour period and gradually continued decreasing to 40.6 °C. After preparation of the second cycle influent, the detected temperature values were 37.8 °C and 34.2 °C, respectively. The significant increase in temperature in comparison with the initial temperature of cycle 1 demonstrated that the first cycle remaining effluent plays a dominating role in increasing the temperature of the mixed raw wastewater and effluent. Unexpectedly, both experiments resulted a semi identical trend through the second cycle exposure time and the offset decreased to a maximum 0.3 °C. Both experiment temperatures increased steadily to 41.8 °C and 42.1 °C at 96.5 hours (the end of day 1, cycle 2) while the tendency of the last 24 hour period was downward and both temperatures were decreased to 40.3 °C and 40.5 °C, respectively. The reason for obtaining a higher temperature for the Exp.45 in which 50% H₂O₂ was used as an oxidizing agent was related to a higher possibility of hydrogen peroxide electrolysis through the exposure to electric field. Consequently, electro-Fenton oxidation was accelerated, and the exothermic reactions development would be intensified which led to a higher heat convection in the system and reaching higher temperature. Finally, the offset between the temperature curves of the Exp.42 and Exp.45 was 3.11 °C.

The characteristics of the SBR cycle 2 influent are presented in Table 4-4. Ammonia removal efficiency (Fig.4-30a) of the Exp.42 (30% H₂O₂) was 99.24% ± 0.1% while the efficiency of the Exp.45 (50% H₂O₂) was 99.54% ± 0.12%. It provided a 0.3% higher efficiency in comparison with the Exp.42. Although the removal efficiency of the Exp.45 was reduced to 99.02% ± 0.12% at 96.5 hours (The first day of cycle 2), it is superior in comparison with Exp.42's result with 98.43%

$\pm 0.1\%$ at 96.5 hours. At the end of the second cycle, the Exp.42 and Exp.45 gave $99.03\% \pm 0.1\%$ and $99.23\% \pm 0.12\%$. Comparing the first day and second days results of the second SBR cycle revealed that the Exp.45's ammonia removal efficiency at 96.5 hours was approximately the same as the Exp.42's one at 120.5 hours. It means that the acceptable concentration of ammonia reached 24 hours sooner in comparison with Exp.42's acceptable one.

TKN removal efficiency values (Fig.4-30b) of Exp.42 and Exp.45 were $98.35\% \pm 0.12\%$ and $99.01\% \pm 0.14\%$ at 72 hours. In the first 24 hour period of the second SBR cycle, TKN removal efficiency of both experiments were enhanced and reached $98.71\% \pm 0.12\%$ and $99.13\% \pm 0.14\%$, respectively. However, the magnitudes of removal efficiency fell and gave $98.35\% \pm 0.12\%$ and $98.63\% \pm 0.14\%$. It would be probable that nitrite formation was boosted in the last 24 hours of cycle 2 (120.5 hours) Consequently, the TKN degradation reaction was reversed.

Total nitrogen removal efficiency (Fig.4-30c) also followed the same trend as the TKN results and the highest efficiency was achieved with $99.04\% \pm 0.15\%$ and $99.54\% \pm 0.17\%$ at 96.5 hours (end of the first day of cycle 2) for the Exp.42 and Exp.45, respectively. The Exp.42's removal efficiency lower than the first day of cycle 2 during the last 24 hour exposure time (from 96.5 hours to 120.5 hours) and it decreased for 2.73%. Exp.42's removal efficiency was $96.31\% \pm 0.15\%$ at the end of cycle 2. Besides, the Exp.45's removal efficiency declined for 1.84% in comparison with the first 24 hour exposure time of cycle2 and provided 97.7% efficiency. The removal efficiency values of the last day of the first cycle (72 hours) was approximately similar to the results obtained at the end of the second day of cycle 2 (120.5 hours) for both experiments. The removal efficiency magnitudes at 72 hours were $96.5\% \pm 0.15\%$ and $97.5\% \pm 0.17\%$ for the Exp.42 and Exp.45, respectively.

Organic nitrogen removal efficiency (Fig.4-30d) of both experiments were acceptable at the end of the first cycle with the values of 96.4% and 97.06%, respectively. However, the best results among all phases of the study were achieved at the end of the first day of the second cycle (96.5 hours) with the values of 99.6% and 99.67%, respectively. But, both experiments experience a decline throughout the last day and obtained 95.87% and 94.56%, respectively.

In conclusion, using 50% hydrogen peroxide provided the best removal efficiency for the target pollutants and the electro-Fenton sequential batch reactor (EF-SBR) leads the process to achieve the desirable removal efficiencies in 4 days instead of 6 days (running two serial experiments with Phase 2 experimental design). It means that reduction for 48 hours in the exposure time. In addition, the removal efficiency of the TKN, total nitrogen, and specifically organic nitrogen were significantly increased in comparison with previous process design (72 hours exposure time) by using EF-SBR.

Table 4- 4 Characteristics of the initial concentrations of the ammonia, TKN, total nitrogen and, organic nitrogen in the raw wastewater and beginning of the second cycle; medium scale results

No. Exp.	Ammonia [mg/L]	TKN [mg/L]	Total nitrogen [mg/L]	Organic nitrogen [mg/L]
Initial (Cycle 1)	11000.0	14000.0	14500.0	3000.0
42-72.5h (Cycle 2)	8707.5	11100.1	11560.0	2392.6
45-72.5h (Cycle 2)	8700.6	11198.6	11817.5	2388.5

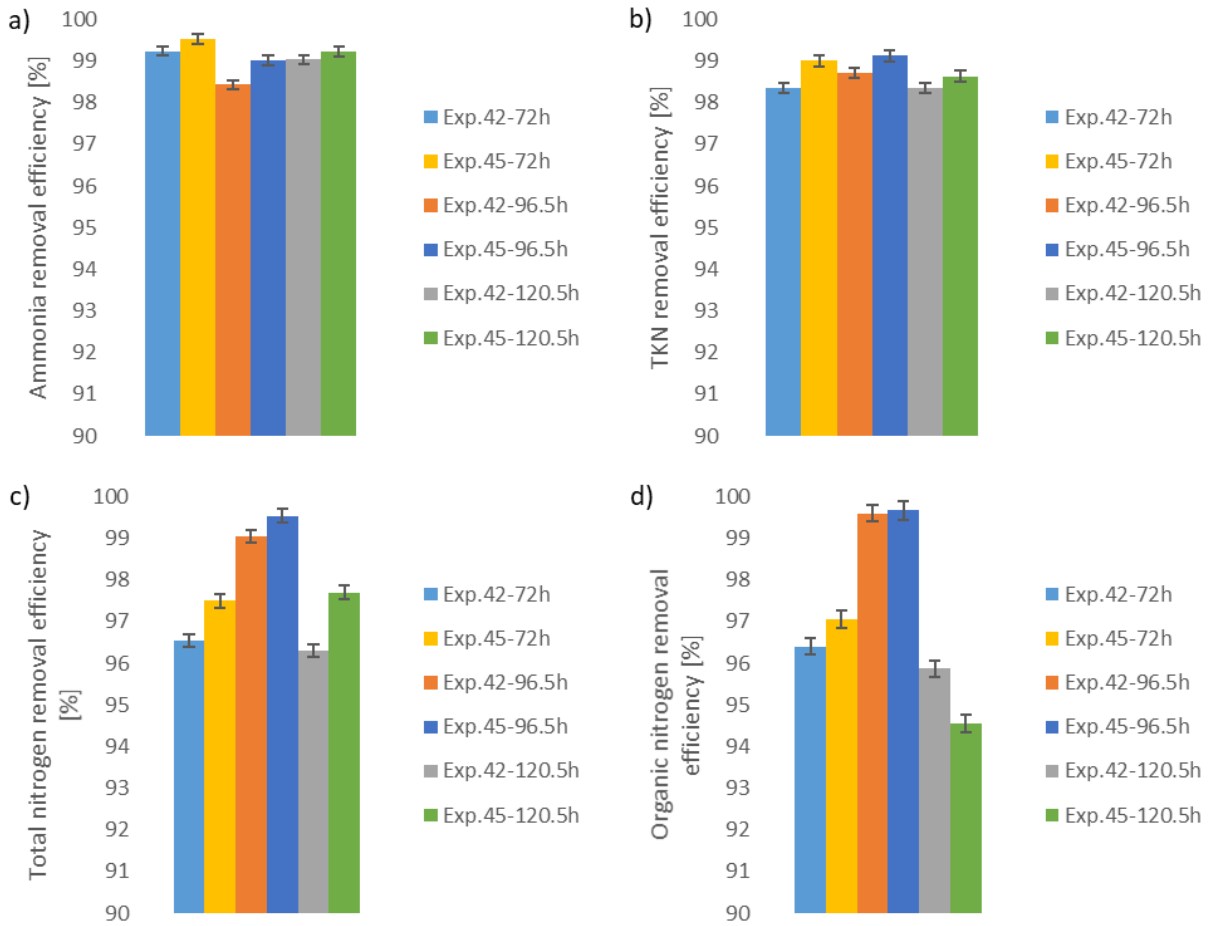


Figure 4- 30 Removal efficiencies of the pollutants for Stage 4-1, medium scale EF-SBR; a) ammonia removal efficiency; b) TKN removal efficiency; c) total nitrogen removal efficiency; d) organic nitrogen removal efficiency

4-4-1-2. Impact of hydrogen peroxide purity on large scale EF-SBR efficiency

The second scope of Stage 4-1 is related to the investigation of the impact of the hydrogen peroxide purity in the large scale EF-SBR removal efficiency. The cell design is identical to the Exp.40, in which the best removal efficacies were achieved. Two experiments were determined to assess the impact of using 50% and 30% hydrogen peroxide purity, respectively. The time interval of adding hydrogen peroxide was 12 hours and the molar ratio of $\frac{\text{Fe}^{2+}}{\text{H}_2 \text{O}_2}$ was equal to 3:81/1 which

gave the best results in Phase 3. The analyzed experiments were the Exp.44 (50% purity H₂O₂) and Exp.46 (30% purity H₂O₂), respectively.

For the compartment 1 results, the voltage variations (Fig.4-31a) of the Exp.44 (50% purity H₂O₂) demonstrated that the voltage fluctuated in the first, second, and third 12 hour time interval. In addition, the voltage values reached to 3.63 V at 12 hours, increased to 3.86 V at the end of the second 12 hour period, and finally declined to 3.67 mV at the end of the third 12 hour exposure time. After a gradual increase to 3.8 V in the fourth 12 hour period, the tendency of variations was smoothed and the detected value of voltage at the end point of the cycle 1 was 3.75 V. On the other hand, the Exp.46 (30% purity H₂O₂)'s voltage steadily increased in the first 12 hour exposure time and the second 12 hours and reached 4.8 V from initial 4.2 V at 24 hours. Voltage gradually and smoothly declined meanwhile the third, fourth and, fifth 12 hour period and obtained 4.5 V at 60 hours. Throughout the last 12 hour period of the first cycle, voltage steadily fell and reached 4.3 V. Once the second cycle commenced, the Exp.44's voltage increased to 4.72 V at the start point of cycle 2 which indicates that the conductivity experienced a sharp drop (From 261 mS/cm to 57.9 mS/cm). However, the voltage steadily and strongly fell in the second cycle and it was 3.52 V at 108.5 hours (the third 12 hour period of the second cycle). The voltage stabilized during the last 12 hour exposure time and provided 3.51 V at 120.5 hours. In contrast, the Exp.46 sustained stabilized voltage throughout the first and second 12 hour period of cycle 2 and reached 4.3 V at 96 hours. Although the voltage dropped to 4 V in the third 12 hour exposure time of cycle 2, the cell potential recovered throughout the last 12 hour period and provided 4.3 V at 120.5 hours.

The results of compartment 3 indicate that the Exp.44 and Exp.46 had identical initial voltage which was equal to 5.39 V. The Exp.44's voltage steadily declined in the first and second 12 hour exposure time and reached 4.01 V at 24 hours. Throughout the third 12 hour period, the voltage

gradually decreased to 3.85 V at 36 hours. For the remaining 36 hour exposure time of the first cycle, voltage experienced weak fluctuations and the final observed voltage of cycle 1 was 3.77 V at 72 hours. On the other hand, the Exp.46's voltage remained unchanged throughout the first 12 hour exposure time. A peak was obtained at 24 hours with the value of 6.5 V. While a sharp decline observed in the third 12 hour period and the voltage reached 5.1 V. Throughout the remaining 36 hour exposure time, the voltage continuously dropped and the measured voltage (end of cycle 1) was 4.43 V at 72 hours. In the start point of the second SBR cycle, the voltage of the Exp.44 and Exp.46 were 6.65 V and 6.7 V, respectively which was significantly increased in comparison with the end point of cycle 1. The reason is a significant decline in the conductivity magnitude of both experiments at the start point of cycle 2. Exp.44's voltage sharply decreased to 4.72 V meanwhile the first 12 hour interval of the second cycle. Afterwards, it experienced a gradual increase throughout the second 12 hour period of cycle 2 and gave 4.8 V at 96.5 hours. For the remaining 24 hour period, the voltage steadily declined and provided 4.04 V at 120.5 hours. Whereas, Exp.46's voltage smoothly decreased throughout the first, second and third 12 hour period and gave 5.15 V at 108.5 hours. The trend was upwards in the last 12 hour exposure time and the final measured voltage was 5.31 V.

Based on the achieved results, the cell potential was remarkably increased for the second cycle of the Exp.46 in which 30% purity H_2O_2 was used. On the other hand, the Exp.44 (50% purity H_2O_2) kept outpacing the first cycle's cell potential during the first 24 hour period although the voltage was slightly lower than the cycle 1 cell potential throughout the last day.

Due to the fact that pH values (Fig.4-31b) of all compartments were similar while taking to account negligible difference (less than 0.05) for each individual experiment, juxtaposing both experiments in one compartment as a representative state of the system would be a logical

approach. Therefore, the results of compartment 1 were selected to analyze pH variations. The pH results of compartment 1 demonstrated the similar tendency for both Exp.44 (50% purity H_2O_2) and Exp.46 (30% purity H_2O_2) in the first and second 12 hour exposure time which proved that the pH variations were independent on the purity of hydrogen peroxide throughout the first day. Both experiments experienced a sharp decline and provided pH equal to 1 at 24 hours from the initial 6.85. During the third and the fourth 12 hour period, the Exp.44's pH slightly increased and the measured pH was 1.54 at 48 hours. In the fifth and sixth 12 hour exposure time, pH changed to 1.52 at 60 hours and 1.59 at 72 hours. While on the other hand, the Exp.46's pH slightly declined to 0.86 during the third 12 hour interval. Then, pH raised to 1.21 at 48 hours and kept fluctuating throughout the fifth and sixth 12 hour period of the cycle 1. The final pH of the Exp.46 at 72 hours is 1.32. After mixing the effluent with raw wastewater, the initial pH magnitudes of cycle 2 were significantly increased and gave 2.3 and 4.55 for the Exp.44 and Exp.46, respectively. After a steady decline and recording pH equal to 1.69 for the Exp.44 during the first 12 hour interval of cycle 2, a stabilized behavior was observed throughout the remaining 36 hour exposure time of the second cycle and the final detected pH at 120.5 hours was equal to 1.66. The average offset was 0.15 and the Exp.44's ORP was higher than the Exp.46's one.

ORP variations (Fig.4-31c) showed that the Exp.44's ORP was dominantly higher than the Exp.46's ORP. The reason was utilizing 50% purity H_2O_2 in the Exp.44 which led to a higher number of hydroxyl radicals. Therefore, the tendency of reactions would be oxidizing organic compounds. Consequently, ORP as an indicator of the oxidation state is expected to give higher values for the Exp.44 in which 50% purity hydrogen peroxide was used.

Compartment 1 results demonstrated that the Exp.44's ORP slightly declined toward reduction state and it was -25.97 mV at 12 hours. The identical behavior was also observed for the Exp.46

(30% purity H₂O₂) and the detected ORP was equal to -25.7 mV at 12 hours. The tendency of the ORP variation was strongly upwards for both Exp.44 and Exp.46. It showed that the oxidation of organic compounds was taken place. The provided ORP at 24 hours were 276.57 mV and 144 mV, respectively. Throughout the third 12 hour period Exp.44 faced a gradual decline to 270.9 mV while Exp.46 experienced the slight increase to 152.17 mV during the same time interval. Meanwhile the fourth and fifth 12 hour exposure time, Exp.44's ORP steadily increased to 311.87 mV at 48 hours and consistently fell to 281.23 mV at 60 hours. However, Exp.46's ORP demonstrated a reversed behavior in which a steady decline to 122.5 mV at 48 hours occurred and then recovered to 155.9 mV at 60 hours. In the last 12 hour period of cycle 1, ORP of both experiments increased to 373.1 mV and 269.93 mV, respectively. Based on the analysis conducted on removal efficiency, remarkable enhancement was achieved throughout the last 24 hour exposure time of SBR cycle 1.

Once the influent of cycle 2 was introduced to the system, the initial ORP of the Exp.44 and Exp.46 significantly declined in comparison with cycle 1's end point and gave -33.8 mV and -26.2 mV correspondingly. The obtained ORP values of the medium scale at the second cycle of SBR were significantly higher (66.16 mV at 72.5 hours) which showed that current density played an important role in obtaining oxidation state at the start point of cycle 2. The current density of the medium scale (33.33 mA/cm²) was remarkably higher than the large scale one (21.37 mA/cm²) which led to a higher ORP. The Exp.44's ORP sharply increased to 310.24 mV at the first 12 hour exposure time of cycle 2 and continued increasing meanwhile the second 12 hour period of cycle 2. The achieved ORP was 367.13 mV at 96.5 hours. Throughout the third and fourth 12 hour period, the ORP variation slightly stabilized and the final achieved ORP was 375.9 mV at 120.5 hours. On the other hand, Exp.46 experienced a sharp increase meanwhile the first and second 12

hour interval of cycle 2 and gave 62.5 and 192 mV at 84.5 hours and 96.5 hours, respectively. Exp.46's ORP kept steadily increasing meanwhile the third and fourth 12 hour period of cycle 2 and gave 257.6 mV at 120.5 hours. The average offset between Exp.44 and Exp.46 curves was equal to 115.9 mV.

The results of compartment 2 indicate that Exp.44's ORP outpaced Exp.46's one and the tendency of variations was slightly like compartment 1's changes. Exp.44's ORP gradually declined during the first 12 hour period and it was in reduction state with the value of -36.72 mV (slightly lower than compartment 1 congruous results). The ORP changes were strongly upwards meanwhile the second and the third 12 hour period and the given value at 24 hours and 36 hours were 234.9 mV and 348.17 mV, respectively. The upward tendency weakened throughout the fourth 12 hour interval and the recorded ORP was equal to 355.5 mV.

Then, the ORP declined to 325.23 mV at 60 hours during the fifth 12 hour period. Throughout the last 12 hour interval, the Exp.44's ORP steadily increased to 387 mV. On the other hand, the Exp.46's ORP variation was slightly downwards in the first 12 hour period and the given ORP at 12 hour interval was -26.47 mV. The tendency of the Exp.46's variations was strongly upwards during the second and third 12 hour period and the ORP magnitudes sharply increased. The measured values at 24 hours and 36 hours were 122.9 mV and 166.3 mV, respectively. However, the Exp.46's ORP declined consistently throughout the fourth 12 hour period and the measured ORP at 48 hours was tantamount to 136.77 mV. Meanwhile the fifth and sixth 12 hour exposure time, the Exp.46's ORP was sharply increased and it was 271.83 mV.

Once the cycle 2's influent formulated, the monitored ORP significantly declined and obtained -33.8 mV and -26.2 mV. However, the ORP of both experiments recovered meanwhile the first 12

hour period of the second cycle. Exp.44's ORP was obtained an approximate equivalent value with the second 12 hour period of the first cycle which was equal to 317.8 mV. It demonstrated that EF-SBR would lead the reactions to the oxidation state in the shorter exposure time. In the second and third 12 hour interval, the Exp.44's ORP was consistently increased although the slope of the curves was much smoother than the first 12 hour period. The obtained ORP was 380.3 mV at 108.5 hours (the third 12 hour exposure time of the second cycle). Throughout the last 12 hour interval, the Exp.44's ORP stabilized and gave 381.9 mV. The upward tendency was also observed for Exp.46's variations although the given ORP at the first 12 hour period of the second cycle was lower than the representative value for the primary 12 hour exposure time of the first cycle. In the following 12 hour period, the slope of the changes increased and the recorded ORP at the second 12 hour period of the second cycle was equal to 205 mV. The obtained ORP was 82.1 mV higher than ORP of the second 12 hour exposure time of the first cycle. Throughout the remaining 24 hour exposure time, Exp.46's ORP kept steadily increasing and the obtained value was equal to 260.6 mV at 120.5 hours. Finally, the average offset between ORP curves of the Exp.44 and Exp.46 was 116.57 mV and Exp.44's ORP was higher than Exp.46's one.

The results of compartment 3 indicate that the overall ORP magnitudes of the Exp.44 was the lowest among all three compartments. On the other hand, the highest ORP was achieved by the compartment 3 of the Exp.46. Therefore, it can be concluded that utilizing 50% H₂O₂ promotes the oxidation state through compartment 2 where the electrolyte was affected by a lower temperature. Whereas, achieving the lowest temperature range in the compartment 3 of Exp.46 led to the highest ORP. The relationship between ORP and temperature is introduced by Rodkey based on the conducted research on Diphosphopyridine Nucleotide System^[4-11]. Based on the previous compartment ORP results, the tendency of the first cycle was distinctive while the variations of

the second cycle demonstrated the similar behavior as the other compartments. Therefore, the entire investigation is essential to assess the trends of the changes for the first cycle. Meanwhile the first 12 hour interval, the Exp.44's ORP steadily declined toward reduction state and gave -39.77 mV at 12 hours. However, the ORP of the Exp.44 increased to 186.73 mV throughout the second 12 hour period and kept raising up to 291.47 mV which was recorded at the end of the third 12 hour interval. As it was discussed previously, ORP sharp raising was the illustrative of oxidation reactions evolution in the electrokinetic cell. During the fourth and fifth 12 hour exposure time, the Exp.44's ORP gradually decreased and provided 275.5 mV at 60 hours. Then, ORP is sharply increased to 359.23 mV which was the peak of the first cycle. On the other hand, the Exp.46 provided a consequence with respect to ORP variations. ORP kept increasing throughout the remained 60 hour exposure time (from 12 hours to 72 hours) and the final measured ORP is equal to 275.63 mV.

Due to the fact that mixing the remaining volume of effluent with raw wastewater leads to a homogenous distribution, all monitoring parameters except voltage (e.g. pH, conductivity, ORP and, temperature) were identical in all three compartments. Therefore, the same ORP as compartment 1 and compartment 2 was achieved for the Exp.44 and Exp.46 which were -33.8 mV and -26.2 mV, respectively. Once the second cycle of SBR commenced for the Exp.44, the reactions showed distinguishable tendency to oxidation state and gave 295.93 mV at the first 12 hour period of the second cycle (84.5 hours). Also, the ORP of the Exp.44 consistently increased to 361.9 mV throughout the second 12 hour period of the second cycle (96.5 hours). Meanwhile the third and fourth 12 hour interval of cycle 2, the ORP gradually raised and it was 379.1 mV at 120.5 hours. Contrary to the Exp.44's results, the tendency of reactions to the oxidation state slowly evolved in the first 12 hour exposure time of the second cycle and provided 53.8 mV at

84.5 hours. Throughout the second 12 hour period of cycle 2, the Exp.46 experienced a sharp increase in ORP and it was 203.65 mV. Therefore, the potential nitrogen contained compounds mineralization was expected to be progressive during the second 12 hour period of cycle 2. Subsequently, the mentioned improvement was confirmed once the ammonia, TKN, total nitrogen, and organic nitrogen were observed to be declined to 0.19, 0.50, 0.51 and, 0.64 of analyzed concentration at 84.5 hours. The reference concentration of the nitrogen contained compounds were 3838.7 mg/L, 7516 mg/L, 7937.3 mg/L and 3677.33 mg/L for ammonia, TKN, total nitrogen and organic nitrogen, correspondingly. The ORP of Exp.46 steadily increased in the remaining 24 hour exposure time and the final measured ORP was 258.6 mV at 120.5 hours. Finally, the averaged offset between Exp.44 and Exp.46 ORP curves was 84.33 mV which was lower than other compartment relevant offset values.

Because of the fitted curves of conductivity for each compartment (except for 108.5 hours for Exp.44 and 48 hours and 120.5 hours for Exp.46), compartment 1 results would be discussed and the mentioned unfitted points would be investigated.

Conductivity results (Fig.4-31d) of the Exp.44 (50% H₂O₂) was dominantly higher than Exp.46 (30% H₂O₂) in compartment 1 which demonstrated the impact of hydroxide and hydrogen ions on providing conductivity in the system. Therefore, due to the higher number of electrolyzed ions in Exp.44 which resulted from utilizing 50% hydrogen peroxide, the significant excellency of Exp.44 with respect to conductivity values could be justified.

In the first 12 hour exposure time, Exp.44's conductivity sharply increased to 112.67 mS/cm from initial 61.4 mS/cm and continued raising gradually meanwhile the following 12 hour interval. The measured conductivity at 24 hours was 117.8 mS/cm. The slope of the curve intensified, and

conductivity values consistently increased meanwhile the remained 48 hours of the first cycle and the final obtained conductivity was 261 mS/cm at 72 hours. In contrast the conductivity variations of Exp.46 fluctuated throughout the first cycle. Besides, conductivity steadily increased during the first and second 12 hour period and the obtained conductivity was 98.9 mS/cm at 24 hours. Afterwards, Exp.46 experienced a sharp increase throughout the third 12 hour period although the conductivity fell to 119.77 mS/cm during the fourth 12 hour exposure time. The second significant fluctuation was observed in the sixth and seventh 12 hour exposure time in which it fell to 153.8 mS/cm at 72 hours after a sharp increase which provided 163.45 mS/cm at 60 hours.

At the second cycle start point, the conductivity values of all three compartments were 57.9 mS/cm and 54.8 mS/cm for Exp.44 and Exp.46, respectively. The tendency of Exp.44's conductivity was strongly upwards and the given magnitude at 108.5 hours (the third 12 hours of cycle 2) was 256 mS/cm. Unexpectedly, the conductivity significantly fell to 192.2 mS/cm during the last 12 hour interval. Based on the observed decline, it can be speculated that once the concentrations of the target electrochemically active compounds reduced, the conductivity faced a significant decline. The second reason might be related to a decrease in the number of ions which impacts the strength of the electrolyte. Consequently, the outcome would be a significant decline in conductivity. The remarkable increase in removal efficiency of the target compounds justifies the sharp decline of the conductivity referring to previously mentioned two reasons. On the other hand, the Exp.46 experienced linear steadily increased throughout the first and second 12 hour period of the cycle 2 and provided 88.2 mS/cm at 96.5 hours. A sharp increase to 133.5 S/cm was detected in the third 12 hour interval of the second cycle. After a gradual decline, the final obtained conductivity was 131.2 mS/cm.

Comparing the peak values of each cycle provides a significant increase in number of electroactive ions resulted on the exact measurement time of the peak. The reason for obtaining a lower peak in the second cycle is originated from availability of lower ions due to a lower initial concentration of the second cycle. The zero-time concentration of each cycle is given in Table 4-5.

The time interval in which the conductivity curves of the Exp.44 were not fitted was the third 12 hour period of the second cycle (108.5 hours). The reason is related to available ions which can be related to the remaining concentration. The lowest remaining concentration was achieved in compartment 1 which resulted the highest conductivity among all compartments. However, the proper justification for unfitted time intervals of the Exp.46 (the fourth 12 hour exposure time of the first cycle and the last 12 hour period of the second cycle) is a flint difference in the remaining concentration of compartment 2 with the rest of the components. Once, the remaining concentration was lower, the available number of electroactive ions would be affected and declined. Therefore, a decline in conductivity was expected to take place. Considering compartment 1 as a representative of the conductivity of the electrochemical reactor led to have 52.37 mS/cm offset between conductivity curves. It showed that utilizing 50% hydrogen peroxide gives higher conductivity.

The temperature variations (Fig.4-31e) of compartment 1 demonstrated a distinctive trend for the first cycle of both experiments. However, the second cycle results of Exp.44 and Exp.46 was meaningfully fitted. Also, results prove that the EF-SBR approach leads the system to respond independently to initial hydrogen peroxide purity during the second cycle of compartment 1. The fitted curves of temperature were also obtained in two other compartments. Therefore, it would be possible to extend the second cycle temperature findings to entire large-scale EF-SBR, impact of hydrogen peroxide purity analysis.

Exp.44's temperature increased to 45.3 °C from an initial temperature of 12.5 °C while the tendency of variations was smoothly downwards throughout the second, the third and the fourth 12 hour period. The measured temperature at 48 hours was 40.3 °C. After a negligible increase for 0.1 °C, Exp.44 faced a sharp decline during the sixth 12 hour exposure time and the measured temperature at 72 hours was 31.6 °C. On the other hand, Exp.46 experienced a remarkable sharp increase in temperature during the first 12 hour period and it was 36.1 °C considering the initial temperature equal to 12.3 °C. In the second 12 hour exposure time, temperature kept raising and the obtained temperature was 43 °C at 24 hours. However, the temperature fell significantly throughout the third 12 hour interval and reached 30 °C at 36 hours. In the remaining 36 hour exposure time, the temperature gradually and smoothly decreased to 28.5 °C at 72 hours.

The initial temperature magnitudes of the second cycle were 17.9 °C and 18.6 °C for the Exp.44 and Exp.46, respectively. Due to the fact that the temperature curves of the second cycle were fitted, investigating the tendency of the temperature variation of one experiment would be adequate for this study. Also, the same approach would be followed for the rest compartments. The Exp.44, the representative of the second cycle temperature variations, experienced a sharp increase during the first 12 hour period of the second cycle and provided 35.6 °C at 84.5 hours. The tendency of the changes switched to downwards and the given temperature at 96.5 hours was 29.2 °C. The last 24 hours of the exposure time can be described as a period in which the temperature was gradually increased to 30.2 °C in the third 12 hour exposure time of the second cycle. It fell to 28.9 °C meanwhile the last 12 hour period. Also, the overall offset was equal to 3.83 °C. The significant point that should be considered for the second cycle was its noteworthy overall lower temperature in comparison with the first cycle of EF-SBR. The reason was related to a remarkable lower

electrochemical reaction heat loss that was obtained in cycle 2. The observed phenomenon was associated with the lower required concentration of the target compounds to be mineralized.

Compartment 2 results of the Exp.44 presented the similar tendency as compartment 1 corresponded one during the first and second 12 hour exposure time and the achieved temperature were 46.2 °C and 43 °C at 12 hours and 24 hours, respectively. Therefore, the peak of the Exp.44's temperature in compartment 2 was 0.9 °C higher than compartment 1's peak. Throughout the third and fourth 12 hour period, the trend of variations was upward, and the obtained temperature was 40.3 °C at 48 hours. However, the Exp.44 experienced a gradual raise during the fifth 12 hour exposure time and given 42.6 °C at 60 hours. However, the Exp.44's temperature fell significantly during the fifth and the sixth 12 hour period and the final obtained temperature is 31.7 °C. On the other hand, the Exp.46's variations showed that the temperature faced two steps increasing during the first and second 12 hour period and gave 34.5 °C and 42 °C at 12 hours and 24 hours, respectively. During the third 12 hour exposure time, the tendency changed to be strongly downward and the measured temperature was 29.6 °C at 36 hours. Although the temperature stabilized during the fourth 12 hour exposure time, the variations were steadily downwards in the last 24 hour period of cycle 1. Also, the cycle 1's final temperature was 27.8 °C.

Once the second cycle is instigated, the temperature significantly declined in comparison with the recorded temperature at 72 hours for both experiments. However, the obtained temperature at the cycle 2's zeroth point was higher than initial temperature of cycle 1 which were 17.9 °C and 18.6 °C for the Exp.44 and Exp.46, congruently. Because of the identical observed behavior for both experiments in cycle 2, the temperature changes of the Exp.44's compartment 2 could be the representative of the reactor temperature. During the first 12 hour period of cycle 2, the Exp.44's temperature sharply increased to 34.8 °C at 84.5 hours. However, the temperature steadily declines

in the second 12 hour exposure time of cycle 2 and gave 29.6° C at 96.5 hours. Throughout the final 24 hour period, the Exp.46's temperature slowly increased and provided 30.3° C at 120.5 hours. Finally, the total offset between the Exp.44 and Exp.46 temperature curves was 4.11° C.

Based on the observation, it can be interpreted that the Exp.44 provided a temperature range of variations which was above 40° C from 12 hours to 48 hours. It showed that the electrochemical reactions provided significant Gibbs free energy meanwhile the dissociation, mineralization, and electrolysis reactions.

The results of compartment 3 showed that the highest temperature among all compartments was achieved by Exp.44 at 12 hours with the value of 50.1° C. The temperature reached 45.6° C at 36 hours after a sharp decrease during the second 12 hour period. Throughout the fourth 12 hour interval, the Exp.44's temperature continuously declined to 40° C at 48 hours. Although the temperature slightly stabilized during the fifth 12 hour exposure time, the variation was strongly downward throughout the last 12 hour period of cycle 1 and provided 31° C at 72 hours. The similar tendency as compartment 1 and compartment 2's variations of Exp.46 was observed throughout the first and second 12 hour period. The measure temperature was 42° C at 24 hours. However, Exp.46's temperature declined sharply to 28.5° C during the third 12 hour period and kept decreasing gradually during the remained 36 hour exposure time of cycle 1. The final measured temperature of Exp.46's cycle 1 was equal to 27.2° C.

Once the second cycle of SBR started, the initial temperature magnitudes were 17.9° C and 18.6° C for Exp.44 and Exp.46, respectively. Due to achieving complete fitted curves for the Exp.44 and Exp.46, the Exp.44 is selected to describe the tendency of temperature variations. During the first 12 hour period of cycle 2, the temperature increased to 33.8° C from initial 17.9° C. While, the

variations of the second 12 hour period of the second cycle were smoothly downwards and it gave 30.5 °C at 96.5 hours. The temperature slightly stabilized in the third and fourth 12 hour exposure time of cycle 2 and the resulting temperature was 30.2 °C at 120.5 hours. Finally, the average offset between Exp.44 and Exp.46 curves was 5.15 °C.

First of all, the removal efficiency of both Exp.44 and Exp.46 were juxtaposed with respect to ammonia removal efficiency (Fig.4-32a). According to the achieved results of 60 hours, the removal efficiency of Exp.44 (50% H₂O₂) was slightly higher than Exp.46's removal efficacy and the obtained results were 99.46 % ± 0.15% and 98.72% ± 0.17%, respectively. Exp.44 kept outpacing during the last 12 hour period of cycle 1 and gave 99.48 % ± 0.15% removal efficiency at 72 hours which was 0.32 % higher than the Exp.46's relevant result. At the end of the second 12 hour exposure time of cycle 2 (96.5 hours), the Exp.44 provided a tenable removal efficiency with respect to ammonia removal efficiency which was equal to 86.85 % ± 0.15%. In contrast, Exp.46's results demonstrated significant difference in comparison with Exp.44's removal efficacy at 96.5 hours. However, the difference between Exp.44 and Exp.46 removal efficiency decreased to 0.01% (tantamount to 1.1 mg/L) which can be considered as negligible difference corresponding to an initial 11000 mg/L concentration. At last, the removal efficiencies of 99.06 % ± 0.15% and 99.05 % ± 0.17% were achieved at 120.5 hours.

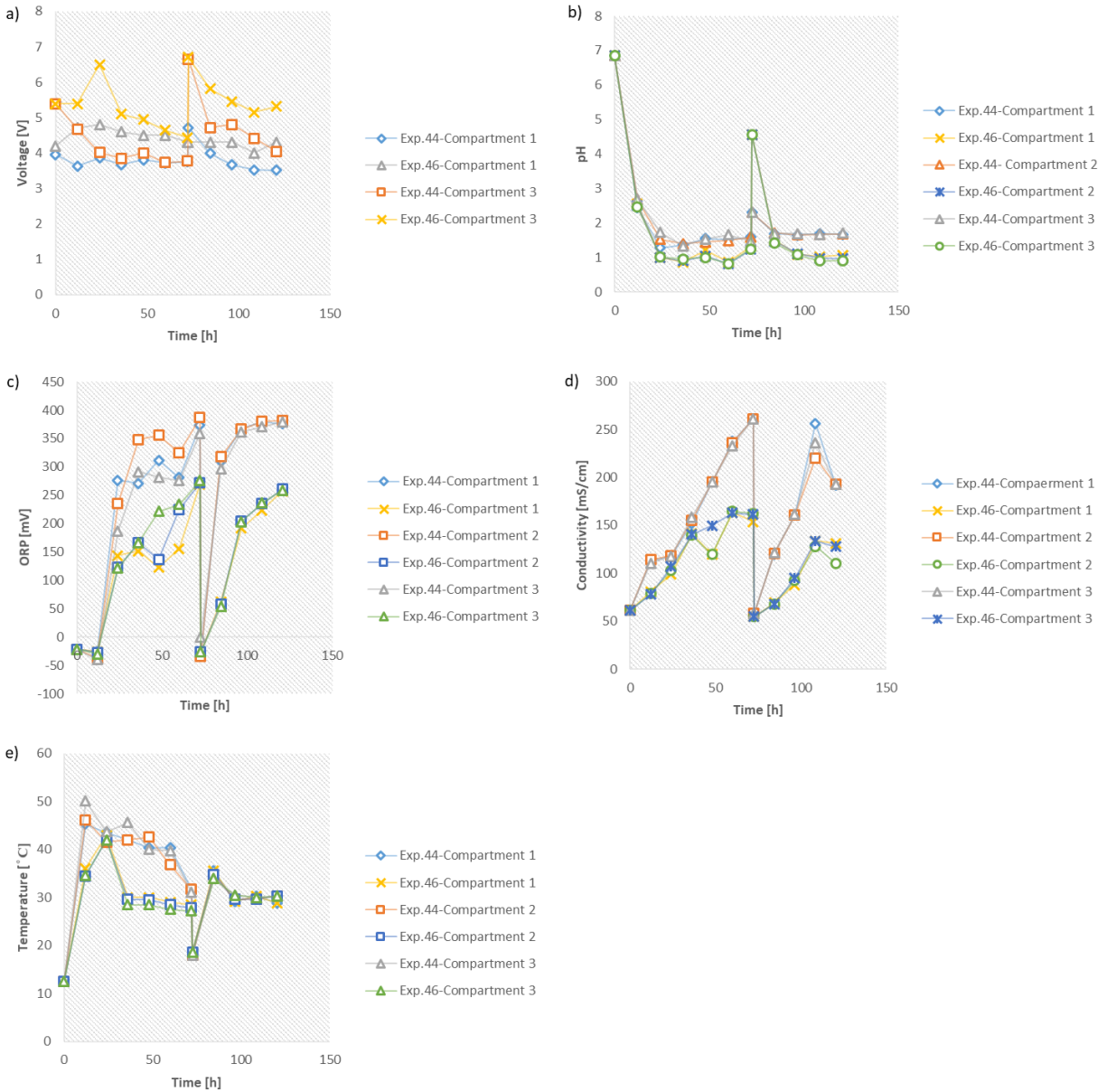


Figure 4- 31 Variations of monitored parameters for the relevant experiments of the Stage 4-1, large scale EF-SBR; a) voltage versus time; b) pH versus time c) ORP versus time; conductivity versus time e) temperature versus time

The Exp.44 (50% H₂O₂) gave outstanding results at the end of the fifth 12 hour exposure time of cycle 1 (60 hours) with respect to TKN removal efficiency (Fig.4-32b) with the value of 99.46% ± 0.17%. It can be considered as the best achieved removal efficiency among all experiments of Stage 4-1. Also, the significant difference attained between the removal efficiency of the Exp.44

and Exp.46 (with $96.25 \% \pm 0.17\%$ removal efficiency at 60 hours) that was 3.21% . Due to formation of nitrate and nitrite during the last 12 hour period of cycle 1 in the Exp.44, the removal efficiency was significantly declined to $97.18\% \pm 0.17\%$. Although the efficiency of Exp.46 was slightly improved meanwhile the last 12 hour exposure time of the first cycle by giving $96.45\% \pm 0.17\%$ at 72 hours. After analyzing the sample of the second 12 hour period of cycle 2, a poor removal efficiency was achieved which demonstrated that one-day exposure would not be applicable in large scale EF-SBR. Although the medium scale EF-SBR results provided acceptable removal efficiency at 96.5 hours (one-day cycle 2 exposure time), it would not be feasible to lessen the exposure time. The achieved removal efficiency at 96.5 hours was $72.95\% \pm 0.17\%$ which was 5.68% higher than Exp.46's one. In order to provide sensible description for the mentioned difference it should be mentioned that Exp.46 maintained around 795 mg TKN /L higher concentration in comparison with Exp.44's persisted TKN concentration. The final analyzed results of the second cycle provided remarkable improvements in comparison with the second 12 hour exposure time of the second cycle (96.5 h) for both Exp.44 and Exp.46. In addition, the achieved removal efficiency were $96.64 \% \pm 0.17\%$ and $92.85\% \pm 0.17\%$, respectively. Therefore, using $50\% \text{ H}_2\text{O}_2$ as an oxidizing agent led to reducing the exposure time of cycle 1 and cycle 2 for 12 hours and 24 hours, correspondingly.

Total nitrogen removal efficiency (Fig.4-32c) results demonstrated that the analyses of 60 hours and 72 hours of the Exp.44 ($50\% \text{ H}_2\text{O}_2$) gave the identical values which was equal to $95.76 \% \pm 0.20\%$. However, the Exp.46's removal efficiency experienced a slight increase during the last 12 hour period of the first cycle from $93.98 \% \pm 0.22\%$ at 60 hours to $94.88\% \pm 0.22\%$ at 72 hours. Once 24 hours passed from the initiation of the second cycle, the analyzed samples provided a poor removal efficiency as well as TKN representative one with the value of $71.01 \% \pm 0.20\%$ and

63.45%± 0.22% for the Exp.44 and Exp.46, respectively. In the following 24 hour exposure time of cycle 2, remarkable transmute was achieved and the results provided 95.74% ± 0.20% and 92.84% ± 0.22% efficiency at 120.5 hours for the Exp.44 and Exp.46, correspondingly. It can be implied that it is feasible to obtain similar total nitrogen removal efficiency at the last 12 hour period of cycle 1 with using 50% hydrogen peroxide which led to 24 hour reduction in exposure time.

Organic nitrogen removal efficacy (Fig.4-32d) of the Exp.44 gave the highest value (92.2 % ± 0.32%) at 60 hours while the best results of the Exp.46 (86.48 %± 0.34%) was achieved at 72 hours (the last 12 hour period of cycle 1). Furthermore, the Exp.44 faces a decrease equals to 1.17% during the last 12 hour exposure time of cycle 1. On the other hand, Exp.46 experienced a slight increase which was equal to 0.22% (6.6 mg/L more removal reference to 3000 mg/L initial organic nitrogen concentration). A catastrophic decline was obtained at the second 12 hour interval of cycle 2 for both Exp.44 and Exp.46 with the magnitudes of 22% ± 0.32% and 2.37% ± 0.34%, respectively. The extremely poor results of 96.5 hours draw attention that it would not be feasible to assess acceptable removal of the target compounds while considering 24 hours as the exposure time of the second cycle. In the upcoming third and fourth 12 hour interval of the second cycle, the removal efficiency of both experiments were remarkably improved and gave 87.79% ± 0.32% and 70.58% ± 0.34% at 120.5 hours. The difference between 60 hours and 72 hours results of the Exp.44 was 4.43% (132.9 mg/L more removal for the results of 60 hours based on initial 3000 mg ON/L).

Table 4- 5 Characteristics of the initial concentrations of the ammonia, TKN, total nitrogen, and organic nitrogen in the raw wastewater and the beginning of the second cycle; large scale results

No. Exp.	Ammonia [mg/L]	TKN [mg/L]	Total nitrogen [mg/L]	Organic nitrogen [mg/L]
Initial (Cycle 1)	11000.0	14000.0	14500.0	3000.0
44-72.5h (Cycle 2)	9030.3	11551.1	12000.7	2508.3
46-72.5h (Cycle 2)	9100.8	11680.5	12280.5	2715.6

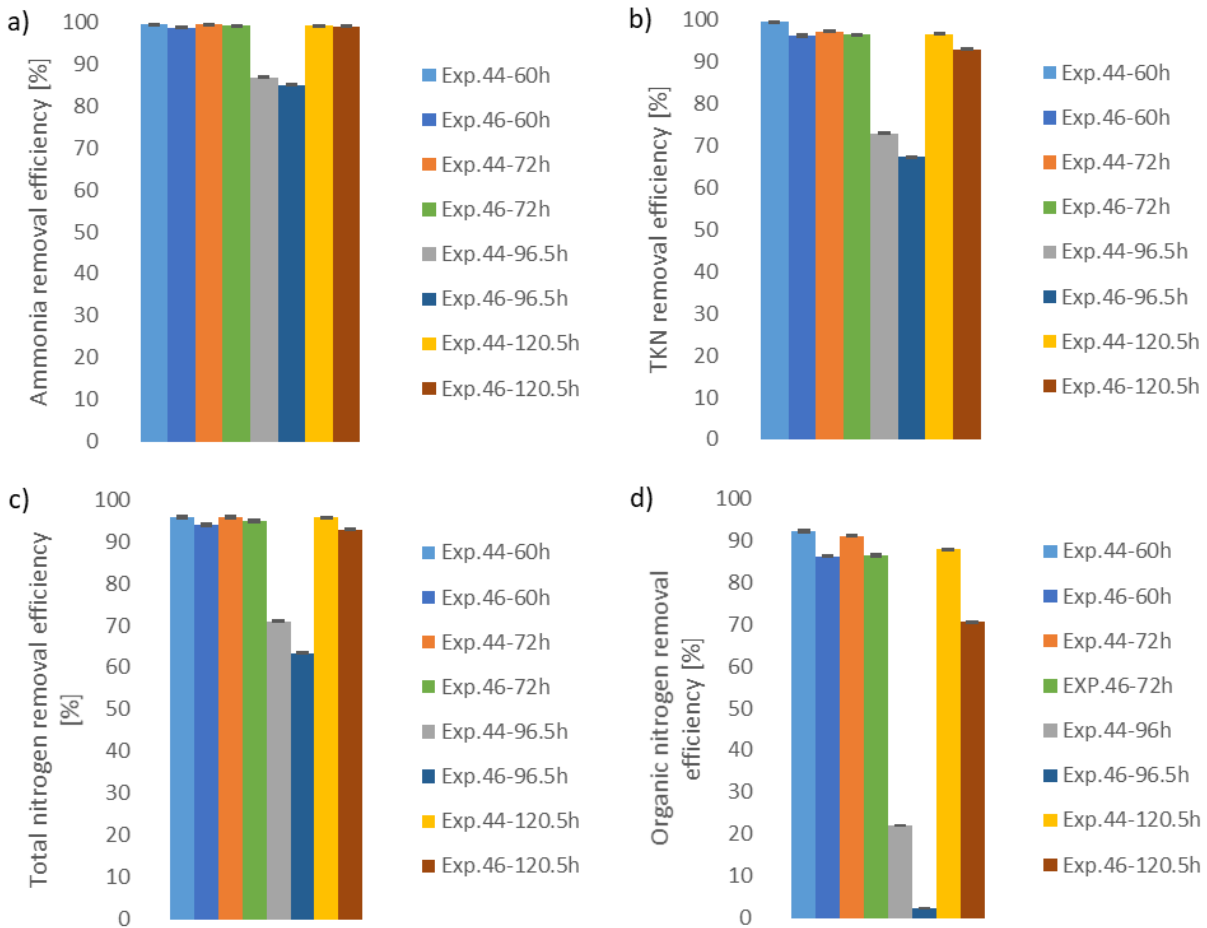


Figure 4- 32 Removal efficiencies of the pollutants for Stage 4-1, large scale EF-SBR; a) ammonia removal efficiency; b) TKN removal efficiency; c) organic nitrogen removal efficiency; d) total nitrogen removal efficiency

Due to the fact that, the main objective of this research is removing TKN and the acceptable efficiencies were achieved at 60 hours and 120.5 hours, it could be determined that the overall efficiency of EF-SBR was promising while the exposure time of the first and second cycle were 60 hours and 48 hours correspondingly. It leads to shorten the conventional large-scale process time from 144 hours to 108 hours. In addition, the change (36 hours) is equal to the half of initial 72 hours (Large-scale retention time).

4-4-2. Stage 4-2 analysis

4-4-2-1. Impact of number of cycles on medium scale EF-SBR efficiency

The last parameter which is studied in this research is the impact of the number of cycles on EF-SBR removal efficiency. The research is conducted on both medium and large scale experiments and the first part of Stage 4-2's study is devoted to medium scale outcomes. Based on the achieved results in Stage 4-1, it would be practical to reduce the exposure time of cycle 2 to 24 hours for medium scale once 50% purity hydrogen peroxide was used as an oxidizing agent (Exp.45). However, using 30% hydrogen peroxide (Exp.42) gave acceptable removal efficiency in a 1-day exposure time of cycle 2 although the efficiency was not as high as Exp.45. Consequently, the approach of the Stage 4-2, medium scale EF-SBR, would be the investigation of the impact of number of cycles on reducing exposure time to 24 hours with utilizing 30% H₂O₂. The proposed mechanism is continuing the treatment for 48 hours in cycle 3 and considering 24 hours for cycle 4's exposure time. The analyzed experiment of the first scope of Stage 4-2 is the Exp.42.

The variations of monitoring parameters, voltage, pH, ORP, conductivity, and temperature of cycle 1 and cycle 2 were discussed in Stage 4-1, medium scale EF-SBR section in detail. So, the

overall tendency of cycle 1 and cycle 2 variations would be considered to juxtapose with cycle 3 and cycle 4's changes. The initial voltage (Fig.4-33a) of cycle 3 was 5.84 V at 121 hours. In the first 24 hour period of cycle 3, the voltage magnitude consistently declined to 4.89 V and kept decreasing gradually throughout the second 24 hour exposure time of cycle 3. The measured voltage was 4.71 V at 169 hours (end of the second 24 hour period of cycle 3). Once the fourth cycle commenced, the initial voltage was remarkably decreased in comparison with the initial voltage of cycle 3. The recorded voltage at 169.5 hours was 5.4 V. The observed decline in zero-time voltage of cycle 3 and cycle 4 could be interpreted by a significant increase in initial conductivity value. Throughout the fourth cycle, the voltage sharply reduced to 4.24 V from the initial 5.4 V. The reason is a sharp increase in the conductivity of the relevant time interval.

pH variations (Fig.4-33b) of the third and fourth cycle demonstrated distinctive behaviors specifically at the start point of cycle 3. The measured pH was 2.47 at 121 hours (cycle 3 start point) which is 0.5 higher than the initial pH of the second cycle. During the first 24 hour period of cycle 3, the pH steadily declined to 2.05 while the intensity of variations dumped throughout the second 24 hours of cycle 3 and gave pH equal to 2 at 169 hours. Then, the initial pH of cycle 4 was 1.96 whereas the typical trend was observed throughout the last 24 hour period of retention time. The pH gradually increased to 2.08 which is noteworthy to assess. The reasons could be related to an increase in the number of hydroxide ions due to poorer ammonia oxidation reactions (See Eq. 3-5). The 0.66% reduction in ammonia removal efficiency in comparison with the first 24 hour exposure time of cycle 3 proves the described justification.

Although the obtained ORP (Fig.4-33c) at the end of each 24 hours was congruous with the results of previous cycles (cycle 1 and cycle 2), the initial ORP of cycle 3 and cycle 4 showed a strongly reduction state with the amount of - 68.83 mV and -29.5 mV at 121 hours and 169.5 hours,

respectively. During the first 24 hour period of cycle 3, ORP increased to 387.8 mV at 145 hours which was 10 mV lower than the ORP of the second 24 hour exposure time of cycle 2. ORP constantly declined to 366.9 mV while the slope of variation was - 0.87 mV/h which was significantly higher than the second 24 hour period of cycle 2's variation slope. In the exposure time of the cycle 4 (the last 24 hour exposure time of overall exposure time), the ORP sharply increased to 374.8 mV which was 13 mV lower than ORP of the first 24 hour interval of cycle 3.

The conductivity curve (Fig.4-33d) of cycle 3 demonstrated that the initial conductivity significantly dropped to 34.6 mS/cm which was 49.5 mS/cm lower than initial conductivity of the second cycle. Although the conductivity increased sharply in the first and second 24 hour period of cycle 3 and was 118.67 mS/cm and 160 mV/cm at 145 hours and 160.3 hours, the end point conductivity of the third cycle was remarkably lower than cycle 2's relevant conductivity (206.8 mS/cm). Besides, a congruous trend was observed for voltage variation meanwhile the third cycle in which the voltage declined to 4.71 V at 169 hours (end point of cycle 3) from 5.84 V at 121 hours (start point of cycle 3). The initial value of conductivity of cycle 4 with the magnitude of (58.5 mS/cm) considerably recovered in comparison with the third cycle's initial value. However, the resulted conductivity of cycle 4 was pointedly lower than initial conductivity of cycle 2 (84.1 mS/cm). During the last 24 hour period, the conductivity raised to 130.3 mS/cm. One of the highlight of the conductivity curve would be the sensible decline once the peaks of cycle 2, cycle 3 and cycle 4 are compared with cycle 1's peak. The reason is related to available electrochemically active ions which were existed at the relevant monitoring time. Therefore, the highest number of ions fits in cycle 1's peak.

The temperature variations (Fig.4-33e) presented that the initial temperature of cycle 3 with the value of 21.2 °C was remarkably higher than the zeroth time of the process (15.5 °C) although the

recorded difference between the second and the third cycle initial temperature was high. Furthermore, the measured difference showed that the initial temperature of cycle 3 was 14° C lower than cycle 2's one. In the first 24 hour exposure time of cycle 3, temperature increased to 32° C while the trend of the second 24 hour period was slightly downward and the given temperature at the end of cycle 3 was 31° C. According to cycle 4's results, the obtained temperature at 169.5 hours (start point of the fourth cycle) was 20° C and the temperature sharply increased during the last 24 hour period and reached 30° C at 193.5 hours.

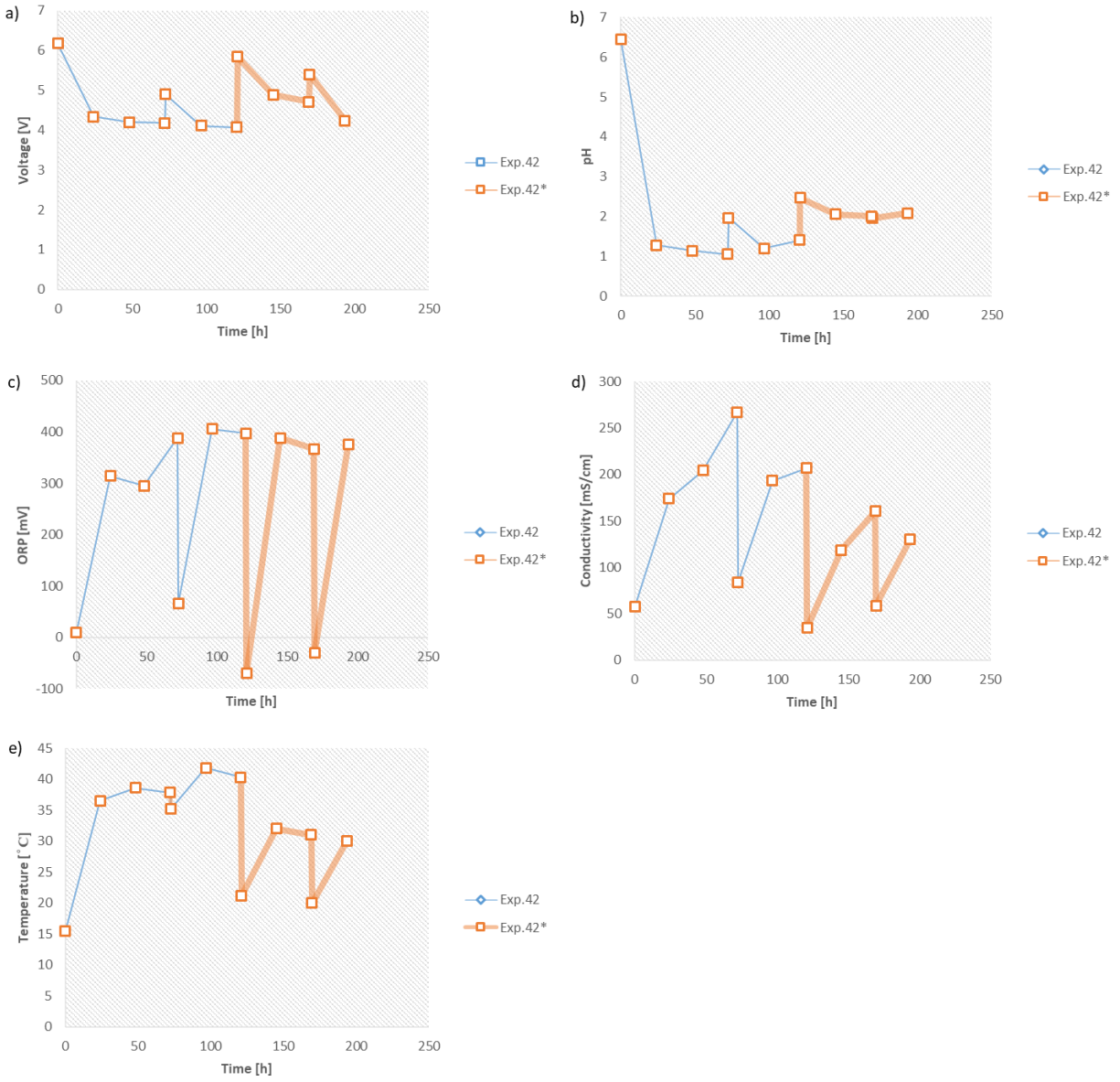


Figure 4- 33 Variations of monitored parameters for the relevant experiments of the Stage 4-2, medium scale EF-SBR; a) voltage versus time; b) pH versus time c) ORP versus time; conductivity versus time e) temperature versus time

Ammonia removal efficiency (Fig.4-34a) of the third cycle provided a significant improvement comparing to the relevant results of each individual 24 hours of the second cycles. For instance, the removal efficiencies of the first and the second 24 hour period of the third cycle were $99.2\% \pm 0.12\%$ and $99.62\% \pm 0.12\%$ while the achieved efficacies of the second cycles were $98.43\% \pm$

0.12% and $99.03\% \pm 0.12\%$ at 96.5 hours (the first day of cycle 2) and 120.5 hours (the second day of cycle 2), respectively. Also, the highest removal efficiency was achieved at the end of the third cycle with the magnitude of $99.62\% \pm 0.12\%$. Although the removal efficiency of the first 24 hour period of cycle 3 declined in comparison with the first 24 hour period of the third cycle, the achieved efficiency with the value of 98.54% still outpaced the removal efficiency of the first 24 hour exposure time of cycle 2 that was equal to $98.43\% \pm 0.12\%$. Therefore, it can be speculated that the increase in the number of cycles will improve the ammonia removal efficiency and make it feasible to decrease the exposure time to 24 hours after completing 2 cycles from the zero time in case the aim is removing ammonia predominantly.

The results indicate that the removal efficiency of TKN (Fig.4-34b) significantly declined at the end of the first day of cycle 3 and showed $91.86\% \pm 0.14\%$ at 145 hours. Comparing the results of the first 24 hour period of the third cycle with the first day of the second cycle showed that the efficiency dropped, and the obtained difference was 6.49% which was equal to 908.6 mg/L excess in the remaining TKN concentration. Although the efficiency of cycle 3 recovered at the end of the cycle 3 (169 hours), cycle 2's end point provided 1.17 % higher efficiency. During the 24 hour exposure time of cycle 4, the removal efficiency of TKN was lower compared with the first 24 hour period of the third cycle and the analyzed value at the end of exposure time was $91.14\% \pm 0.14\%$. The difference between the analyzed magnitude of cycle 4 and the removal efficiency of the first 24 hour period of cycle 3 was 0.72%. So, increase in number of SBR cycles would have an adverse effect on removal efficiency of TKN and leads to lower removal efficacy.

Total nitrogen removal efficiency (Fig.4-34c) of the first 24 hour exposure time of the cycle 3 fell to $90.82\% \pm 0.17\%$ which was 5.49% lower than the first 24 hour period of the second cycle's one. However, a significant increase in removal efficiency was observed at the end of cycle 3 with

the removal efficiency of $98.26\% \pm 0.17\%$ and it outpaced the relevant cycle's 3 removal efficiency by giving 1.98% higher efficacy. Cycle 4's results demonstrated a slight difference with cycle 3's total nitrogen removal efficiency and gave $90.34\% \pm 0.17\%$ at 193.5 hours (end of cycle 4). In case the first 24 hour period of cycle is considered as reference of juxtaposition, it would not be feasible to achieve a similar allowable remained concentration as cycle 2 by increasing the number of cycles. It might be questionable why we increased the number of cycle although the excellent removal effectiveness was obtained at the end of the first 24 hour exposure time of cycle 2. The response is providing identical condition to analyze all target compounds at the same time intervals.

The last target compounds which is assessed in analysis is organic nitrogen (Fig.4-34d). The poor results of the first 24 hour period of cycle 3 and cycle 4 with the magnitudes of $64.93\% \pm 0.17\%$ and $64.03\% \pm 0.17\%$ make it untenable to shorten the exposure time of the following cycles to 24 hours. In addition, the final removal efficiency of cycle 3 with the value of 88.26% was significantly lower than cycle 2's one (95.87%).

Therefore, an increase in the number of cycles would not lead to a higher removal efficiency in the first 24 hour exposure time of the fourth cycle and a harmonic decline was observed in the first 24 hour period results once the number of cycles was increased.

Table 4- 6 Characteristics of the initial concentrations of the ammonia, TKN, total nitrogen and, organic nitrogen in the raw wastewater and the beginning of each cycle medium scale results; cycle 1, cycle 2, cycle 3 and cycle 4 initial concentration

No. Exp.	Ammonia [mg/L]	TKN [mg/L]	Total nitrogen [mg/L]	Organic nitrogen [mg/L]
Initial (Cycle 1)	11000.0	14000.0	14500.0	3000.0
42-72.5h (Cycle 2)	8707.5	11100.1	11560.0	2392.6
42-121h (Cycle 3)	8912.7	11361.6	11824.1	2448.9
42-169.5h (Cycle 4)	9195.9	11759.1	12202.9	2564.0

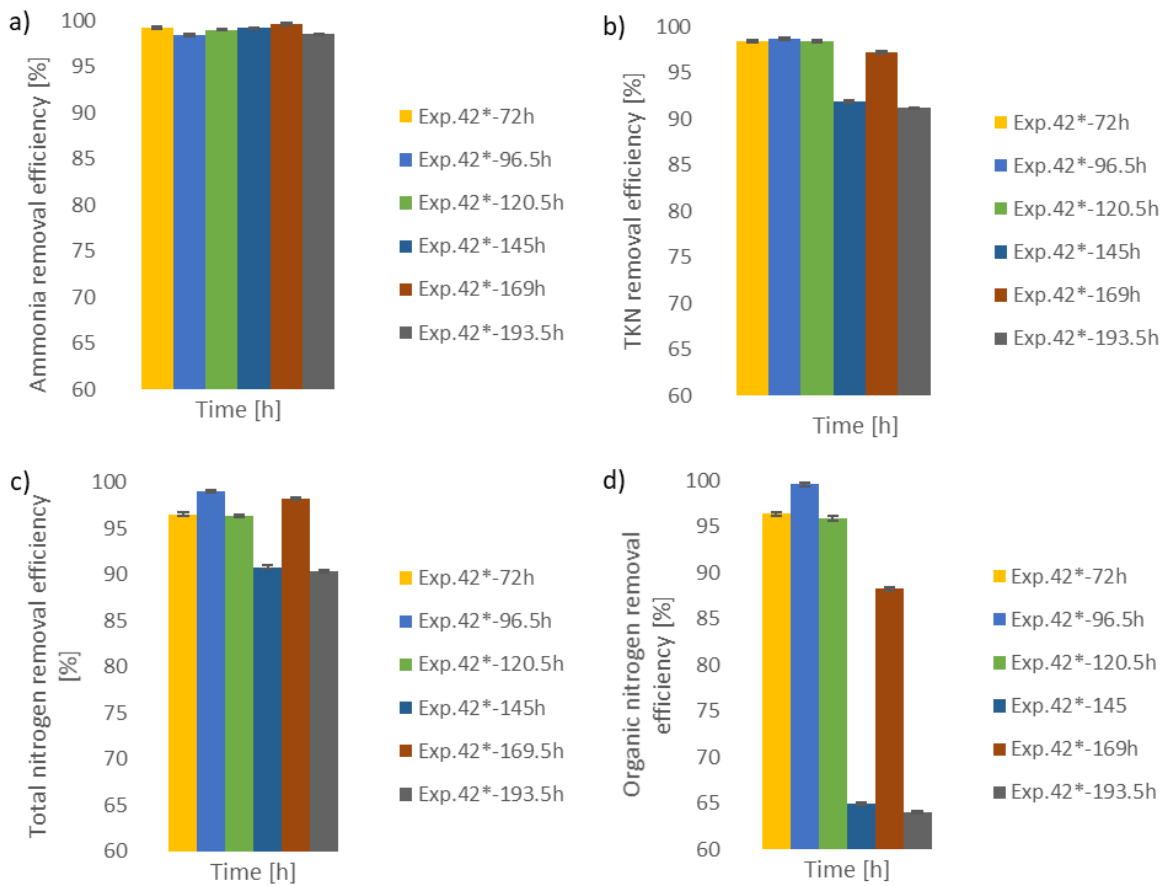


Figure 4- 34 Removal efficiencies of the pollutants versus time for Stage 4-2, medium scale EF-SBR; a) ammonia removal efficiency, b) TKN removal efficiency; c) organic nitrogen removal efficiency; d) total nitrogen removal efficiency

4-4-2-2. Impact of number of cycles on large scale EF-SBR efficiency

The second scope of Stage 4-2 is related to the investigation of the impact of the number of cycles on removal efficiency and consequent feasibility analysis of lessening exposure time for each individual cycle. Thereafter, the overall exposure time would be analyzed to assess the possibility of decreasing it. The Exp.46 is selected for study for the second scope of Stage 4-2 in which 30% hydrogen peroxide is utilized as oxidizing agent. The analyzed experiment of the second scope of Stage 4-2 is the Exp.46.

The variations of voltage (Fig.4-35a) in compartment 1 showed that increasing current did not result in a higher cell potential in the system at the start point of the third cycle. To clarify the statement, it should be mentioned that the initial voltage of cycle 3 was 4.4 V while the voltage of the fourth 12 hour exposure time of cycle 2 was equal to 4.3 V. Meanwhile the first 12 hour period of the third cycle, the voltage steadily decreased to 4 V while the Exp.46 experienced a stabilized condition throughout the second 12 hour exposure time with an identical voltage at 145 hours. Then, gradual decline was observed and the measured voltage was 3.8 V at 157 hours (end of the third 12 hours). While on the other hand voltage magnitude stabilized during the last 12 hour period. Therefore, the voltage fluctuated between 3.8 V to 4.4 V which was a relatively narrower range in comparison with compartment 3's variations.

The curve of voltage variations in compartment 3 demonstrated that the initial voltage of the third cycle was 6.47 V which was slightly lower than initial voltage of the second cycle with the value of 6.7 V. Although the obtained initial voltage of cycle 3 was lower than cycle 2's one, the initial conductivity of cycle 3 also gave lower magnitude in comparison with the second cycle which is anticipated to be reversed. The reason could be related to prevalence of electron-transfer control instead of Butler-Volmer control state. To clarify the difference between Butler-Volmer and

electron-transfer control, it is important to consider the concentration of target oxidized compound on the surface of electrode and the bulk concentration. Once the Butler-Volmer equation is governing condition, the concentration at the surface is equal to the concentration in the bulk electrolyte ($C^s = C^b$). While on the other hand, electron - transfer control leads to a lower concentration at the electrode surface compared with the bulk one ($C^s < C^b$) [4-12]. Therefore, heterogenous distribution of concentration directs to a lower initial cell potential. In the first 12 hour period of cycle 3, the voltage significantly fell to 5.25 V. However, the tendency of the changes during the second 12 hour period of the third cycle was slightly upward and gave 5.32 V at 145 hours. Throughout the remaining 24 hours, the Exp.46 faced a sharp decline during the third 12 hour exposure time of cycle 3 which provided 4.85 V at 157 hours while the slope of decrease dampened and gave 4.8 V at the end of the exposure time.

The pH curves (Fig.4-35b) of all three compartments fitted and the offset between each pair of curves was less than 0.05. Therefore, compartment 2 is selected as the zone of investigation to analyze the pH variations meanwhile the third cycle. At the initial point of cycle 3, the measured pH was 2.7. A significant decline in comparison with initial pH of the second cycle demonstrated that the electrochemical oxidation reactions led the electrolyte to be in stronger acid state. In the first, the second and the third 12 hours of the third cycle, pH sharply decreased to 0.85 at 157 hours (end of the third 12 hours of cycle 3), while the tendency of variation was upwards and provided pH equal to 1.13 at 169 hours.

Unexpectedly, the initial ORP (Fig.4-35c) of cycle 3 with the value of -51.83 mV was remarkably lower than the initial ORP of the second cycle (-26.2 mV at 72.5 hours). During the first, the second and the third 12 hour period of the third cycle, all three compartments gave the approximately similar value with less than 5 mV difference while the offset between compartment 3's ORP curve

and two other components emerged. In the second 12 hour exposure time of cycle 3, the reactions took place in the reaction state due to attained negative value for ORP (-26.1 mV) at the end of the time interval (133 hours). Then, ORP increased to 220.7 mV at 157 hours which showed that the reactions were in a strong oxidation state. During the third 12 hour period of cycle 3, ORP kept increasing and the obtained ORP was equal to 256.2 mV at 157 hours. Comparing cycle 2 and cycle 3 results, the peak was obtained at the end of the last 12 hour exposure time of cycle 2 while the similar ORP (with 2 mV difference) was obtained at the third 12 hour period of the cycle 3. Therefore, it can be interpreted that oxidation reactions were evolved relatively quicker during the third cycle in comparison with the second cycle which can be considered as one of the advantages of increasing the number of SBR cycles. For the last 12 hour interval, ORP variations demonstrated distinctive behavior due to giving similar ORP for compartment 1 and compartment 2. While on the other hand, compartment 3's ORP was 36 mV lower than the rest components. Therefore, it can be speculated that the oxidation reactions were not homogeneously taken place in the EF-SBR meanwhile the last 12 hour period of cycle 3. It might be initiated from the absence of mixing in the system.

Conductivity curves (Fig.4-35d) of all three compartments were fitted while conductivity of compartment 1 was slightly lower and the difference was less than 5 mS/cm. The minimal initial conductivity was achieved in cycle 3 with the value of 25 mS/cm that was significantly lower than the conductivity of raw wastewater electrolyte (61.4 mS/cm). during the first and second 12 hour period of the third cycle, conductivity was sharply increased and given 76.5 mS/cm at 145 hours. Throughout the third and fourth 12 hour exposure time, the changes increased, and the final achieved conductivity was 113.18 mS/cm at 169 hours. The differences among the slopes of conductivity curves originated from distinctive initial concentrations of each cycles. As presented

in Table 4-6, available concentrations of target electroactive compounds determine the pathway of conductivity raising throughout each individual cycle. Once the available concentration is higher, the conductivity ascending variations of the first and second 12 hour period develop quicker (See Fig.35d). However, subsequent effects of available conductive ions (hydroxide ions) on the ORP and the conductivity leads to have relative behavior in evolving conductivity respect on obtainable concentration and hydroxide ions. The hydroxide ions increased in the electrolyte. As a result, the conductivity slope increased faster.

Temperature variations (Fig.4-35e) demonstrated that the initial temperature of the third cycle was 18.7 °C which was like the initial temperature of cycle 2 with a 0.1 °C difference. The reason was the slightly equal temperature at the end of cycle 1 and cycle 2 which contributed as remained effluent temperature in the initial point of their relative following cycle. Due to identical temperature of influent, initial temperature of cycle n is dependent on the final temperature of cycle n-1's effluent. During the first 12 hour exposure time of cycle 3, temperature sharply increased to 32.4 °C because of majorly electrochemical oxidation reactions and minorly ohmic heat. In the second 12 hour period of cycle 3, temperature consistently declined to 29.6 °C while the tendency of variations was stable throughout the third 12 hour exposure time of the third cycle and given 29.5 °C at 157 hours. During the last 12 hour period, temperature gradually decreased to 29 °C which is 1.2 °C lower than the final temperature of cycle 2.

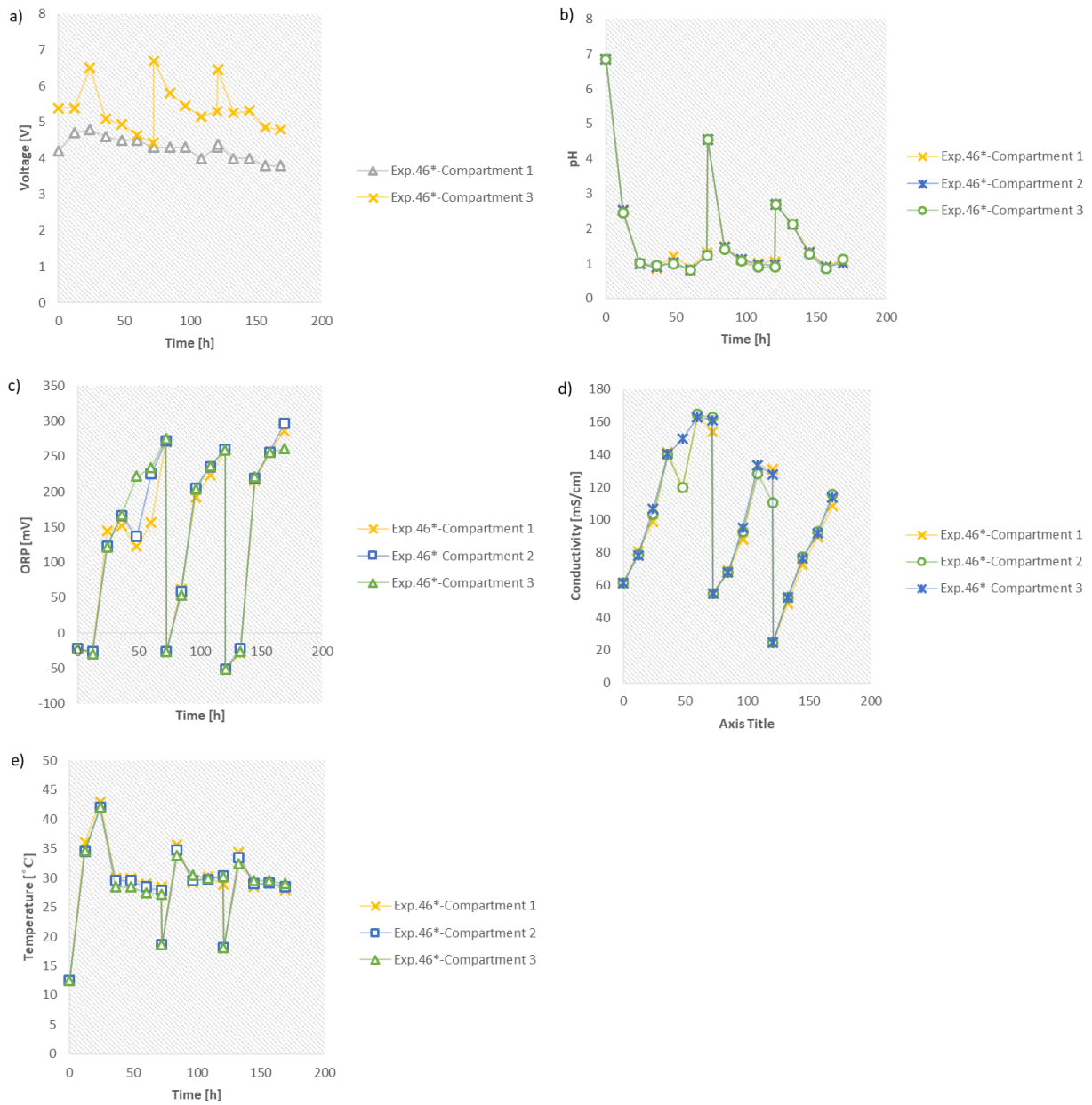


Figure 4- 35 Variations of monitored parameters for the relevant experiments of the Stage 4-2, large scale EF-SBR; a) voltage versus time; b) pH versus time c) ORP versus time; conductivity versus time e) temperature versus time

Considering Figure 4-36 and Table 4-7 which describe the removal efficiencies of target compounds and initial concentration of each cycle, removal efficiency analysis reveals that increase in number of cycles leads to higher efficiency for all target compounds at the end of the

second 12 hour exposure time of the third SBR cycle (145 hours). To support the statement, ammonia removal efficiency (Fig.4-36a) increased for 0.67% from $84.97\% \pm 0.17\%$ at 96.5 hours (end of the second 12 hour period of the second cycle). In addition, TKN removal efficiency significantly improved and outpaced cycle 2's relevant results. The achieved TKN removal efficiency at 145 hours (the second 12 hour exposure time of the third cycle) was $72.39\% \pm 0.17\%$ which was 5.12% higher than cycle 2's one. Furthermore, total nitrogen removal efficiency also increased for 8.13% which was tantamount to 1178.85 mg/L TKN removal concentration and the obtained removal efficiency at the second 12 hour interval of the third cycle was $71.58\% \pm 0.17\%$. The offset between the second 12 hour period of cycle 2 and cycle 3 was emerged once organic nitrogen removal analysis was assessed. The removal efficiency was enhanced for 21.46% which was around 9 times higher than the efficiency at 96.5 hours (the second 12 hour period of cycle 2) and the obtained efficiency was $23.83\% \pm 0.17\%$.

In addition, slightly improvement (0.11%) was observed for TKN removal efficiency (Fig.4-36b) at the end of exposure time (end of cycle 3) in juxtaposition with the recorded removal efficiency at the relative time (120.5 hours) of cycle 2 in which $92.84\% \pm 0.17\%$ efficiency was achieved. In contrast, total nitrogen removal efficiency (Fig.4-36c) slightly declined at the end of cycle 3 in comparison with cycle 2's end point results ($92.84\% \pm 0.22\%$) and gave $92.08\% \pm 0.22\%$ at 169 hours (end of cycle 3). Ammonia and organic nitrogen removal efficiencies reached identical values individually which were equal to cycle 2's corresponding efficiencies at the end of the third cycle. The obtained values were $99.05\% \pm 0.17\%$ and $70.58\% \pm 0.34\%$, respectively.

According to significant improvement in the second 12 hour exposure time of the third cycle, increasing the number of cycles led to better removal efficiency. In addition, the final results of cycle 3 also demonstrated a slight improvement with respect to TKN removal efficiency. Since the

aim of this research is obtaining high removal efficiency for TKN, increasing the number of SBR cycle is recommended. Also, approximately similar ammonia removal efficiency as the final results of cycle 1 supports the conclusion. The difference between mentioned ammonia removal efficiencies is equal to 0.11% and cycle 3'one is lower.

It might be questionable if it is possible to extend the conclusions of Stage 4-2 to medium and large-scale experiments with 50% hydrogen peroxide purity. The justification proposes that considering the worst condition by utilizing 30% hydrogen peroxide and obtaining tangible results would guarantee that enhancing experimental conditions (utilizing 50% hydrogen peroxide) increases the probability of achieving a better removal efficiency. It is suggested to analyze the enhanced experimental condition results in future work.

Table 4- 7 Characteristics of the initial concentrations of the ammonia, TKN, total nitrogen and, organic nitrogen in the raw wastewater and the beginning of each cycle of the large scale; cycle 1, cycle 2, and cycle 3 initial concentration

No. Exp.	Ammonia [mg/L]	TKN [mg/L]	Total nitrogen [mg/L]	Organic nitrogen [mg/L]
Initial (Cycle 1)	11000.0	14000.0	14500.0	3000.0
46-72.5h (Cycle 2)	9100.8	11680.5	12280.5	2715.6
46-121h (Cycle 3)	9365.6	12048	12480.8	2682.4

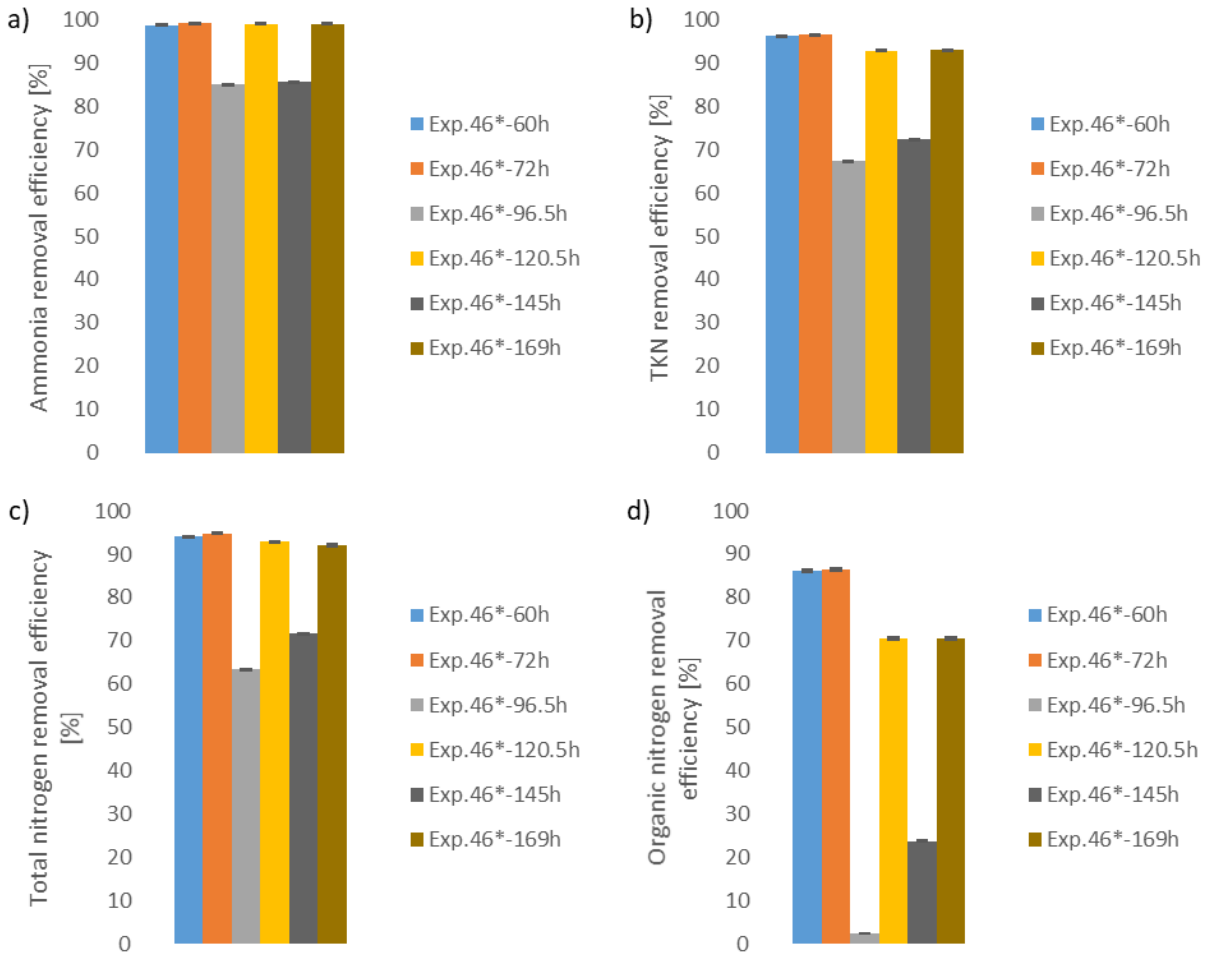


Figure 4- 36 Removal efficiencies of the pollutants with time for Stage 4-2, large scale EF-SBR; a) ammonia removal efficiency; b) TKN removal efficiency; c) total nitrogen removal efficiency; d) organic nitrogen removal efficiency

Table 4- 8 Removal efficiencies of ammonia, TKN, total nitrogen, and organic nitrogen for all experiments of Phase 4

Stage	No. of Exp.	Ammonia removal [%]	TKN removal [%]	Total nitrogen removal [%]	Organic nitrogen removal [%]	Remarks
Stage 4-1; medium scale	42-72 h	99.24 ± 0.1	98.35 ± 0.12	96.55± 0.15	96.4± 0.26	30% purity H ₂ O ₂ ; 2 SBR Cycle
	45-72 h	99.54 ± 0.12	99.01± 0.14	97.5± 0.17	97.06± 0.28	50% purity H ₂ O ₂ ; 2 SBR Cycle
	42-96.5 h	98.43 ± 0.1	98.71± 0.12	99.04± 0.15	99.6± 0.26	30% purity H ₂ O ₂ ; 2 SBR Cycle
	45-96.5 h	99.02± 0.12	99.13± 0.14	99.54± 0.17	99.67± 0.28	50% purity H ₂ O ₂ ; 2 SBR Cycle
	42-120.5 h	99.03 ± 0.1	98.35± 0.12	96.31± 0.17	95.87± 0.26	30% purity H ₂ O ₂ ; 2 SBR Cycle
	45-120.5 h	99.23 ± 0.12	98.63± 0.14	97.7± 0.17	94.56± 0.28	50% purity H ₂ O ₂ ; 2 SBR Cycle
Stage 4-1; large scale	44-60 h	99.46 ± 0.15	99.46± 0.17	95.76± 0.17	92.22± 0.32	50% purity H ₂ O ₂ ; 2 SBR Cycle
	46-60 h	98.72 ± 0.17	96.26± 0.17	93.98± 0.17	86.26± 0.34	30% purity H ₂ O ₂ ; 2 SBR Cycle
	44-72 h	99.48 ± 0.15	97.18± 0.17	95.76± 0.17	91.05± 0.32	50% purity H ₂ O ₂ ; 2 SBR Cycle
	46-72 h	99.16 ± 0.17	96.45± 0.17	94.88± 0.17	86.48± 0.34	30% purity H ₂ O ₂ ; 2 SBR Cycle
	44-96.5 h	86.85 ± 0.15	72.95± 0.17	71.01± 0.17	2.00± 0.32	50% purity H ₂ O ₂ ; 2 SBR Cycle
	46-96.5 h	84.97 ± 0.17	67.27± 0.17	63.45± 0.17	2.37± 0.34	30% purity H ₂ O ₂ ; 2 SBR Cycle
	44-120.5 h	99.06 ± 0.15	96.64± 0.17	95.74± 0.17	87.79± 0.32	50% purity H ₂ O ₂ ; 2 SBR Cycle
	46-120.5 h	99.05 ± 0.17	92.95± 0.17	92.84± 0.17	70.58± 0.34	30% purity H ₂ O ₂ ; 2 SBR Cycle

Table 4-8 Continued- removal efficiencies of ammonia, TKN, total nitrogen, and organic nitrogen for all experiments of Phase 4

Stage 4-2; medium scale	42*-72 h	99.24± 0.1	98.35± 0.12	96.55± 0.15	96.4± 0.26	30% purity H ₂ O ₂ ; 4 SBR Cycle
	42*-96.5 h	98.43± 0.1	98.71± 0.12	99.04± 0.15	99.6± 0.26	30% purity H ₂ O ₂ ; 4 SBR Cycle
	42*-120.5 h	99.03± 0.1	98.35± 0.12	96.31± 0.15	95.87± 0.26	30% purity H ₂ O ₂ ; 4SBR Cycle
	42*-145 h	99.2± 0.1	91.86± 0.12	90.82± 0.15	64.93± 0.26	30% purity H ₂ O ₂ ; 4 SBR Cycle
	42*-169 h	99.62± 0.1	97.19± 0.12	90.34± 0.15	64.03± 0.26	30% purity H ₂ O ₂ ; 4 SBR Cycle
	42*-193.5 h	98.54± 0.1	91.14± 0.12	98.26± 0.15	88.26± 0.26	30% purity H ₂ O ₂ ; 4 SBR Cycle
Stage 4-2; large scale	46*-60 h	98.72± 0.17	96.26± 0.17	93.98± 0.17	86.26± 0.34	30% purity H ₂ O ₂ ; 3 SBR Cycle
	46*-72 h	96.45± 0.17	96.45± 0.17	94.88± 0.17	86.48± 0.34	30% purity H ₂ O ₂ ; 3SBR Cycle
	46*-96.5 h	84.97± 0.17	67.27± 0.17	63.45± 0.17	2.37± 0.34	30% purity H ₂ O ₂ ; 3 SBR Cycle
	46*-120.5 h	99.05± 0.17	92.84± 0.17	92.84± 0.17	70.58± 0.34	30% purity H ₂ O ₂ ; 3 SBR Cycle
	46*-145 h	85.63± 0.17	72.39± 0.17	71.58± 0.17	23.83± 0.34	30% purity H ₂ O ₂ ; 3 SBR Cycle
	46*-169 h	99.05± 0.17	92.95± 0.17	92.08± 0.17	70.58± 0.34	30% purity H ₂ O ₂ ; 3 SBR Cycle

Table 4-8 provides the removal efficiencies of Stage 4-1 and Stage 4-2 for both medium and large scales. The highest ammonia removal efficiency of Stage 4-1, medium scale, was achieved by the Exp.45 (50% purity hydrogen peroxide) at the end of the first cycle. It was 99.54% ±0.12%. In addition, the highest detected TKN removal efficiency was at the first 24 hour period of cycle 2 in the Exp.45 with the value of 99.13% ± 0.14%. Furthermore, the highest removal efficiency of total nitrogen and organic nitrogen were achieved at the end of the first 24 hour exposure time of the

second cycle of the Exp.45 with the value of $99.54\% \pm 0.17\%$ and $99.67\% \pm 0.28\%$, respectively. According to large scale results of Stage 4-1, specifically, the Exp.44, the best efficiency of target components were achieved at 60 hours with the magnitudes of $99.24\% \pm 0.15\%$, $98.35\% \pm 0.17\%$, $96.55\% \pm 0.2\%$, and $96.4\% \pm 0.32\%$ for ammonia, TKN, total nitrogen, and organic nitrogen, respectively. The final results of the Exp.44 which were achieved at the end of the second cycle were tenable. The reason is achieving promising removal efficiency in 48 hours. Besides, other target compounds were also achieved acceptable removal efficiency values. The values of $99.06\% \pm 0.15\%$, $96.64\% \pm 0.17\%$, $95.74\% \pm 0.2\%$, and $87.79\% \pm 0.32\%$ were obtained for ammonia, TKN, total nitrogen, and organic nitrogen at the end of cycle 2 correspondingly.

the medium scale EF-SBR (Stage 4-2) results demonstrated that the best removal efficiency was reached at the end of the first cycle. The achieved values were $99.24\% \pm 0.12\%$, $98.35\% \pm 0.14\%$, $96.55\% \pm 0.17\%$, and $96.4\% \pm 0.28\%$ for ammonia, TKN, total nitrogen, and organic nitrogen, respectively. The removal efficiency of total nitrogen enhanced at the end of the fourth cycle and it reached $98.26\% \pm 0.17\%$ at 193.5 hours. It is essential to mention that total nitrogen was the only compound that faced enhancement once the number of SBR cycles were increased to 4. Outstanding removal efficiency was achieved after one-day exposure time at 96.5 hours (the first 24 hour period of cycle 2) for all target compounds. The achieved results were 98.43%, 98.71%, 99.04%, and 99.6% for ammonia, TKN, total nitrogen, and organic nitrogen, respectively.

The results of large scale EF-SBR (Stage 4-2) showed that the removal efficiency of ammonia was $99.05\% \pm 0.17\%$ at the end of the third cycle. The achieved value was the best removal efficiency among all analyzed points in large scale E. In addition, it was identical with the final results of the second cycle. the best TKN removal efficiency was achieved at 72 hours with the value of 96.45%

$\pm 0.17\%$. On the other hand, increasing number of cycles leads to TKN removal efficiency with the value of $92.95\% \pm 0.17\%$ at the end of the third cycle.

The results of large scale EF-SBR (Stage 4-2) demonstrated that the best efficiency was obtained at the end of the first cycle (72 hours) with the value of $94.88\% \pm 0.22\%$. In addition, the highest removal efficiency among the following cycles belonged to the end point of cycle 2 with the value of $92.84\% \pm 0.22\%$. Due to obtaining a lower total nitrogen removal efficiency at the end of the third cycle, it can be interpreted that nitrite and nitrate compounds evolved throughout the third cycle in EF-SBR.

The final target compound which was analyzed in large scale EF-SBR (Stage 4-2) was organic nitrogen. The best removal efficiency was achieved at the end of the first cycle (72 hours). The obtained value was $86.48\% \pm 0.34\%$. In addition, an identical value of $70.58\% \pm 0.34\%$ was obtained at the end of the second and third cycle. Therefore, it is fair to speculate that the contribution of increasing the number of SBR cycles is enhancing the removal efficiency of TKN and all three remained target compounds are provided slightly or identically similar magnitudes in the second and third cycle. So, increasing the number of cycle is expected to be functional in decreasing the hydraulic retention time (HRT) and subsequently overall exposure time for the following cycles and the results are validated by the three-cycle experiment.

Table 4-9 describes the sludge production of a group of experiments which are selected among each phase of this study. Small scale experiments gave significant amount of sludge per liter while the upscaling mitigates the sludge production per liter. In the other words, considering four individual run with the exposure volume and experimental conditions of the Exp.17 (500 mL) is expected to give a significantly higher amount of sludge production. While on the other hand the

obtained sludge production per liter is much lower than upscaling expectations. Surprisingly, increasing the number of SBR cycles resulted in a negligible increase in the amount of sludge production which proves the promising performance of EF-SBR.

Table 4- 9 Amount of sludge production and sludge mass per liter for small scale, large scale, and medium and large EF-SBR

No. of Experiment	Sludge production (g)	Sludge mass per Liter (g/L)
1-small scale	2.75	5.50
17-small scale	2.35	4.70
19- small scale	10.58	21.16
26 – small scale	5.78	11.56
40- large scale	42.96	7.39
45 – medium scale 2 SBR cycle	22.51	5.86
42 – medium scale 4 SBR cycles	44.90	7.91
44- large scale 2 SBR cycles	79.64	7.46

Chapter 5 Investigation of EF-SBR process kinetics

Chapter 5 demonstrated that a novel EF-SBR achieved objectives of the thesis, i.e. decrease the TKN and ammonia content in wastewater by 67.96 % and 70.3%, respectively for around 1.7 times higher concentration of TKN and ammonia. However due to the novelty of the system, the physicochemical processes taking place in the system are unknowns. Subsequently, additional study was conducted with attempting to recognize kinetics of contaminant degradation taking place in the EF-SBR.

5-1. Experimental analysis

The raw wastewater was sampled after one year from the same point source as previous investigated influent. The concentrations of pollutants were significantly increased in comparison with the previous sample. The initial concentrations of compounds and characteristics of wastewater are provided in Table 5-1. To find out the kinetics of degradation for each individual compound, 37 points were considered for monitoring and 111 samples were collected from all compartments of the EF-SBR during 5 consecutive days of the observations. The experimental conditions of the Exp.48 are identical to the Exp.44 (see Table 3-17).

Table 5- 1 Characteristics of the studied wastewater for investigation of the kinetics

Characteristics of the wastewater	Value
Ammonia (NH₃) [mg/L]	18000.0
Total kjeldahl nitrogen (TKN) [mg/L]	23600.0
Organic nitrogen (ON) [mg/L]	5600.0
Nitrate (NO₃⁻) [mg/L]	210.0
Nitrite (NO₂⁻) [mg/L]	5.0
Total nitrogen (TN) [mg/L]	23815.0
Sulfate (SO₄²⁻) [mg/L]	34500.0
Ferrous (Fe²⁺) [mg/L]	2901.4
Total suspended solids [g]	19.8
pH	6.8
Conductivity [mS/cm]	100.6
Oxidation reduction potential (ORP) [mV]	-61.4

The monitoring parameters are voltage, pH, ORP, conductivity, and temperature. The variations of the mentioned parameters are illustrated in Figure 5-1, Figure 5-2 , Figure .5-3, Figure .5-4, and Figure 5-5, respectively. The first cycle exposure time was 73.5 hours while the second cycle exposure time was 44.83 hours. Furthermore, 2.67 hours was considered for the preparation of the influent of cycle 2.

According to Figure 5-1, the variations of the voltage values demonstrated the smooth fluctuations meanwhile 37.4 hours for both compartments. In addition, the obtained voltage at 37.4 hours were 3.45 V and 4.75 V for compartment 1 and compartment 3, respectively. During 2.6 hour-period (from 37.4 hours to 39 hours) , both compartments experienced a sharp decline and the voltage of the compartment 1 and 2 decreased and gave 2.73 V and 3.97 V, respectively at 39 hours. The observed decline can be expressed as the initiation of a high fluctuation region which was observed throughout the time interval between 37.41 hours and 73.5 hours. The lowest detected voltage and

the highest one for compartment 1 were 2.46 V at 61.75 hours and 3.86 V at 50.75 hours. The analysis of the voltage variations of compartment 3 in the time interval between 37.41 hours and 73.5 hours demonstrated that the lowest and highest voltages were 3.51 V at 61.75 hours and 4.3 V at 59.25 hours, respectively. It is important to consider that the detected voltage of compartment 3 at the same monitoring point (50.75 hours) in which compartment 1 gave the highest voltage was 4.28 V. Consequently, it can be fairly described that the highest and lowest voltage of both compartments were observed at the congruous monitoring time. Those monitoring-time points were 50.75 hours and 61.75 hours, respectively.

Once the second cycle of the SBR commenced at 76.17 hours, the current set as the initial current of the first cycle, and the resulted voltage for both compartments were 3.5 V and 4.92 V, respectively. It is fair to consider three regions to assess the variations of voltage during the second cycle. The first time interval of the second cycle is between 76.17 hours and 85.34 hours. The second region is between 86.34 hours and 99.18 hours, and finally the last time interval is started from 99.18 hours and continued for 21.82 hours. Throughout the first time interval of the cycle 2, the variations of the voltage values were smooth in both compartments. The obtained voltage magnitudes at 86.34 hours are 3.42 V and 4.66 V for compartment 1 and compartment 3, respectively. During the second time interval, the variations were adverse and the predominant trend of voltage variations changed, and gave higher voltage for compartment 1. At 97.34 hours, the compartment 1's voltage increased quickly and reached 4.42 V while compartment 3's voltage was 3.26 V. However, the predominant trend reobtained at 99.18 hour and compartment 3's voltage outpaced compartment 1's one. The detected voltage values were 3.22 V and 4.26 V for compartment 1 and compartment 3, respectively. Meanwhile the third time segment of the cycle 2, the variations were smooth except at 110.35 hours for compartment 3 in which the measured

voltage fell to 3.81 V from 4.09 V at 109.35 hours. The final values which were detected at the end of the second cycle (121 hours) were 3.16 V and 3.96 V. Due to the presence of extremely high concentrations of the pollutants, considering the conventional relationship between voltage and conductivity was not practical. Since the conventional relationship was applicable for lower concentrations of pollutant which are present in the electrolyte ^[4-12].

pH variations of all three compartments were provided in Figure 5-2. Due to similar obtained pH values in each monitoring point for all compartments, it is a fair simplification to assess one compartment (e.g. compartment 2) as a representative of the system. However, initial 3.33 hour exposure time and the time interval between 12.65 hours and 17.4 hours require individual investigation for each compartment because of the distinctive obtained values in each compartment.

The initial pH of raw wastewater was 6.85. After 1.83 hours, compartment 3's pH adversely changed toward the acidic condition and reached 5.42. At the same monitoring point (1.83 hours) the pH of the compartment 1 and compartment 2 gave 6.28 and 6.12, respectively. The pH values of all three compartments converged at 3.33 hours to 4.71. Throughout the time interval between 3.33 hours to 12.65 hours, the tendency of the pH variation of all compartment was sharply descending and the obtained pH was around 2.8 at 12.65 hours for all three compartments. The second time segment which required individual assessment was started from 12.65 hours and continued for 4.75 hours. At 14.4 hours, compartment 3's electrolyte was the most acidic among all compartments with the value of 2.2. Although, the differences among the pH values were not significant like the pH magnitudes of initial 3.33 hours, the pH of compartment 1 and compartment 2 provided 2.2 and 2.23 at 14.4 hours, respectively. In the following 3 hour- period, the pH values declined and all compartments reached identical pH at 17.4 hours which was equal to 2.09.

For the remaining 56.1 hours of cycle 1, the pH values were similar in all three compartments and the tendency was downwards for a time interval between 17.4 hours to 67 hours. The sharpest decrease was observed for the time interval between 17.4 hours and 24 hours and pH was declined to 1.31 from 2.09. The pH values smoothly decreased during the time interval between 24 hours and 67 hours and the detected pH was equal to 0.05 at 67 hours. Unexpectedly, the tendency was upwards for the rest of the 6.5 hours of cycle 1. The final achieved pH was 0.64 at 73.5 hours which was around 13 times larger than the observed pH at 67 hours.

The initial pH value of cycle 2 was 3.4. Meanwhile the time interval between 76.17 hours (cycle 2's start point) and 86.34 hours, the trends were decreasing. Furthermore, the measured pH at 86.34 hours was 1.45. Throughout the time segment between 86.34 hours and 97.34 hours, pH kept declining and the obtained pH was 0.78 at 97.34 hours. The fluctuations of pH were smooth during the remained 23.66 hours. Although the tendency was declining throughout the remained 23.66 hours, two time segment should be considered to determine the distinctive behaviour of pH raising. The first time segment is 107.35 hours and 109.35 hours in which pH gradually increased to 0.56 at 109.35 hours from 0.49 at 107.35 hours. The second allocated time interval in which pH changes demonstrated distinctive behavior starting from 117.35 and continued up to the end point (121 hours). pH was increased to 0.36 from 0.27.

To find out the reason of the relatively lower pH in Exp.48, it should be mentioned that the justification is the presence of 34500 mg/L sulfate ions in new sampled wastewater which can be considered as extremely high concentration. Whereas, the sulfate concentration of assessed raw wastewater for all four phases of study is 4190 mg/L. Therefore, it can be interpreted that high concentration of sulfate ions in the raw wastewater of the Exp.48 results lower pH at the end of

cycle 1 and cycle 2 in comparison with Exp.44 (2 SBR cycle large scale EF-SBR). It is crucial to mention that the experimental condition of the Exp.44 is identical to the Exp.48.

ORP variations of all three compartments are illustrated in Figure 5-3. According to cycle 1's results, all three curves of variations fitted except in the time interval between 11.15 hours and 17.4 hours in which ORP of compartment 1 was significantly higher than ORP values of compartment 2 and compartment 3. During the time segment between initial and 11.15 hours, the tendency was downward, and the process moved toward reduction state in which the ORP declined from -60.77 mV to -110.9 mV. Meanwhile the time segment between 11.15 hours and 17.4 hours, compartment 1's ORP increased sharply and it was -32.5 mV at 14.4 hours. While on the other hand, ORP of the compartment 2 and compartment 3 gave identical value which was equal to -87.8 mV. The measured ORP at 17.4 hours provided -79.6 mV for all three compartments. During the remaining 56.1 hours, the measured ORP values resulted the same magnitude. Therefore, one value would be reported to assess the tendency of ORP changes in the system. During the time interval of 17.4 hours to 24 hours, ORP increased to -4.55 mV at 24 hours.

To compare the required time to observe the process in oxidation state, it should be considered that Exp.44's required time was 12 hours while it took more than 24 hours to obtain oxidation state in Exp.48. Throughout the time segment between 24 hours and 27.75 hours, ORP increased to 309.2 mV which demonstrated a that the process was in strong oxidation state. Throughout the time interval between 27.75 hours and 37.41 hours, ORP steadily increased to 349.2 mV at 37.41 hours. At 37.41 hours to 55 hours, the fluctuations of ORP magnitudes intensified and the maximum ORP of Exp.48 achieved at 50.75 hours which was equal to 399.9 mV. Throughout 55 hours to 73.5 hours the fluctuations and ORP changed in the range between 370.2 mV and 387.55 mV and the final ORP of cycle 1 was equal to 378.3 mV.

After preparing the influent of the second cycle, the initial ORP of cycle 2 was -47.6 mV which was higher than the initial ORP of cycle 1 (-60.77 mV). The reason is the contribution of the remaining effluent on increasing the initial ORP of purely raw wastewater by mixing. A sharp decline detected after 1.17 hours and the recorded ORP was -126.9 mV at 77.34 hours. However, ORP recovered to -79.9 mV at 85.34 hours. Throughout the time segment between 85.34 hours and 86.34 hours, ORP increased sharply to 324.3 mV which demonstrated that the process was in relatively strong oxidation state. It is notable to take into account that the required time to reach oxidation state is in the range between 9.17 hours and 10.17 hours. So, increasing the number of cycles significantly decreases the required time to reach oxidation state.

During the time segment between 86.34 hours and 107.35 hours, ORP smoothly changed and gave 352.1 mV at 107.35 hours. From 107.35 hours to 121 hours, fluctuations intensified, and the lowest and highest obtained values were 335.5 mV at 109.35 hours and 387.5 mV at 121 hours, respectively. It is crucial to mention that the compartment 1's ORP was remarkably lower than the compartment 2 and compartment 3's one at 117.35 hours, and the recorded ORP of compartment 1 was 358.4 mV while obtained ORP values for compartments 2 and 3 were identical and equal to 376.8 mV at the same monitoring point.

According to Figure 5-4, the conductivity variations of all compartments demonstrated adverse fluctuations during the first and second cycles. However, the final conductivity of each compartment was remarkably higher than the initial conductivity of the system (101.37 mS/cm). Furthermore, the final conductivity of cycle 1 and cycle 2 were 193.6 mS/cm and 211.5 mS/cm, respectively. The maximum conductivity of cycle 1 was achieved by compartment 2 with the value of 235.5 mS/cm at 59.25 hours. Besides, relatively high voltage also obtained at 59.25 hours. So, it proves that the studied electrolyte does not follow the conventional governing equation for dilute

electrolyte. In addition, the maximum conductivity of cycle 2 was obtained by compartment 1 with the magnitude of 236 mS/cm.

Figure 5-5 illustrates the variations of temperature in all three compartments. The fluctuations of temperature in all three compartments was adverse and it was not possible to determine overall trend for each compartment. The initial and final temperature of cycle 1 were 18.4 °C and 27.8 °C, respectively. Also, the maximum temperature of cycle 1 was obtained by compartment 1 with the value of 40 °C. Furthermore, the highest temperature of cycle 2 was observed at 85.34 hours with the value of 38.5 °C.

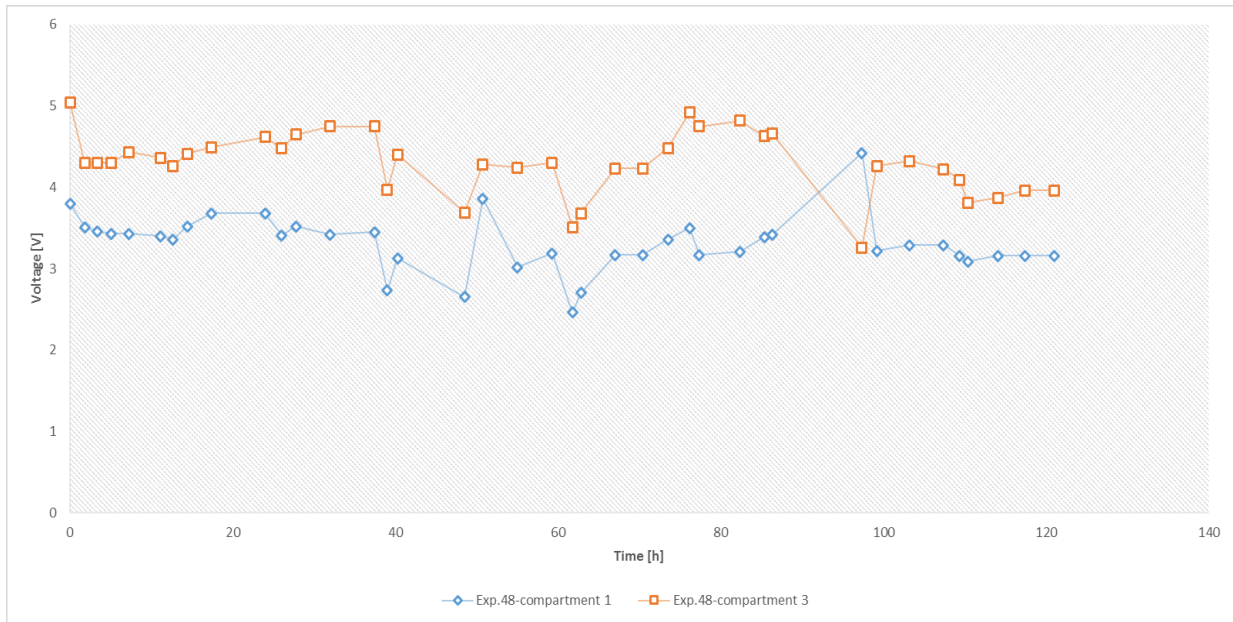


Figure 5- 1 Voltage variations versus time for large scale EF-SBR

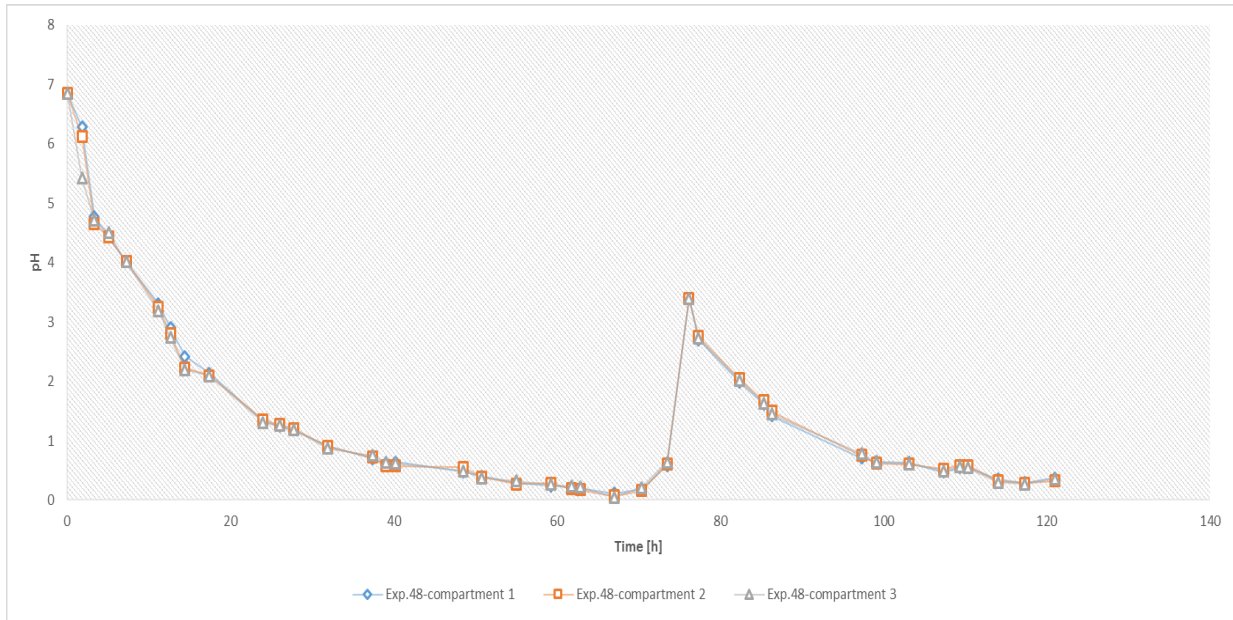


Figure 5- 2 pH variations versus time for large scale EF-SBR

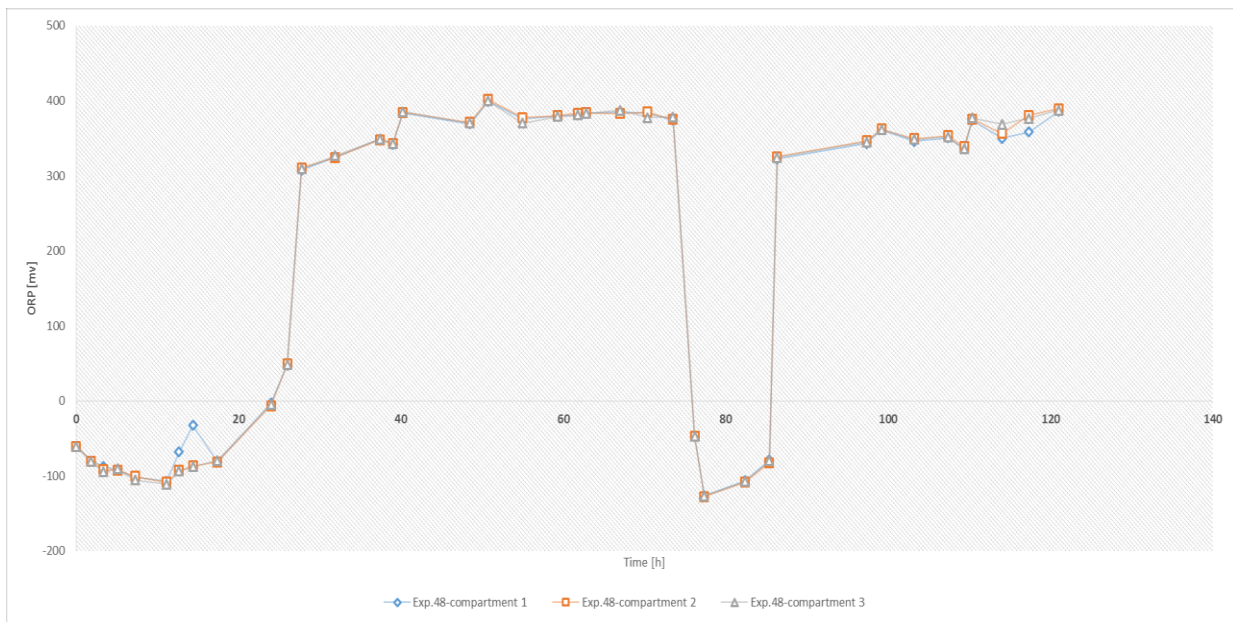


Figure 5- 3 ORP variations versus time for large scale EF-SBR

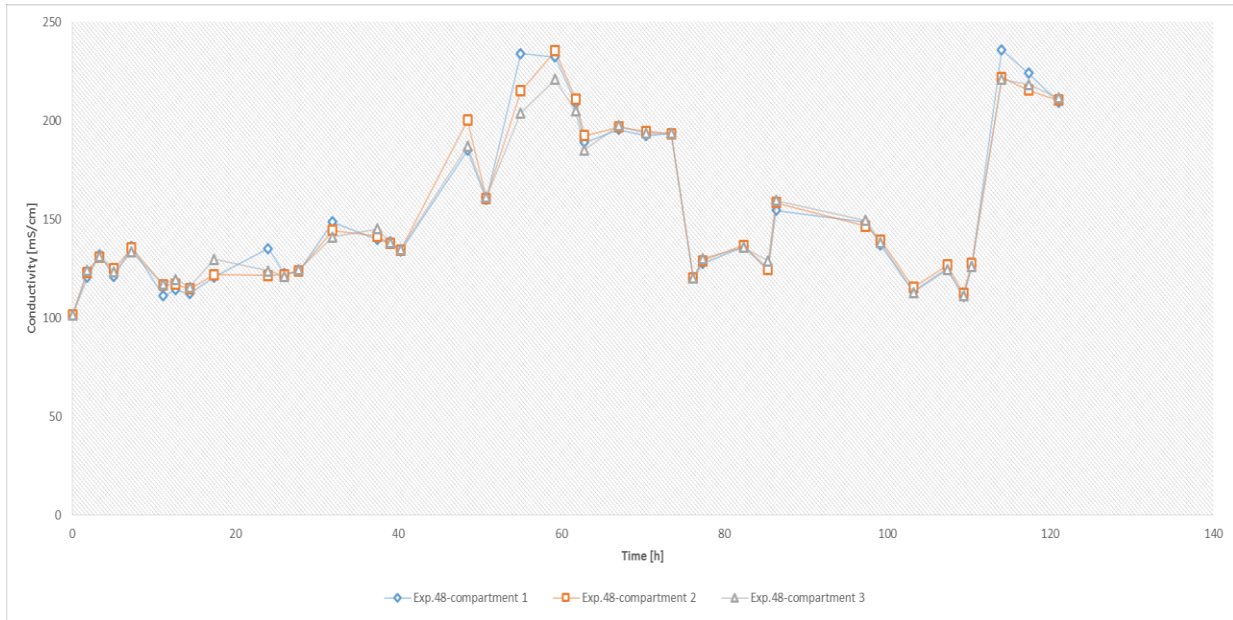


Figure 5- 4 Conductivity variations versus time for large scale EF-SBR

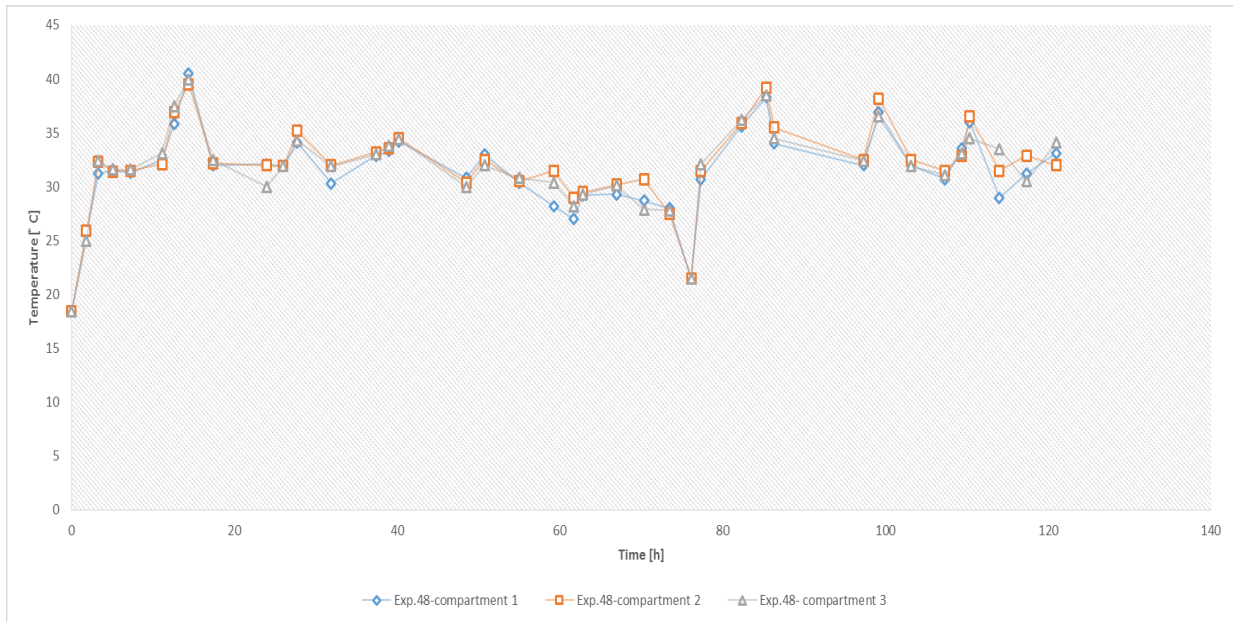


Figure 5- 5 Temperature variations versus time for large scale EF-SBR

Figure 5-6 presents the variations of ammonia concentrations. Meanwhile the time segment between initial and 27.75 hours, all compartments experienced high and adverse fluctuations and production of ammonia observed in the electrolyte. During the time interval between 27.75 hours and 50.75 hours ammonia concentrations steadily declined and reached 7100 mg/L, 7490 mg/L,

and 8440 mg/L in compartment 1, compartment 2 and compartment 3, respectively. A distinctive behavior observed at 55 hours in which compartment 2 and compartment 3 were 9320 mg/L and 7890 mg/L while compartment 1's concentration kept declining, and provided 6820 mg/L at 55 hours. The final ammonia concentration of cycle 1 was 4710 mg/L at 73.5 hours.

Table 5-2 provides the initial concentrations of cycle 1 and cycle 2 for ammonia, TKN, total nitrogen, organic nitrogen, nitrate, nitrite, and sulfate, respectively. When the second SBR cycle started, the transient behavior observed for 10.17 hours and the obtained concentrations at 86.34 hours were 15800 mg/L, 14700 mg/L, and 14300 mg/L for compartment 1, compartment 2, and compartment 3, respectively. For the remained 24.66 hours, the overall trend was descending except for the time segment between 107.35 hours and 110.35 hours. At 109.35 hours, compartment 2 gave the highest concentration among all compartments with the value of 10000 mg/L. In contrast, the ammonia concentrations of compartment 1 and compartment 3 with the values of 8690 mg/L and 8840 mg/L kept descending which was predominant in monitoring point of the last 24.66 hours of cycle 2. Finally, the concentration of all three compartments converged at 121 hours

Table 5- 2 The initial concentrations of ammonia, TKN, total nitrogen, organic nitrogen, nitrate, nitrite, and sulfate at the beginning of cycle 1 and cycle 2

No. Exp.	Ammonia [mg/L]	TKN [mg/L]	Total nitrogen [mg/L]	Organic nitrogen [mg/L]	Nitrate [mg/L]	Nitrite [mg/L]	Sulfate [mg/L]
Initial (Cycle 1)	18000	23600	23815	5600	210	5.0	34500
46-73.5h (Cycle 2)	15200	20200	20500	5000	81.7	218.3	33700

According to Figure 5-7, the fluctuations of the TKN concentrations in each compartment were high for compartment 1 and compartment 3 meanwhile the time segment between initial and 40.25

hours. The resulted concentrations were identical at 40.25 hours for compartment 1 and compartment 3 and equal to 14500 mg/L. In addition, the results of compartment 2 demonstrated a transient behavior throughout the time interval between initial and 31.91 hours. For 19 hours (from 40.25 hours to 59.25 hours), compartment 1 showed a steady decline and reached 7090 mg/L while compartment 3 maintained the declining trend for 21.5 hours (from 40.25 hours to 61.75 hours) and gave 5880 mg/L at 61.75 hours. Compartment 3 preserved a consistent decline for a large time extent in comparison with the other compartments. The consistent decline in compartment 3 continued for 30.92 hours and gave 6480 mg/L at 62.83 hours. A distinctive behavior detected for the last 3.82 hours of cycle 1 in compartment 2 and the final recorded concentration of compartment 2 was 5280 mg/L at 73.5 hours which increased from 4930 mg/L at 70.38 hours. In addition, the final concentrations of cycle 1 were identical for compartment 1 and compartment 3 with the value of 4870 mg/L.

Once the second cycle started, the intensive fluctuations lasted for 10.17 hours and the highest concentration of cycle 2 obtained in compartment 1 with the value of 18900 mg/L. Also, the time segment between 107.35 hours and 110.35 hours should be assessed for the distinctive trend of variations compartment 1 and 2. Subsequently, an ascending and descending variations observed for each compartment. While on the other hand, the second transient behavior of compartment 3 initiated at 109.35 hours and continued for 4.67 hours. The final concentrations of compartment 1, compartment 2, and compartment 3 were 4970 mg/L, 5280 mg/L and, 4870 mg/L, respectively.

The variations of total nitrogen concentrations of compartment 1 were transient throughout the whole exposure time of cycle 1 and adverse fluctuations observed. The same behavior observed from the second cycle in compartment 1 and gave the final concentrations equal to 5370 mg/L and 8130 mg/L at the end of cycle 1 and cycle 2, correspondingly (Fig.5-8).

Compartment 2 also showed strong fluctuations during the first 27.75 hour exposure time, and the obtained concentration was 20200 mg/L at 27.75 hours. During the time interval between 27.75 hours and 61.75 hours, the declining trend maintained for compartment 2 and the achieved concentration was 6170 mg/L. After a slight fluctuation, the concentration was first increased to 6930 mg/L. Then declined to 6750 mg/L. Also, an ascending behavior observed for the last 3.28 hours of cycle 2 in which total nitrogen concentration of compartment 2 increased from 5480 mg/L at 70.28 hours to 5710 mg/L at 73.5 hours. The results of compartment 3 demonstrated a transient behavior for 48.5 hours to 9280.5 mg/L at 48.5 hours. From 40.25 hours to 61.75 hours, variations showed a descending trend and reached 6170 mg/L at 61.75 hours. However, total nitrogen slightly increased to 6750 mg/L at 62.83 hours. However, the tendency was descending throughout the last 10.67 hours and the final measured concentration of cycle 1 was 4870 mg/L. It is noteworthy to mention that the maximum total nitrogen concentration was observed in compartment 3 with the value of 27600 mg/L at 11.15 hours.

The behavior of all compartments was transient throughout the second cycle and the final obtained concentration of cycle 2 were 8130 mg/L, 7530 mg/L and, 7730 mg/L for compartment 1, compartment 2, and compartment 3, respectively.

According to Figure 5-9, organic nitrogen concentrations variations did not follow any specified trend and the continuous adverse fluctuations were observed throughout the entire exposure time of cycle 1 and cycle 2. The recorded organic nitrogen concentrations at the end of cycle 1 were 440 mg/L, 520 mg/L, and 160 mg/L, respectively. The observed negative value was detected for compartment 2 and 3 with the magnitude of -1810 mg/L and -780 mg/L at 55 hours. The reason to observe negative values was obtaining a higher concentration of ammonia in comparison with TKN that was originated from faster degradation of TKN. During the last 21.82 hour- period (from

99.18 hours to 121 hours) of the second cycle, the overall tendency of all compartment was ascending. The measured concentration of compartment 1, compartment 2 and, compartment 3 at 121 hours were 2740 mg/L, 1810 mg/L and, 2090 mg/L, respectively.

The similar random behavior observed for the nitrate degradation throughout the entire cycle 1 and cycle 2. The minimal concentration of the nitrate resulted at 39 hours in compartment 3 with the value of 28.5 mg/L. In addition, the concentration of the nitrate in compartment 1 and compartment 2 were identical to 95 mg/L at 39 hours. The highest concentration of the nitrate observed at 107.35 hours in which compartment 1 was 249.5 mg/L. To have an overview about the removal of the nitrate in both cycles, it should be mentioned that the recorded concentration at the end of the first cycles were 108.5 mg/L, 121 mg/L and, 117.5 mg/L for compartment 1, compartment 2 and, compartment 3, respectively. Also, the final analyzed concentrations of cycle 2 were 106.5 mg/L, 118 mg/L and, 97.8 mg/L, correspondingly (Fig.5-10).

According to Figure 5-11, all compartments gave similar sulfate concentration at all monitoring points except the time interval between 50.75 hours and 59.25 hours. Compartment 3 gave the lowest sulfate concentration with the value of 73500 mg/L at 59.25 hours. While on the other hand, the detected concentration for both compartment 1 and compartment 2 was identical to 78200 mg/L. The overall trend of both cycles was ascending, and sulfate evolved in the reactor meanwhile the process in both cycles. Except a sharp decrease which was observed at 12.65 hours, the ascending tendency preserved throughout the first cycle. The final measured sulfate concentration of cycle 1 which was the maximum obtained value of cycle 1 and equal to 88500 mg/L at 73.5 hours. Throughout the second cycle, sulfate concentrations were identical for all compartments and a steady increase observed from the start point of cycle 2 to 86.34 hours. In addition, the obtained concentration at 86.34 hours was 70300 mg/L. Sulfate concentration gradually increased

during the time interval between 86.34 hours and 97.34 hours and 71500 mg/L recorded at 97.34 hours. During the time segment between 97.34 hours and 110.35 hours, strong fluctuations observed. Subsequently, a sharp increase resulted through 110.35 hours to 117.35 hours and the maximum value of sulfate concentration in cycle 2 was obtained with the value of 84900 mg/L at 117.35 hours. Meanwhile the last 3.65 hours of cycle 2, the tendency was downwards and the final measured concentration was 82100 mg/L.

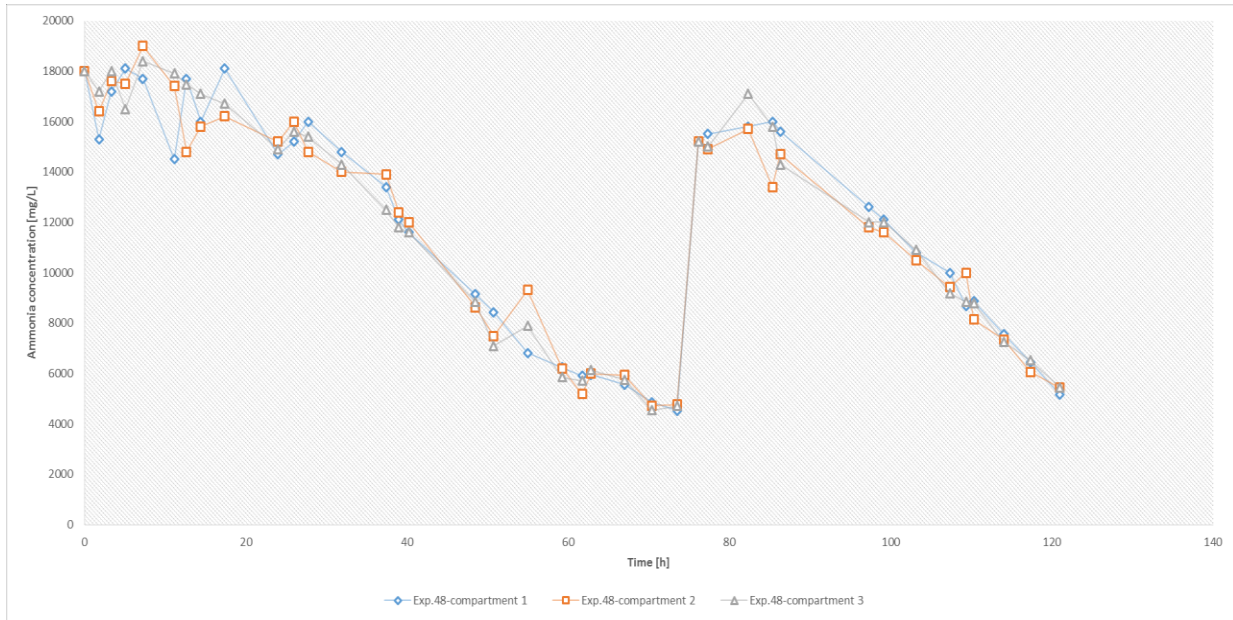


Figure 5- 6 Ammonia concentrations variations versus time for large scale EF-SBR

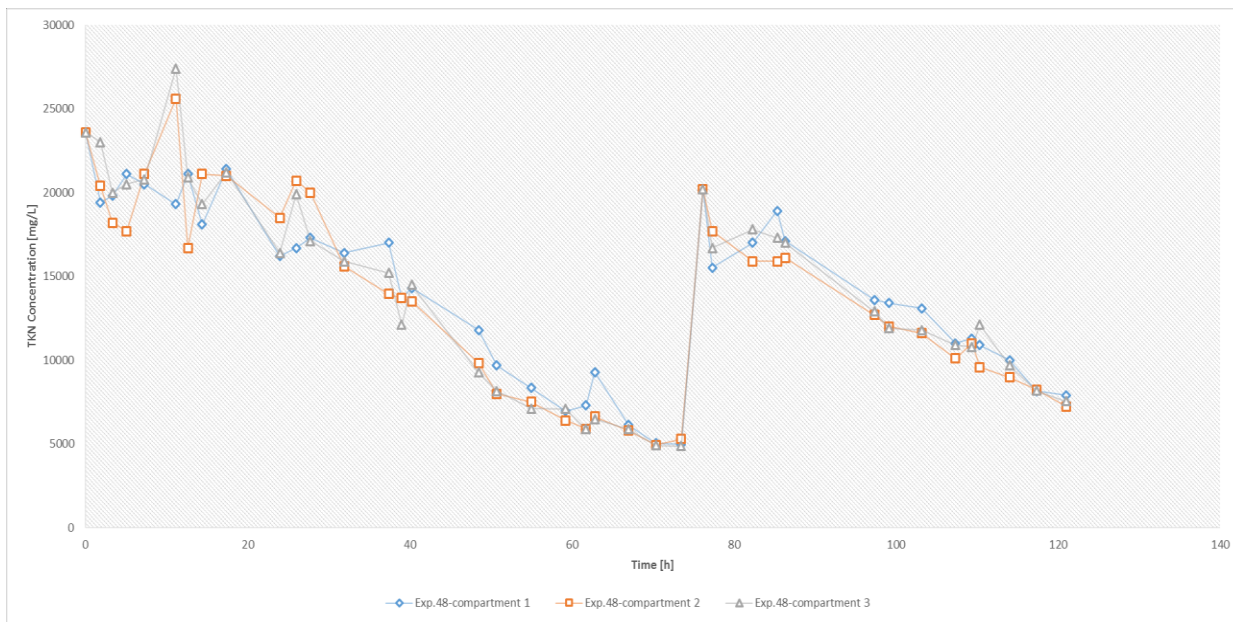


Figure 5- 7 TKN concentrations variations versus time for large scale EF-SBR

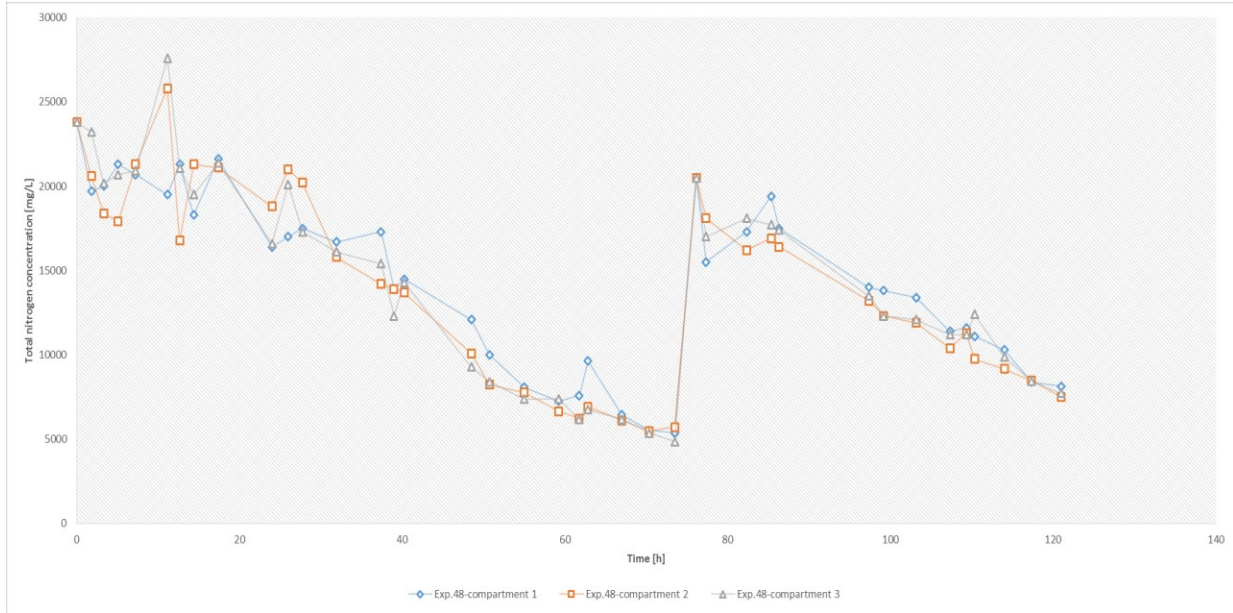


Figure 5- 8 Total nitrogen concentrations variations versus time for large scale EF-SBR

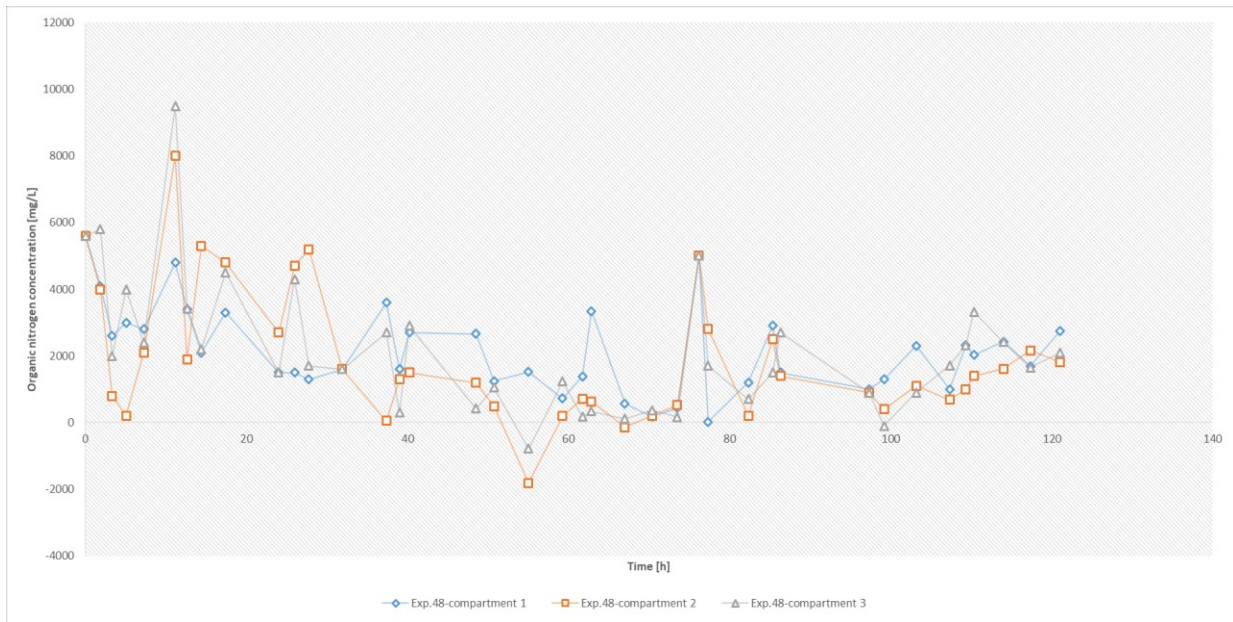


Figure 5- 9 Organic nitrogen concentrations variations versus time for large scale EF-SBR

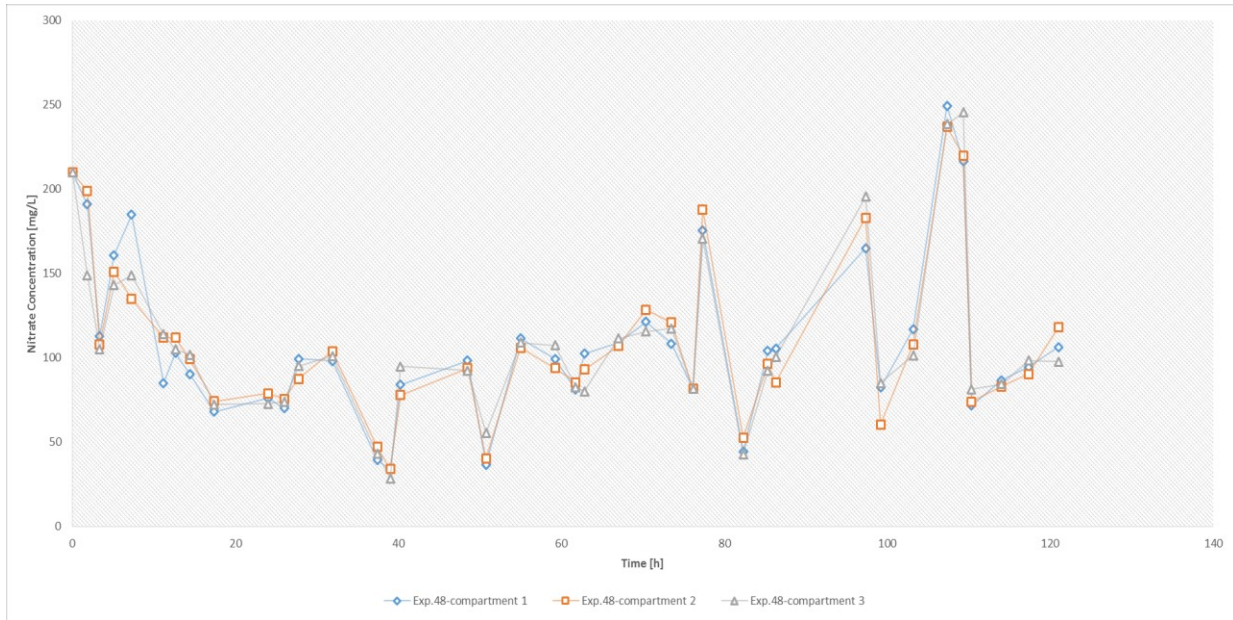


Figure 5- 10 Nitrate concentrations variations versus time for large scale EF-SBR

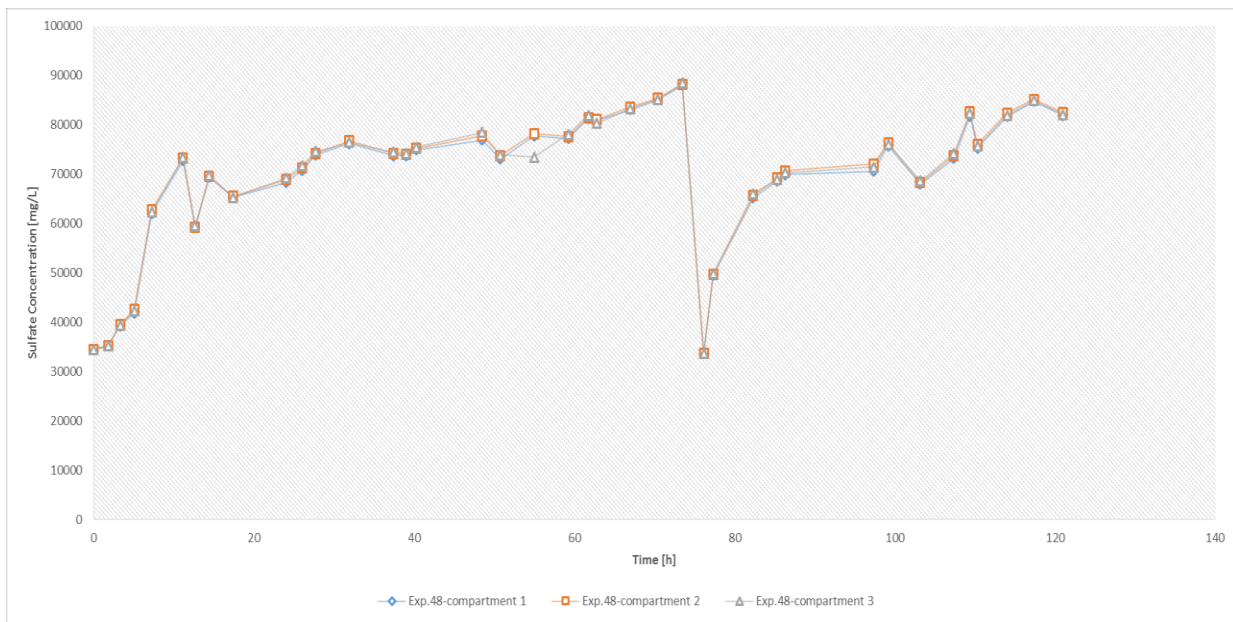


Figure 5- 11 Sulfate concentration variations versus time for large scale EF-SBR

Due to the transient behaviors of the concentration variations for all pollutant except sulfate, possibility of the time-dependent mechanism comes into consideration. To construe the variations nature, two approaches were considered. The first approach was the investigation of kinetics of the target pollutant degradation. And the second approach was using fractal analysis to find the behavior of the dynamical system of this study.

5-2. Kinetics of the degradation

To assess the kinetics of the target pollutant, the finite difference for differential method of analysis was proposed (See Section 3-4-3). Due to the transient changes of ammonia, TKN, and total nitrogen concentrations mainly in the first and second cycle, it is not feasible to use a differential method. The reason is that the resultant negative differential values would not be determinable in the domain of applied natural logarithm.

Even if, the negative $(-dC_A/dt)$ values are considered as consumption and effected as a multiplier of natural logarithm, the function of $\ln(-dC_A/dt)$ vs. $\ln(C_A)$ would be nonlinear and finding the reaction order and reaction constant would not be possible.

An alternative method which is considered by Fogler ^[3-33] is using nonlinear regression by polymath 6.10 and calculating reaction order (α) and reaction kinetics (k) for transient data. The approach is proposing two initial guess values (α and k) to see the R-squared value for both initial guesses. In case R-squared gives higher than 0.99 for α or k , the resultant value would be replaced in Eq.5-1 and the second parameter would be calculated.

$$[5-1] \quad t = \frac{1}{k'} \frac{(0.05)^{(1-\alpha)} - C_A^{(1-\alpha)}}{(1-\alpha)}$$

According to literature review conducted on expected reaction order of ammonia degradation [3-35], the initial guess value of α should be close to 1. Also, the proper reaction order (α) of TKN was near 2. A set of values with the step of 0.02 in range (0.02 to 1) considered for α to assess ammonia degradation kinetics. While α values of TKN placed from 1 to 3 with the step size of 0.02. In addition, based on the literature review, k considered as initial 0.1 for both ammonia [5-1] and TKN increased to 0.15 with step size of 0.05. It is crucial to mention that for each set of initial values of α , one magnitude of k was considered, and each new value of k applied on the entire set of α . No convergence observed neither for ammonia nor for TKN reaction order or reaction constant. So, applying nonlinear regression would not lead to predict reaction mechanism. Moreira et al. [2-126] also faced the similar behavior in curve fitting the experimental results with pseudo first order kinetics for DOC removal. They could not propose reaction constant for the DOC degradation mechanism.

5-3. Fractal analysis

Therefore, the strong dependency of reaction kinetics to initial values draws the attention to fractal dynamical system analysis. Due to the successful application of the fractal analysis in diffusion-influenced reaction kinetics by Barzykin et al. [5-2], fractal analysis could be justified to be applied in this study. Barzykin et al's research also proposed that it would be possible to apply the resultant fractal dimensions in the well-known Smoluchowski framework to investigate the transient variations. Furthermore, interpreting time-dependent diffusion results could be permissible while analyzing the transient behavior of target compounds concentrations (See Section 3-4-2).

Fractal analysis permits quantifying the signal complexity by a single value, the fractal dimension. Based on the model provided by regularization fractal analysis, one of the limitations of box-

counting method is covered. The described solution was provided by Rimpault et. al [5-3], [5-4] and successful results were obtained in the scope of cutting force and acoustic emission signals. In addition, the same model is used to describe the transient behavior of concentration variations.

To describe the methodology of applied regularization fractal analysis, regularization dimension is estimated from the convolutions of the signal “s” with different kernels g_a and a width of “a”. Each convolution product s_a is given in Eq. 5-2.

$$[5-2] \quad s_a = s * g_a$$

The kernels g_a are calculated based on a rectangle kernel which is an affine function. The hypothesis is s_a has a finite length which is called l_a and it is set for the size of ‘a’. The regularization dimension D_R is computed using:

$$[5-3] \quad D_R = 1 - \lim_{a \rightarrow 0} \frac{\log l_a}{\log a}$$

The slope estimation is resulted from where ‘a’ values are the smallest and R-squared of a part of curve ($\log l_a$ vs. $\log a$) is close to 1.

Figure 5-3 provides the curves of $\log l_a$ vs. $\log a$ for ammonia, TKN, total nitrogen, organic nitrogen, nitrate and sulfate in the order of Figure 5-12, Figure 5-13, Figure 5-14, Figure 5-15, Figure 5-16, and Figure 5-17, respectively. For instance, “Ammonia 1” is representative of the results of ammonia in compartment 1 of Exp.48 and the same pattern is used to label curves for all target pollutants. TKN (Fig. 5-13) and total nitrogen (Fig.5-14) provided the best results with respect to the linear variations of $\log l_a$ for a wider range of $\log a$.

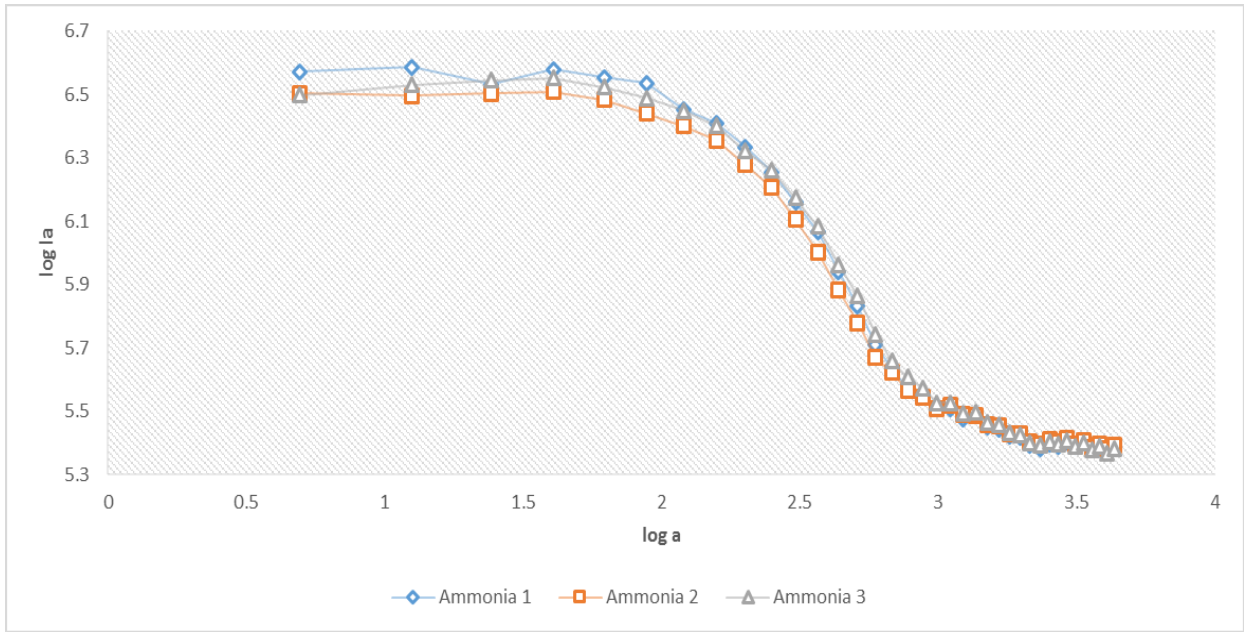


Figure 5- 12 regularization dimension curves for ammonia concentrations in compartment 1, compartment 2 and, compartment 3 of Exp.48

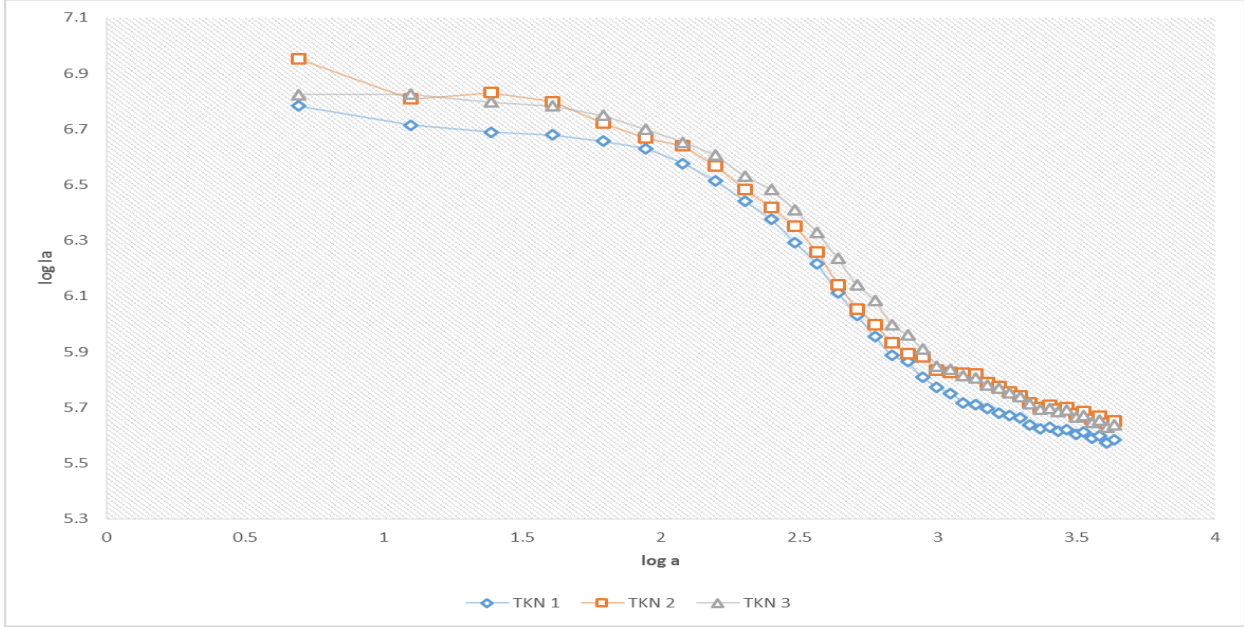


Figure 5- 13 regularization dimension curves for TKN concentrations in compartment 1, compartment 2 and, compartment 3

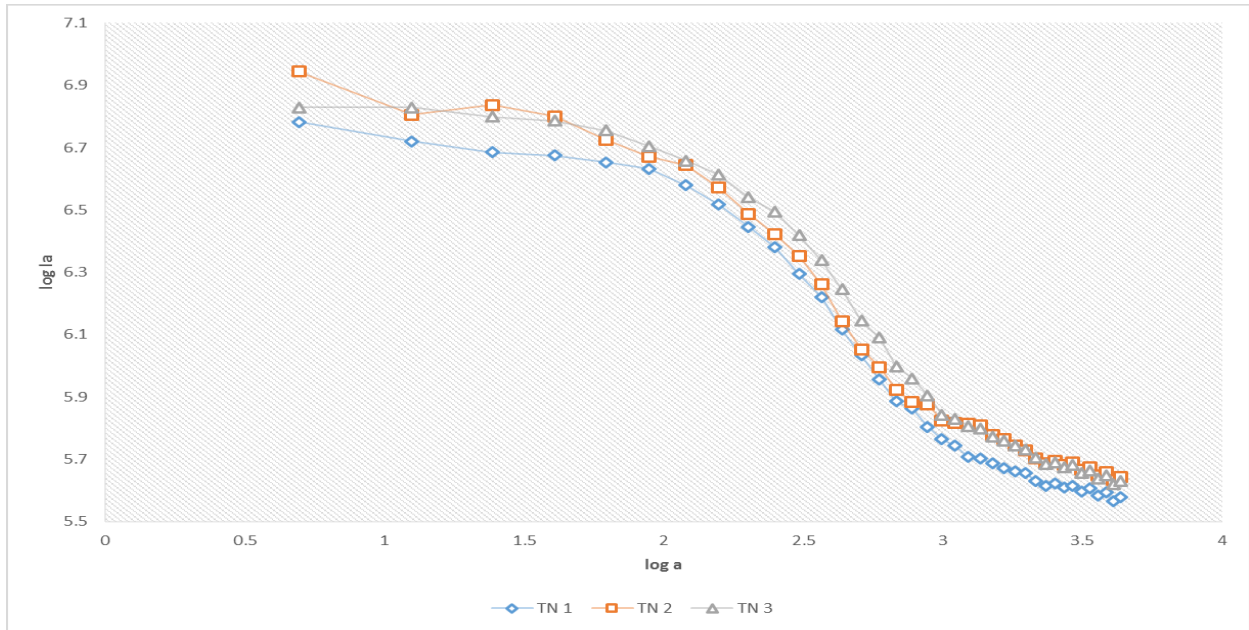


Figure 5- 14 Regularization dimension curves for total nitrogen concentrations in compartment 1, compartment 2 and, compartment 3

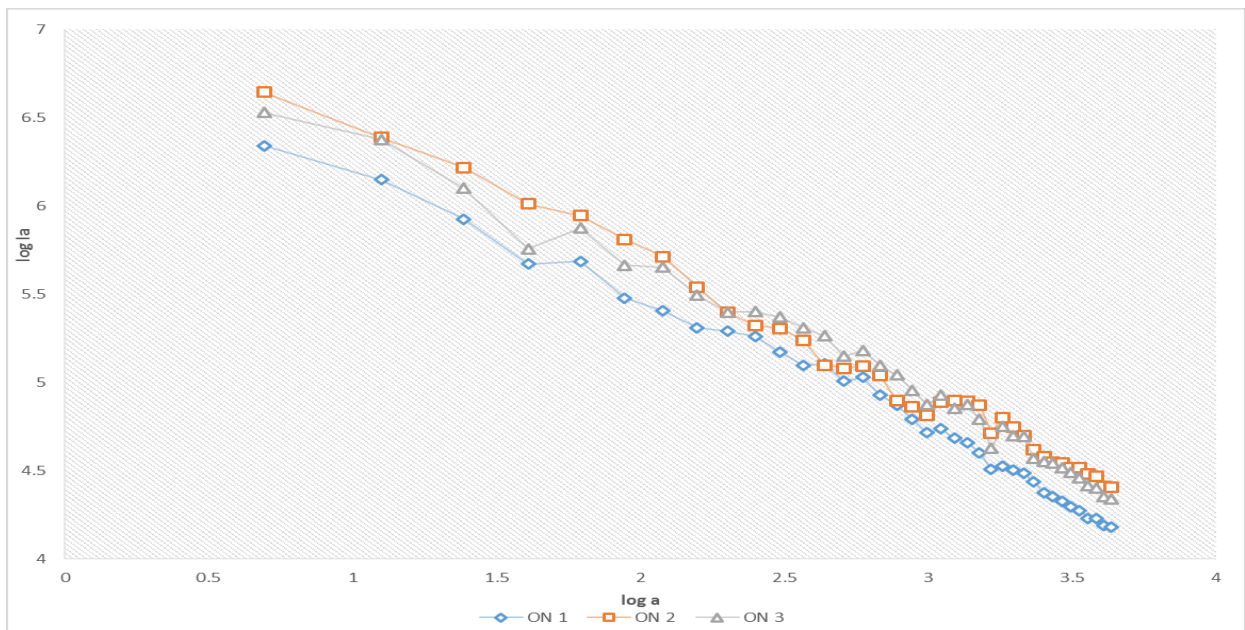


Figure 5- 15 Regularization dimension curves for organic nitrogen concentrations in compartment 1, compartment 2 and, compartment 3

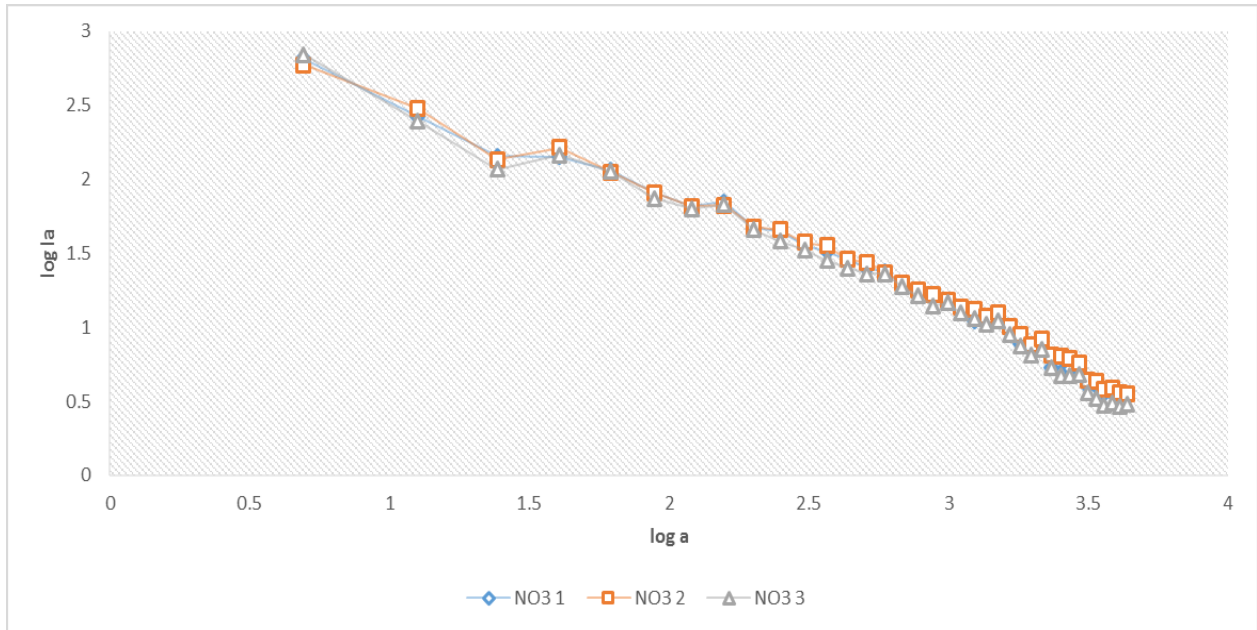


Figure 5- 16 Regularization dimension curves for nitrate concentrations in compartment 1, compartment 2 and, compartment 3

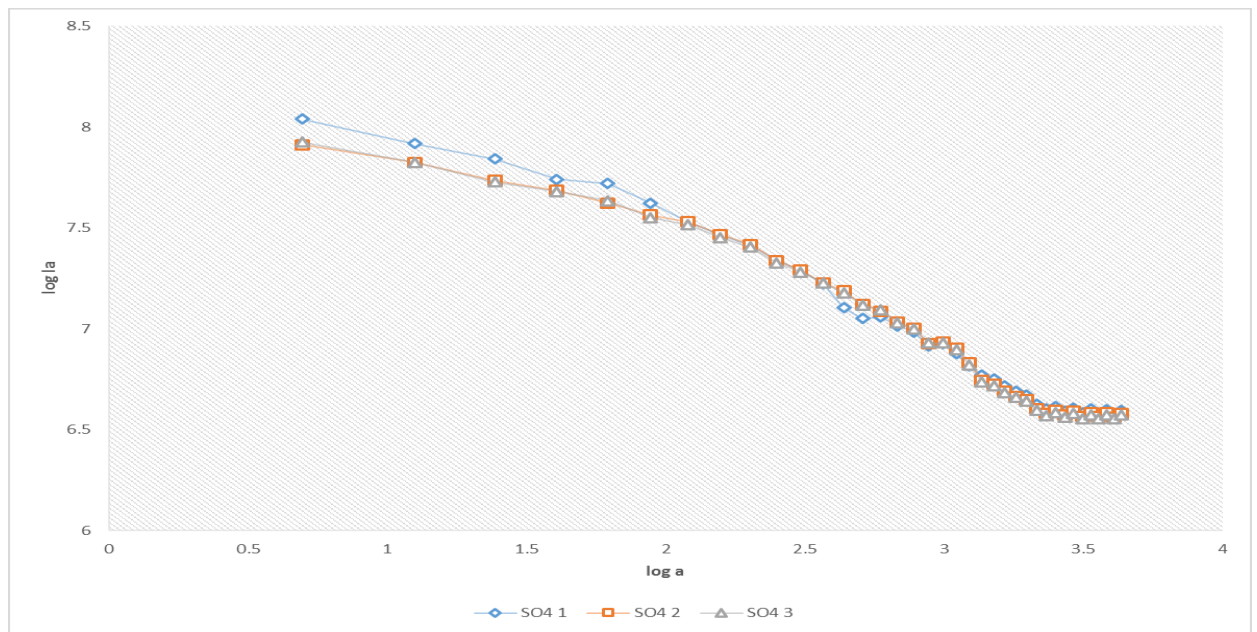


Figure 5- 17 Regularization dimension curves for sulfate concentrations in compartment 1, compartment 2 and, compartment 3

Ammonia (Fig. 5-12) gives fair results while organic nitrogen (Fig. 5-15), nitrate (Fig.5-16), and sulfate (Fig. 5-17) provided relatively poor results due to a narrower range of log (a) for linear changes of log I_a .

The study of a complex system such as physicochemical phenomena in EF-SBR concluded necessity of further investigation using more sophisticated tools.

Chapter 6 Conclusions and future work

Chapter 6 contains conclusions from obtained results of the four phases of the study. It also discusses future development and potential investigations on practicability of the proposed process. The future work discussion is based on precise investigations and feasibility study of kinetics of electro-oxidation mechanism and fractal analysis while decreasing the monitoring time.

6-1. Conclusions

The best reactor design of the large scale (Phase 3) permitted to decrease the concentration of ammonia and TKN from 11000 mg/L and 14000 mg/L/L to 59.4 mg/L and 75.6 mg/L, respectively. Also, the novel electro-Fenton Sequential Batch Reactor (EF-SBR) permitted to achieve 103.4 mg/L, 470.4 mg/L, and 366.3 mg/L for ammonia, TKN, and organic nitrogen while the exposure time of the second cycle was reduced to 24 hours.

Medium scale EF-SBR design provides the highest removal providing a final concentration of 107.8 mg/L, 121.8 mg/L, and 9.9 mg/L for ammonia, TKN, and organic nitrogen at the end of cycle 2, correspondingly. Furthermore, the exposure time was declined to 48 hours which can be considered as one of the notable advantages of EF-SBR.

Phase 1

- Phase 1 results demonstrate that anode to cathode surface area ratio plays an important role in obtaining a satisfactory removal efficiency. However, the predominant parameter is the dimensional quotient (DQ) which should be critically considered for designing EK reactor. The optimal DQ was equal to 1.
- The results show that allocating 12 hours as the time interval of adding hydrogen peroxide would give a superior efficiency for ammonia, TKN, total nitrogen, and organic nitrogen meanwhile the 60 hour exposure time.

- Pretreatment of the present sulfate in the influent would not give an acceptable removal of target compounds. The contribution of sulfate ions in declining pH during relatively short exposure time is visible. Its production would generate a range of pH to proceed electro-oxidation and electro-Fenton reactions in the nitrogen contaminated electrolyte.
- Supplying Fenton agent (e.g. ferrous sulfate) would significantly enhance the removal efficiencies in a small scale. However, due to the externally surge in the sulfate concentration when the ferrous sulfate is introduced to EK system, it is suggested to restrain of heterogeneous catalyst into the system. It was preferable to maintain the homogenous catalytic reactions in the medium.
- Minimal and maximal current density values of the selected ranges gave unsatisfactory results with respect to the pollutant removal. On the other hand, among two moderate values, which provided tenable results (at a small scale), 33.33 mA/cm² was selected as an optimal current density.
- Implementing continuous airflow as a source of an oxidizing agent provides a fair removal efficiency for low range of flowrate values. It led to applying airflow in the medium scale to evaluate the removal efficiency in the presence of oxygen instead of hydrogen peroxide.

Phase 2

- According to Stage 2-1 and Stage 2-2 results, using a graphite plate was preferred due to an increase in TKN, total nitrogen, and organic nitrogen removal efficiency.
- The results of Stage 2-3 prove that minimizing current density would lead to poor mineralization of the target pollutants and it is crucial to consider a lower limit for current density. Then, 21.37 mA/cm² would be an appropriate value to assess for upscaling due to significant decrease in energy consumption.
- Based on achieved results in Stage 2-4, applying a high airflow rate causes poor removal efficiency of pollutants, specifically for ammonia and organic nitrogen. It is recommended to use a low flowrate to observe the feasibility of substituting oxygen with hydrogen peroxide at a medium scale of the EK reactor.

Phase 3

- Based on obtained results for the removal efficiency analysis, applying 5 cm as the separation of electrodes would be an appropriate approach to follow in Phase 3 and Phase 4 of the research. Applying 7.5 cm distance requires higher current density due to nonlinear changes in the resistivity of the cell once the distance among electrode is increased.
- Based on the achieved removal efficiencies, it is preferable to use hydrogen peroxide with 50% purity. The reason for a higher removal efficiency of TKN, total nitrogen, and organic nitrogen is providing more hydroxyl radicals in the system. Also, shortening the exposure time to 60 hours is feasible due to present efficiencies. Based on Stage 3-3 results, an increase in hydrogen peroxide input volume will significantly enhance the removal efficiencies of ammonia, TKN, total nitrogen, and organic nitrogen, respectively. In addition, obtaining molar ratio equals to $3.81/1 \frac{\text{H}_2\text{O}_2}{\text{Fe}^{2+}}$ would be a logical approach for Phase 4.

Phase 4

- Applying 50% hydrogen peroxide results the best removal efficiency for the target pollutants in medium scale EF-SBR. Electro-Fenton sequential batch reactor (EF-SBR) achieved the desirable removal efficiencies in 4 days instead of 6 days (running two serial experiments with Phase 2 experimental design). It leads to reduction in exposure time for 48 hours. Also, the removal efficiency of TKN, total nitrogen, and specifically organic nitrogen are significantly boosted with EF-SBR comparing to previous (Phase 2) process design (72 hours exposure time).
- Large scale EF-SBR results proved that it is possible to decrease exposure time to 12 hours once 50% hydrogen peroxide was used. Also, the applicability of molar ratio of ferrous to hydrogen peroxide ($\frac{\text{Fe}^{2+}}{\text{H}_2\text{O}_2}$) equal to 3.81/1 was validated and approved in large scale EF-SBR by giving the best efficiency in Phase 3.
- The removal efficiency of EF-SBR was investigated in the worst experimental condition (applying 30% hydrogen peroxide) by increasing the number of SBR cycle. The outcomes help minimizing the cost of the chemicals.
- Determining the worst experimental condition obtained in Stage 4-1 (e.g. using 30% hydrogen peroxide) helps to investigate the impact of increasing number of SBR cycles

in Stage 4-2. Although significant improvement has been observed in the first 24 hours of each individual SBR cycle, the desirable removal efficiency (Stage 4-1, using 50% hydrogen peroxide) was not achieved at the end of the newly introduced cycles (cycle 3 and cycle 4 for medium scale; cycle 3 for large scale).

- Increasing number of EF-SBR cycles at large scale contributed to enhance the removal efficiency of TKN. Therefore, it is feasible to take into account the positive impact of increased number of cycles on the upscaling EF-SBR multicomponent reactor considering the best experimental condition determined in Stage 4-1.
- Although pH lower than 3 was declared as an unsuitable pH, based on the results of the large scale EF-SBR, the resultant removal was significant at the end of the first and second cycle, with pH around 1.1 and 1.4 respectively. It proves that utilizing EF-SBR decreases the demand of pH adjustment or ideally eliminates it.
- The most notable drawbacks of Fenton and electro-Fenton process is relatively high amount of sludge production. Although the number of cycles increased, the sludge mass produced per liter slightly increased in both medium and large scale. It shows that EF-SBR would be a promising process to overcome one of the major drawbacks of the Fenton and electro-Fenton process, sludge generation.

6-2. Contributions

A novel electro-Fenton Sequential batch reactor was developed. To our knowledge, no sequential batch reactor has been implemented in electrokinetics yet. A novel system was validated for high nitrogen industrial wastewater containing 11000 mg/L, 14000 mg/L and, 3000 mg/L ammonia, TKN, and organic nitrogen, respectively. Above 99% removal efficiency resulted in medium scale EF-SBR for ammonia, TKN, and organic nitrogen, respectively. Above 99%, 96%, and 87% removal efficiency was obtained at a large scale EF-SBR for ammonia, TKN, and organic nitrogen, correspondingly.

This system proved its sustainability with respect to two scopes:

- i) Use a homogenous catalyst present in the industrial wastewater instead of introducing Fenton agent as heterogeneous catalyst;
- ii) Decrease the exposure time for 48 hours and 24 hours for medium and large scale EF-SBR, respectively.

The experimental upscaling results helped to understand that the concentration variations within the system are nonlinear. Based on the additional work, regularization fractal analysis provided promising results and made the interpretation of nonlinear behavior feasible.

6-3. Future work

Based on regularization fractal analysis results, the future study can be determined as followed:

- Use fractal dimensions to solve the Smoluchowski framework numerically for TKN and total nitrogen
- Simulate the new sets of data based on obtained experimental values to increase a number of points for a higher precision of the regularization fractal dimension output.
- Determine a pathway to assess time segments in which the time-dependent diffusion mechanism is predominant.
- Conduct fine multifractal analysis to investigate the behavior of fractal dimension curves and evaluate the enhancement of previous results of regularization fractal analysis (e.g. organic nitrogen, nitrate, and sulfate).

Based on experimental results of four phases of this study, the following future work are proposed:

- Investigate the possibility of reducing retention time by modifying the operational conditions.

- Upscale the EF-SBR process for 40 L and subsequently for pilot scale to find out the efficiency of the system at an industrial scale.
- Conduct coulometric methods to analyze the controlled-current electrolysis and find the current-voltage curves to assess current efficiency.
- Analyze the gas emissions and determine the gas phase components resulted throughout the exposure time.

References

Chapter 1

- [1-1] Dongke, Y, “Evaluation of effluent organic nitrogen and its impacts on receiving water bodies”, MA.Sc thesis, *University of Massachusetts - Amherst*, USA, 2012.
- [1-2] Reglementation municipale, “Reglement relative aux rejets dans les ouvrages d’assainissement sur le territoire de l’agglomeration de Montreal (RCG 08-041)”, *Montreal*, Canada, 2012.
- [1-3] Papadopoulou, A., Fatta, D., Liorizi, M., “Development and optimization of dark Fenton oxidation for the treatment of textile wastewaters with high organic load”, *Journal of Hazardous Materials*, vol.146, issue 3, 2007,pp. 558-563.
- [1-4] Elektorowicz, M., Ibied, S., Olesziewicz J., “Simultaneous superior removal of carbon, phosphorus, nitrogen in a novel single electro-bioreactor”, *Patent 12030689*, 2011.
- [1-5] Nakada, N., Shinohara, H., Murata, A., Kiri, K., Managaki, S., Sato, N., Takada, H., “Removal of selected pharmaceuticals and personal care products (PPCPs) and endocrine-disrupting chemicals (EDCs) during sand filtration and ozonation at a municipal sewage treatment plant”, *Water Research*, vol.41, 2007, pp. 4373–4382.
- [1-6] Shaojun, J., Shourong, Z., Daqiang, Y., Lianhong, W., Liangyan, C., “Aqueous oxytetracycline degradation and the toxicity change of degradation compounds in photoirradiation process”, *Journal of Environmental Science*, vol. 20, 2008,pp. 806-813.
- [1-7] Homem, V., Santos, L., “Degradation and removal methods of antibiotics from aqueous matrices - A review”, *Journal of Environmental Management*, vol. 92, 2011, pp.2304-2347.
- [1-8] Boreen, A., Arnold, W., McNeill, K., “The photochemical fate of sulfa drugs in the aquatic environment: sulfa drugs containing five-membered heterocyclic groups”, *Environmental Science Technology*, vol.38, 2004, pp.3933-3940.
- [1-9] Kümmerer, K., “Antibiotics in the aquatic environment - a review- Part I.”, *Chemosphere*, vol.75, 2009, pp.417-434.

[1-10] Ruppert, G., Bauer, R., Heisler, G., "The photo-Fenton reaction - an effective photochemical wastewater treatment process", *Journal of Photochemistry and Photobiology, A* 73, 1993, pp.75-78.

[1-11] Asghar, A., Raman, A. A. A., Daud, W. M. A. W., "Advanced oxidation processes for in-situ production of hydrogen peroxide/hydroxyl radical for textile wastewater treatment: a review", *Journal of Cleaner Production*, vol. 87, 2015, pp. 826-838

[1-12] Bauer, R., Fallmann, H., "The photo-Fenton oxidation – a cheap and efficient wastewater treatment method", *Research on Chemical Intermediates*, vol.23, 1997, pp. 341-354.

[1-13] Zhukovskaya, N., "Enhanced electrokinetic process for industrial wastewater treatment containing a high concentration of Total Kjeldahl Nitrogen (TKN)", Master thesis, *Concordia University, Montreal, Canada*, 2015.

Chapter 2

[2-1] Salvaggio, N., Basic photographic materials and processes, *Elsevier Publishing*, third Edition, 2009, pp. 382-394

[2-2] Wang, L., Tselung Y., *Handbook of industrial and hazardous wastes treatment*, New York, 2004.

[2-3] Jeyaseelan, S., Sathananthan, S., "Clean Technology for Treatment of Photographic Wastes and Silver Recovery", *Journal of Environmental Monitoring and Assessment*, Springer, 1997, pp.44- 219

[2-4] Bensalah, N., Bedoui, A., Chellam, S., Abdel-Wahab, A., "Electro-Fenton Treatment of Photographic Processing Wastewater". *Clean – Soil, Air, Water*, vol.41, 2013, pp.635–644

[2-5] Lunar, L., Sicilia, D., Rubio, S., Pérez-Bendito, D., Nickel, U., "Degradation of photographic developers by Fenton's reagent: condition optimization and kinetics for metal oxidation", *Water Research*, vol. 34, Issue 6, 2000. pp. 1791-1802

[2-6] United States Environmental Protection Agency, Photographic Processing Effluent Guidelines; Effluent Guides, Electronic code of federal regulations Title 40, Chapter I, Subchapter N, Part 459

- [2-7] Zabicky, J., "the chemistry of amides", *John Wiley and Sons publishing*, 1970
- [2-8] Sunners, B., Piette, L., Schneider, W., "Proton magnetic resonance measurements of formamide". *Canadian Journal of Chemistry*, vol.38, 1966, pp. 681-688
- [2-9] Cheng, C., Hong, S., "Oxidative amide synthesis directly from alcohols with amines". *Organic and Biomolecular Chemistry*, vol. 9, 2010, pp. 20-26
- [2-10] Cadoni, R., Porcheddu, A., Giacomelli, G., De Luca, L., "One-Pot Synthesis of Amides from Aldehydes and Amines via C-H Bond Activation". *Organic Letters*, Vol.14, 2012, pp. 19
- [2-11] Pattabiraman, V. R., Bode, J. W., "Rethinking amid bond synthesis", *Nature review*, vol.480, 2011, pp. 471–479
- [2-12] Hunt, I., Spinney, R., "Organic Chemistry On-Line Learning Center", *McGraw-Hill*, 2009
- [2-13] Carey, F. A., Giuliano, R. M., *Organic chemistry*, *McGraw-Hill*, 7th edition
- [2-14] Lawrence, S. A., *Amines; Synthesis, Properties and Application*, *Cambridge University Press*, 2004
- [2-15] Wallis, E. S., Lane, J. F., *The Hofmann Reaction- Organic Reactions*, vol.3, 2011, pp.267–306
- [2-16] Ahmed, M. B., Zhou, J. L., Ngo, H. H., Guo H., Thomaidis, N. S., Xu, J., "Progress in the biological and chemical treatment technologies for emerging contaminant removal from wastewater: A critical review", *Journal of Hazardous Materials*, vol. 323, Part A, 2017, pp.274-298
- [2-17] Luo, Y., Guo, W., Ngo, H.H., Nghiem, L.D., Hai, F.I., Zhang, J., Liang, S., Wang, X.C., "A review on the occurrence of micro pollutants in the aquatic environment and their fate and removal during wastewater treatment", *Science of The Total Environment*, vol. 473, 2014, pp.619–641.
- [2-18] Rivera-Utrilla, M., Sánchez-Polo, J., Ferro-García, M.Á., Prados-Joya, G., Ocampo-Pérez, R., "Pharmaceuticals as emerging contaminants and their removal from water: a review", *Chemosphere*, vol.93, 2013, pp.1268–1287

- [2-19] Benner, J., Helbling, D.E., Kohler, H.-P. E., Wittebol, J., Kaiser, E., Prasse, C., Ternes, T.A., Albers, C.N, Amand, J., Horemans, B., "Is biological treatment a viable alternative for micropollutant removal in drinking water treatment processes", *Water Research* Vol.47, 2013, pp. 5955–5976
- [2-20] Radjenović, J., Matosić, M., Mijatović, I., Petrović, M., Barceló, D., "Membrane bioreactor (MBR) as an advanced wastewater treatment technology, in: D. Barceló, M. Petrović (Eds.) ", *Emerging Contaminants from Industrial and Municipal Waste*, Springer, 2008, pp. 37–101.
- [2-21] Deegan, A., Shaik, B., Nolan, K., Urell, K., Oelgemöller, M., Tobin, J., Morrissey, A., "Treatment options for wastewater effluents from pharmaceutical companies", *International Journal of Environmental Science and Technology*, vol. 8, 2011, pp.649–666.
- [2-22] Raj, D. S. S., Anjaneyulu, Y., "Evaluation of biokinetic parameters for pharmaceutical wastewaters using aerobic oxidation integrated with chemical treatment", *Process Biochemistry*, vol.40, 2005, pp. 165–175
- [2-23] Sreekanth D., Sivaramakrishna, D., Himabindu, V., Anjaneyulu Y., "Thermophilic treatment of bulk drug pharmaceutical industrial wastewaters by using hybrid up flow anaerobic sludge blanket reactor", *Bioresource Technology*, Vol. 100, 2009, pp. 2534–2539
- [2-24] Töre, G.Y., Meric S., Lofrano, G., De Feo, G., "Removal of trace pollutants from wastewater in constructed wetlands, in: G. Lofrano (Ed.) ", *Emerging Compounds Removal from Wastewater*, Springer, 2012, pp. 39–58.
- [2-25] Matamoros, V., Gutiérrez, R., Ferrer I., García, J., Bayona, J.M., "Capability of microalgae-based wastewater treatment systems to remove emerging organic contaminants: a pilot-scale study", *journal of hazardous materials*. Vol. 288, 2015, pp. 34–42
- [2-26] Yang, W., Cicek, N., Ilg J., "State-of-the-art of membrane bioreactors: worldwide research and commercial applications in North America", *J. Membrane Sci.* vol.270, 2006, pp. 201–211.
- [2-27] Arana, J., Melián, J.H., Rodríguez, J. D., Diaz, O.G., Viera, A., Pena, J. P., Sosa P.M., Jiménez, V.E., "TiO₂-photocatalysis as a tertiary treatment of naturally treated wastewater", *Catalysis Today*, vol.76, 2002, pp. 279–289.

- [2-28] Malato, S., Maldonado, M. I., Oller, I., Zapata, A., "Removal of pesticides from water and wastewater by solar-driven photocatalysis, G. Lofrano (Ed.) ", *Emerging Compounds Removal from Wastewater*, Springer, 2012, pp.59–76
- [2-29] Le Truong, G., De, Laat J., Legube, B., "Effects of chloride and sulfate on the rate of oxidation of ferrous ion by H_2O_2 ", *Water Research*, Vol.38, 2004, pp.2384–2394
- [2-30] Prieto-Rodriguez, L., Miralles-Cuevas, S., Oller, I., Agüera, A., Puma, G. L., Malato, S., "Treatment of emerging contaminants in wastewater treatment plants (WWTP) effluents by solar photocatalysis using low TiO_2 concentrations", *Journal of Hazardous Materials*, vol. 211, 2012, pp.131–137
- [2-31] Snyder, S. A., Adham, S., Redding, A. M., Cannon, F. S., DeCarolis, J., Oppenheimer, J., Wert E.C., Yoon Y., "Role of membranes and activated carbon in the removal of endocrine disruptors and pharmaceuticals", *Desalination*, vol.202, 2007, pp. 156–181.
- [2-32]. Poyatos, J. M, Muñio, M. M., Almecija, M. C., Torres, J. C., Hontoria, E., Osorio, F., "Advanced Oxidation Processes for Wastewater Treatment: State of the Art", *Water Air Soil Pollution* , Springer Netherlands, vol.205 , 2009, pp.187–204
- [2-33] Skoumal, M., Cabot, P. L., Centellas, F., Arias C., Rodríguez R. M., Garrido J. A., Brillas E., "Mineralization of paracetamol by ozonation catalyzed with Fe^{2+} , Cu^{2+} and UVA light". *Applied Catalysis B Environmental*, Elsevier Publishing, vol.66, 2006, pp.228–240
- [2-34] Rosenfeldt, E. J., Chen, P. J., Kullmanc, S., Linden, K. G., "Destruction of estrogenic activity in water using UV Advanced oxidation". *The Science of the Total Environment*, vol.377, 2007, pp.105–113
- [2-35] Hoign'e, J., Bader, H., Haag, W.R., Staehelin, J., "Rate constants of reactions of ozone with organic and inorganic compounds in water. III". Inorganic compounds and radicals". *Water Research*, vol.19, 1985, pp.993–1004
- [2-36] Alaton, I. A., Balcioglu, I. A., Bahnemann D. W. "Advanced oxidation of a reactive dyebath effluent: Comparison of O_3 , $H_2O_2/UV-C$ and $TiO_2/UV-A$ processes", *Water Research*, vol.36, 2002, pp.1143–1154

- [2-37] Guittoneau S., Duguet J. P., Bonnel C., Dore, M., "Oxidation of parachloronitrobenzene in dilute aqueous solution by O_3+UV and H_2O_2+UV : a comparative study", *Ozone Science and Engineering*, vol.12, 1990, pp.73–94
- [2-38] Kasprzyk-Hordern, B., Zi'olek, M., Nawrocki, J., "Catalytic ozonation and methods of enhancing molecular ozone reactions in water treatment", *Applied Catalyst B: Environmental*, vol. 46, 2003, pp.639–669
- [2-39] Glaze W. H., Kwang J. W., Chapin, D. H., "Chemistry of water treatment process involving ozone, hydrogen peroxide and ultraviolet radiation", *Ozone Science and Technology*, vol.9, 1987, pp.335–352.
- [2-40] Muruganandham M., Chen S., Wu J., "Mineralization of N-methyl-2-purolidone by advanced oxidation process", *Separation and Purification Technology*, vol. 55, 2007, pp.360–367
- [2-41] Yonar, T., Yonar, G. K., Kestioglu, K., Azbar, N. "Decolorisation of textile effluent using homogeneous photochemical oxidation processes". *Coloration Technology*, vol.121, 2005, pp.258–264.
- [2-42] Peternel, I., Koprivanac, N., and Kusic, H., "UV-based processes for reactive azo dye mineralization". *Water Research*, vol. 40, 2006, pp.525–532.
- [2-43] He, Z., Song, S., Ying, H., Xu, L., Chen, J., "P-Aminophenol degradation by ozonation combined with sonolysis: operating conditions influence and mechanism". *Ultrasonics Sonochemistry*, vol.14, 1987, pp.568–574
- [2-44] Fenton, H. J. H., "Oxidation of tartaric acid in the presence of iron", *Journal of Chemical Society Transactions*, vol.65, 1894, pp. 899–910
- [2-45] Sychev, A.Y., Isak, V.G., "Iron compounds and the mechanism of the homogeneous catalysis of the activation of O_2 and H_2O_2 and of the oxidation of organic substrates", *Russian Chemical Reviews*, vol.64, 1995, pp.1105–1129.
- [2-46] Pignatello, J.J., Oliveros, E., Mackay, A., "Advanced oxidation processes for organic contaminant destruction based on the Fenton reaction and related chemistry", *Critical Reviews in Environmental Science and Technology*, Taylor and Francis, vol.36, 2006, pp.1–84

- [2-47] Neyens, E., Baeyens, J., "A review of classic Fenton's peroxidation as an advanced oxidation technique", *Journal of Hazardous Materials*, vol.98, 2003, pp.33–50
- [2-48] Babuponnusami, A., Muthukumar, K., "A review on Fenton and improvements to the Fenton process for wastewater treatment", *Journal of Environmental Chemical Engineering*, Vol.2, Issue 1, 2014, pp.57-572
- [2-49] Rivas, F.J., Beltran, F.J., Frades, J., Buxeda, P., "Oxidation of p-hydroxybenzoic acid by Fenton's reagent", *Water Research*, vol.35, 2001, pp.387–396.
- [2-50] Eisenhauer, H.R., "Oxidation of phenolic wastes", *Journal of Water Pollution Control Federation*, vol.36, 1964, pp.1116–1128
- [2-51] Ma, Y.S., Huang, S.T., Lin, J.G., "Degradation of 4-nitro phenol using the Fenton process", *Water Science and Technology*, vol.42, 2000, pp.155–160
- [2-52] Babuponnusami, A., Muthukumar, K., "Degradation of phenol in aqueous solution by Fenton, sono-Fenton, Sono-photo-Fenton methods", *Clean-Soil Air Water*, vol.39, 2011, pp.142–147
- [2-53] Lin, S. H., Lo, C.C., "Fenton process for treatment of desizing wastewater", *Water Research*, vol.31, 1997, pp.2050–2056
- [2-54] Ito, K., Jian, W., Nishijima, W., Baes, A. U., Shoto, E., Okada, M., "Comparison of ozonation and AOPs combined with biodegradation for removal of THM precursors in treated sewage effluents", *Water Science and Technology*, vol.38, 1998, pp.179–186
- [2-55] Benatti, C. T., Da-Costa, A. C. S., Tavares, C .R. G., "Characterization of solids originating from the Fenton's process", *Journal of Hazardous Materials*, vol.163, 2009, pp. 1246–1253
- [2-56] Boonrattanakij, N., Lu, M-C., Anotai J., "Kinetics and mechanism of 2, 6-dimethyl-aniline degradation by hydroxyl radicals", *Journal of Hazardous Materials*, vol.172, Issues 2–3, 2009, pp.952-957
- [2-57] Siedlecka, E. M., Stepnowski, P., "Phenols degradation by Fenton reaction in the presence of chlorides and sulfates", *Polish Journal of Environmental Studies*, vol.14, 2005, pp.823–828

- [2-58] Lin, S. H., Lin, C.M., Leu, H.G., "Operating characteristics and kinetics studies of surfactant wastewater treatment by Fenton oxidation", *Water Research*, vol.33, 1999, pp.1735–1741
- [2-59] Zhang, H., Choi, H. J., Huang, C-P, "Optimization of Fenton process for the treatment of landfill leachate", *Journal of Hazardous Materials*, vol.125, Issues 1–3, 2005, pp.166-174
- [2-60] Kang, Y.W., Hwang, K.Y., "Effects of reaction conditions on the oxidation efficiency in the Fenton process", *Water Research*, vol.34, 2000, pp.2786–2790
- [2-61] Francony, A., Petrier, C., "Sonochemical degradation of carbon tetrachloride in aqueous solution at two frequencies: 20 kHz and 500 kHz", *Ultrasonic Sonochemistry*. vol.3, 1996, pp.77–82
- [2-62] Mason, T.J., Cordemans, E.D., "Ultrasonic intensification of chemical processing and related operations: a review", *Chemical Engineering Research and Design*, vol.74, 1996, pp.511–516
- [2-63] Susick, K.S., Doktycz, S.J., Flint E.B, "On the origin of sonoluminescence and sonochemistry", *Ultrasonic Sonochemistry*, vol.28, 1990, pp.280–290
- [2-64] Dahlem, O., Demaiffe, V., Halloin, V., Reisse, J., "Direct sonication system suitable for medium-scale sonochemical reactors", *AIChE Journal*, vol.44, 1998, pp.2724–2730
- [2-65] Liang, J., Komarov, S., Hayashi, N., Eiki, K., "Recent trends in the decomposition of chlorinated aromatic hydrocarbons by ultrasound irradiation and Fenton's reagent", *Journal of Material Cycles and Waste Management*, vol.9, 2007, pp.47–55
- [2-66] Fischer, C.H., Hart, E.J., Henglein, A., "Ultrasonic irradiation of water in the presence of oxygen¹⁸, ¹⁸O₂: isotope exchange and isotopic distribution of hydrogen peroxide", *Journal of Physical Chemistry*, vol.90, 1986, pp.1954–1956
- [2-67] Serpone, N., Terzian, R., Hisdaka, H., Pelizzetti, E., "Ultrasonic induced dehalogenation and oxidation of 2-, 3-, and 4-chlorophenol in air-equilibrated aqueous media. Similarities with irradiated semiconductor particulates", *Journal of Physical Chemistry*, vol.98, 1994, pp.2634–2640

- [2-68] Kotronarou, A., Mills, G., Hoffmann, M.R., "Ultrasonic irradiation of p-nitrophenol in aqueous solution", *Journal of Physical Chemistry*, vol.95, 1991, pp.3630–3638
- [2-69] Drijvers, D., Langenhove, H.V., Beckers, M., "Decomposition of phenol and trichloroethylene by the ultrasound/H₂O₂/CWO process", *Water Research*, vol.33, 1999, pp.1187–1194
- [2-70] Nam, S.N., Han, S.K., Kang, J.W, Choi, H., "Kinetics and mechanism of the sonolytic destruction of non-volatile organic compounds: investigation of the sonochemical reaction zone using several OH_• monitoring techniques", *Ultrasonic Sonochemistry*, vol.10, 2003, pp.139–147
- [2-71] Sun, Y., Pignatello, J. J., "Photochemical reactions involved in the total mineralization of 2,4-D by Fe³⁺/H₂O₂/UV", *Environmental Science & Technology*, vol.27,1993, pp.304–310
- [2-72] Gogate, P. R., Pandit, A. B., "A review of imperative technologies for wastewater treatment II: hybrid methods", *Advances in Environmental Research*, vol.8, 2004, pp.553–597
- [2-73]. Zepp, R.G, Faust, B.C., Hoigne J., "Hydroxyl radical formation in aqueous reactions (pH 3–8) of iron (II) with hydrogen peroxide: the photo-Fenton reaction", *Environmental Science & Technology*, vol.26, 1992, pp.313–319
- [2-74] McGinnis, B.D., Adams, V.D., Middlebrooks E.J., "Degradation of ethylene glycol in photo Fenton systems", *Water Research*, vol.34, 2000, pp.2346–2354
- [2-75] Safarzadeh-Amiri, A., Bolton, J. R., Cater, S. R., "Ferrioxalate-mediated photodegradation of organic pollutants in contaminated water", *Water Research*, vol.31, 1997, pp.787–798
- [2-76] De Oliveira, I.S., Viana, L., Verona, C., Fallavena, V.L.V., Azevedo C.M.N., Pires M., "Alkydic resin wastewaters treatment by Fenton and photo-Fenton processes", *Journal of Hazardous Materials*, vol.146, 2007, pp.564–568
- [2-77] Kim, S.M., Geissen, S.U.,Vogelpohl A., "Landfill leachate treatment by a photo-assisted Fenton reaction", *Water Science and Technology*, vol.35, 1997, pp. 239–248
- [2-78] Amat, A.M., Arques, A., Miranda, M.A., Segui S., "Photo-Fenton reaction for the abatement of commercial surfactants in a solar pilot plant", *Solar Energy*, vol.77, 2004, pp.559–566

- [2-79] Candeias, L.P., Stratford, M.R.L., Wardman, P., "Formation of Hydroxyl Radicals on Reaction of Hypochlorous Acid with Ferrocyanide, a Model IRON (II) Complex", *Free Radical Research*, Taylor and Francis Publishing, vol.20, 1994, pp. 241–249
- [2-80] Bokare, A. D., Choi, W., "Review of iron-free Fenton-like systems for activating H₂O₂ in advanced oxidation processes", *Journal of Hazardous Materials*, vol.275, 2014, pp.121-135
- [2-81] Brillas, E., Calpe, J. C., Casado, J., "Mineralization of 2,4-D by advanced electrochemical oxidation processes", *Water Research*, vol.34, Issue 8, 2000, pp.2253-2262
- [2-82] Oturan, M., "An ecologically effective water treatment technique using electrochemically generated hydroxyl radicals for in situ destruction of organic pollutants: Application to herbicide 2, 4-D", *Journal of Applied Electrochemistry*, vol.30, 2000, pp.475
- [2-83] Kapałka, A., Baltruschat, H., Comninellis, C., "Electrochemical Oxidation of Organic Compounds Induced by Electro-Generated Free Hydroxyl Radicals on BDD Electrodes" *Synthetic Diamond Films: Preparation, Electrochemistry, Characterization, and Applications*, 2011, pp. 237-260.
- [2-84] Nguyen-Manh, D., Ntoahae, P. S., Pettifor, D. G., Ngoepe, P. E., "Electronic Structure of Platinum-Group Minerals: Prediction of Semiconductor Band Gaps", *Molecular simulation*, Taylor and Francis Publishing, vol. 22, 1999, pp.23-30
- [2-85] Nidheesh, P.V., Gandhimathi, R., "Removal of Rhodamine B from aqueous solution using graphite–graphite electro-Fenton system", *Desalination and Water Treatment*, Taylor and Francis Publishing, vol.52, 2014, Issue 10-12, pp.1872-1877
- [2-86] Özcan, A., Yücel, S., Savaş, Koparal, A., Oturan, M.A., "Carbon sponge as a new cathode material for the electro-Fenton process: Comparison with carbon felt cathode and application to degradation of synthetic dye basic blue 3 in aqueous medium", *Journal of Electroanalytical Chemistry*, vol.616, Issues 1–2, 2008, pp.71-78
- [2-87] Sirés, I., Garrido, J. A., Rodríguez, R. M., Brillas, E., Oturan, N., Oturan, M. A., "Catalytic behavior of the Fe³⁺/ Fe²⁺ system in the electro-Fenton degradation of the antimicrobial chlorophene", *Applied Catalysis B: Environmental*, vol.72, Issues 3–4, 2007, pp.382-394

[2-88] Kishimoto, N., Kitamura, T., Kato, M., Otsu, H., "Reusability of iron sludge as an iron source for the electrochemical Fenton-type process using $\text{Fe}^{2+}/\text{HOCl}$ system", *Water Research*, vol.47, Issue 5, 2013, pp.1919-1927

[2-89] Kishimoto, N., Kitamura, T., Nakamura, Y., "Applicability of an electrochemical Fenton-type process to actual wastewater treatment", *Water Science and Technology*, vol.72, 2015, pp.850-857

[2-90] Flox ,C., Garrido, J.A., Rodríguez, R.M., Cabot, P.L., Centellas F., Arias C., Brillas E., "Mineralization of herbicide mecoprop by photoelectro-Fenton with UVA and solar light", *Catalysis Today*, vol.129, Issues 1–2, 2007, pp.29-36

[2-91] Hammami, S., Oturan, N., Bellakhal, N., Dachraoui, M., Oturan, M.A., "Oxidative degradation of direct orange 61 by electro-Fenton process using a carbon felt electrode: Application of the experimental design methodology", *Journal of Electroanalytical Chemistry*, vol.610, Issue 1, 2007, pp.75-84

[2-92] Isarain-Chávez, E., Rodríguez, R. M., Garrido, J. A., Arias, C., Centellas, F., Cabot, P. L., Brillas, E., "Degradation of the beta-blocker propranolol by electrochemical advanced oxidation processes based on Fenton's reaction chemistry using a boron-doped diamond anode", *Electrochimica Acta*, vol.56, Issue 1, 2010, pp.215-221

[2-93] El-Ghenymy, A., Rodríguez, R. M., Arias, C., Centellas, F., Garrido J. A., Cabot P. L., Brillas E., "Electro-Fenton and photoelectro-Fenton degradation of the antimicrobial sulfamethazine using a boron-doped diamond anode and an air-diffusion cathode", *Journal of Electroanalytical Chemistry*, vol.701, 2013, pp.7-13

[2-94] Labiadh L., Oturan M.A., Panizza M., Hamadi N. B., Ammar S., "Complete removal of AHPS synthetic dye from water using new electro-fenton oxidation catalyzed by natural pyrite as heterogeneous catalyst", *Journal of Hazardous Materials*, vol.297, ISSN 0304-3894,2015, pp.34-41

[2-95] Iranifam M., Zarei M., Khataee A. R., "Decolorization of C. I., "Basic Yellow 28 solution using supported ZnO nanoparticles coupled with photoelectro-Fenton process", *Journal of Electroanalytical Chemistry*, vol.659, Issue 1, 2011, pp.107-112

[2-96] Wu, J., Zhang H., Oturan, N., Wang, Y., Chen, L., Oturan, M.A., "Application of response surface methodology to the removal of the antibiotic tetracycline by electrochemical process using carbon-felt cathode and DSA (Ti/RuO₂-IrO₂) anode", *Chemosphere*, vol.87, Issue 6, 2012, pp.614-620

[2-97] Khataee, A., Marandizadeh, H., Zarei, M., Aber, S., Vahid, B., Hanifehpou, Y., Joo, S. W., "Treatment of an Azo Dye by Citrate Catalyzed Photoelectro-Fenton Process Under Visible Light using Carbon Nanotube-polytetrafluoroethylene Cathode", *Journal of Current Nanoscience*, vol.9, Issue 3, 2013

[2-98] Garcia-Segura, S., Cavalcanti, E. B., Brillas, E., "Mineralization of the antibiotic chloramphenicol by solar photoelectro-Fenton: From stirred tank reactor to solar pre-pilot plant", *Applied Catalysis B: Environmental*, vol.144, 2014, pp.588-598

[2-99] Boye, B., Dieng, M.M., Brillas, E., "Degradation of Herbicide 4-Chlorophenoxyacetic Acid by Advanced Electrochemical Oxidation Methods", *Environmental Science & Technology*, vol.36, 2002, pp.3030-3035

[2-100] Serra, A., Domènech, X., Arias, C., Brillas, E., Peral J., "Oxidation of α -methylphenylglycine under Fenton and electro-Fenton conditions in the dark and in the presence of solar light", *Applied Catalysis B: Environmental*, vol.89, Issues 1–2, 2009, pp.12-21

[2-101] Antonin, V.S., Garcia-Segura, S., Santos, M.C., Brillas, E., "Degradation of Evans Blue diazo dye by electrochemical processes based on Fenton's reaction chemistry", *Journal of Electroanalytical Chemistry*, vol.747, 2015, pp.1-11

[2-102] Skoumal, M., Arias, C., Cabot, P.L., Centellas F, Garrido J.A., Rodríguez R.M., Brillas E., "Mineralization of the biocide chloroxylenol by electrochemical advanced oxidation processes", *Chemosphere*, vol.71, Issue 9, 2008, pp.1718-1729

[2-103] Flox C., Cabot, P.L., Centellas, F., Garrido, J.A., Rodríguez, R.M., Arias, C., Brillas, E., "Solar photoelectro-Fenton degradation of cresols using a flow reactor with a boron-doped diamond anode", *Applied Catalysis B: Environmental*, vol.75, Issues 1–2, 2007, pp.17-28

- [2-104] Santos, A., Yusts, P., Rodriguez, S., Simon, E., Garcia-Ochoa, F., "Abatement of phenolic mixtures by catalytic wet oxidation enhanced by Fenton's pretreatment: Effect of H₂O₂ dosage and temperature", *Journal of Hazardous Materials*, vol.146, Issue 3, 2007, pp.595-601
- [2-105] El-Ghenymy, A, Garrido, J.A., Rodríguez, R.M., Cabot, P.L., Centellas, F., Arias, C., Brillas, E., "Degradation of sulfanilamide in acidic medium by anodic oxidation with a boron-doped diamond anode", *Journal of Electroanalytical Chemistry*, vol.689, 2013, pp.149-157
- [2-106] Malato, S., Fernández-Ibáñez, P., Maldonado, M.I., Blanco J., Gernjak W., "Decontamination and disinfection of water by solar photocatalysis: Recent overview and trends", *Catalysis Today*, vol.147, Issue 1, 2009, pp.1-59
- [2-107] Pignatello, J. J., "Dark and photoassisted iron (3+)-catalyzed degradation of chlorophenoxy herbicides by hydrogen peroxide", *Environmental Science & Technology*, vol.26, 1992, pp.944-951
- [2-108] Meeker, R.E., inventors. Stabilization of hydrogen peroxide. United States, Patent 3208825 A. 1965 September 28.
- [2-109] Daneshvar, N., Aber, S., Vatanpour, V., Rasoulifard, M. H., "Electro-Fenton treatment of dye solution containing Orange II: Influence of operational parameters", *Journal of Electroanalytical Chemistry*, vol.615, Issue 2, 2008, pp.165-174
- [2-110] Chiang, L-C, Chang, J-E, Wen, T-C, "Indirect oxidation effect in electrochemical oxidation treatment of landfill leachate", *Water Research*, vol.29, Issue 2, 1995, pp.671-678
- [2-111] Anglada, A., Urtiaga, A., Ortiz, I., Mantzavinos, D., Diamadopoulos, E., "Boron-doped diamond anodic treatment of landfill leachate: Evaluation of operating variables and formation of oxidation by-products", *Water Research*, Vol.45, Issue 2, 2011, pp.828-838
- [2-112] Orescanin, V., Kollar, R., Nad, K., Mikelic, I.L., Gustek, S.F., "Treatment of winery wastewater by electrochemical methods and advanced oxidation processes", *Journal of Environmental Science and Health, Part A*, vol.48, Issue 12, 2013
- [2-113] El-Desoky, H.S., Ghoneim, M. M., Zidan, N. M., "Decolorization and degradation of Ponceau S azo-dye in aqueous solutions by the electrochemical advanced Fenton oxidation", *Desalination*, vol.264, Issues 1–2, 2010, pp.143-150

- [2-114] Rosales, E., Pazos, M., Longo, M. A., Sanromán, M. A., "Electro-Fenton decoloration of dyes in a continuous reactor: A promising technology in colored wastewater treatment", *Chemical Engineering Journal*, vol.155, Issues 1–2, 2009, pp.62-67
- [2-115] Gözmen, B., Kayan, B., Gizir, A. M., Hesenov, A., "Oxidative degradations of reactive blue 4 dye by different advanced oxidation methods", *Journal of Hazardous Materials*, vol.168, Issue 1, 2009, pp.129-136
- [2-116] Almeida, L.C., Garcia-Segura, S., Arias ,C., Bocchi, N., Brillas, E., "Electrochemical mineralization of the azo dye Acid Red 29 (Chromotrope 2R) by photoelectro-Fenton process", *Chemosphere*, vol.89, Issue 6, 2012, pp.751-758
- [2-117] Garcia-Segura, S., Almeida, L.C., Bocchi, N., Brillas, E., "Solar photoelectro-Fenton degradation of the herbicide 4-chloro-2-methylphenoxyacetic acid optimized by response surface methodology", *Journal of Hazardous Materials*, vol.194, 2011, pp.109-118
- [2-118] Moreira, F.C., Boaventura, R.A.R, Brillas E., Vitor V.J.P, "Electrochemical advanced oxidation processes: A review on their application to synthetic and real wastewaters" *Applied Catalysis B: Environmental*, vol.202, 2017, pp.217–261
- [2-119] Zhang, H., Zhang, D., Zhou, J., "Removal of COD from landfill leachate by electro-Fenton method", *Journal of Hazardous Materials*. vol.135, 2006, pp.106–111
- [2-120] Yuan, S., Tian, M., Cui, Y., Lin, L., Lu, X., "Treatment of nitrophenols by cathode reduction and electro-Fenton methods", *Journal of Hazardous Materials*, vol.137, 2006, pp.573–580.
- [2-121] Oturan, M.A., Pimentel, M., Oturan, N., Sirés, I., "Reaction sequence for the mineralization of the short-chain carboxylic acids usually formed upon cleavage of aromatics during electrochemical Fenton treatment", *Electrochimica Acta*, vol.54, Issue 2, 2008, pp.173-182
- [2-122] Pimentel, M., Oturan, N., Dezotti, M., Oturan, M.A., "Phenol degradation by advanced electrochemical oxidation process electro-Fenton using a carbon felt cathode", *Applied Catalysis B: Environmental*, vol.83, Issues 1–2, 2008, pp.140-149
- [2-123] Oturan, N., van Hullebusch, E. D., Zhang, H., Mazeas, L., Budzinski, H., Menach, K .L., Oturan, M. A., "Occurrence and Removal of Organic Micropollutants in Landfill Leachates

Treated by Electrochemical Advanced Oxidation Processes", *Environmental Science & Technology*, vol.49,2015, pp.12187-12196

[2-124] Brillas, E., Casado, J., "Aniline degradation by Electro-Fenton and peroxi-coagulation processes using a flow reactor for wastewater treatment", *Chemosphere*, vol.47, Issue 3, 2002, pp.241-248

[2-125] Moreira, F. C., Boaventura, R. A. R., Brillas, E., Vilar, V.J.P, "Remediation of a winery wastewater combining aerobic biological oxidation and electrochemical advanced oxidation processes", *Water Research*, vol.75, 2015, pp.95-108

[2-126] Wang, C., Chou, W., Chung, M., Kuo, Y., "COD removal from real dyeing wastewater by electro-Fenton technology using an activated carbon fiber cathode", *Desalination*, vol.253, Issues 1–3, 2010, pp.129-134

[2-127] Kurt, U., Apaydin, O., Gonullu, M.T., "Reduction of COD in wastewater from an organized tannery industrial region by Electro-Fenton process", *Journal of Hazardous Materials*, vol.143, Issues 1–2, 2007, pp.33-40

[2-128] Brillas, E., Mur, E., Sauleda, R., Sánchez, L., Peral, J., Domènech, X., Casado, J., "Aniline mineralization by AOP's: anodic oxidation, photocatalysis, electro-Fenton and photoelectro-Fenton processes", *Applied Catalysis B: Environmental*, vol.16, Issue 1, 1998, pp.31-42

[2-129] Cañizares, P., Paz, R., Sáez, C., Rodrigo, M. A., "Costs of the electrochemical oxidation of wastewaters: A comparison with ozonation and Fenton oxidation processes", *Journal of Environmental Management*, vol. 90, Issue 1, 2009, pp. 410-420

Chapter 3

[3-1] Kushwaha, J. P., Srivastava, V. C., Mall, I. D., "Sequential batch reactor for dairy wastewater treatment: Parametric optimization; kinetics and waste sludge disposal", *Journal of Environmental Chemical Engineering*, vol 1, Issue 4, 2013, pp. 1036-1043

[3-2] EMD Millipore MColortest™ Sulfate Test Kits, colorimetric with color-disk comparator method, 25 – 50 – 75 -100 – 130 – 160 – 190 – 240 – 300 -400 mg/L MColortest, EMD Millipore 1183890001

- [3-3] Boopathy R., Mandal A. B., Sekaran G., “Electrochemical treatment of evaporated residue of reverse osmosis concentrate generated from the leather industry”, *RSC Advances*, 4, 2014, pp.54-61.
- [3-4] Avis, D., Fukuda, K., “Reverse Search for Enumeration”, *Discrete Applied Mathematics*, vol. 65, 1996, pp. 21-46.
- [3-5] Nitrogen, Simplified TKN, 0 to 16 mg/L TKN, s-TKN™ Method, Hach Method 10242, DOC316.53.01258, (01/2017), Edition 4
- [3-6] Nitrogen, Ammonia, High Range 2 to 47 mg/L NH₃-N, Salicylate Method, Hach Method 10205, DOC316.53.01083, (11/2016), Edition 10
- [3-7] Nitrate high Range, 5 to 35 mg/L NO₃⁻-N or 22 to 155 mg/L NO₃⁻, Dimethylphenol Method, Hach Method 10206, DOC 316.53.01071, (09/2015), Edition 9
- [3-8] Sulfate High Range (150 to 900 mg/L SO₄²⁻) Turbidimetric Method, Hach Method 10227, DOC 316.53.01232, (2012), Edition 7
- [3-9] Haber, F., Weiss, J., “The Catalytic Decomposition of Hydrogen Peroxide by Iron Salts” *Mathematical, Physical and Engineering Science*, 147, 1934, pp. 332–351.
- [3-10] Brillas, E., Sirés, I., Oturan, M.A., “Electro-Fenton Process and Related Electrochemical Technologies Based on Fenton’s Reaction Chemistry” , *Chemical Reviews*, 109 (12), 2009, pp. 6570–6631.
- [3-11] Nidheesh, P., Gandhimathi, R., “Trends in the electro-Fenton process for water and wastewater treatment: An overview”. *Desalination*, vol. 299, 2012, pp. 1-15.
- [3-12] Girault, H., “Analytical and Physical Electrochemistry”, *EPFL Press*, 2004, pp. 141-175.
- [3-13] Rajeshwar, K., Ibanez, J.,” Environmental Electrochemistry: Fundamentals and Applications in Pollution Sensors and Abatement” *Academic Press*, 1997, pp. 62-64.
- [3-14] Jianrong, Wu, Berland K. M., “Propagators and Time-Dependent Diffusion Coefficients for Anomalous Diffusion”, *Biophysical Journal*, vol. 95, Issue 4, 2008, pp. 2049-2052
- [3-15] Weiss, M., Elsner, M., Kartberg, F., Nilsson, T., “Anomalous subdiffusion is a measure for cytoplasmic crowding in living cells.” *Biophys. J.*, 2004, pp. 87:3518–3524.

[3-16] Feder, T. J., Brust-Mascher, I., Slattery, J. P., Baird B., and Webb W. W., “Constrained diffusion or immobile fraction on cell surfaces: a new interpretation”, *Biophysical Journal* 1996, pp.70:2767–2773.

[3-17] Segre, P. N., and Pusey, P. N., “Scaling of the dynamic scattering function of concentrated colloidal suspensions”, *Physical Review Letters*, vol.77, 1996, pp .771–774

[3-18] Thompson, N. L.,” Fluorescence correlation spectroscopy. In *Topics in Fluorescence Spectroscopy*. J. R. Lakowicz, editor. Plenum Press, New York, 1991, pp. 337–378.

[3-19] Elson, E. L., Magde, D., “Fluorescence Correlation Spectroscopy I. Conceptual Basis and Theory”, *Biopolymers*, 1974, pp.13:1–27.

[3-20] Scott, K.,” Electrochemical processes for clean technology”. *Cambridge, UK: The Royal Society of Chemistry*, 1995, pp. 12– 62.

[3-21] de Grotthuss, C. J. T. "Sur la décomposition de l'eau et des corps qu'elle tient en dissolution à l'aide de l'électricité galvanique". *Annali Di Chimica*, vol.58,1806, pp. 54–73.

[3-22] IUPAC Compendium of Chemical Terminology, 2nd ed. (the "Gold Book"). Compiled by A. D. McNaught and A. Wilkinson. Blackwell Scientific Publications, Oxford (1997). XML on-line corrected version: <http://goldbook.iupac.org> (2006) created by M. Nic, J. Jirat, B. Kosata; updates compiled by A. Jenkins

[3-23] Chen, X., Chen, G., You, P., “Investigation on the electrolysis voltage of electrocoagulation”, *Chemical Engineering Science*, vol. 57, 2002, pp. 2449 – 2455

[3-24] Gallagher, K., G., Fuller, T. F., “Kinetic model of the electrochemical oxidation of graphitic carbon in acidic environments”, *Physical Chemistry Chemical Physics*, vol.11, 2009, pp. 11557–11567

- [3-25] Colmenares, L. C., Wurth, A., Jusys, Z., Behm, R. J., “Model study on the stability of carbon support materials under polymer electrolyte fuel cell cathode operation conditions”, *Journal of Power Sources*, vol. 190, Issue 1, 2009, pp. 14-24
- [3-26] Kangasniemi, K. H., Conditb, D. A., and Jarvic, T. D., “Characterization of Vulcan Electrochemically Oxidized under Simulated PEM Fuel Cell Conditions”, *Journal of Electrochemical Society*, vol. 151, 2004, issue 4, pp. E125-E132.
- [3-27] Kinoshita K., Bett J. A. S., “Potentiodynamic analysis of surface oxides on carbon blacks”, *Carbon Journal, Elsevier Publishing (1973)*, vol. 11, 1973, Issue 4, pp. 403-411.
- [3-28] Leon y Leon, C. A., Radovic, L. R., “Interfacial Chemistry and Electrochemistry of Carbon Surfaces” *Chemistry and Physics of Carbon*, Thrower, P. A., Ed.; Marcel Dekker: New York, Vol. 24, 1994, pp. 213- 310.
- [3-29] Zhang, H., Fei, C., Zhang, D., Tang, F., “Degradation of 4-nitrophenol in aqueous medium by electro-Fenton method”, *Journal of Hazardous Materials*, 145, 2007, pp. 227–232.
- [3-30] Bard, A. J., Faulkner, L. R., “Electrochemical Methods”, 1980, New York: Wiley. pp. 42-45.
- [3-31] Bieniasz, L. K., “Use of dynamically adaptive grid techniques for the solution of electrochemical kinetic equations. Part 14: extension of the patch-adaptive strategy to time-dependent models involving migration–diffusion transport in one-dimensional space geometry, and its application to example transient experiments described by Nernst–Planck–Poisson equations”, *Journal of Electroanalytical Chemistry*, vol. 565, 2004, pp. 251–271,
- [3-32] Moya, A. A., and Horno, J., “Application of the Network Simulation Method to Ionic Transport in Ion-Exchange Membranes Including Diffuse Double-Layer Effects”, *Journal of Physical Chemistry B*, 103 (49), 1999, pp. 10791–10799

[3-33] Fogler, H. S., “Elements of chemical reaction engineering”, *Fifth edition, Pearson Education Prentice-Hall Publishing*, January 2016.

[3-34] Kapałka, A., Fóti, G., Comninellis, C., Kinetic modelling of the electrochemical mineralization of organic pollutants for wastewater treatment, *Journal of Applied Electrochemistry*, vol. 38, Issue 1, 2008, pp 7–16.

[3-35] Li, L., Liu, Y., “Ammonia removal in electrochemical oxidation: Mechanism and pseudo-kinetics”, *Journal of Hazardous Materials*, vol. 161, 2009, Issues 2–3, pp. 1010-1016

Chapter 4

[4-1] Abbassi-Guendouz, A., Brockmann, D., Trably E., Dumas, C., Delgenès, J.P., Steyer J. P., Escudié, R., “Total solids content drives high solid anaerobic digestion via mass transfer limitation”, *Bioresource Technology*, vol. 111, 2012, pp. 55–61.

[4-2] Sillanpää, M., Shestakova, M., “Electrochemical Water Treatment Methods; Fundamentals, Methods and Full Scale Applications”, *1st Edition, Butterworth-Heinemann Elsevier Publishing*, 2017, pp. 95-96.

[4-3] Anglada, A., Urtiaga, A., Ortiz I., “Electrochemical Water Treatment Methods; Fundamentals -water treatment: fundamentals and review of applications”, *Journal of Chemical Technology and Biotechnology*, vol. 84, 2009, pp. 1747–1755

[4-4] Gabrielli, C., Huet, F., and Keddam, M., “Fluctuations in electrochemical systems. I. General theory on diffusion limited electrochemical reactions”, *The Journal of Chemical Physics* vol. 99, Issue 9, 1993, pp. 7232-7239

[4-5] Xu, J.J., Peng, Y., Bao, N., Xia, X., Chen, H., “Simple method for the separation and detection of native amino acids and the identification of electroactive and non-electroactive analytes”, *Journal of Chromatography A*, vol. 1095, 2005, pp.193–196,

[4-6] Bennett, W. B., Lubin D. L., “Electrochemical cell having electrode additives”, *Patent WO 2000030198 A1*, Published in 25 May 2000, Application number PCT/US1999/026814.

- [4-7] Ebrahiem, E. E., Al-Maghrabi, M. N., Mobarki A. R., “Removal of organic pollutants from industrial wastewater by applying photo-Fenton oxidation technology”, *Arabian Journal of Chemistry*, vol. 10, 2017, pp. S1674-S1679
- [4-8] De Maubeugez, H. L., “Calculation of the Optimal Geometry of Electrochemical Cells Application to the Plating on Curved Electrodes”, *Journal of The Electrochemical Society*, 149 (8), 2002, C413-C422.
- [4-9] Panizza, M., Cerisola, G., “Removal of organic pollutants from industrial wastewater by electrogenerated Fenton's reagent”, *Water Research*, vol. 35, 2001, Issue 16, pp. 3987-3992
- [4-10] Lin, S., Chang, C., “Treatment of landfill leachate by combined electro-Fenton and sequencing batch reactor”, *Water Research*, Vol. 34, 2000, No. 17, pp. 4243-4249
- [4-11] Rodkey F. L., “The effect of temperature on the Oxidation-Reduction Potential of the Diphosphopyridine Nucleotide System”, *Journal of Biological Chemistry*, vol. 234, 1959, pp. 188-190.
- [4-12] Hamann C., H., Hamnett A., Vielstich W., “Electrochemistry; second, completely revised and updated edition”, 2nd edition, 2007, *Wiley-VCH Verlag GmbH & Co. KGaA*

Chapter 5

- [5-1] Szpyrkowicz, L., Naumczyk, J., Zilio-Grandi, F., “Electrochemical treatment of tannery wastewater using TiPt and Ti/Pt/Ir electrodes”, *Water Research*, vol. 29, Issue 2, 1995, pp. 517-524
- [5-2] Barzykina, A. V., Tachiyab, M., “Diffusion-influenced reaction kinetics on fractal structures”, *The Journal of Chemical Physics* 99, 1995, 9591
- [5-3] Rimpault, X., Chatelain, J.-F., Klemberg-Sapieha, J.E., Balazinski, M., “Tool wear and surface quality assessment of CFRP trimming using fractal analyses of the cutting force signals”, *CIRP Journal of Manufacturing Science and Technology*, vol. 16, 2017, pp. 72-80
- [5-4] Rimpault, X., “Tool condition monitoring and surface topography analysis during the machining of CFRP composites” (PhD thesis), Polytechnique Montreal, *Université de Montréal, Montréal, Canada*, 2016